University of Alberta

Antagonistic modulation of spontaneous neural network activities in isolated newborn rat brainstem preparations by opioids and methylxanthines

by

Bogdan Alexandru Panaitescu

A thesis submitted to the Faculty of Graduate Studies and Research
in partial fulfillment of the requirements for the degree of

Doctor of Philosophy

Department of Physiology

Fall, 2012
Edmonton, Alberta

Abstract

Apnea of prematurity is a common problem among the infants born before term pregnancy. Administration of respiratory stimulating drugs methylxanthines is the most frequent therapy, often in combination with the use of intubation. Opioids are used to reduce the pain associated with intubation, although they can depress breathing by acting on inspiratory neural networks located in the lower medulla, such as pre-Bötzinger Complex (preBötC). The aim of this thesis was to study the effects of methylxanthines and opioids on the respiratory active network preBötC and to compare the findings with those in the spontaneously active newborn network, *locus coeruleus* (LC).

In a first project, it was found that novel 400 μm thick slices with centered preBötC showed stable inspiratory rhythm for >5 h in a solution with 5-6 mM K^+ and 1 mM Ca^{2+}. Elevated Ca^{2+} concentrations (1.5-2 mM Ca^{2+}) blocked rhythm without postsynaptic changes in membrane potential or input resistance, while concentrations lower than 0.75 mM evoked seizure-like discharges. Similar to elevated Ca^{2+}, the μ-opioid agonist [D-Ala^2,N-Me-Phe^4,Gly^5-ol]-enkephalin (DAMGO) abolished preBötC neuron bursting with minor postsynaptic effects, which was reversed by methylxanthines without changes on membrane properties. The same methylxanthine dose evoked non-respiratory discharges in spinal inspiratory motor networks, while the preBötC remained largely unaffected.

Based on these findings it was studied whether spontaneous bursting of LC networks in horizontal brainstem slices was perturbed by low millimolar methylxanthine. The results showed that the LC is similarly resistant to methylxanthines which can evoke a depolarization that reverses the DAMGO-induced hyperpolarization. Ca^{2+} imaging in either preBötC or LC revealed that DAMGO lowers Ca^{2+} baseline in neurons and abolishes their rhythm-related Ca^{2+} rises, which are restored by low millimolar methylxanthines without a hypothesized store-mediated effect. Neither DAMGO nor methylxanthines affected Ca^{2+} in silent small cells, likely representing astrocytes.

These novel electrophysiological and optical findings provide the basis for future studies dedicated to analyze whether the lack of obvious postsynaptic membrane effects of both opioids and methylxanthines are an indication of a major role of presynaptic inhibition, which potentially underlies also the strong preBötC inhibition by raised extracellular calcium.

Acknowledgments

I would like to thank my supervisor, Dr. Klaus Ballanyi for the opportunity he gave me to work in his laboratory and for introducing me to the world of neuroscience. His support and motivation were invaluable for me. I appreciate greatly the intellectual and scientific training that I received in his laboratory. I would like to thank to all the past and present members of the Ballanyi laboratory: Lucia Sechia, Araya Ruangkittisakul, Nicoleta Bobocea, Junya Kuribayashi, and Chase Kantor for their help, support and friendship throughout all these years.

I also would like to thank to my committee members, Drs. Peter Smith and Simon Gosgnach for their helpful advice and feedback throughout my graduate program. Members of my defense examining committee (Drs. Anthony Ho, Gregory Funk, and Christopher Del Negro) deserve a thank you for taking the time to review my proposal and dissertation and for their comments and suggestions.

A big thanks goes to my family (wife, sister, and parents) for their support and unconditional love. I would not be who I am today without them.

Table of Contents

List of Figures

Chapter 1

Chapter 2

Chapter 3

Chapter 4

Chapter 5

Chapter 6

List of Abbreviations

5HT	5-hydroxytryptamine (serotonin)
$A_{1,2A}$	Adenosine receptors
AC	Adenylyl cyclase
AMPA	α-amino-3-hydroxy-5-methyl-4-isoxazolepropionic acid
AP	Area postrema
BA	Basilar artery
BAPTA	1,2-bis(o-aminophenoxy)ethane-N,N,N',N'-tetraacetic acid
Bic	Bicuculline
BötC	Bötzinger complex
C	Caudal
C_{1-8}	Cervical nerve roots
C+preBötC	Slice containing "caudal" tissue plus the preBötC
Caff	Caffeine
cAMP	Cyclic-adenosine monophosphate
CCA	Caudal cerebellar artery
CPA	Cyclopiazonic acid
D	Dorsal
DAMGO	[D-Ala^2, *N*-Me-Phe^4, Gly^5-ol] Enkephalin
Dbx1	Developing brain homeobox 1
DHPG	3,5-dihydroxy-phenylglycine

DMCC	Dorsomedial cell column of inferior olive
DMSO	Dimethyl sulfoxide
DMPX	8-Cyclopentyl-1,3-dipropylxanthine
DRG	Dorsal respiratory group
EGTA	Ethylene glycol tetraacetic acid
GABA	γ-aminobutyric acid
Glu	Glutamate
Gly	Glycine
GIRK	G protein-coupled inward-rectifying K^+ channels
IBMX	Isobuthylmethylxanthine
IC_{50}	Half maximal inhibitory concentration
I_{CAN}	Ca^{2+}-activated nonspecific cationic current
I_{NaP}	Persistent Na^+ current
IO	Inferior olive
IRC	Ictal respiratory changes
IX	Glossopharyngeal nerve
LC	Locus coeruleus
LRN	Lateral reticular nucleus
mGluR,	Metabotropic glutamate receptor
m-preBötC	Slices containing the preBötC in the middle
Mus	Muscimol
NA	Nucleus ambiguous
Nalo	Naloxone

NK1	Neurokinin-1
NMDA	N-methyl-D-aspartic acid
NTB	Nucleus trapazoid body
P	Postnatal day
P2Y	Purinergic receptors, G-protein coupled
PDE	Phosphodiesterase
pFRG	Parafacial respiratory group
Phox2b	Paired-like homeobox 2b
PKA	Protein kinase A
preBötC	Pre-Bötzinger complex
Pre-I	Pre-inspiratory
PRG	Pontine respiratory group
R	rostral
r+preBötC	Slice containing “rostral” tissue plus the preBötC
ROI	Region of interest
RTN	Retrotrapezoid nucleus
RYR	Ryanodine receptors
SD	Sprague Dawley
SP	Substance-P
SR101	Sulforhodamine-101
Strych	Strychnine
Theo	Theophylline
$T_{2,3}$	Thoracic nerve roots

TRH	Thyrotropin releasing hormone
TTX	Tetrodotoxin
v	Ventral
V_4	Fourth ventricle
V	Trigeminal nerve
VGCC	Voltage-gated Ca^{2+} channels
VGLUT	Vesicular glutamate transporter
VI	Abducens nerves
VII	Facial motonucleus
VII_c	Caudal end of facial motonucleus
VIII	Vestibulocochlear nerves
VRC	Ventral respiratory column
VRG	Ventral respiratory group
W	Wistar
X	Vagal nerves
XI	Accessory nerves
XII	Hypoglossal motonucleus/nerves

CHAPTER 1

General Introduction

1.1. Rationale for Thesis

In preterm infants, the function of various organs is yet not fully developed. This includes an immaturity of central nervous respiratory control mechanisms resulting in irregular breathing movements. Such irregular breathing, also termed apnea of prematurity, is typical for premature infants, but can also occur in term newborns although normally at lower incidence and severity. At present, the gold standard for pharmacological treatment of such apneas is methylxanthines. Specifically, these are caffeine, but also theophylline and aminophylline. While methylxanthines counter apneas of prematurity effectively, they can exert severe systemic side effects such as nausea, tachycardia, tachypnea, sleep disruption, and seizures. Consequently, there is a need for developing novel drugs that specifically target the primary anatomical sites of the respiratory stimulating action of methylxanthines. Most important in that regard are lower brainstem respiratory networks that initiate and control breathing movements. Consequently, these networks need to be studied for specific treatment of central respiratory diseases.

Research on various *in vitro* and *in vivo* animal models indicated that a dual respiratory center is involved in nervous control of breathing during the 'perinatal' time period around birth. One component of this dual 'respiratory oscillator', the parafacial respiratory group (pFRG), is presumably responsible for expiratory-related breathing movements. Moreover, during birth the pFRG seems to stimulate its inspiratory counterpart, the pre-Bötzinger complex (preBötC),

whose neurons are directly depressed by a surge of endogenous opioids associated with stress during the transition to air breathing. Later after birth, the preBötC constitutes the vital part of the dual respiratory center, whereas active expiration becomes less important for normal breathing. Because of the pivotal role of the preBötC for breathing, it is important to understand the basic operation and mutual interaction of its cellular elements which are interneurons, glial cells (particularly astrocytes) and immuno-related microglia.

Central to this thesis is the hypothesis that methylxanthines act as respiratory stimulants by targeting primarily the preBötC. To study this, I used mostly a brainstem slice model for depressing preBötC activity with opioids before applying methylxanthines for studying the mechanisms of their hypothesized countering effects on this depression. There is some disagreement regarding the exact subcellular sites within the preBötC of inhibitory opioid actions. Some groups propose that this inhibition is caused by postsynaptic hyperpolarization of preBötC neurons, whereas others, including our laboratory, presented evidence for a major involvement of presynaptic mechanisms. To exclude potential influences of experimental conditions on presynaptic *versus* postsynaptic effects, I compared responses of the isolated preBötC to opioids and methylxanthines with those on *locus coeruleus* (LC) neurons in brainstem slices because robust postsynaptic hyperpolarizing opioid actions were pioneered in these cells.

1.2 Isolation of the Dual Respiratory Center in Neonates

Apnea of prematurity occurs frequently in (preterm) infants. Presumably, they originate from immature nervous structures in the lower brainstem (*medulla oblongata*) that normally initiate and control respiratory muscle contractions. For specific novel treatment of these developmentally-related apneas and other central respiratory diseases, knowledge is therefore required particularly on the structure and function of such medullary respiratory networks. It has been hypothesized since long that breathing movements are controlled by a respiratory center, a so-called *noeud vital* (Flourens, 1858; Feldman, 1986; Bianchi et al., 1995; Feldman & Del Negro, 2006). The latter review articles summarize lesioning studies that have established, in concert with *in vivo* work using microelectrodes to categorize respiratory-related neuronal activities, the existence of three major respiratory groups **(Fig. 1-1)**. Each of these neural networks is distributed within bilaterally organized columns to form the pontine, dorsal and ventral respiratory groups, with the latter being part of the ventral respiratory column (VRC) (Feldman, 1986; Bianchi et al., 1995; Feldman & Del Negro, 2006; Smith et al., 2009). The pontine and dorsal respiratory groups are important particularly for integrating reflexes, that are triggered by (peripheral) mechano- and chemoreceptors, and also for subsequent shaping of respiratory neuronal activity patterns (Bianchi et al., 1995; Dutschmann et al., 2004). These activity patterns with different phase relationships to each other are transmitted to respiratory muscle groups for generating three neural respiratory phases, i.e. inspiration, post-inspiration and expiration (Richter & Spyer, 2001; Duffin, 2004).

Previous *in vivo* work indicated that the *noeud vital* is located in a specific aspect of the VRC, but ultimately it was successfully identified and isolated using an *in vitro* approach. As a pivotal step toward this, Suzue (1984) developed an isolated newborn rat brainstem-spinal cord preparation that retains spontaneous respiratory-like rhythmic activity **(Fig. 1-2)**. Since almost three decades, this so-called '*en bloc*' model is used for unravelling pharmacological and cellular respiratory network features (Ballanyi et al., 1999; Feldman & Del Negro, 2006). This *en bloc* preparation was seminal for identification of the respiratory center in a milestone study in 1991 by Smith and colleagues, involving our group. This study revealed firstly by serial brainstem transection in rostral-to-caudal *versus* caudal-to-rostral direction that *in vitro* respiratory rhythm stopped when an overlapping brainstem area of ~200 µm thickness was affected. It was concluded that this area, tagged as the preBötC, is the *noeud vital*. It was then hypothesized by the authors that a transversal brainstem slice containing this region generates rhythm that is inspiratory-related (tagged 'inspiratory' in the following). Indeed, preBötC-containing slices as thin as 350 µm showed synaptically-mediated rhythmic discharge in neurons positioned in the ventrolateral aspect, corresponding to the VRC location in newborn rats (Smith et al., 1991) **(Fig. 1-2)**. A notable portion of preBötC neurons in that study (Smith et al., 1991) was capable of intrinsic ('conditional') bursting upon membrane potential depolarization due to current injection via the patch electrode used for 'blind' whole-cell recording (Blanton et al., 1989). Rhythmic synaptic activity of such

isolated preBötC neurons is inspiratory because it is synchronous with discharge of hypoglossal (XII) nerve rootlets that are contained in these slices **(Fig. 1-2)** and normally innervate the inspiratory active genioglossus muscle (Smith et al., 1990; Ballanyi et al., 1999; Greer & Funk, 2005).

Work on the newborn rat *en bloc* model by the group of Onimaru and Homma starting in 1987, thus several years before preBötC identification, has established that a group of pre-inspiratory ('Pre-I') neurons mutually interacts with inspiratory networks **(Fig. 1-1)** (Onimaru et al., 1987; Ballanyi et al., 1999). Onimaru and colleagues used sectioning and focal cooling or lesioning to show that inspiratory rhythm is depressed in the absence of functional Pre-I neurons which are located (in newborn rats) several hundred micrometer rostral to the preBötC **(Figs. 1-2, 1-3)** (Onimaru et al., 1987). In 2003, Onimaru and Homma used voltage imaging to visualize the activity of Pre-I neurons and tagged them as the pFRG because they represent a rhythmogenic respiratory group that is located in the 'para-facial' region, i.e. around facial (VII) motor nucleus **(Figs. 1-1, 1-3)**. While their earlier work was somehow over-shadowed by the discovery of the preBötC, interest in the potential function of pFRG/Pre-I neurons was boosted by more recent studies, e.g. from the laboratories of Onimaru and Homma plus Feldman, with one seminal study done in collaboration between these groups (Janczewski et al., 2002). In their excellent review article, Feldman & Del Negro (2006) summarize the important role of opioids for identification of the dual respiratory center comprised of the inspiratory preBötC and the expiratory pFRG

(Fig. 1-1) as described in detail below (Chapter **1.5**). In brief, the pFRG seems pivotal for initiating fetal breathing movements and for breathing immediately after birth (Jaquin et al., 1996; Feldman & Del Negro, 2006). Later in life, it may at least partly transform into one class of central chemosensitive neurons that regulate breathing because of their ability to directly respond to a (metabolism-related) change in pH within lower brainstem tissues (Guyenet & Mulkey, 2010). However, there is recent evidence that pFRG neurons remain respiratory active and contribute to (active) expiration during the need for strong respiratory efforts, e.g. during severe hypoxia or hypercapnia (Guyenet & Mulkey, 2010; Abdala et al., 2009). For studying this expiratory oscillator without interference from rhythmogenic inspiratory networks, Onimaru's group has isolated the pFRG in a newborn rat brainstem 'slab' whose caudal margin is anterior to the preBötC (Onimaru et al., 2006).

During the past two decades, many important findings were derived from studies using both the *en bloc* and slice models. For example, video camera imaging in the rhythmic slices enabled optic monitoring of the activity of superficial preBötC neurons that were loaded with membrane-permeant fluorescent Ca^{2+} dye (Koshiya & Smith, 1999; Frermann et al. 1999). These cells flashed up when rhythmic bursting increased their free cytosolic Ca^{2+} concentration mainly due to depolarization-related Ca^{2+} influx through voltage-activated Ca^{2+} channels (Yuste et al., 2006, Ruangkittisakul et al., 2009). Such Ca^{2+} imaging also consolidated the above described finding that preBötC neurons are conditional bursters (also

tagged ‘pacemakers’) that remain active upon blockade of synaptic transmission **(Fig. 1-4)** (Koshiya & Smith, 1999). At about the same time, it was shown that (phasic) synaptic inhibition involving anion channel-coupled A-type □-aminobutyric acid ($GABA_A$) and glycine receptors is functional and hyperpolarizes VRC neurons already at birth, but is not essential for *(in vitro)* inspiratory rhythm (Shao & Feldman, 1997; Brockhaus & Ballanyi, 1998). This was not in line with previous *in vivo* findings (Pierrefieche et al., 1998), suggesting that rhythm is generated by a primary oscillator comprised of early-inspiratory and post-inspiratory neurons. These two antagonistically active neuron populations are thought to mutually inhibit each other via $GABA_A$ and glycine receptors and to innervate, also primarily via inhibitory synapses, other types of VRC neurons to generate the three phase respiratory pattern (Richter et al., 1992; Funk & Feldman, 1995; Smith et al., 2000).

Most review articles, including the latter ones, propose that rhythmogenic preBötC networks constitute a ‘hybrid network-pacemaker’ system. In fact, ‘classical’ conductances mediating intrinsic bursting, i.e. a persistent subtype of voltage-activated Na^+ channels and a non-selective cation channel, are functional in a notable number of preBötC neurons while their relevance for rhythm generation is yet not clear **(Fig. 1-4)** (Smith et al., 2000, 2009; Del Negro et al., 2002; Ramirez & Viemari, 2005; Feldman & Del Negro, 2006; Ramirez & Garcia, 2007). According to a recent ‘group pacemaker’ model, rhythm emerges from a network of glutamatergic preBötC neurons that produce an inspiratory

burst by recurrent excitatory ('feed forward') synaptic activity (Del Negro et al., 2002, 2010; Feldman & Del Negro, 2006; Gray et al., 2011) **(Fig. 1-4)**.

1.3 Calibrated preBötC Slices

The use of preBötC slices from perinatal rodents in a large number of studies has substantially improved the understanding of inspiratory network functions. However, until recently several issues were not solved that may potentially diminish the relevance of at least some of that work. Specifically, these issues were: (*i*) although the anatomical preBötC location has been determined in the original report on its discovery (Smith et al., 1991), the anterio-posterior ('rostrocaudal') thickness of preBötC slices used since then varies between 200 µm (e.g. Koshiya & Smith, 1999) and 1100 µm (e.g. Rekling et al., 1996), and no histological proof is typically given for their boundaries; (*ii*) preBötC slices are routinely studied in superfusate with a $[K^+]$ of 7-11 (mostly 8-9) mM **(Fig. 1-2)** and a $[Ca^{2+}]$ of 0.7-2.4 mM (for references see Ruangkittisakul et al., 2007; Ballanyi & Ruangkittisakul, 2009). This contrasts with physiological values for these cations in interstitial brain tissues, which are 3 mM for K^+ and 1-1.2 mM for Ca^{2+} (Somjen, 2002). Because of the utmost importance of both cations for neuronal excitability (Somjen, 2002; Hille, 2002), major differences in their superfusate levels may, at least partly, explain discrepant findings on preBötC slices between laboratories, e.g. regarding the incidence of occurrence or the relevance of intrinsic bursting, (*iii*) superfusate Ca^{2+} <1 mM and K^+ >4 mM are

established *in vitro* epilepsy models because they induce rhythmic seizure-like activity in cortical brain slices (Jefferys, 1999; Kilb et al., 2007) raising the question whether preBötC rhythm in such solutions is indeed inspiratory-related, (*iv*) studies on >500 µm thick newborn mouse slices demonstrated that preBötC neurons can reconfigure their activity patterns between 'eupnea-like' and 'sigh-like' bursting **(Fig. 1-2)** (Lieske et al., 2000; Ramirez & Viemari, 2005). Contrary, sigh-like bursting has not been reported for newborn rat preBötC slices and it was not clear whether preBötC networks in thinner rodent slices are capable of reconfiguring burst patterns, (*v*) in preBötC slices in high K^+, some neuromodulators need to be applied at concentrations that are sometimes several orders of magnitude higher than necessary for their specific effects in less reduced *in vitro* or *in vivo* models. For example, opioids need to be administered to 'respiratory networks in the dish' at doses close to 1 µM (Johnson et al., 1994; Takeda et al., 2001; Feldman & Del Negro, 2006; Montandon et al., 2011), whereas they inhibit respiratory rhythm in a perfused working-heart-brainstem model already in the low nanomolar range (Manzke et al., 2003).

All these issues were solved in studies published by our laboratory between 2006-2011, partly in collaboration with the groups of Funk and Schwarzacher. In a first report (Ruangkittisakul et al., 2006), anatomically 'calibrated' preBötC slices were generated based on the finding that the rostrocaudal extent of 'respiratory marker structures', particularly the inferior olive (IO) and VII nucleus, is constant in brainstems from postnatal day (P) 0-4 old Sprague-Dawley or Wistar rats,

which are mostly used for 'breathing' rat slices **(Fig. 1-3)**. By generating a reference newborn rat brainstem atlas and comparing it with anatomical landmarks given in the study on the preBötC discovery for its location (Smith et al., 1991), 500 or 600 μm thick calibrated slices were generated in which the preBötC was located approximately in the middle ('m-preBötC slices') of the slice. In the ventrolateral aspect corresponding to the VRC location **(Figs. 1-1, 1-2, 1-3)**, these slices generated inspiratory rhythm with intermingled eupnea-like and sigh-like bursts for several hours in solution with physiological K^+ (3 mM) and Ca^{2+} (1 mM). After several hours, rhythm in such '$3K^+/1Ca^{2+}$' solution was 'washed out', but was reactivated by various neuromodulators including low nanomolar doses of thyrotropin-releasing hormone and low millimolar doses of the methylxanthine theophylline (Chapter **1.7**) **(Fig. 1-3)**. Contrary, the μ-opioid receptor agonist [D-Ala^2,N-Me-Phe^4,Gly^5-ol]-Enkephalin (DAMGO) blocked preBötC rhythm in $3K^+/1Ca^{2+}$ at low nanomolar doses. In a recent review article, Ballanyi & Ruangkittisakul (2009) showed that this blockade is attenuated by raising K^+ to 9 mM in the presence of low nanomolar DAMGO **(Fig. 1-5)**.

As a further aspect of the first study on calibrated preBötC slices (Ruangkittisakul et al., 2006), multiphoton/confocal Ca^{2+} imaging was for the first time applied for monitoring the activity and the soma shape plus primary dendrites of preBötC neurons at greatly improved spatial resolution compared to earlier camera imaging (Chapter **1.2**) (Koshiya & Smith, 1999; Frermann et al., 1999). To exemplify recent Ca^{2+} imaging findings from our group (Bobocea et al., 2010;

Ruangkittisakul et al., 2012), **Fig. 1-6** indicates an asymmetric distribution and density of preBötC neurons and demonstrates that the same cells are active in 3 and 7 mM K^+. The latter finding argues against the above mentioned potential concern that high K^+ evokes seizure-like activity in (non-respiratory) preBötC neurons. Multiphoton Ca^{2+} imaging was also used in the first follow-up study from our group on calibrated newborn rat preBötC slices, again in collaboration with the groups of Drs. Funk and Schwarzacher (Ruangkittisakul et al., 2008). One aspect of that work showed that individual preBötC neurons are indeed capable of reconfiguring their activity between fictive eupnea and fictive sigh burst patterns. This was, e.g., achieved by applying, after the onset of '*in vitro* apnea' in $3K^+/1Ca^{2+}$, an agonist of the neurokinin-1 subtype of substance-P receptors to evoke a mixed eupnea-sigh burst pattern, whereas a solely eupnea-like burst pattern was induced by thyrotropin-releasing hormone. Also, raising K^+ from 3 to 7-9 mM transformed a mixed fictive eupnea-sigh pattern into regular eupnea-like bursting **(Fig. 1-6)**. Moreover, in this follow-up study 700 µm thick slices with the preBötC exposed to the rostral or caudal margin showed in $3K^+/1Ca^{2+}$ either exclusively eupnea-like bursts or a mixed eupnea-sigh burst pattern, respectively. The latter finding unraveled that structures rostral to the preBötC drive its rhythmogenic neurons to generate fictive sighs whereas structures caudal to the preBötC drive it toward more regular bursting. Therefore, brainstem structures included within respiratory active slices determine the modulatory drives to the preBötC and hence properties of its output. As a final result in that study, 175-250 µm thin m-preBötC slices were capable of rhythm in

$3K^+/1Ca^{2+}$, but *in vitro* apnea occurred typically within <2 h (Ruangkittisakul et al., 2008).

A steadily increasing number of reports use the preBötC slices from mice. This is because rhythmic slices can be obtained from up to two weeks-old animals and, importantly, 'knock-out' mice or otherwise genetically modified animals can be studied (Gray, 2008; Gaultier & Gallego, 2008; Ballanyi & Ruangkittisakul, 2009). For example, and as outlined in more detail below (Chapter **1.6**), mice can either lack a particular cellular feature, such as the 'NMDA' subtype of ionotropic glutamate receptors (Funk et al. 1997) or express fluorescent proteins in specific neurons (Winter et al., 2007; Gray, 2008; Gray et al., 2011) or astrocytes (Grass et al., 2004; Härtel et al., 2009). My training for this thesis involved participation in a recent study of our group that served to generate calibrated preBötC slices from C57/BL6 mice (that are often used for genetic engineering) and describe basic features of their rhythmic activity in $3K^+/1Ca^{2+}$ (Ruangkittisakul et al., 2011). Regarding the most important anatomical finding in that study, we showed that a slice of identical thickness in this newborn mouse species, compared to newborn Sprague-Dawley and Wistar rats, contains by a factor of ~1.5 more rostrocaudal extent of respiratory marker nuclei. Consequently, observations in e.g. 400 µm thick mouse slices would have to be compared with those in 600 µm thick rat slices if the extent of the preBötC and adjacent modulatory structures also corresponds to that scale. As a further result, we established that a 'Ca^{2+}/K^+ antagonism' determines the rate and 'longevity' (in $3K^+/1Ca^{2+}$) of preBötC slice

rhythm from C57/BL6 mice. This is in line with recent findings from Del Negro's group on this mouse strain (Del Negro et al., 2009) and from our group on newborn rat respiratory networks in the dish, as dealt with in the following.

1.4 Ca^{2+}/K^{+} Antagonism of Isolated preBötC Rhythm

The 'References and Notes' section in the study on the preBötC discovery (Smith et al., 1991) contains the statement that 'inspiratory XII nerve bursting occurs in 3 mM K^{+} in >500 to 600 µm thick slices while similar XII nerve bursting is revealed in 350-500 µm thick slices only in superfusate with 9-11 mM K^{+} (which accelerates rhythm in the thicker slices)'. Moreover, it was stated in follow-up studies that preBötC and XII rhythms are seen in 3 mM K^{+}, but are not stable (Funk et al., 1993; Tryba et al., 2003). Based on these notions, preBötC slices are routinely studied in high (mostly 8-9 mM) K^{+} (for references see Ruangkittisakul et al., 2007; Ballanyi & Ruangkittisakul, 2009) **(Fig. 1-2)**. However, our group showed that ≥500 µm thick calibrated newborn rat preBötC slices are rhythmic in 3 mM K^{+} for several hours **(Fig. 1-3)** (Ruangkittisakul et al., 2006, 2008). In these studies, the superfusate contained 1 mM Ca^{2+}, whereas most groups, including earlier work from us, use at least 1.5 mM, while various laboratories prefer 2.4 mM Ca^{2+} according to the recipe by Suzue (1984) in the first study on the *en bloc* model (for references see Ruangkittisakul et al., 2007; Ballanyi & Ruangkittisakul, 2009). A study on the newborn rat *en bloc* model showed that raised Ca^{2+} (or Mg^{2+}) depresses inspiratory rhythm (Kuwana et al., 1998) and they

cited *in vivo* work (Leusen, 1974) pointing out that Ca^{2+} injection into respiratory brainstem regions depresses breathing and that this is countered by K^+ injection. This was the starting point of a thorough study by our group (Ruangkittisakul et al., 2007) to quantify such an apparent Ca^{2+}/K^+ antagonism for calibrated preBötC slices **(Fig. 1-5)**. Moreover, calibrated *en bloc* preparations were developed in that study which had a specific amount of tissue rostral to the preBötC based on defined sectioning using ventral brainstem surface landmarks. The aim for establishing a calibrated *en bloc* model was to analyze whether the more or less exposed preBötC would show a different sensitivity to the proposed Ca^{2+}/K^+ antagonism. Indeed, even modest elevation of superfusate Ca^{2+}, specifically from 1 to 1.5 mM, greatly depressed preBötC rhythm if the inspiratory center was close to or exposed to the surface. This potent Ca^{2+} block of preBötC rhythm in both models was countered by raising K^+ to 7-9 mM **(Fig. 1-5)**.

As a further finding in that study (Ruangkittisakul et al., 2007) and a related report from our laboratory (Taccola et al., 2007), expiratory activity in lumbar nerve roots was abolished when the rostral section level was located 0.75 mm or caudal to the posterior end of VII nucleus (VII_c), which is the designated reference point for generating and tagging calibrated preBötC slices (Ruangkittisakul et al., 2006; Ballanyi & Ruangkittisakul, 2009). In the classical 'Suzue-type' brainstem-spinal cord preparation that is widely used (Onimaru et al., 1987; Smith et al., 1990; Ballanyi et al., 1999; Onimaru & Homma, 2003; Mellen et al., Ballanyi et al., 2009), the rostral brainstem transection level is just

anterior to the caudal cerebellar artery **(Figs. 1-2, 1-3)**. Such preparations contain a functional pFRG expiratory oscillator that mutually interacts with the preBötC **(Fig. 1-1)** as summarized in the following.

1.5 Opioids as Tool for Dual Respiratory Center Analysis

While overdoses of opioids can be fatal primarily by their depressing action on brainstem respiratory networks, they are at the same time of utmost importance for clinical treatment of pain, with frequent use in (preterm) infants (Durrmeyer et al., 2010; Walter-Nicolet et al., 2010). By definition, opioids act on opioid receptors and include natural plant-derived opiates plus synthetic agents. In addition to these exogenous agents, there are different classes of endogenous opioids that include endorphins, endomorphins, dynorphines and nociceptin-orphanin. These endogenous opioids are involved in (mostly inhibitory) modulation of central nervous signalling pathways, such as presynaptic inhibition of pain sensation, and can also induce euphoric feelings, e.g. during sustained physical exercise (Waldhoer et al., 2004). Opioids act on particular receptor subtypes in the mammalian brain (Pert & Snyder, 1973; Simon et al., 1973; Terenius, 1973). Specifically, these opioid receptors are either μ-type (μ for morphine), κ-type (κ for ketocyclazocine), δ-type (δ for *deferens*, being first identified in mouse *vas deferens*) and NOR-type (nociceptin/orphanin FQ receptor) (Waldhoer et al., 2004). Regarding the cellular mechanisms of opioid actions, the most established pathway is via inhibition of adenylyl cyclase induced

by receptor-coupled pertussis toxin-sensitive G_i/G_o proteins as the initial step. The subsequent fall of cellular cyclic-adenosine monophosphate (cAMP) and resulting blockade of the protein kinase-A signalling system modulates the activity of various cellular proteins including receptor-coupled and voltage-activated ion channels via phosporylation (Santiago & Edelman, 1985; Richter et al., 1997; Connor & Christie, 1999; Loh & Smith, 1990). As examples for effector targets, opioids can block presynaptic voltage-activated Ca^{2+} channels or activate postsynaptic G protein-coupled inward-rectifying K^+ (GIRK) channels. Importantly, whether such or other targets are indeed located pre- or post-synaptically depends on a given cell type in a particular nervous tissue (Loh & Smith, 1990; Christie, 1991; Nestler et al., 1999; Williams et al., 2001) **(Figs. 1-7, 1-8)**.

Use of opioids for pain treatment can be associated with side effects like nausea, vomiting, constipation, sedation, and, as already mentioned, respiratory depression. Systemic respiratory opioid effects are diverse, including slowing of breathing rate, reduction of upper airway patency, abdominal and chest wall rigidity and reduction of respiratory responses to hypoxia (Santiago & Edelman, 1985; Pattinson, 2008; Dahan et al., 2010). The incidence of respiratory depression evoked by clinical opioid administration during surgeries is ~17% and this depression can be fatal (Cashman & Dolin, 2004). Because respiratory depression is a major safety concern related to clinical (and recreational) use of opioids, there is a need for novel pharmacological strategies to rapidly and

selectively counter this depression. Naloxone and naltrexone are the two established clinical opioid antagonists for countering severe side effects of opioids, but their main drawback is that they also reverse their analgesic effects (Dahan et al., 2010). Therefore, the current focus is on developing drugs that stimulate breathing while retaining the analgesic effect of opioids such as agonists of 5-$HT_{4(a)}$ receptors (Richter et al., 1997; Manzke et al., 2003), ampakines which enhance endogenous activation of α-amino-3-hydroxy-5-methyl-4-isoxazole-proprionic acid (AMPA) receptors **(Fig. 1-7)** (Ren et al., 2006, 2009; Greer & Ren, 2009; Oertel et al., 2010) or agents that stimulate cAMP-PKA signalling pathways directly, such as rolipram (Chapter **1.7**) (Ballanyi et al., 1997; Ruangkittisakul & Ballanyi, 2006, 2010).

Experiments in adult cats established that both μ- and δ-opioid receptors are functional in brainstem respiratory neurons (Morin-Surun et al., 1984). More recently, it was shown in both *in vivo* and *in vitro* studies that these receptor subtypes are already active in newborn rodents, though with a dominance of μ-opioid receptors immediately after birth (Greer et al., 1995; Ballanyi et al., 1997; Gray et al., 1999; Dahan et al., 2001; Takeda et al., 2001; Manzke et al., 2003). Several of these, and also more recent studies, proposed that rhythmogenic preBötC neurons are directly inhibited via a μ-opioid receptor-mediated postsynaptic conductance increase and concomitant hyperpolarization due to activation of GIRK channels (Gray et al., 1999; Manzke et al., 2003; Lorier et al., 2008; Montadon et al., 2011). Also others, including our group (Ballanyi et al.,

1997; Takeda et al., 2001) have revealed a (mostly modest) hyperpolarization and conductance increase in some unidentified inspiratory VRC neurons in newborn rat *en bloc* medullas. However, in these studies seemingly similarly active cells did not show a postsynaptic response during opioid-evoked depression of inspiratory nerve bursting. Related research using opioids as tools has established that breathing is initiated by a dual respiratory oscillator, at least in newborns **(Fig. 1-1)** (Chapter **1.2**). Firstly, Feldman's group reported that opioids depress inspiratory rhythm in quantal fashion **(Fig. 1-9)** (Mellen et al., 2003). This is evident from the fact that during μ-opioid receptor activation in that report and follow-up studies (Janczewski et al. 2002; Janczewski & Feldman, 2006; Onimaru et al., 2006; Ballanyi et al., 2009) various inspiratory activities, both *in vitro* or *in vivo*, are skipped to cause slowing of rhythm, whereas rates of Pre-I neuron bursting *in vitro* or expiratory lumbar nerve and abdominal muscle activities are not changed (or even accelerated). A recent collaborative study of our group with Onimaru's laboratory has, on the one hand, substantiated the idea that presynaptic inhibition is pivotal for inspiratory depression by opioids (Ballanyi et al., 2009). Specifically, DAMGO did not hyperpolarize histologically identified 'Onimaru type-I' inspiratory preBötC neurons that are the only target of excitatory synaptic input from pFRG neurons (Ballanyi et al., 1999). On the other hand, DAMGO prolonged pre-inspiratory Pre-I neuron bursting as indication of presynaptic inhibition. Regardless of whether opioids depress the preBötC primarily via pre- or postsynaptic mechanisms, this inhibitory action would cause a problem during the process of birth that is presumably associated with a stress-induced surge of

endogenous opioids (Jansen & Chernick, 1983; Ballanyi, 2004; Feldman & Del Negro, 2006). In this situation, the opioid-insensitive (or rather opioid-stimulated) pFRG (Tanabe et al., 2005; Onimaru et al., 2006) presumably boosts preBötC activity to counter inspiratory inhibition (Jaquin et al., 1996; Feldman & Del Negro, 2006).

1.6 Identification of Cell Types in Isolated preBötC

Inspiratory active preBötC neurons and pFRG/Pre-I neurons that are active during both the pre-inspiratory and expiratory phases **(Fig. 1-9)** constitute functionally different oscillators. However, inspiratory neurons are also found in the newborn rat *en bloc* model in regions rostral to the preBötC, which overlap with the pFRG, while numerous Pre-I neurons (also tagged as 'biphasic-expiratory' neurons) are located within the preBötC **(Fig. 1-2)** (Smith et al., 1990; Ballanyi et al., 1999, 2009). The latter finding is in line with the observation in adult cats *in vivo* that various respiratory neuron types are active within the preBötC (Schwarzacher et al., 1995). This overlap of respiratory neuron classes in the preBötC does not necessarily mean that the rhythmogenic aspect of the yet anatomically undefined rhythmogenic portion of the pFRG overlaps with the anatomically defined preBötC. It is more likely that these areas are separated for both oscillators and that cells in these rhythmogenic spots activate 'follower neurons' that are more widely distributed (Ballanyi & Ruangkittisakul, 2009). It appears though that these other respiratory neuron types are becoming increasingly inactive (or

transform their activities into inspiratory bursting or tonic discharge) when the preBötC is isolated in a transversal slice of a thickness less than ~500 μm for newborn rats (Ballanyi & Ruangkittisakul, 2009). This may be related to a decreased functional expression of (recurrent) phasic synaptic inhibition via $GABA_A$ and glycine receptors in thin preBötC slices because combined pharmacological blockade of these receptors in the newborn rat *en bloc* model transforms pre/post-inspiratory Pre-I neuron bursting into inspiratory bursting that is often indiscernible from that of 'normal' inspiratory neurons in that model (Brockhaus & Ballanyi, 1998, 2000). Moreover, some of the densely distributed tonically active neurons within the isolated newborn rat preBötC may also represent intrinsically chemosensitive cells that provide on-going excitatory drive to rhythmogenic inspiratory neurons (Kawai et al., 1996; Ballanyi & Ruangkittisakul, 2009). Based on these considerations, the 'real' inspiratory neurons would optimally have to be identified in (thin) slices to discriminate them from other types of respiratory neurons that are not, or less specifically, active in more reduced preparations. One possibility in that regard is to exclude Pre-I/pFRG neurons by an immunohistochemical approach, i.e. labeling for the transcription factor Phox2b that is presumably characteristic for these cells (Onimaru et al., 2009; Guyenet & Mulkey, 2010). Moreover, inspiratory neurons that are glycinergic or GABAergic, and thus do not contribute to the recurrent excitatory processes that is proposed to be involved in rhythm generation (Feldman & Del Negro, 2006; Del Negro et al., 2010) **(Fig. 1-4)**, can be fluorescence-labeled in genetically engineered mouse models for exclusion from

study (Kuwana et al., 2006; Winter et al., 2009). Rather, inspiratory active mouse cells that express fluorescent-labeled transcription factor Dbx1 as marker for glutamatergic inspiratory preBötC neurons should be studied (Gray et al., 2011). Optimally, recording from such neurons should be combined with other markers for their potential rhythmogenic role. One possibility for additional marking in that regard is to apply to the acute slice fluorescence-tagged substance-P that is presumably taken up via neurokinin-1 receptors (Pagliardini et al., 2005). The importance of these receptors **(Fig. 1-7)** is indicated by findings from an *in vivo* lesioning study in which selective poisoning of NK1 receptor-expressing preBötC cells severely impedes normal breathing (Gray et al., 2001). However, it has to be considered that preBötC Pre-I neurons and astrocytes also express NK1 receptors (Härtel et al., 2008; Onimaru et al., 2009). The latter considerations already indicate that it is not trivial to distinguish rhythmogenic inspiratory neurons from other classes of respiratory neurons within the preBötC and there is yet a very limited number of studies that have combined two (or more) methods for marking such candidate rhythmogenic inspiratory neurons (Hayes & Del Negro, 2007; Lorier et al., 2008; Gray et al., 2011).

This scenario is even more complex because of the likely role of astrocytes in modulation of preBötC neuronal activities. Particularly the group of Hülsmann (initially in collaboration with Richter's group), has pioneered the identification and functional characterization of preBötC astrocytes (Grass et al., 2004; Härtel et al., 2009). Also our group has started several years ago to identify astrocytes

versus neurons in the preBötC area of newborn rat brainstem slices using multiphoton/confocal Ca^{2+} imaging. This revealed, for example, that presumptive preBötC astrocytes do not show inspiratory cytosolic Ca^{2+} rises, but respond with a major (oscillatory) Ca^{2+} rise to phenylephrine, adenosine triphosphate or anoxia, whereas neurons respond with rather modest Ca^{2+} increases to these neuromodulators **(Fig. 1-7)** (Ruangkittisakul et al., 2009). Contrary, neurons show in our hands a robust Ca^{2+} rise in response to thyrotropin-releasing hormone and neurokinin-1 receptor agonists, whereas astrocytes respond rather modestly, if at all (Ruangkittisakul et al., 2009). Moreover, our group contributed with Ca^{2+} imaging in acute preBötC slices to a study on a role of astrocytic P2Y receptors in modulation of inspiratory rhythm-generating networks by adenosine triphosphate **(Fig. 1-7)** (Huxtable et al., 2011). In our recent 'perspective' article (Ballanyi et al., 2010), we provide an overview on neuronal and glial receptors that are likely active in the preBötC **(Fig. 1-7)**. We also note in that article that, in other neural circuits, mutual interactions of neurons with astrocytes are influenced by microglial mediators such as brain-derived neurotrophic factor or interleukin-1□ that are released into the spinal cord to initiate hypersensitivity related to neuropathic pain (Gustafson-Vickers et al., 2008; Hutchinson et al., 2008; Lu et al., 2009). With respect to opioids as a tool for studying the dual respiratory oscillator, it needs to be considered that these drugs also affect both astrocytes and microglia in addition to neurons (Ballanyi et al., 2010; Hutchinson et al., 2008). In that regard, also adenosine affects various processes in all three cell types to eventually contribute to neurological diseases such as Alzheimer's or Parkinson's

(Matute & Cavaliere, 2011; Daré et al., 2007). This raises the possibility that respiratory stimulating effects of methylxanthines may, at least partly, also arise from their blocking action on adenosine receptors on (micro)glia.

1.7 Pharmacology of Methylxanthines

Methylxanthines, which are contained, e.g., in beans, coffee, tea or cocoa, are the most commonly used psychoactive substances. They are methylated derivatives of xanthine (which is derived from guanine) and include caffeine, theophylline, aminophylline, paraxanthine, theobromine, pentoxifylline and others. Caffeine, theophylline and theobromine are ingredients of many commercial products, such as coffee, soda and energy drinks and particularly caffeine is also used in combination with non-prescription medications like painkillers and cold remedies. Caffeine, consumed from dietary sources, is rapidly absorbed from the gastrointestinal tract and reaches a peak plasma concentration within 15-120 min to 8-10 mg/l for doses of 5-8 mg/kg (Arnaud, 2011). It is metabolized by the liver through demethylation to three active metabolites, paraxanthine, theobromine, and theophylline (Kennedy et al., 1987; Berthou et al., 1992), but there are differences between humans and animal species regarding both their fractioning percentages and pharmacokinetics (Arnaud, 2011). Methylxanthines cross the blood-brain barrier easily and, after long-term caffeine ingestion, theophylline levels in the brain tend to be higher than those for caffeine implying that caffeine is metabolized through some local brain pathways (Johansson et al., 1996).

Though, studies in humans showed that the main metabolite of caffeine is paraxanthine, a less studied central nervous stimulant (Arnaud, 2011) and it has been suggested that some *in vivo* effects of caffeine are in fact mediated by paraxanthine (Hetzler et al., 1990). Methylxanthines have multiple desired actions like bronchodilation and positive inotropic and chronotropic cardiac plus anti-inflammatory effects. As examples for stimulatory central nervous effects, caffeine increases arousal (Barry et al., 2005) and locomotor activity (Nehlig et al., 1992), improves performance on learning and memory tasks (Angelucci et al., 1999) and enhances feelings of well-being (Garrett & Griffiths, 1997), cognitive performance (Smit & Rogers, 2000), auditory vigilance and reaction time (Lieberman et al., 1987). At the same time, caffeine has a minimal addictive potential (Fredholm et al., 1999).

Due to their similar structure, the different (metabolites of) methylxanthines display common mechanisms of brain actions, although with different potency and in dose-dependent manner (Fredholm et al., 1999) **(Fig. 1-10)**. The most established mechanism of methylxanthine actions is antagonism of adenosine receptors (Fredholm et al., 1999). Four types of adenosine receptors have been identified, namely A_1, A_{2A}, A_{2B}, and A_3 receptors, with the latter being insensitive to methylxanthines. The IC_{50} values for inhibition of adenosine receptors by caffeine are about 40-50 μM while values for theophylline are around 10 μM (Ukena et al., 1993; Fredholm et al., 1999). A_1 receptor activation can block adenylyl cyclase and the resulting decrease of cAMP might decrease

phospholipase C and D activities and thus, e.g., inhibit voltage-activated Ca^{2+} channels or activate K^+ channels, similar to the main mechanism of opioid actions (Chapter **1.5**) (Fredholm et al., 1999). In contrast, A_{2A} receptors typically stimulate adenylyl cyclase and also some types of voltage-activated Ca^{2+} channels. Consequently, A_1 and A_2 receptors have usually opposing effects and the antagonizing mechanism of methylxanthines will have different neuron type- and brain tissue-specific outcomes (Fredholm et al., 1999). A_1 receptor signaling is implicated in the inhibitory actions of adenosine on respiratory frequency in different animal species (Funk et al., 2008; Herlenius et al., 2002; Wilson et al., 2004; Koos et al., 2005). In vitro studies revealed conflicting results, some groups showing that adenosine has inhibitory effects on respiratory frequency (Mironov et al., 1999; Wang et al., 2005; Lorier et al., 2007) while others did not see an inhibitory effect (Ballanyi et al., 1999; Ruangkittisakul & Ballanyi, 2010). Huxtable et al. (2009) demonstrated that adenosine through A_1 receptors depresses inspiratory rhythm in fetal, but not postnatal rats. Another study revealed that adenosine has an inhibitory effect on newborn mice, but no effect on newborn rats (Zwicker et al., 2011). In humans, adenosine stimulates breathing, although it appears that this action is dominated by excitation of peripheral chemoreceptors (Fuller et al., 1987; Reid et al., 1991). More studies are needed to characterize the relationship between adenosine and respiratory system further.

As another mechanism of methylxanthine actions, caffeine and theophylline were the first identified inhibitors of cyclic nucleotide-dependent phosphodiesterases

(PDEs) which serve to break down cAMP or other cyclic nucleotides **(Fig. 1-10)** (Francis et al., 2011). The PDE family is composed of eleven isoenzymes with a specific tissue, cellular, and subcellular localization pattern (Soderling & Beavo, 2000). Because modulation of cellular nucleotide levels has potentially substantial effects on various organs and inflammatory processes, there is a long-standing search for specific antagonists of PDE subtypes to improve therapeutic use and reduce side effects associated with nonspecific inhibitor drugs, particularly methylxanthines (Daly, 2000). Because cAMP seems to be a major stimulus to rhythmogenic preBötC networks (Ballanyi et al., 1997, 1999; Richter et al., 1997; Manzke et al., 2003; Ballanyi, 2004), our group explored the respiratory stimulating effect of the blocker of cAMP-dependent PDE4, rolipram. This research on the newborn rat *in vitro* respiratory model revealed that rolipram accelerates slow fetal preBötC rhythm and counters spontaneous *in vitro* apnea in $3K^+/1Ca^{2+}$, as well as opioid-evoked blockade of inspiratory rhythm (Ballanyi et al., 1999; Ballanyi, 2004; Ruangkittisakul & Ballanyi, 2006, 2010; Ruangkittisakul et al., 2006, 2007, 2008). However, rolipram is not suitable for clinical use because of various adverse effects including nausea and vomiting (Ruangkittisakul & Ballanyi, 2010). The fact that low millimolar methylxanthine doses were necessary to mimic the stimulatory rolipram effects in the latter studies indicates that they might act primarily via blocking PDE4.

A third action of low millimolar methylxanthine doses is induction of Ca^{2+} release from cellular stores **(Fig. 1-10)**. Through this mechanism, caffeine stimulates

contraction of skeletal, cardiac and smooth muscles by increasing the Ca^{2+} sensitivity of ryanodine-sensitive Ca^{2+} release channels (Magkos & Kavouras, 2005; McPherson et al., 1991). This mechanism seems also to be functional in nervous structures as evidenced by effect on neurons, e.g. in hippocampus, midbrain or cerebellum (Berridge, 1998; Rizzuto, 2001; Guerreiro et al., 2011).

Methylxanthines are extensively used in neonatal intensive care units. The main indication is for treatment of apnea of prematurity. Each episode of such apneas can last for >15 s, thus leading to oxygen desaturation and bradycardia, and they are presumably caused by immaturity of 'medullary respiratory rhythm generators' (Miller & Martin, 1992; Martin & Abu-Shaweesh, 2005; Bancalari, 2006; Zhao et al., 2011). Early studies demonstrated that methylxanthines are counteracting these apneas by decreasing the incidence of occurrence to ultimately increase minute ventilation and diaphragmatic activity, thus decreasing hypoxic depression of breathing (Kuzemko & Paala, 1973; Bancalari, 2006). Initially, aminophylline was used in a form of suppositories as an 'off-label' drug to treat apnea of prematurity (aminophylline is metabolized to theophylline), but it turned out that it was not always effective (Bhatt-Mehta & Schumacher, 2003). An *in vitro* study showed that aminophylline accelerates inspiratory rhythm in preBötC slices from early neonatal mice with no effect on burst amplitude, but augments burst amplitude in slices from mice older than P7 with no effect on burst rate (Wilken et al., 2000). Despite principally similar clinical effects of caffeine and theophylline, caffeine has a wider therapeutic range, thus being the

current drug of choice in treatment of apnea of prematurity (Henderson-Smart & De Paoli, 2010; Henderson-Smart & Steer, 2010; Johnson, 2011). Long-term studies showed that caffeine given to premature infants improved the rate of survival and decreased both the incidence of cerebral palsy and cognitive delay and bronchopulmonary dysplasia at 18 months of age (Schmidt et al., 2007). Moreover, in neonatal rats methylxanthines might be neuroprotective in postnatal hypoxia (Bona et al., 1997; Kumral et al., 2010). Contrary to this, other studies suggested that caffeine alters adenosine receptor expression and distribution (Montandon et al., 2008a), induces long-term changes in sleep and hypoxic response in adult rats (Montandon et al 2008b, 2009), causes neuronal apoptosis (Kang et al., 2002) and transiently inhibits astrocytogenesis (Desfrere et al., 2007). Clinical studies suggested that methylxanthines can reduce blood flow in the cerebral and intestinal arteries (Hoecker et al., 2002), disrupt sleep (Hayes et al., 2007), increase the oxygen consumption and reduce weight gain (Bauer et al., 2001), increase blood glucose levels (Srinivasan et al., 1983), and correlate with a proinflammatory cytokine profile (Chavez-Valdez et al., 2011). Premature infants are given oral caffeine in combination with intubation and ventilation; the latter procedures also require morphine administration for analgesia. An animal study showed that caffeine has a neurotoxic effect which increases when morphine is administered concomitantly while morphine alone does not appear to be neurotoxic (Black et al., 2008). Based on all this, there is an on-going debate whether methylxanthine are safe or not in preterm infants (Millar & Schmidt, 2004).

As one major adverse effect on central nervous actions, methylxanthine effects, e.g. upon consumption of high caffeine containing energy drinks, decrease the threshold for the occurrence of seizures (Fredholm et al., 1999; Kaufman & Sachdeo, 2003; Iyadurai & Chung, 2007; Tchekalarova et al., 2007; Boison, 2011). Similarly, for theophylline (which has been widely used for bronchial asthma, chronic obstructive pulmonary disease or apnea of prematurity), it was recognized that the clinical entity called 'theophylline-induced seizures' is a neurological emergency (Dunn & Parekh, 1991; Korematsu et al., 2008; El-Bitar & Boustany, 2009). Compared to caffeine, theophylline has a narrower therapeutic window regarding seizures (Aitken & Martin, 1987; Bonfiglio & Dasta, 1991; Delanty et al., 1998; Sugimoto et al., 2001; El-Bitar & Boustany, 2009), but theophylline-evoked seizures can not be categorized as simple intoxication because serum concentrations for the agent do not correlate with seizures (Aitken & Martin, 1987). Conventional anticonvulsant therapy is ineffective in controlling these seizures because the gold standard in that regard, diazepam, fails to show beneficial response, suggesting that theophylline might interact with benzodiazepines (Nakada et al., 1983; Yoshikawa, 2007). The proconvulsive role of theophylline is presumably due to the following mechanisms (Boison, 2011) (*i*) decrease of seizure threshold through inhibition of adenosine receptors, (*ii*) inhibition of blood flow through adenosine antagonism, (*iii*) inhibition of pyridoxal 5'-phosphate, which may decrease GABA synthesis or (*iv*) direct inhibition of $GABA_A$ receptors. Finally, findings on newborn rat

hippocampal slices indicate that caffeine is proconvulsive via A_1 receptor blockade at least during anoxia, i.e. tissue oxygen depletion (Dzhala et al., 1999). Periods of anoxia are associated with increased adenosine levels in extracellular brain tissue, which depresses neuronal activity and hence prevents seizures in the neonatal hippocampus. Through antagonism of A_1 adenosine receptors, caffeine evokes seizures which might disturb development of neonatal networks thus resulting in neurological sequelae in adults (Holmes & Ben-Ari, 1998).

1.8 Hyperpolarization of LC Neurons by Opioids

The LC represents a cluster of noradrenergic neurons that are located in the dorsal pons adjacent to the fourth ventricle. It was first described by Reil in 1809, but the name *locus coeruleus* was coined in 1812 by the Wenzels (Maeda, 2000). The LC is associated with arousal and sleep-wake cycle and is the major noradrenergic nucleus in the brain providing noradrenergic projections to various nervous structures, including cortex, hippocampus, cerebellum, brainstem and spinal cord (Mason & Fibiger, 1979; Foote et al., 1983; Berridge & Waterhouse, 2003; Samuels & Szabadi, 2008). LC neurons synthesize norepinephrine starting from the amino-acid L-tyrosine, having dopamine β-hydroxylase as the rate-limiting enzyme (Smythies, 2005). Norepinephrine stimulates different signalling pathways in the effector cells through activation of α_1, α_2, and β adrenergic receptors (Hein, 2006). α_1 and α_2 receptors are coupled to the $G_{q/11}$ and G_i/cAMP second messenger systems, respectively, while β adrenergic receptors are coupled

to the G_s/cAMP system. Although the LC is considered as a rather homogenic noradrenergic nucleus, there is evidence suggesting that norepinephrine is co-released with other neuromodulators such as BDNF, enkephalin, neuropeptide-Y or somatostatin (Olpe & Steinmann, 1991; Sutin & Jacobowitz, 1991), which likely serve to fine tune norepinephrine action (Berridge & Waterhouse, 2003). Axons from LC neurons are characterized by profuse branching to innervate wide areas, mainly ipsilaterally (Mason & Fibiger, 1979). LC neuronal axon terminals have a classical structure, but they also possess varicosities that promote norepinephrine release at various spots of their passage through different brain areas. This 'volume transmission release' affects not only neurons, but also glia and blood vessels (Paspalas & Papadopoulos, 1996; Porter & McCarthy, 1997; Fuxe et al., 2010).

Previous studies showed that the noradrenergic LC system is already present at birth, but continues to develop postnatally (Dreyfus et al., 1983; Nakamura et al., 1987; Marshall et al., 1991; Maubecin & Williams, 1999; Murrin et al., 2007). In rats, LC neurons differentiate at embryonic day 12 (E12) while norepinephrine can be determined at E14 (Lauder & Bloom, 1974). Norepinephrine is important in brain maturation by regulating the development of Cajal-Retzius cells, the first type of cortical neurons (Naqui et al., 1999). In the neonatal period, norepinephrine is also implicated in olfactory learning, maternal recognition and hence infant survival (Moriceau et al., 2010). The LC in neonatal rats has unique

characteristics and presumably at ~P10 it appears to have matured to an almost adult-like neural circuit (Moriceau et al., 2010).

LC neurons in the adult brain fire in both tonic and phasic modes (Hobson et al., 1975; Aston-Jones & Cohen, 2005). The tonic mode is characterized by a low-frequency regular pattern with a higher discharge during wakefulness, lower discharge during non-REM sleep and no activity during REM sleep. LC neuronal discharge rates are modified by a change in behavioural states. Specifically, in wakefulness, tonic discharge is maintained by environmental stimuli and correlated with arousal. Contrary, the phasic mode of LC discharge is characterized by a burst pattern associated with error-free responses in signal-detection tasks (Aston-Jones & Cohen, 2005). Additionally, the phasic LC response exhibits accommodation after a repeated stimulus. LC neurons display spontaneous electrical activities that are synchronized during development. Nakamura and colleagues (1987) showed that LC neurons in anesthetized rats *in vivo* display a spontaneous firing rate which is significantly greater in P7-18 rats compared to P1-6. Specifically, LC neurons fire tonically at 0.2-3 Hz according to the latter *in vivo* study, and also discharge at comparable frequencies in brain slices. Early studies on rats revealed that LC neuronal excitability depends on various conductances, including a persistent Ca^{2+} current, a tetrodotoxin (TTX)-sensitive persistent Na^{+} current and Ca^{2+} activated K^{+} currents (Williams et al., 1984). More recent studies indicated the additional involvement of an inward-directed non-specific cation current carried primarily by Na^{+} (Nestler et al., 1999;

Murai & Akaike, 2005). In contrast, Ca^{2+} currents are seemingly not involved in pacemaker activity of mouse LC neurons and the strengths of Na^{+} and K^{+} currents are increasing during development (De Oliveira et al., 2010 2011). As further example for interspecies differences regarding their excitability, the incidence of spontaneous firing in mouse LC neurons is decreasing during development. *In vitro* studies showed that early postnatal LC neurons display Ca^{2+} dependent subthreshold membrane potential oscillations which become less pronounced during maturation, contrary to the increasing (tonic) discharge rate (Williams et al., 1984; Williams & Marshall, 1987; Christie et al., 1989). Synchronous activity of the LC neurons is apparently mediated by electrotonic coupling through gap junctions (Maubecin & Williams, 1999; Alvarez et al., 2002; Bennett & Zukin, 2004), which was demonstrated by electrical and dye-coupling experiments between pairs of neurons (Christie et al., 1989; Christie & Jelinek, 1993; Oyamada et al., 1999; Ballantyne et al., 2004). Based on a reduced synchrony of discharge between LC neurons in adult rats, it was suggested that electrotonic coupling is decreasing with age similar to neurons in other brain regions (Bennett & Zukin, 2004). In adult rat LC slices, spontaneous membrane potential oscillations are rarely seen, but can be induced by bath-application of barium or tetraethylamonium (Ishimatsu & Williams, 1996).

Opioid effects on LC neurons are extensively studied, both *in vivo* and *in vitro* (Aghajanian, 1978; Williams et al., 1982; Aghajanian & Wang, 1987). For example, the LC and endogenous opioids are implicated in a hypotensive stress

response (Van Bockstaele et al., 2010). Corticotropin-releasing factor activates LC neurons during the hypotensive stress, and in turn, the LC activates the cortex through norepinephrine release. After stress termination, basal neuronal activity in the LC is restored by endogenous opioids through an inhibition, protecting the system from over-activation (Curtis et al., 2001; Van Bockstaele et al., 2010). In LC neurons, all three classes of opioid receptors (Chapter **1.5**) are functional, specifically μ-receptors on postsynaptic neuronal processes, contrary to δ- and κ-receptors on axon terminals (Christie, 1991). Neuronal LC μ-opioid receptors are co-localized with α_2-adrenoceptors and they share similar intracellular second messenger pathways. Specifically, opioids suppress LC neuronal activity through activation of μ-receptors and exert their actions through stimulation of pertussis toxin-sensitive $G_{i/o}$-proteins for inhibition of adenylyl cyclase and GIRK channel activation (Williams et al., 1982, 1984; Christie, 1991; Law et al., 2000). GIRK channel activation leads to membrane hyperpolarization and depression of neuronal activity, thus preventing cells from firing action potentials. Inhibition of adenylyl cyclase is usually followed by a decrease of cellular cAMP and consequent reduction of phosphorylation of the nonspecific cation current implicated in LC neuron bursting (Wang & Aghajanian, 1990; Alreja & Aghajanian, 1991, 1993; Nestler et al., 1999). In summary, LC studies contributed significantly to our understanding of cellular opioid responses and provided a classical pharmacological example for a postsynaptic action of opioids via μ-receptors.

Besides its role in arousal and control of performance, the LC is implicated in homeostatic functions, including cardiovascular regulation (Guyenet, 1991) and breathing (Oyamada et al., 1998, 1999; Hakuno et al., 2004; Hilaire et al., 2004; Viemari et al., 2004; Hilaire, 2006; Gargaglioni et al., 2010). The LC is not considered as a part of respiratory rhythm-generating networks, but norepinephrine secreted by pontine structures is involved in their modulation. Norepinephrine exerts a combination of α_1 facilitatory and α_2 inhibitory effects on medullary inspiratory networks with apparent species differences between rats and mice (Errchidi et al., 1991; Funk et al., 1994; Hilaire et al., 2004; Adachi et al., 2005). LC neurons send information and receive feedback from medullary respiratory networks, which allows them to exhibit central respiratory-modulated firing (Guyenet et al., 1993; Oyamada et al., 1998, 1999). Oyamada and colleagues (1998) showed that spontaneous activity of LC neurons in the newborn rat *en bloc* model is related to inspiratory rhythm. Moreover, transneuronal tracing studies demonstrated an anatomical pathway between LC and medullary respiratory networks. Specifically, neurotropic viruses applied to phrenic motoneurons were found to be localized in some LC neurons in adult rats and mice (Dobbins & Feldman, 1994; Burnet et al., 2001) and also in neonatal mice (Hilaire et al., 2004).

1.9 Objectives and Hypotheses

In synopsis of the information in the previous sections, the main aim of this thesis was to test the hypothesis that one major aspect of respiratory stimulating actions of methylxanthine is direct stimulation of preBötC networks. I will use newborn rats for this work because previous findings from our group on central respiratory methylxanthine effects were obtained in the *en bloc* and slice models from that species. One option to study methylxanthine actions on the isolated inspiratory center is to use calibrated slices with the preBötC exposed to one surface. I chose this approach for multiphoton/confocal Ca^{2+} imaging combined with suction electrode recording of contralateral preBötC population activity (Ruangkittisakul et al., 2007, 2008, 2009). However, for whole-cell recording combined with suction electrode recording from the contralateral preBötC, I decided to develop novel 400 μm thick 'm-preBötC[400]' slices that contain the inspiratory *noeud vital* approximately in their center. The major rationale for this was to make sure that the dendritic tree, which spans <400 μm in rostrocaudal direction in most of preBötC neurons (Ballanyi & Ruangkittisakul, 2009) remains mostly intact. This would increase the probability that contribution to the likely antagonistic effects of opioids and methylxanthines on conductances, such as μ-opioid receptor-coupled GIRK channels or channels coupled to dendritic metabotropic glutamate receptors (Del Negro et al., 2010) that are possibly located on distal dendrites, is preserved for detection via blind whole-cell recording (Smith et al., 1991, 1992). Recordings were planned primarily from inspiratory preBötC neurons located close to the center of these slices, but effects on neighboring tonic neurons that

may represent chemosensitive cells or other types of neurons that transformed their activities in the thin slices may also be of interest (Ballanyi & Ruangkittisakul, 2009) (Chapter **1.6**).

Using this two-pronged approach of blind patch recording from non-superficial neurons plus Ca^{2+} imaging, four major projects were conducted according to four chapters of this thesis. Importantly, in one chapter, findings on m-preBötC slices were complemented by observations based on suction electrode recordings of nerve bursts in the newborn rat *en bloc* model.

Project-1: Ca^{2+}/K^{+} Antagonism of Isolated preBötC Bursting

The isolated preBötC should be studied (*i*) in slices that are thin enough to minimize the influence from adjacent respiratory brainstem structures and (*ii*) in superfusate with close-to-physiological Ca^{2+} and K^{+} levels (Chapter **1.4**). The first aim of this study was to generate and study basic properties of novel newborn rat 400 μm thick 'm-preBötC[400]' brainstem slices. In these calibrated preBötC slices, population activity in the preBötC and the preBötC-driven XII motor nucleus or nerve was going to be recorded in combination with blind whole-cell recording of membrane potential or from identified inspiratory and tonic preBötC neurons in the center of these slices. While membrane potential recording served to provide information on the pre-synaptic *versus* postsynaptic nature of the blocking action of Ca^{2+} on preBötC rhythm, combined suction electrode recording

from the preBötC and XII aimed at determining for m-preBötC[400] slices the optimum Ca^{2+}/K^{+} ratio for long-term stability of inspiratory rhythm.

I hypothesize for *Project-1*:

I) Rhythm in m-preBötC[400] slices in 3 mM, or modestly elevated (5-6 mM) K^{+} persists at physiological (1-1.2 mM) Ca^{2+} at reasonable rates (>5 bursts/min) for time periods >2 h, thus long enough for pharmacological and intracellular analyses.

II) Block of rhythm by high Ca^{2+} does not hyperpolarize inspiratory or tonically active preBötC neurons.

Project-2: Methylxanthine Reversal of Opioid Depression of preBötC Neurons

As outlined above, the main hypothesis for this thesis is that methylxanthine-evoked stimulation of inspiratory rhythm is due to effects on the preBötC. For this approach, I used the novel m-preBötC[400] newborn rat slices developed for *Project 1* for inducing a sustained depression of inspiratory rhythm via on-going bath-application of the μ-opioid receptor agonist DAMGO. Our laboratory has recently shown that such depression of preBötC rhythm is effectively antagonized by low millimolar caffeine and theophylline (Ruangkittisakul & Ballanyi, 2010). While these findings already indicate a direct methylxanthine action, the evidence would be stronger if supported by revealing a direct postsynaptic response on identified preBötC neurons. In that regard, it was also relevant to find out if

opioid-evoked postsynaptic hyperpolarizations are possibly more pronounced in neurons of slices (Gray et al., 1999; Montandon et al., 2011) *versus* the *en bloc* model (Takeda et al., 2001; Ballanyi et al., 2009) (Chapter **1.5**). In a parallel approach, multiphoton/confocal Ca^{2+} imaging was done using 400 μm thick slices with the preBötC exposed to the caudal surface ('r+preBötC[400] slices') (Ruangkittisakul et al., 2008; Ballanyi & Ruangkittisakul, 2009). The major rationales for such imaging were to reveal, on the one hand, whether arrest of inspiratory rhythm evoked by DAMGO leads to a major decrease of cytosolic Ca^{2+} based on blockade of Ca^{2+} channels in association with a presumptive direct hyperpolarization of preBötC neurons. Such a mechanism has been demonstrated by our group for dorsal vagal neurons in juvenile rat brainstem slices which have a similar resting potential as neonatal preBötC neurons (Ballanyi & Kulik, 1998). Specifically, it was shown in these studies that block of tonic action potential discharge during the initial phase of an anoxia-evoked hyperpolarization is accompanied by a notable fall of cytosolic Ca^{2+} in these neurons. On the other hand, I wished to analyze whether reactivation of slice rhythm by low millimolar methylxanthine is associated with a major Ca^{2+} rise that is eventually caused by Ca^{2+} release from cellular stores as outlined above (Chapter **1.7**). However, because the countering effect of methylxanthines on opioid depression of slice rhythm occurs already at <10 mM, it is possible that Ca^{2+} stores are not much affected and that blockade of PDE4 plays a bigger role in mediating this effect. This is indicated by the fact that the PDE4 blocker rolipram countered opioid

depression of slice rhythm in a fashion similar to methylxanthines (Ruangkittisakul & Ballanyi, 2010).

I hypothesize for *Project-2*:

I) Opioids block inspiratory rhythm in preBötC[400] slices without hyperpolarizing inspiratory or tonic preBötC neurons.

II) Methylxanthines recover opioid-depressed preBötC rhythm also primarily via preynaptic processes.

III) Lack of opioid-evoked hyperpolarization of preBötC neurons is reflected by lack of an effect on cytosolic Ca^{2+} and recovery of rhythm by methylxanthines also occurs in absence of a change of Ca^{2+}.

IV) Methylxanthines reactivate opioid-depressed slice rhythm via PDE4 blockade in preBötC neurons which is mimicked by the specific PDE4 blocker rolipram.

Project-3: Methylxanthine-Evoked Hyperexcitability in Isolated Inspiratory Networks

Methylxanthines represent the gold standard for treatment of apnea of prematurity (Martin et al., 2004, 2005, Mishra et al., 2008, Abu-Shaweesh & Martin, 2008). However, their administration to preterm infants (as well as intake by adults via leisure drinks) can be associated with various side effects including seizures (Comer et al., 2001; Schmidt et al., 2006). One proposed mechanism for induction

of seizures by methylxanthines is blockade of $GABA_A$ receptors (Lopez et al., 1989; Uneyama et al., 1993; Amabeoku, 1999; Fredholm et al., 1999; Shi et al., 2003; Sugimoto et al., 2001). It is not clear whether methylxanthines also evoke seizure-like activities in respiratory models and, if so, what would be the underlying mechanism. I propose to study this in two newborn rat *in vitro* respiratory models. Firstly, nerve recordings will be done in calibrated *en bloc* preparation to elucidate which types of inspiratory-related motor bursting are particularly affected. In m-preBötC[400] slices suction electrode recording in the preBötC and XII nerve or nucleus will be combined with whole-cell recording from contralateral inspiratory and tonic preBötC neurons for unraveling cellular mechanisms of such hyperexcitability.

I hypothesize for *Project-3*:

I) Methylxanthines perturb inspiratory-related (motor) rhythms in the newborn rat *en bloc* model and m-preBötC[400] slices.

II) These perturbations of inspiratory rhythm are due to $GABA_A$ receptor blockade.

III) Rhythm in both models will be restored by caffeine and theophylline following depression with the $GABA_A$ receptor agonist muscimol.

IV) preBötC neurons in m-preBötC[400] slices are hyperpolarized by muscimol along with a decrease in input resistance and that methylxanthines will reverse these effects.

Project 4: Methylxanthine countering of opioid-evoked depression of spontaneous locus coeruleus network oscillations in newborn rat brain slices

Clinical administration of methylxanthines for treatment of apnea of prematurity is often accompanied by seizures. Methylxanthine effects are not known on other neural networks that are spontaneously active in newborns and it is thus possible that high doses of these agents evoke neuronal overexcitation in these networks. This was studied here in LC neurons that show rhythmic bursting or tonic activity in newborn rat brainstem *en bloc* and slice models (Christie et al., 1989; Christie & Jelinek, 1993; Oyamada et al., 1998, 1999; Ballantyne et al., 2004; Kantor et al., 2012) (Chapter **1.8**) **(Fig. 1-11)**. A further rationale for studying these neurons is related to the fact that GIRK channels involvement in strong opioid-evoked postsynaptic hyperpolarizations were pioneered in this model (Williams et al., 1982, 2001; Alreja & Aghajanian, 1993; Christie, 1991; Law et al., 2000). Accordingly, opioid effects on membrane potential of these neurons under experimental conditions identical to those applied to the m-preBötC[400] slices in the other projects will serve also as a reference for discussing whether 'methodological artifacts' potentially causing the hypothesized lack of opioid-evoked hyperpolarization in preBötC neurons. In addition to blind whole-cell recordings from LC neurons, that was sometimes combined with suction electrode recording of rhythmic population bursting, multiphoton/confocal Ca^{2+} imaging was conducted under conditions very similar to those in *Project-2*. This served to investigate whether opioid hyperpolarization causes a major fall of the baseline of

cytosolic Ca^{2+} which might be due to a blockade of voltage-activated Ca^{2+} channels and whether methylxanthine actions are associated with Ca^{2+} release as discussed for Project-3. Moreover, it was investigated whether application of methylxanthines to control slices causes LC neuronal hyperexcitability.

I hypothesize for *Project-4* that:

I) LC neurons in newborn rat brainstem slices are active and fire synchronously in superfusate with physiological ion content.

II) Methylxanthines evoke hyperexcitability by $GABA_A$ receptor blockade as hypothesized for respiratory (motor) networks which will lead to major changes of cytosolic Ca^{2+}.

III) Opioid depression of LC rhythm involves a major postsynaptic hyperpolarization under experimental conditions identical to those used for studying isolated preBötC networks.

IV) Methylxanthines recover LC neuronal bursting depressed by opioids via PDE4 inhibition, similar to stimulatory effects on the isolated preBötC.

1.10 Figures and Legends

Fig. 1-1

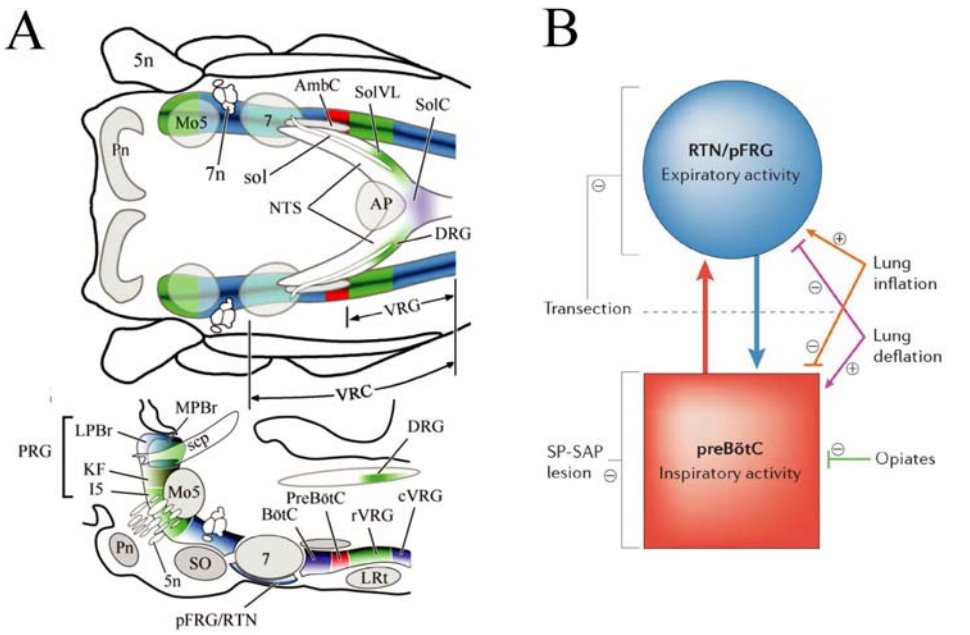

Fig. 1-1: Respiratory groups and centers in the lower brainstem of mammals. **A**, respiratory related regions of the rhombencephalon (pons + lower brainstem) of the rat shown in horizontal (upper schema) and sagittal (lower schema) views. Abbreviations: 5n, trigeminal nerve; 7, facial nucleus (note that the terminology 'VII' is used for this thesis); AmbC, compact part of nucleus ambiguus; AP, area postrema; BötC, Bötzinger complex; cVRG, caudal division of ventral respiratory group; DRG, dorsal respiratory group; I5, intertrigeminal area; icp, inferior cerebellar peduncle; KF, Kölliker-Fuse nucleus; LPBr, lateral parabrachial region; LRt, lateral reticular nucleus; Mo5, motor nucleus of the trigeminal nerve; MPBr, medial parabrachial region; NTS, nucleus of the solitary tract; pFRG, parafacial respiratory group; Pn, basilar pontine nuclei; preBötC, preBötzinger complex; PRG, pontine respiratory group; RTN, retrotrapezoid nucleus; rVRG, rostral division of ventral respiratory group; SO, superior olive; sol, solitary tract; SolC, commissural subdivision of the nucleus of the solitary tract; SolVL, ventrolateral subdivision of the nucleus of the solitary tract; sp5, spinal trigeminal tract; VRC, ventral respiratory column of the medulla; VRG, ventral respiratory group (modified from Alheid & McCrimmon, 2008). **B**, dual respiratory center in (newborn) mammals comprised by the inspiratory preBötC and the more rostral RTN/pFRG that appears to drive expiratory activity and may not be rhythmic in mammals at rest showing no active expiration. Substance P-saporin (SP-SAP) lesion of preBötC neurokinin 1 receptor (NK1R) neurons disrupts breathing. Transections between the two oscillators disrupt expiratory motor outflow, while inspiratory activity continues unabated. Lung inflation enhances the activity of the expiratory oscillator and depresses the inspiratory oscillator (from Feldman & del Negro, 2006).

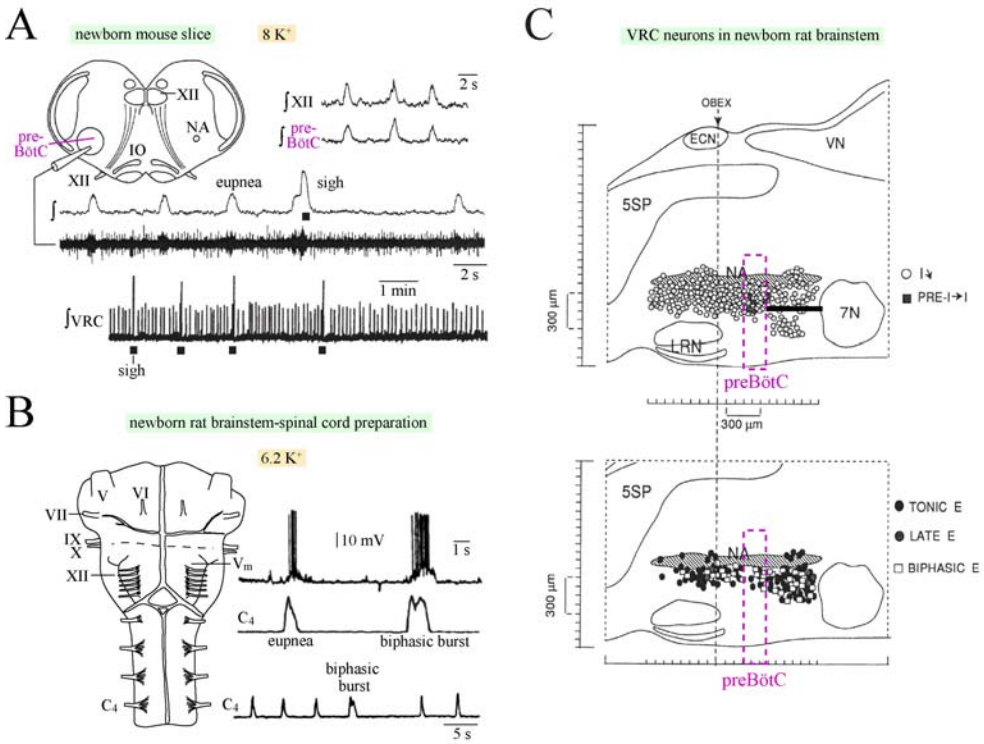

Fig. 1-2. Inspiratory burst patterns and neuron types in newborn rodent brainstem preparations. A, in preBötC slices from 0-2 weeks-old mice, inspiratory-related bursting (shown as raw differential and/or integrated signals) is monitored in superfusate with 8 mM K^+ and 1.5 mM Ca^{2+} ('$8K^+/1.5Ca^{2+}$ solution') with suction electrodes in the ventrolateral slice region and from hypoglossal (XII) nerve (upper right inset). The lowermost trace shows 'fictive eupneic' bursts of regular rate and amplitude that are interrupted at intervals >1 min by larger amplitude 'fictive sighs' and a postsigh period of inhibition of bursting. **B**, In $6.2K^+/1.5Ca^{2+}$, brainstem-spinal cords from postnatal day (P) 0-4 rats generate fictive eupneia cervical (C_4) nerve bursts that alternate with 'biphasic bursts' of similar amplitude, likely comprising two partially-overlapping eupneic bursts. The lowermost trace shows that biphasic bursts are less frequent than eupnea-like bursts. Abbreviations: IO, inferior olive; VRC, ventral respiratory column; NA, nucleus ambiguus; V, VI, VII, IX, X: trigeminal, abducens, facial, glossopharyngeal, vagal nerves; V_m, membrane potential. **C**, sagittal projection of neurons with (pre)inspiratory (top) and expiratory (bottom) activity in VRC between caudal end of VII nucleus and lateral reticular nucleus (LRN). Each symbol indicates point of maximum extracellular field potential of unit recorded along a single-electrode tract. Cell locations were reconstructed from dye marks at recording sites. Abbreviations: VN, vestibular nucleus; ECN, external cuneate nucleus; 5SP, spinal trigeminal nucleus. Shaded region demarcating nucleus ambiguus represents compact, semicompact, and loose formations of this nucleus only (**A** modified from Lieske et al., 2000, **B** modified from Shvarev et al., 2003, **C** modified from Smith et al., 1990)

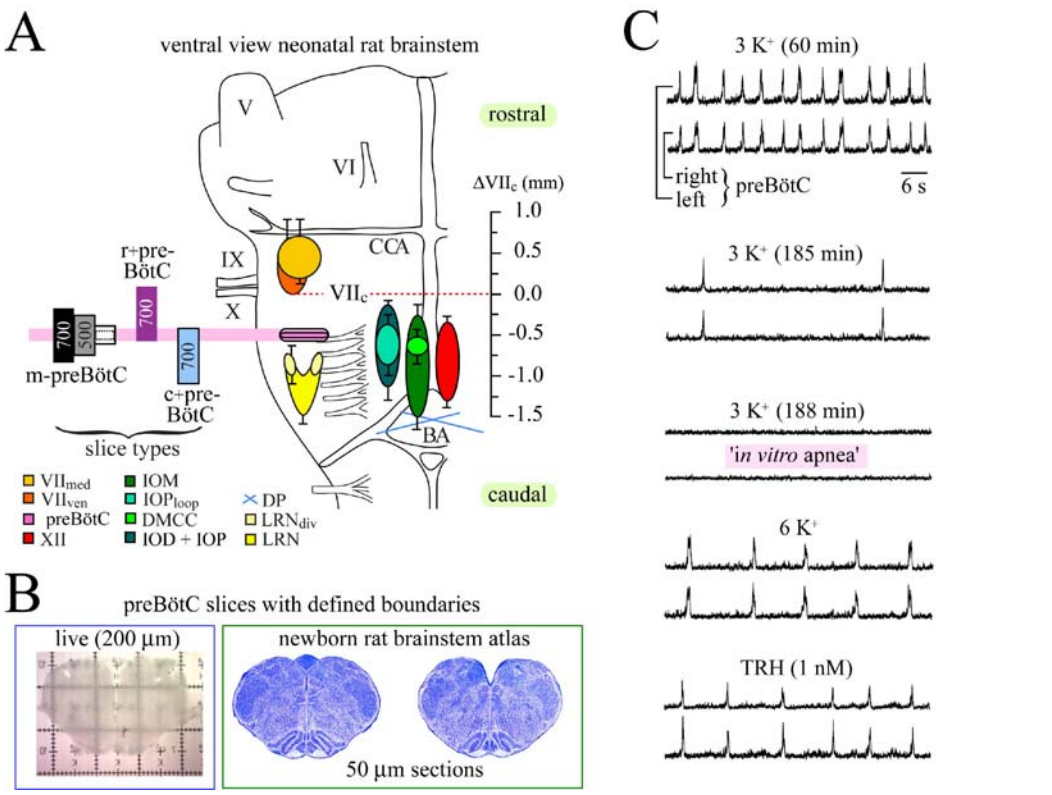

Fig. 1-3: Rhythm in physiological K^+ of calibrated preBötC inspiratory center slices. A, rostrocaudal extents of respiratory brainstem marker nuclei such as subnuclei of the IO and VII motor nucleus, projected onto the ventral brainstem surface, are constant (see small standard deviations of bars) in P0-4 Sprague-Dawley and Wistar rats enabling with 'online histology' various types of preBötC slices with defined anatomical boundaries referred to the caudal end of VII nucleus, (VII_c). 'm-preBötC' slices have the preBötC in the middle. r+preBötC or c+preBötC slices contain the <100 µm small preBötC kernel necessary for generation of rhythm plus additional rostral or caudal tissue, respectively. **B**, shows in the left a 200 µm thin living rhythmic m-preBötC slice after an experiment next to 2 sections from a newborn rat reference atlas used to determine the margins of rhythmic slices. **C**, rhythm recorded with two suction electrodes in $3K^+/1Ca^{2+}$ in a 500 µm thick m-preBötC (m-preBötC[500/-0.70]W-P3) slice was stable for ~3 h before burst rate dropped from >10 to <4 bursts/min. After rhythm stopped spontaneously shortly after 185 min ('*in vitro* apnea'), it was restored by raising K^+ to 6 mM or bath-application of thyrotropin-releasing hormone (TRH) (details in Ruangkittisakul et al., 2006, 2008). Abbreviations: CCA, caudal cerebellar artery; DMCC: dorsomedial cell column of IO, IOM: medial IO, IOD: dorsal IO, IOP: principal IO, IOP_{loop}: lateral loop of IOP, LRN: lateral reticular nucleus, LRN_{div}: LRN divided into medial and lateral subnuclei, VII_{med}: medial subnucleus of VII, VII_{ven}: ventral subnucleus of VII, DP: pyramidal decussation (from Ruangkittisakul et al., 2012).

Fig. 1-4

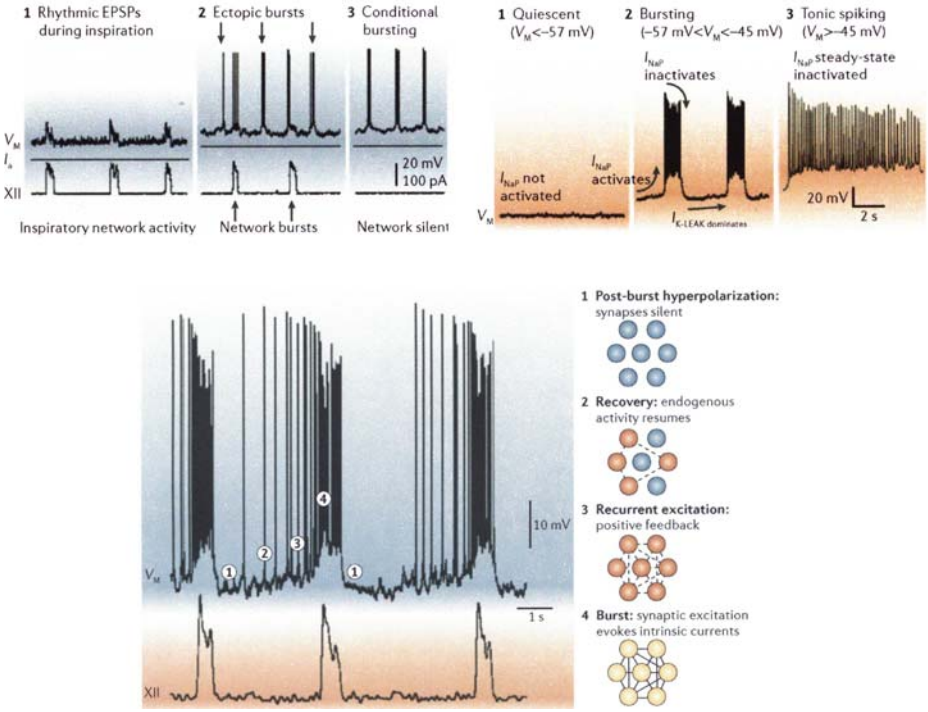

Fig. 1-4: Group-pacemaker hypothesis of respiratory rhythm generation. Upper left panel, conditional bursting ('pacemaker') preBötC neurons are capable of ectopic bursting, i.e. bursting out of phase with inspiratory XII rhythm, upon current-evoked membrane depolarization and continue to burst when network activity is blocked. **Upper right panel**, pacemaker neurons maintain voltage-dependent bursting in the range of -57 to -45 mV after synaptic isolation. When depolarization exceeds -45 mV, bursting gives way to tonic spiking. Voltage-dependent bursting depends on persistent Na^+ current (I_{NaP}) and leakage K^+ current ($I_{K\text{-}LEAK}$). I_{NaP} causes burst depolarization and $I_{K\text{-}LEAK}$ regulates excitability. **Lower panel**, membrane potential of rhythm-generating neuron is shown (V_M, top trace) with network activity, represented by XII motor output (XII, bottom). Images to the right of the traces depict neuronal activity at different stages of the cycle. **1:** refractory state following inspiration, in which activity-dependent outward currents depress membrane potential, and excitatory synapses are inactive. **2**: the most excitable neurons recover from post-burst hyperpolarization and begin to spike at a low rate. **3:** these cells begin to synaptically activate other neurons, leading to aggregation of network activity itself due to recurrent synaptic excitation ('positive-feedback'). **4**: inspiratory burst ensues once a critical number of cells is activated by recurrent excitation. In this final step, synaptic inputs recruit burst-generating intrinsic currents such as Ca^{2+}-activated nonspecific cationic current (I_{CAN}) and persistent Na^+ current (I_{NaP}), which give rise to large inspiratory burst potentials with high-frequency spike activity. Inspiratory bursts terminate owing to Ca^{2+}-dependent K^+ currents and electrogenic pumps (from Feldman & Del Negro, 2006).

Fig. 1-5

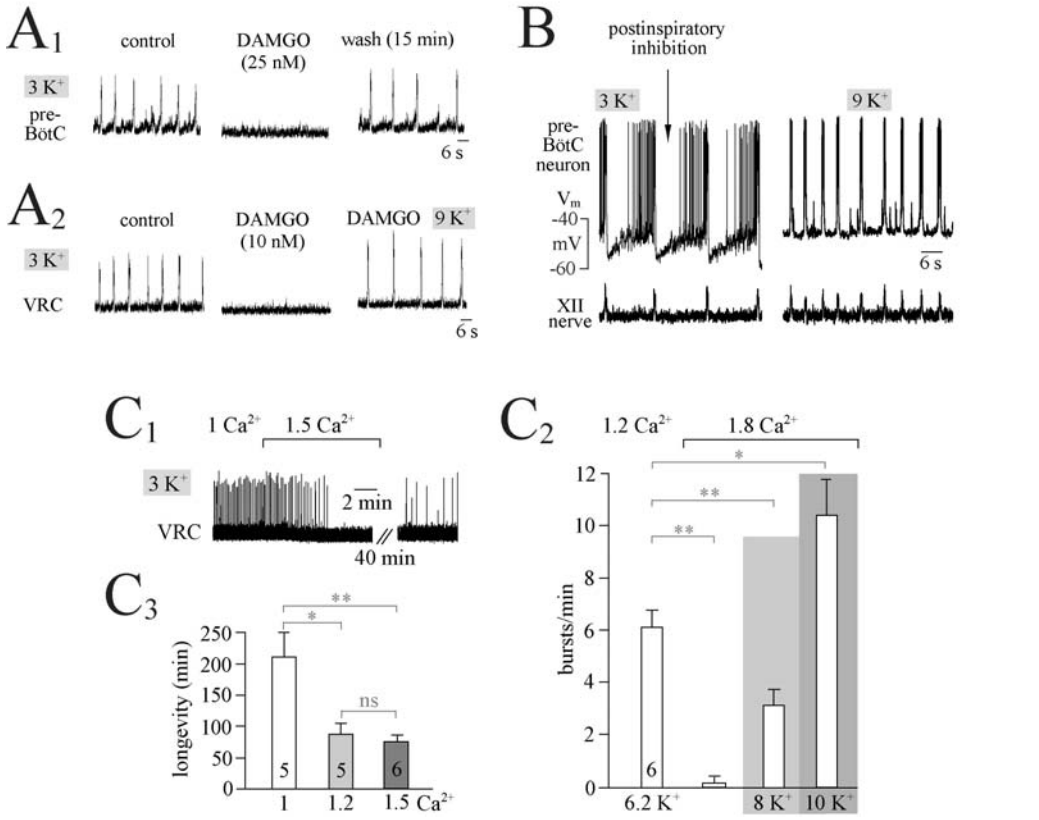

Fig. 1-5. Modulation of newborn rat preBötC slice rhythm by opioids, Ca^{2+}, and K^+. A, depression of rhythm by opioids, **A_1** in a m-preBötC[400] slice in $3K^+/1Ca^{2+}$ a low nanomolar concentration of the bath-applied μ-opioid receptor agonist [D-Ala^2,N-Me-Phe^4,Gly^5-ol]-Enkephalin (DAMGO) reversibly abolished inspiratory-related bursting in the VRC region. **A_2**, a similar block of rhythm by DAMGO in a m-preBötC[600] slice in $3K^+/1Ca^{2+}$ was reversed by raising K^+ to 9 mM. **B**, raising K^+ from 3 to 9 mM in a m-preBötC[500] slice not only accelerate the rate of rhythm, but also changed membrane potential trajectory in an inspiratory preBötC neuron notably. **C**, Ca^{2+}/K^+ antagonism, **C_1**, inspiratory-related bursting in the VRC region of an m-preBötC[600] slice in $3K^+/1Ca^{2+}$ was abolished by raising Ca^{2+} to 1.5 mM. **C_2**, mean rate of VRC bursts in six m-preBötC[600] slices during variation of superfusate Ca^{2+} and K^+. In control, slices were kept in $6.2K^+/1Ca^{2+}$. Subsequently, rhythm was blocked upon elevation of Ca^{2+} to 1.8 mM and reactivated by raising K^+, first to 8 mM, then to 10 mM. **C_3**, longevity of rhythm in m-preBötC[600] slices that were each generated and studied in $3K^+$ solution of different Ca^{2+} content. Note that rhythm persists for notably longer time periods in 1 *versus* 1.2 or 1.5 mM Ca^{2+}. Digits in bars indicate number of slices. (**A** and **B** from Ballanyi & Ruangkittisakul, 2009; **C** from Ruangkittisakul et al., 2007).

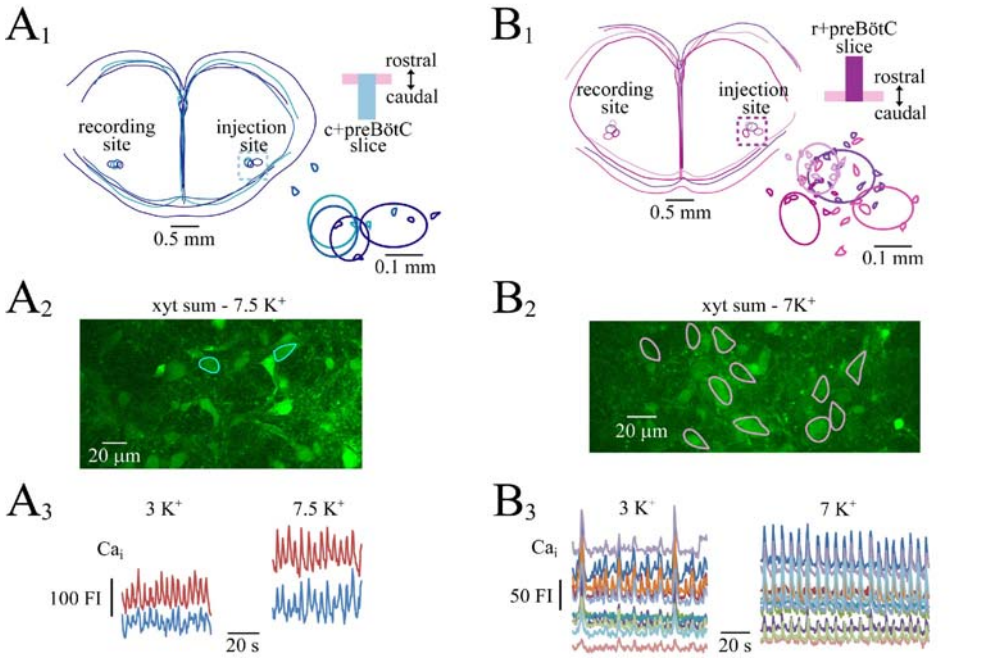

Fig. 1-6: Multiphoton/confocal Ca^{2+} imaging in the isolated newborn rat preBötC. A, location, soma size/shape and activity of inspiratory neurons in superficial layers (30-80 µm) of slices with the preBötC exposed to the rostral border ('c+preBötC slices'). **A_1**, locations in 4 superimposed slices of inspiratory neurons loaded with membrane-permeant Ca^{2+}-sensitive dye (Fluo-4-AM) via pressure injection (25-50 mmHg, 10 min) into the preBötC, correspond with positions in contralateral preBötC of suction electrodes for recording inspiratory rhythm with maximal amplitude. Overlapping dye injection sites outlined by dotted square are shown in the lower right inset at higher magnification. Inspiratory active neurons are marked by regions of interest (ROIs) with equal shading indicating the same injection site (one per slice). **A_2**, examples for cellular morphology in one injection spot of **A_1** with inspiratory neurons indicated by ROIs. Cells were located 0.43 mm caudal to VII_c, i.e., 70 µm rostral to the preBötC center, located 0.50 mm caudal to VII_c. **A_3**, inspiratory-related rises of cytosolic Ca^{2+} (Ca_i) shown by plotting Fluo-4-AM fluorescence intensity (FI) traces over time in the 2 neurons indicated by ROIs of **A_2** were synchronous with electrophysiologically recorded population bursting in contralateral preBötC (not shown). Raising superfusate K^+ from 3 to 7.5 mM produced more robust oscillations with a concomitant increase in Ca_i baseline. **B**, location (**B_1**), morphology (**B_2**) and activity (**B_3**) of inspiratory neurons in superficial layers (30-80 µm) of slices with the preBötC exposed to the caudal border ('r+preBötC slices'). **B_1**, overlapping dye injection sites are shown in lower right inset. **B_2**, examples for cellular morphology in one injection spot of **B_1**. Cells were within the preBötC center at 58 µm caudal to VII_c. **B_3**, raising K^+ from 3 to 7 mM transformed inspiratory Ca_i rises from an eupnea-sigh to regular eupnea pattern in the neurons outlined in **B_2** (from Ruangkittisakul et al., 2012).

Fig. 1-7

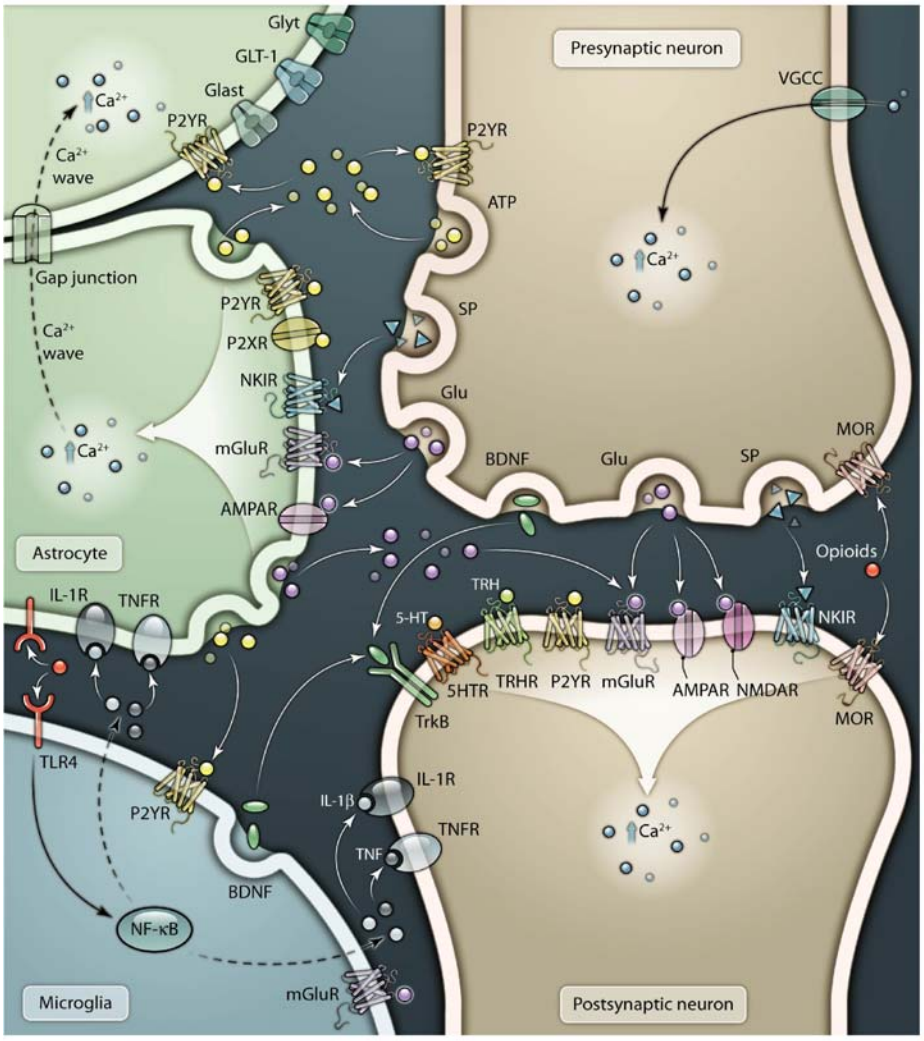

Fig. 1-7: Signaling pathways between presynaptic and postsynaptic areas of inspiratory preBötC neurons and adjacent astrocytic glial cells and microglial cells. Experimental evidence for most of these pathways has been obtained primarily from studies on rhythmically active preBötC slices from perinatal rodents. Interactive signaling of preBötC neurons and astrocytes with microglia is hypothetical. 5HT(R), serotonin (receptor); AMPAR, α-amino-3-hydroxy-5-methyl-4-isoxazole propionic acid receptor; Ca^{2+}, calcium; Glast, glutamate-aspartate transporter; GLT-1, glutamate transporter; Glu, glutamate; Glyt, glycine transporter; IL1(R), interleukin-1 (receptor); mGluR, metabotropic glutamate receptor; MOR, μ-opioid receptor; NF-κB, nuclear factor κB; NK1R, neurokinin-1 receptor; NMDAR, *N*-methyl-D-aspartate receptor; SP, substance P; TLR, Toll-like receptor; TNF(R), tumor necrosis factor (receptor); TRH(R), thyrotropin-releasing hormone (receptor); TrkB, tyrosine receptor kinase B; VGCC, voltage-gated Ca^{2+} channels (from Ballanyi et al., 2010).

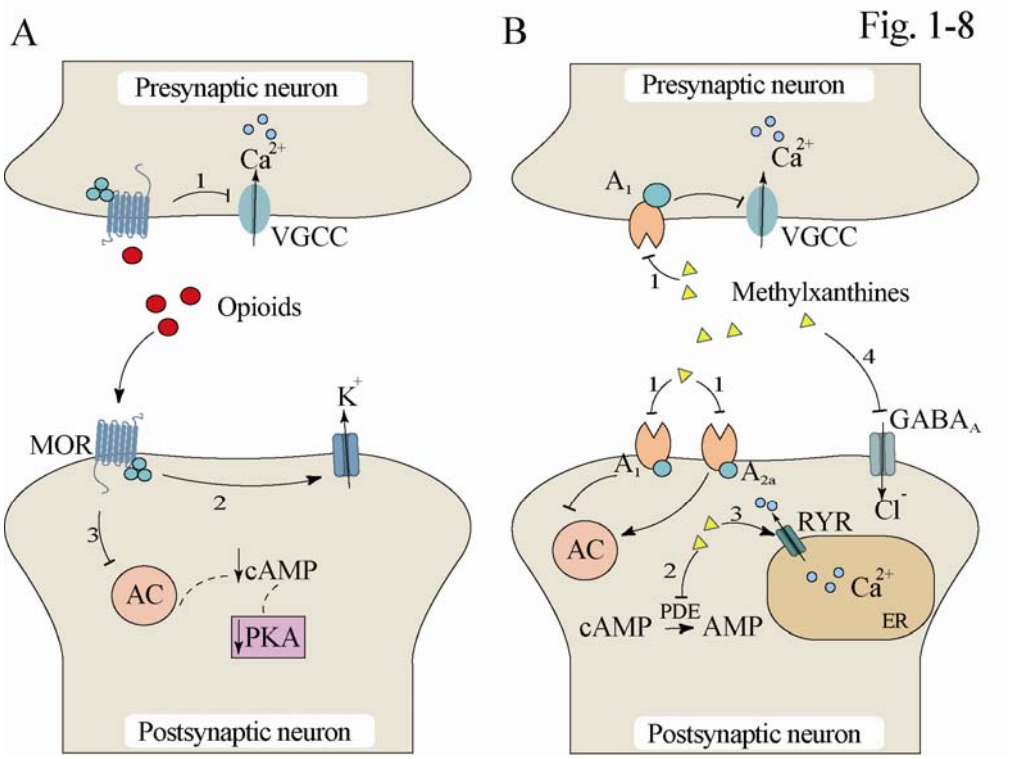

Fig. 1-8: Mechanisms of opioid and methylxanthine actions on neurons. A, Opioids can, e.g., act presynaptically through G protein-coupled opioid receptors, causing (*i*) inhibition of voltage-gated Ca^{2+} channels (VGCCs) or (*ii*) postsynaptic activation of a G protein-coupled inward-rectifying K^+ (GIRK) channel through the same opioid sensitive receptors (), and also (*iii*) inhibition of adenylyl cyclase (modified from Nestler et al., 1999). Abbreviations: AC, adenylyl cyclase; Ca^{2+}, calcium ions; cAMP, cyclic adenosine monophosphate; K^+, potassium ions; MOR, μ-opioid receptors; PKA, protein kinase A; VGCC, voltage-gated Ca^{2+} channels. **B**, main mechanisms of methylxanthine actions are (*i*) antagonism of adenosine receptors (mainly A_1, A_{2A}), (*ii*) inhibition of (cAMP-dependent) phosphodiesterases (PDE), (*iii*) Ca^{2+} release from endoplasmic reticulum (ER) through ryanodine receptors (RYR), and (iv) antagonism of $GABA_A$ receptors (for review, see Fredholm et al., 1999).

Fig. 1-9

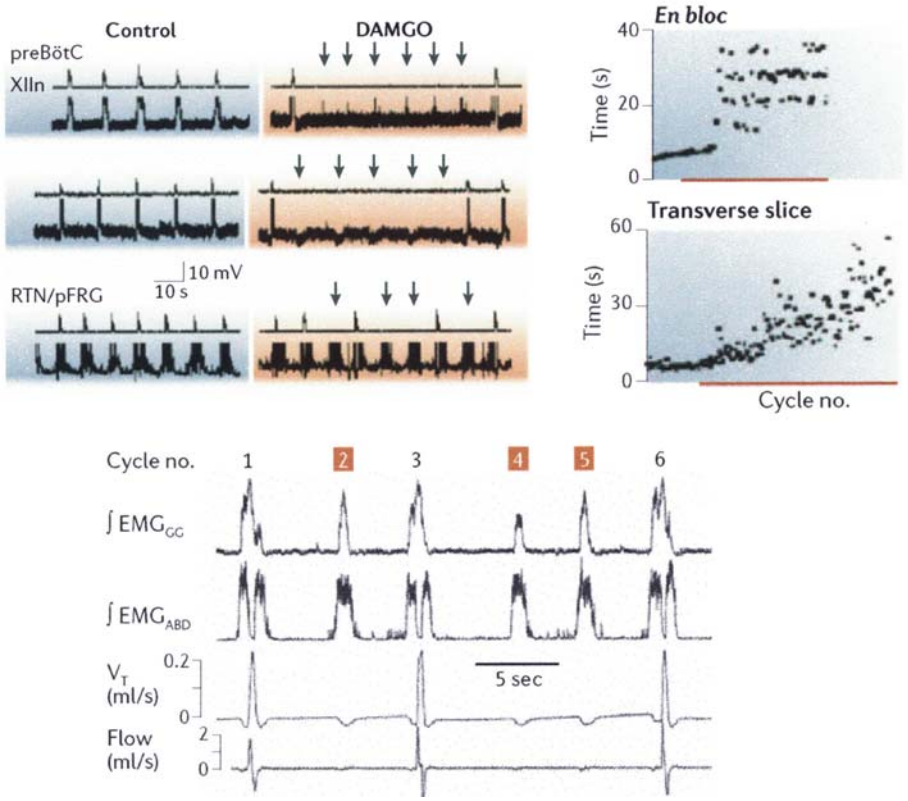

Fig. 1-9: Opiates cause quantal slowing of inspiration but not of active expiration. Upper left panel, simultaneous recordings of inspiratory rhythm in control and DAMGO-treated XII nerve plus inspiratory preBötC neurons (top two pairs of traces; compare **Fig. 1-5**) and XII nerve plus pre-inspiratory (Pre-I) neurons in pFRG (bottom pair). Arrows in DAMGO traces indicate subthreshold events in preBötC neurons during skipped bursts, which occur at the approximate time expected for inspiratory bursts at control frequency, or unperturbed bursting in Pre-I neurons. **Upper right panel**, sequential plots of inspiratory period *in vitro* before and after treatment with DAMGO; bottom plot shows continuous slowing of inspiratory rhythm in newborn rat preBötC slice, top plot shows quantal slowing of rhythm in *en bloc* model. **Lower panel**, *in vivo* recordings in juvenile rats following fentanyl injection. Traces show typical recording with normal cycles (1, 3, 6) interspersed with cycles without inspiratory activity (2, 4, 5). Abbreviations: $\int EMG_{ABD}$, integrated abdominal muscle electromyogram (EMG); $\int EMG_{GG}$, integrated genioglossus muscle EMG; flow, air flow (up or down for inspiratory or expiratory air flow, respectively); V_T, tidal volume (from Feldman & Del Negro, 2006).

Fig. 1-10

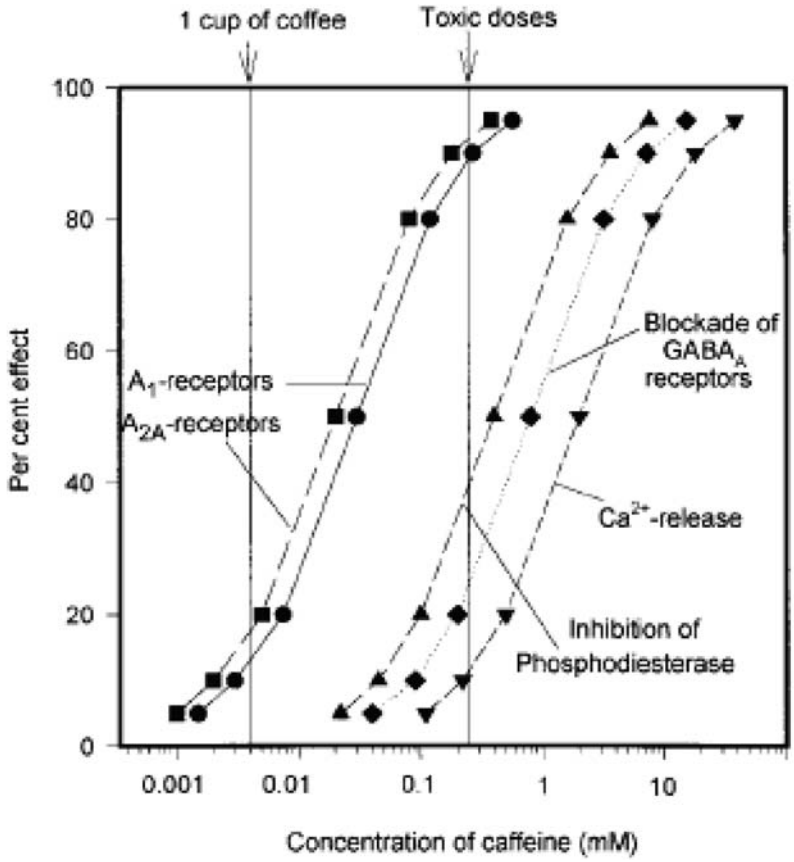

Fig. 1-10: Cellular in vitro effects of caffeine. At low micromolar doses caffeine blocks A_1 and A_{2A} types of adenosine receptors, whereas at higher micromolar doses it inhibits firstly PDEs, then $GABA_A$ receptors and, finally, starting at ~0.5 mM releases $Ca^{2+}$from stores (compare **Fig. 1-8**). Note that the same sequence of events applies principally for theophylline. (from Fredholm et al., 1999).

Fig. 1-11

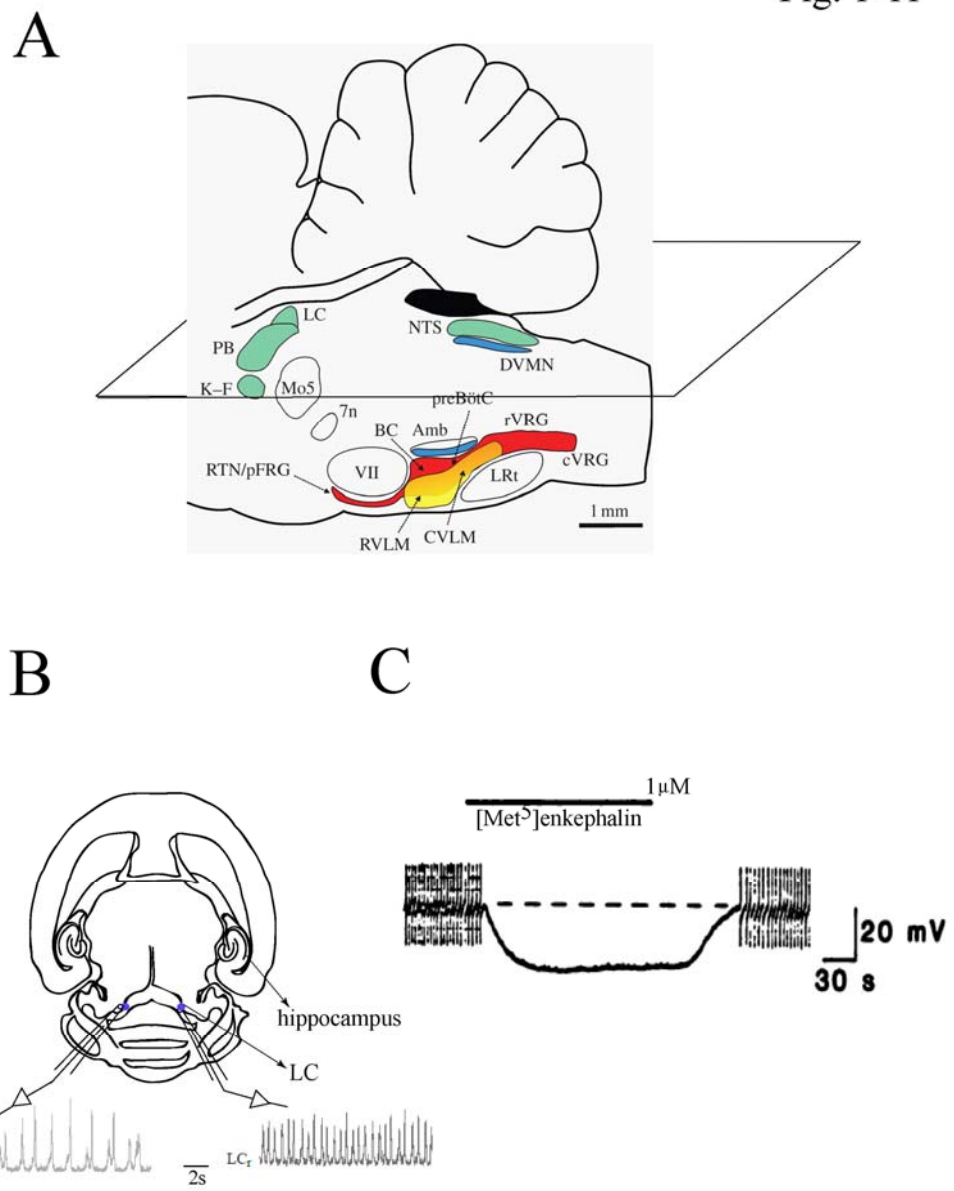

Fig. 1-11: *Locus coeruleus* in the newborn rat brainstem. A, sagittal view of the rat brainstem, indicating *locus coeruleus* (LC) in relation to the other areas involved in neural control of breathing. The brainstem can be cut horizontally at the LC level (rectangle) and this will result in a brain slice similar to the bottom diagram (**B**). This horizontal slice allows the simultaneous recordings of bilateral LC signals with suction electrodes. **C**, activation of LC neuronal µ-opioid receptors with [Met^5]enkephalin induces a membrane hyperpolarization. (**A** modified from Spyer & Gourine, 2009, **B** from Kantor et al., 2012, and **C** modified from Williams & Marshall, 1987.)

1.11 References

Abdala AP, Rybak IA, Smith JC, Paton JF (2009) Abdominal expiratory activity in the rat brainstem-spinal cord in situ: patterns, origins and implications for respiratory rhythm generation. J Physiol 587, 3539-3559

Abu-Shaweesh JM, Martin RJ (2008) Neonatal apnea: what's new? Pediatr Pulmonol 43, 937-944

Adachi T, Robinson DM, Miles GB, Funk GD (2005) Noradrenergic modulation of XII motoneuron inspiratory activity does not involve alpha2-receptor inhibition of the Ih current or presynaptic glutamate release. J Appl Physiol 98, 1297-1308

Aghajanian GK (1978) Tolerance of locus coeruleus neurones to morphine and suppression of withdrawal response by clonidine. Nature 276, 186-188

Aghajanian GK, & Wang YY (1987) Common alpha 2 and opiate effector mechanisms in the locus coeruleus: intracellular studies in brain slices. Neuropharmacology 26, 793-799

Aitken ML, Martin TR (1987) Life-threatening theophylline toxicity is not predictable by serum levels. Chest 91, 10-14

Alheid GF, McCrimmon DR (2008) The chemical neuroanatomy of breathing. Respir Physiol Neurobiol 164, 3-11

Alreja M, Aghajanian GK (1991) Pacemaker activity of locus coeruleus neurons: whole-cell recordings in brain slices show dependence on cAMP and protein kinase A. Brain Res 556, 339-343

Alreja M, Aghajanian GK (1993) Opiates suppress a resting sodium-dependent inward current and activate an outward potassium current in locus coeruleus neurons. J Neurosci 13, 3525-3532

Alvarez VA, Chow CC, Van Bockstaele EJ, Williams JT (2002) Frequency-dependent synchrony in locus ceruleus: role of electrotonic coupling. Proc Natl Acad Sci USA 99, 4032-4036

Amabeoku GJ (1999) Gamma-aminobutyric acid and glutamic acid receptors may mediate theophylline-induced seizures in mice. Gen Pharmacol 32, 365-372

Angelucci ME, Vital MA, Cesario C, Zadusky CR, Rosalen PL, Da Cunha C (1999) The effect of caffeine in animal models of learning and memory. Eur J Pharmacol 373, 135-140

Arnaud MJ (2011) Pharmacokinetics and metabolism of natural methylxanthines in animal and man. Handbook Exp Pharmacol 200, 33-91

Aston-Jones G, Cohen JD (2005) An integrative theory of locus coeruleus-norepinephrine function: adaptive gain and optimal performance. Ann Rev Neurosci 28, 403-450

Ballantyne D, Andrzejewski M, Mückenhoff K, Scheid P (2004) Rhythms, synchrony and electrical coupling in the Locus coeruleus. Resp Physiol Neurobiol 143, 199-214

Ballanyi K (2004) Neuromodulation of the perinatal respiratory network. Curr Neuropharmacol 2, 221-243

Ballanyi K, Kulik A (1998) Intracellular Ca^{2+} during metabolic activation of K_{ATP} channels in spontaneously active dorsal vagal neurons in medullary slices. Eur J Neurosci 10, 2574-2585

Ballanyi K, Ruangkittisakul A (2009) Structure-function analysis of rhythmogenic inspiratory pre-Botzinger complex networks in "calibrated" newborn rat brainstem slices. Resp Physiol Neurobiol 168, 158-178

Ballanyi K, Lalley PM, Hoch B, Richter DW (1997) cAMP-dependent reversal of opioid- and prostaglandin-mediated depression of the isolated respiratory network in newborn rats. J Physiol 504, 127-134

Ballanyi K, Onimaru H, Homma I (1999) Respiratory network function in the isolated brainstem-spinal cord of newborn rats. Progr Neurobiol 59, 583-634

Ballanyi K, Ruangkittisakul A, Onimaru H (2009) Opioids prolong and anoxia shortens delay between onset of pre-inspiratory (pFRG) and inspiratory (preBötC)

network bursting in newborn rat brainstems. Eur J Physiol (Pflüger's Archiv) 458, 571-587

Ballanyi K, Panaitescu B, Ruangkittisakul A (2010) Control of breathing by nerve glue. Sci Signal 3, pe41

Bancalari E (2006) Caffeine for apnea of prematurity. New Engl J Med 354, 2179-2181

Barry RJ, Rushby JA, Wallace MJ, Clarke AR, Johnstone SJ, Zlojutro I (2005) Caffeine effects on resting-state arousal. Clinical Neurophysiol 116, 2693-2700

Bauer J, Maier K, Linderkamp O, Hentschel R (2001) Effect of caffeine on oxygen consumption and metabolic rate in very low birth weight infants with idiopathic apnea. Pediatrics. 107, 660-663

Bennett MV, Zukin RS (2004) Electrical coupling and neuronal synchronization in the mammalian brain. Neuron 41, 495-511

Berridge MJ (1998) Neuronal calcium signaling. Neuron 21, 13-26

Berridge CW, Waterhouse BD (2003) The locus coeruleus-noradrenergic system: modulation of behavioral state and state-dependent cognitive processes. Brain Res Rev 42, 33-84

Berthou F, Guillois B, Riche C, Dreano Y, Jacqz-Aigrain E, Beaune PH (1992) Interspecies variations in caffeine metabolism related to cytochrome P4501A enzymes. Xenobiotica 22, 671-680

Bhatt-Mehta V, Schumacher RE (2003) Treatment of apnea of prematurity. Paediatric Drugs 5, 195-210

Bianchi AL, Denavit-Saubie M, Champagnat J (1995) Central control of breathing in mammals: neuronal circuitry, membrane properties, and neurotransmitters. Physiol Rev 75, 1-45

Black AM, Pandya S, Clark D, Armstrong EA, Yager JY (2008) Effect of caffeine and morphine on the developing pre-mature brain. Brain Res 1219, 136-142

Blanton MG, Lo Turco JJ, Kriegstein AR (1989) Whole cell recording from neurons in slices of reptilian and mammalian cerebral cortex. J Neurosci Methods 30, 203-210

Bobocea N, Ruangkittisakul A, Ballanyi K (2010) Multiphoton/confocal Ca^{2+} imaging of inspiratory pre-Bötzinger complex neurons at the caudal or rostral surface of newborn rat brainstem slices. Adv Exp Med Biol 669, 81-85

Boison D (2011) Methylxanthines, seizures, and excitotoxicity. Handbook Exp Pharmacol 200, 251-266.

Bona E, Aden U, Gilland E, Fredholm BB, Hagberg H (1997) Neonatal cerebral hypoxia-ischemia: the effect of adenosine receptor antagonists. Neuropharmacology 36, 1327-1338

Bonfiglio MF, Dasta JF (1991) Clinical significance of the benzodiazepine-theophylline interaction. Pharmacotherapy 11, 85-87

Brockhaus J, Ballanyi K (1998) Synaptic inhibition in the isolated respiratory network of neonatal rats. Eur J Neurosci 10, 3823-3839

Brockhaus J, Ballanyi K (2000) Anticonvulsant A_1 receptor-mediated adenosine action on neuronal networks in the brainstem-spinal cord of newborn rats. Neuroscience 96, 359-371

Burnet H, Bevengut M, Chakri F, Bou-Flores C, Coulon P, Gaytan S, Pasaro R, Hilaire G (2001) Altered respiratory activity and respiratory regulations in adult monoamine oxidase A-deficient mice. J Neurosci 21, 5212-5221

Cashman JN, Dolin SJ (2004) Respiratory and haemodynamic effects of acute postoperative pain management: evidence from published data. Br J Aneaesth 93, 212-223

Comer AM, Perry CM, Figgitt DP (2001) Caffeine citrate: a review of its use in apnoea of prematurity. Paediatr Drugs 3, 61-79

Connor M, Christie MD (1999) Opioid receptor signalling mechanisms. Clin Exp Pharmacol Physiol 26, 493-499

Chavez Valdez R, Ahlawat R, Wills-Karp M, Nathan A, Ezell T, Gauda EB (2011) Correlation between serum caffeine levels and changes in cytokine profile in a cohort of preterm infants. J Pediatr 158, 57-64

Christie MJ (1991) Mechanisms of opioid actions on neurons of the locus coeruleus. Progr Brain Res 88, 197-205

Christie MJ, Jelinek HF (1993) Dye-coupling among neurons of the rat locus coeruleus during postnatal development. Neuroscience 56, 129-137

Christie MJ, Williams JT, North RA (1989) Electrical coupling synchronizes subthreshold activity in locus coeruleus neurons in vitro from neonatal rats. J Neurosci 9, 3584-3589

Curtis AL, Bello NT, Valentino RJ (2001) Evidence for functional release of endogenous opioids in the locus ceruleus during stress termination. J Neurosci 21, RC152

Dahan A, Aarts L, Smith TW (2010) Incidence, Reversal, and Prevention of Opioid-induced Respiratory Depression. Anesthesiology 112, 226-238

Daly JW (2000) Alkylxanthines as research tools. J Auton Nervous System 81, 44-52

Daré E, Schulte G, Karovic O, Hammarberg C, Fredholm BB (2007) Modulation of glial cell functions by adenosine receptors. Physiol Behav 92, 15-20

Delanty N, Vaughan CJ, French JA (1998) Medical causes of seizures. Lancet 352, 383-390

Del Negro CA, Morgado-Valle C, Feldman JL (2002) Respiratory rhythm: an emergent network property? Neuron 34, 821-830

Del Negro CA, Kam K, Hayes JA, Feldman JL (2009) Asymmetric control of inspiratory and expiratory phases by excitability in the respiratory network of neonatal mice in vitro. J Physiol 587, 1217-1231

Del Negro CA, Hayes JA, Pace RW, Brush BR, Teruyama R, Feldman JL (2010) Synaptically activated burst-generating conductances may underlie a group-pacemaker mechanism for respiratory rhythm generation in mammals. Prog Brain Res 187, 111-136

De Oliveira RB, Howlett MC, Gravina FS, Imtiaz MS, Callister RJ, Brichta AM, Van Helden DF (2010) Pacemaker currents in mouse locus coeruleus neurons. Neuroscience 170, 166-177

De Oliveira RB, Gravina FS, Lim R, Brichta AM, Callister RJ, Van Helden DF (2011) Developmental changes in pacemaker currents in mouse locus coeruleus neurons. Brain research 1425, 27-36

Desfrere L, Olivier P, Schwendimann L, Verney C, Gressens P (2007) Transient inhibition of astrocytogenesis in developing mouse brain following postnatal caffeine exposure. Ped Res 62, 604-609

Dobbins EG, Feldman JL (1994) Brainstem network controlling descending drive to phrenic motoneurons in rat. J Comp Neurol 347, 64-86

Dreyfus CF, Markey KA, Goldstein M, Black IB (1983) Development of catecholaminergic phenotypic characters in the mouse locus coeruleus in vivo and in culture. Dev Biol 97, 48-58

Duffin J (2004) Functional organization of respiratory neurones: a brief review of current questions and speculations. Exp Physiol 89:517-529

Dunn DW, Parekh HU (1991) Theophylline and status epilepticus in children. Neuropediatrics 22, 24-26

Durrmeyer X, Vutskits L, Anand KJ, Rimensberger PC (2010) Use of analgesic and sedative drugs in the NICU: integrating clinical trials and laboratory data. Pediatr Res 67, 117-127

Dutschmann M, Morschel M, Kron M, Herbert H (2004) Development of adaptive behaviour of the respiratory network: Implications for the pontine kolliker-fuse nucleus. Respir Physiol Neurobiol 143, 155-165

Dzhala V, Desfreres L, Melyan Z, Ben-Ari Y, Khazipov R (1999) Epileptogenic action of caffeine during anoxia in the neonatal rat hippocampus. Ann Neurol 46, 95-102

El-Bitar MK, Boustany RM (2009) Common causes of uncommon seizures. Ped Neurol 41, 83-87

Errchidi, S, Monteau, R, Hilaire, G (1991) Noradrenergic modulation of the medullary respiratory rhythm generator in the newborn rat: an in vitro study. J Physiol 443, 477-498

Feldman JL (1986) Neurophysiology of breathing in mammals. In Handbook of Physiology. The Nervous System. Intrinsic Regulatory System in the Brain Ed. FE Bloom. Am Physiol Soc, Washington, DC, pp 463-524

Feldman JL, Del Negro CA (2006) Looking for inspiration: new perspectives on respiratory rhythm. Nature Rev Neurosci 7, 232-242

Flourens M (1858) Nouveau details sur le noeud vital. Compt Rend Acad Sci 47, 803–806

Foote SL, Bloom FE, Aston-Jones G (1983) Nucleus locus ceruleus: new evidence of anatomical and physiological specificity. Physiol Rev 63, 844-914

Francis SH, Sekhar KR, Ke H, Corbin JD (2011) Inhibition of cyclic nucleotide phosphodiesterases by methylxanthines and related compounds. Handbook of Exp Pharmacol 93-133

Fredholm BB, Battig K, Holmen J, Nehlig A, Zvartau EE (1999) Actions of caffeine in the brain with special reference to factors that contribute to its widespread use. Pharmacol Rev 51, 83-133

Frermann D, Keller BU, Richter DW (1999). Calcium oscillations in rhythmically active respiratory neurones in the brainstem of the mouse. J Physiol 515, 119-131

Fuller RW, Maxwell DL, Conradson TB, Dixon CM, Barnes PJ (1987) Circulatory and respiratory effects of infused adenosine in conscious man. Br J Clin Pharmacol 24, 309-317

Funk GD, Feldman JL (1995) Generation of respiratory rhythm and pattern in mammals: insights from developmental studies. Curr Opin Neurobiol 5, 778-785

Funk GD, Smith JC, Feldman JL (1993) Generation and transmission of respiratory oscillations in medullary slices: role of excitatory amino acids. J Neurophysiol 70, 1497-1515

Funk GD, Smith JC, Feldman JL (1994) Development of thyrotropin-releasing hormone and norepinephrine potentiation of inspiratory-related hypoglossal motoneuron discharge in neonatal and juvenile mice in vitro. J Neurophysiol 72, 2538-2541

Funk GD, Johnson SM, Smith JC, Dong XW, Lai J, Feldman JL (1997) Functional respiratory rhythm generating networks in neonatal mice lacking NMDAR1 gene. J Neurophysiol 78, 1414-1420

Funk GD, Huxtable AG, Lorier AR (2008) ATP in central respiratory control: a three-part signaling system. Respir Physiol Neurobiol 10, 131-142

Fuxe K, Dahlstrom AB, Jonsson G, Marcellino D, Guescini M, Dam M, Manger P, Agnati L (2010) The discovery of central monoamine neurons gave volume transmission to the wired brain. Progr Neurobiol 90, 82-100

Gargaglioni LH, Hartzler LK, Putnam RW (2010) The locus coeruleus and central chemosensitivity. Respir Physiol Neurobiol 173, 264-273

Garrett BE, Griffiths RR (1997) The role of dopamine in the behavioral effects of caffeine in animals and humans. Pharmacol Biochem Behaviours 57, 533-541

Gaultier C, Gallego J (2008) Neural control of breathing: insights from genetic mouse models. J Appl Physiol 104, 1522-1530

Grass D, Pawlowski PG, Hirrlinger J, Papadopoulos N, Richter DW, Kirchhoff F, Hülsmann S (2004) Diversity of functional astroglial properties in the respiratory network. J Neurosci 24, 1358-1365

Gray PA (2008) Transcription factors and the genetic organization of brain stem respiratory neurons. J Appl Physiol 104, 1513-1521

Gray PA, Rekling JC, Bocchiaro CM, Feldman JL (1999) Modulation of respiratory frequency by peptidergic input to rhythmogenic neurons in the preBotzinger complex. Science 286, 1566-1568

Gray PA, Janczewski WA, Mellen N, McCrimmon DR, Feldman JL (2001) Normal breathing requires preBotzinger complex neurokinin-1 receptor-expressing neurons. Nature Neurosci 4, 927-930

Gray PA, Hayes JA, Ling GY, Llona I, Tupal S, Picardo MC, Ross SE, Hirata T, Corbin JG, Eugenín J, Del Negro CA (2011) Developmental origin of preBötzinger complex respiratory neurons. J Neurosci 30, 14883-14895

Greer JJ, Funk GD (2005) Perinatal development of respiratory motoneurons. Respir Physiol Neurobiol 149, 43-61

Greer JJ, Ren J (2009) Ampakine therapy to counter fentanyl-induced respiratory depression. Respir Physiol Neurobiol 168, 153-157

Greer JJ, Carter JE, Al-Zubaidy Z (1995) Opioid depression of respiration in neonatal rats. J Physiol 485, 845-855

Guerreiro S, Marien M, Michel PP (2011) Methylxanthines and ryanodine receptor channels. Handbook Exp Pharmacol 200, 135-150.

Gustafson-Vickers SL, Lu VB, Lai AY, Todd KG, Ballanyi K, Smith PA (2008) Long-term actions of interleukin-1β on delay and tonic firing neurons in rat superficial dorsal horn and their relevance to central sensitization. Mol Pain 4, 63-74

Guyenet PG (1991) Central noradrenergic neurons: the autonomic connection. Progr Brain Res 88, 365-380

Guyenet PG, Koshiya N, Huangfu D, Verberne AJ, Riley TA (1993) Central respiratory control of A5 and A6 pontine noradrenergic neurons. Am J Physiol 264, 1035-1044

Guyenet PG, Mulkey DK (2010) Retrotrapezoid nucleus and parafacial respiratory group. Respir Physiol Neurobiol 173, 244-255

Härtel K, Schnell C, Hülsmann S (2008) Astrocytic calcium signals induced by neuromodulators via functional metabotropic receptors in the ventral respiratory group of neonatal mice. Glia 57, 815-827

Hakuno H, Oyamada Y, Murai M, Ito Y, Yamaguchi K (2004) Effects of inactivation and stimulation of locus coeruleus on respiratory activity of neonatal rat. Resp Physiology Neurobiol 140, 9-18

Hayes JA, Del Negro CA (2007) Neurokinin receptor-expressing pre-botzinger complex neurons in neonatal mice studied in vitro. J Neurophysiol 97, 4215-4224

Hayes MJ, Akilesh MR, Fukumizu M, Gilles AA, Sallinen BA, Troese M, Paul JA. (2007) Apneic preterms and methylxanthines: arousal deficits, sleep fragmentation and suppressed spontaneous movements. J Perinatol. 27, 782-789Hein L (2006) Adrenoceptors and signal transduction in neurons. Cell Tiss Res 326, 541-551

Henderson-Smart DJ, De Paoli AG (2010) Prophylactic methylxanthine for prevention of apnoea in preterm infants. Cochrane Database Syst Rev, CD000432

Henderson-Smart DJ, Steer PA (2010) Caffeine versus theophylline for apnea in preterm infants. Cochrane Database Syst Rev, CD000273

Herlenius E, Aden U, Tang LQ, Lagercrantz H (2002) Perinatal respiratory control and its modulation by adenosine and caffeine in the rat. Pediatr Res 51, 4-12

Hetzler RK, Knowlton RG, Somani SM, Brown DD, Perkins RM 3rd (1990) Effect of paraxanthine on FFA mobilization after intravenous caffeine administration in humans. J Appl Physiol 68, 44-47

Hilaire G (2006) Endogenous noradrenaline affects the maturation and function of the respiratory network: possible implication for SIDS. Auton Neurosci 126-127, 320-331

Hilaire G, Viemari JC, Coulon P, Simonneau M, Bevengut M. (2004) Modulation of the respiratory rhythm generator by the pontine noradrenergic A5 and A6 groups in rodents. Resp Physiol Neurobiol 143, 187-197

Hille B (2002) Ion channels of excitable membranes. Sunderland, MA: Sinauer Associates.

Hobson JA, McCarley RW, Wyzinski PW (1975) Sleep cycle oscillation: reciprocal discharge by two brainstem neuronal groups. Science 189, 55-58

Hoecker C, Nelle M, Poeschl J, Beedgen B, Linderkamp O (2002) Caffeine impairs cerebral and intestinal blood flow velocity in preterm infants. Pediatrics 109, 784-787

Holmes GL, Ben-Ari Y (1998) Seizures in the developing brain: perhaps not so benign after all. Neuron 21, 1231-1234

Hutchinson MR, Northcutt AL, Chao LW, Kearney JJ, Zhang Y, Berkelhammer DL, Loram LC, Rozeske RR, Bland ST, Maier SF, Gleeson TT, Watkins LR (2008) Minocycline suppresses morphine-induced respiratory depression, suppresses morphine-induced reward, and enhances systemic morphine-induced analgesia. Brain Behavior Immunity 22, 1248-1256

Huxtable AG, Zwicker JD, Alvares TS, Ruangkittisakul A, Fang X, Hahn LB, Posse de Chaves E, Baker GB, Ballanyi K, Funk GD (2010) Glia contribute to the purinergic modulation of inspiratory rhythm generating networks. J Neurosci 30, 3947-3958

Huxtable AG, Zwicker JD, Poon BY, Pagliardini S, Vrouwe SQ, Greer JJ, Funk GD (2009) Tripartite purinergic modulation of central respiratory networks during perinatal development: the influence of ATP, ectonucleotidases, and ATP metabolites. J Neurosci 29, 14713-14725

Ishimatsu M, Williams JT (1996) Synchronous activity in locus coeruleus results from dendritic interactions in pericoerulear regions. J Neurosci 16, 5196-5204

Iyadurai SJ, Chung SS (2007) New-onset seizures in adults: possible association with consumption of popular energy drinks. Epilepsy Behav 10, 504-508

Jaquin TD, Borday V, Schneider-Maunoury S, Topilko P, Ghilini G, Kato F, Charnay P, Champagnat J (1996) Reorganization of pontine rhythmogenic neuronal networks in Krox-20 knockout mice. Neuron 17, 747-758

Janczewski WA, Feldman JL (2006) Distinct rhythm generators for inspiration and expiration in the juvenile rat. J Physiol 570, 407-420

Janczewski WA, Onimaru H, Homma I, Feldman JL (2002) Opioid-resistant respiratory pathway from the preinspiratory neurones to abdominal muscles: In vivo and in vitro study in the newborn rat. J Physiol 545, 1017-1026

Jansen AH, Chernick V (1983) Development of respiratory control. Physiol Rev 63, 437-483

Jefferys JG (1994) Experimental neurobiology of epilepsies. Curr Opin Neurol 7, 113-122

Johansson B, Georgiev V, Kuosmanen T, Fredholm BB (1996) Long-term treatment with some methylxanthines decreases the susceptibility to bicuculline- and pentylenetetrazol-induced seizures in mice. Relationship to c-fos expression and receptor binding. Eur J Neurosci 8, 2447-2458

Johnson PJ (2011) Caffeine citrate therapy for apnea of prematurity. Neonatal Metw 30, 408-412

Johnson SM, Smith JC, Funk GD, Feldman JL (1994) Pacemaker behavior of respiratory neurons in medullary slices from neonatal rat. J Neurophysiol 72, 2598-2608

Kang SH, Lee YA, Won SJ, Rhee KH, Gwag BJ (2002) Caffeine-induced neuronal death in neonatal rat brain and cortical cell cultures. Neuroreport 13, 1945-1950

Kantor C, Panaitescu B, Kuribayashi J, Ruangkittisakul A, Lee TF, Cheung PY, MacTavish D, Jhamandas J, Ballanyi K (2012) Electrophysiological imaging of early network oscillations in brain slices from newborn rats and piglets. In Isolated Central Nervous System Circuits (Ed K Ballanyi), Neuromethods Series Vol 73 (Ed W Walz). Springer Science+Business Media, LLC, New York, NY, 315-356

Kaufman KR, Sachdeo RC (2003) Caffeinated beverages and decreased seizure control. Seizure 12, 519-521

Kawai A, Ballantyne D, Mückenhoff K, Scheid P (1996) Chemosensitive medullary neurones in the brainstem--spinal cord preparation of the neonatal rat. J Physiol 492, 277-292

Kennedy JS, Leduc BW, Scavone JM, Harmatz JS, Shader RI, Greenblatt DJ (1987) Pharmacokinetics of intravenous caffeine: comparison of high-performance liquid chromatographic and gas chromatographic methods. J Chromatogr 422, 274-280

Kilb W, Sinning A, Luhmann HJ (2007) Model-specific effects of bumetanide on epileptiform activity in the in-vitro intact hippocampus of the newborn mouse. Neuropharmacology 53, 524-533

Koos BJ, Kawasaki Y, Kim YH, Bohorquez F (2005) Adenosine A2Areceptor blockade abolishes the roll-off respiratory response to hypoxia in awake lambs. Am J Physiol Regul Integr Comp Physiol 288, 1185-1194.

Korematsu S, Miyahara H, Nagakura T, Suenobu S, Izumi T (2008) Theophylline-associated seizures and their clinical characterizations. Pediatr Int 50, 95-98

Koshiya N, Smith JC (1999). Neuronal pacemaker for breathing visualized in vitro. Nature 400, 360-363

Kumral A, Yesilirmak DC, Aykan S, Genc S, Tugyan K, Cilaker S, Akhisaroglu M, Aksu I, Sutcuoglu S, Yilmaz O, Duman N, Ozkan H (2010) Protective effects of methylxanthines on hypoxia-induced apoptotic neurodegeneration and long-term cognitive functions in the developing rat brain. Neonatology 98, 128-136

Kuwana S, Okada Y, Natsui T (1998) Effects of extracellular calcium and magnesium on central respiratory control in the brainstem-spinal cord of neonatal rat. Brain Res 786, 194-204

Kuwana S, Tsunekawa N, Yanagawa Y, Okada Y, Kuribayashi J, Obata K (2006) Electrophysiological and morphological characteristics of GABAergic respiratory neurons in the mouse pre-Bötzinger complex. Eur J Neurosci 23, 667-674

Kuzemko JA, Paala J (1973) Apnoeic attacks in the newborn treated with aminophylline. Arch Dis Child 48, 404-406

Lauder JM, Bloom FE (1974) Ontogeny of monoamine neurons in the locus coeruleus, Raphe nuclei and substantia nigra of the rat. I. Cell differentiation. J Comp Neurol 155, 469-481

Law PY, Wong YH, Loh HH (2000) Molecular mechanisms and regulation of opioid receptor signaling. Annu Rev Pharmacol Toxicol 40, 389-430

Leusen I (1972) Regulation of cerebrospinal fluid composition with reference to breathing.
Physiol Rev 52, 1-56

Lieberman HR, Wurtman RJ, Emde GG, Roberts C, Coviella IL (1987) The effects of low doses of caffeine on human performance and mood. Psychopharmacology 92, 308-312

Lieske SP, Thoby-Brisson M, Telgkamp P, Ramirez JM (2000) Reconfiguration of the neural network controlling multiple breathing patterns: eupnea, sighs and gasps. Nat Neurosci 3, 600-607

Loh HH, Smith AP (1990) Molecular characterization of opioid receptors. Annu Rev Pharmacol Toxicol 30, 123-147

Lopez F, Miller LG, Greenblatt DJ, Kaplan GB, Shader RI (1989) Interaction of caffeine with the GABAA receptor complex: alterations in receptor function but not ligand binding. Eur J Pharmacol 172, 453-9

Lorier AR, Lipski J, Housley GD, Greer JJ, Funk GD (2008) ATP sensitivity of preBötzinger complex neurones in neonatal rat in vitro: mechanism underlying a P2 receptor-mediated increase in inspiratory frequency. J Physiol 586, 1429-1446

Lorier AR, Huxtable AG, Robinson DM, Lipski J, Housley GD, Funk GD (2007) P2Y1 receptor modulation of the pre-Botzinger complex inspiratory rhythm generating network in vitro. J Neurosci 27, 993-1005

Lorier AR, Lipski J, Housley GD, Greer JJ, Funk GD (2008) ATP sensitivity of preBötzinger complex neurones in neonatal rat in vitro: mechanism underlying a P2 receptor-mediated increase in inspiratory frequency. J Physiol 586, 1429-1446

Lu VB, Biggs JE, Stebbing MJ, Balasubramanyan S, Todd KG, Lai AY, Colmers WF, Dawbarn D, Ballanyi K, Smith PA (2009) Brain-derived neurotrophic factor drives the changes in excitatory synaptic transmission in the rat superficial dorsal horn that follow sciatic nerve injury. J Physiol 587, 1013-1032

Maeda T (2000) The locus coeruleus: history. J Chemical Neuroanatomy 18, 57-64

Magkos F, Kavouras SA (2005) Caffeine use in sports, pharmacokinetics in man, and cellular mechanisms of action. Crit Rev Food Sci Nutr 45, 535-562

Manzke T, Guenther U, Ponimaskin EG, Haller M, Dutschmann M, Schwarzacher S, Richter DW (2003) 5-$HT_{4(a)}$ receptors avert opioid-induced breathing depression without loss of analgesia. Science 301, 226-229

Marshall KC, Christie MJ, Finlayson PG, Williams JT (1991) Developmental aspects of the locus coeruleus-noradrenaline system. Progr Brain Res 88, 173-185

Martin RJ, Abu-Shaweesh JM, Baird TM (2004) Apnoea of prematurity. Paediatr Respir Rev 5, 377-382

Martin RJ, Abu-Shaweesh JM (2005) Control of breathing and neonatal apnea. Biol Neonate 87, 288-295

Mason ST, Fibiger HC (1979) Regional topography within noradrenergic locus coeruleus as revealed by retrograde transport of horseradish peroxidase. J Comp Neurol 187, 703-724

Matute C, Cavaliere F (2011) Neuroglial interactions mediated by purinergic signalling in the pathophysiology of CNS disorders. Semin Cell Dev Biol 22, 252-259

Maubecin VA, Williams JT (1999) Developmental changes that regulate the activity of locus coeruleus neurons. Tokai J Exp Clin Med 24, 41-51

McPherson PS, Kim YK, Valdivia H, Knudson CM, Takekura H, Franzini-Armstrong C, Coronado R, Campbell KP (1991) The brain ryanodine receptor: a caffeine-sensitive calcium release channel. Neuron 7, 17-25

Mellen NM, Janczewski WA, Bocchiaro CM, Feldman JL (2003) Opioid-induced quantal slowing reveals dual networks for respiratory rhythm generation. Neuron 37, 821-826

Millar D, Schmidt B (2004) Controversies surrounding xanthine therapy. Semin Neonatol 9, 239-244

Miller MJ, Martin RJ. (1992) Apnea of prematurity. Clinics Perinatology 19, 789-808

Mironov SL, Langohr K, Richter DW (1999) Al adenosine receptors modulate respiratory activity of the neonatal mouse via the cAMP-mediated signaling pathway. J Neurophysiol 81, 247-255

Mishra S, Agarwal R, Jeevasankar M, Aggarwal R, Deorari AK, Paul VK (2008) Apnea in the newborn. Indian J Pediatr 75, 57-61

Montandon G, Kinkead R, Bairam A (2008a) Adenosinergic modulation of respiratory activity: developmental plasticity induced by perinatal caffeine administration. Resp Physiol Neurobiol 164, 87-95

Montandon G, Bairam A, Kinkead R (2008b) Neonatal caffeine induces sex-specific developmental plasticity of the hypoxic respiratory chemoreflex in adult rats. Am J Physiol Regul Integr Comp Physiol 295, 922-934

Montandon G, Horner RL, Kinkead R, Bairam A (2009) Caffeine in the neonatal period induces long-lasting changes in sleep and breathing in adult rats. J Physiol 587, 5493-5507

Montandon G, Qin W, Liu H, Ren J, Greer JJ, Horner RL (2011) PreBotzinger complex neurokinin-1 receptor-expressing neurons mediate opioid-induced respiratory depression. J Neurosci 31, 1292-1301

Moriceau S, Roth TL, Sullivan RM (2010) Rodent model of infant attachment learning and stress. Dev Psychobiol 52, 651-660

Morin-Surun MP, Gacel G, Champagnat J, Denavit-Saubie M, Roques BP (1984) Pharmacological identification of delta and mu opiate receptors on bulbar respiratory neurons. Eur J Pharmacol 98, 241-247

Murai Y, Akaike T (2005) Orexins cause depolarization via nonselective cationic and K+ channels in isolated locus coeruleus neurons. Neurosci Res 51, 55-65

Murrin LC, Sanders JD, Bylund DB (2007) Comparison of the maturation of the adrenergic and serotonergic neurotransmitter systems in the brain: implications for differential drug effects on juveniles and adults. Biochem Pharmacol 73, 1225-1236

Nakada T, Kwee IL, Lerner AM, Remler MP (1983) Theophylline-induced seizures: clinical and pathophysiologic aspects. Western J Med 138, 371-374

Nakamura S, Kimura F, Sakaguchi T (1987) Postnatal development of electrical activity in the locus ceruleus. J Neurophysiol 58, 510-524

Naqui SZ, Harris BS, Thomaidou D, Parnavelas JG (1999) The noradrenergic system influences the fate of Cajal-Retzius cells in the developing cerebral cortex. Dev Brain Res 113, 75-82

Nehlig A, Daval JL, Debry G (1992) Caffeine and the central nervous system: mechanisms of action, biochemical, metabolic and psychostimulant effects. Brain Res Rev 17, 139-170

Nestler EJ, Alreja M, Aghajanian GK (1999) Molecular control of locus coeruleus neurotransmission. Biol Psychiatry 46, 1131-1139

Oertel BG, Felden L, Tran PV, Bradshaw MH, Angst MS, Schmidt H, Johnson S, Greer JJ, Geisslinger G, Varney MA, Lotsch J (2010) Selective antagonism of opioid-induced ventilatory depression by an ampakine molecule in humans without loss of opioid analgesia. Clin Pharmacol Ther 87, 204-211

Olpe HR, Steinmann M (1991) Responses of locus coeruleus neurons to neuropeptides. Progr Brain Res 88, 241-248

Onimaru H, Homma I (2003) A novel functional neuron group for respiratory rhythm generation in the ventral medulla. J Neurosci 23, 1478-1486

Onimaru H, Arata A, Homma I (1987) Localization of respiratory rhythm-generating neurons in the medulla of brainstem-spinal cord preparations from newborn rats. Neurosci Lett 78, 151-155

Onimaru H, Kumagawa Y, Homma I (2006) Respiration-related rhythmic activity in the rostral medulla of newborn rats. J Neurophysiol 96, 55-61

Onimaru H, Ikeda K, Kawakami K (2009) $Phox_{2b}$, RTN/pFRG neurons and respiratory rhythmogenesis. Respir Physiol Neurobiol 168, 13-18

Oyamada Y, Ballantyne D, Mückenhoff K, Scheid P (1998) Respiration-modulated membrane potential and chemosensitivity of locus coeruleus neurones in the in vitro brainstem-spinal cord of the neonatal rat. J Physiol 513, 381-398

Oyamada Y, Andrzejewski M, Mückenhoff K, Scheid P, Ballantyne D (1999) Locus coeruleus neurones in vitro: pH-sensitive oscillations of membrane potential in an electrically coupled network. Resp Physiol Neurobiol 118, 131-147

Pagliardini S, Adachi T, Ren J, Funk GD, Greer JJ (2005) Fluorescent tagging of rhythmically active respiratory neurons within the pre-Bötzinger complex of rat medullary slice preparations. J Neurosci 25, 2591-2596

Paspalas CD, Papadopoulos GC (1996) Ultrastructural relationships between noradrenergic nerve fibers and non-neuronal elements in the rat cerebral cortex. Glia 17, 133-146

Pattinson KT (2008) Opioids and the control of respiration. Br J Anaesth 100, 747-758

Pert CB, Snyder SH (1973) Opiate receptor: demonstration in nervous tissue. Science 179, 1011-1014

Pierrefiche O, Schwarzacher SW, Bischoff AM, Richter DW (1998) Blockade of synaptic inhibition within the pre-Bötzinger complex in the cat suppresses respiratory rhythm generation in vivo. J Physiol 509, 245-254

Porter JT, McCarthy KD (1997) Astrocytic neurotransmitter receptors in situ and in vivo. Progr Neurobiol 51, 439-455

Ramirez JM, Garcia A 3rd (2007) Point: Medullary pacemaker neurons are essential for both eupnea and gasping in mammals. J Appl Physiol 103, 717-718; discussion 722

Ramirez JM, Viemari JC (2005) Determinants of inspiratory activity. Respir Physiol Neurobiol 147, 145-157

Reid PG, Watt AH, Penny WJ, Newby AC, Smith AP, Routledge PA (1991) Plasma adenosine concentrations during adenosine-induced respiratory stimulation in man. Eur J Clin Pharmacol 40, 175-180

Rekling JC, Champagnat J, Denavit-Saubi M (1996) Electroresponsive properties and membrane potential trajectories of three types of inspiratory neurons in the newborn mouse brain stem in vitro. J Neurophysiol 75, 795-810

Ren, J, Poon, BY, Tang, Y, Funk, GD, Greer, JJ (2006) Ampakines alleviate respiratory depression in rats. Am J Respir Crit Care Med 174, 1384–1391

Ren J, Ding X, Funk GD, Greer JJ (2009) Ampakine CX717 protects against fentanyl-induced respiratory depression and lethal apnea in rats. Anesthesiology 110, 1364-1370

Richter DW, Spyer KM (2001) Studying rhythmogenesis of breathing: comparison of in vivo and in vitro models. Trends Neurosci 24, 464-472

Richter DW, Ballanyi K, Schwarzacher S (1992) Mechanisms of respiratory rhythm generation. Curr Opin Neurobiol 2, 788-793

Richter DW, Lalley PM, Pierrefiche O, Haji A, Bischoff AM, Wilken B, Hanefeld F (1997) Intracellular signal pathways controlling respiratory neurons. Respir Physiol Neurobiol 110, 113-123

Rizzuto R (2001) Intracellular Ca^{2+} pools in neuronal signalling. Curr Opin Neurobiol 11, 306-311

Ruangkittisakul A, Ballanyi K (2006) Reversal by phosphodiesterase-4 blockers of in vitro apnea in the isolated brainstem-spinal cord preparation from newborn rats. Neurosci Lett 401, 194-198

Ruangkittisakul A, Ballanyi K (2010) Methylxanthine reversal of opioid-evoked inspiratory depression via phosphodiesterase-4 blockade. Resp Physiology Neurobiol 172, 94-105

Ruangkittisakul A, Schwarzacher SW, Ma Y, Poon B, Secchia L, Funk GD, Ballanyi K (2006) High sensitivity to neuromodulator-activated signalling pathways at physiological [K^+] of confocally-imaged respiratory centre neurons in online-calibrated newborn rat brainstem slices. J Neurosci 26, 11870-11880

Ruangkittisakul A, Secchia L, Bornes TD, Palathinkal DM, Ballanyi K (2007) Dependence on extracellular Ca^{2+}/K^+ antagonism of inspiratory centre rhythms in slices and en bloc preparations of newborn rat brainstem. J Physiol 584, 489-508

Ruangkittisakul A, Schwarzacher SW, Secchia L, Ma Y, Bobocea N, Poon BY, Funk GD, Ballanyi K (2008) Generation of eupnea and sighs by a spatiochemically organized inspiratory network. J Neurosci 28, 2447-2458

Ruangkittisakul A, Okada Y, Oku Y, Koshiya N, Ballanyi K (2009) Fluorescence Imaging of active respiratory networks. Resp Physiol Neurobiol 168, 26-38

Ruangkittisakul A, Panaitescu B, Ballanyi K (2011) K^+ and Ca^{2+} dependence of inspiratory-related rhythm in novel "calibrated" mouse brainstem slices. Resp Physiol Neurobiol 175, 37-48

Ruangkittisakul A, Secchia-Ballanyi L, Panaitescu B, Bobocea N, Kuribayashi J, Iizuka M, Kantor C, Ballanyi K (2012) Anatomically 'calibrated' isolated respiratory networks from newborn rodents. In Isolated Central Nervous System Circuits (Ed K Ballanyi), Neuromethods Series Vol 73 (Ed W Walz). Springer Science+Business Media, LLC, New York, NY, 61-124

Samuels ER, Szabadi E (2008) Functional neuroanatomy of the noradrenergic locus coeruleus: its roles in the regulation of arousal and autonomic function part II: physiological and pharmacological manipulations and pathological alterations of locus coeruleus activity in humans. Curr Neuropharmacol 6, 254-285

Santiago TV, Edelman NH (1985) Opioids and breathing. J Appl Physiol 59, 1675-1685

Schmidt B, Roberts RS, Davis P, Doyle LW, Barrington KJ, Ohlsson A, Solimano A, Tin W (2007) Long-term effects of caffeine therapy for apnea of prematurity. N Engl J Med 357, 1893-1902

Schmidt B, Roberts RS, Davis P, Doyle LW, Barrington KJ, Ohlsson A, Solimano A, Tin W (2006) Caffeine therapy for apnea of prematurity. N Engl J Med 354, 2112-2121

Schwarzacher SW, Smith JC, Richter DW (1995) Pre-Bötzinger complex in the cat. J Neurophysiol 73, 1452-1461

Shao XM, Feldman JL (1997) Respiratory rhythm generation and synaptic inhibition of expiratory neurons in pre-Bötzinger complex: differential roles of glycinergic and GABAergic neural transmission. J Neurophysiol 77, 1853-1860

Shi D, Padgett WL, Daly JW (2003) Caffeine analogs: effects on ryanodine-sensitive calcium-release channels and GABAA receptors. Cell Mol Neurobiol 23, 331-47

Shvarev YN, Lagercrantz H, Yamamoto Y (2003) Two types of rhythm in the respiratory network output in the isolated ventrolateral medulla in the neonatal rats. Neurosci Lett 347, 53-56

Simon EJ, Hiller JM, Edelman I (1973) Stereospecific binding of the potent narcotic analgesic (3H) Etorphine to rat-brain homogenate. Proc Natl Acad Sci USA 70, 1947-1949

Smit HJ, Rogers PJ (2000) Effects of low doses of caffeine on cognitive performance, mood and thirst in low and higher caffeine consumers. Psychopharmacology 152, 167-173

Smith JC, Greer JJ, Liu GS, Feldman JL (1990) Neural mechanisms generating respiratory pattern in mammalian brain stem-spinal cord in vitro. I. Spatiotemporal patterns of motor and medullary neuron activity. J Neurophysiol 64, 1149-1169

Smith JC, Ellenberger HH, Ballanyi K, Richter DW, Feldman JL (1991) Pre-Botzinger complex: a brainstem region that may generate respiratory rhythm in mammals. Science 254, 726-729

Smith JC, Ballanyi K, Richter DW (1992) Whole-cell patch-clamp recordings from respiratory neurons in neonatal rat brainstem in vitro. Neurosci Lett 134, 153-156

Smith JC, Butera RJ, Koshiya N, Del Negro C, Wilson CG, Johnson SM (2000) Respiratory rhythm generation in neonatal and adult mammals: the hybrid pacemaker-network model. Resp Physiol Neurobiol 122, 131-147

Smith JC, Abdala AP, Rybak IA, Paton JF (2009) Structural and functional architecture of respiratory networks in the mammalian brainstem. Philos Trans R Soc Lond B Biol Sci 364, 2577-2587

Smythies J (2005) Section III. The norepinephrine system. Interntl Rev Neurobiol 64, 173-211

Soderling SH, Beavo JA (2000) Regulation of cAMP and cGMP signaling: new phosphodiesterases and new functions. Curr Opin Cell Biol 12, 174-179

Somjen GG (2002) Ion Regulation in the brain: implications for pathophysiology. Neuroscientist 8, 254-267

Spyer KM, Gourine AV (2009) Chemosensory pathways in the brainstem controlling cardiorespiratory activity. Philos Trans R Soc Lond B Biol Sci 364, 2603-2610

Srinivasan G, Singh J, Cattamanchi G, Yeh TF, Pildes RS (1983) Plasma glucose changes in preterm infants during oral theophylline therapy. J Pediatr 103, 473-476

Sugimoto T, Sugimoto M, Uchida I, Mashimo T, Okada S (2001) Inhibitory effect of theophylline on recombinant $GABA_A$ receptor. Neuroreport 12, 489-493

Sutin EL, Jacobowitz DM (1991) Neurochemicals in the dorsal pontine tegmentum. Progr Brain Res 88, 3-14

Suzue T (1984) Respiratory rhythm generation in the in vitro brain stem-spinal cord preparation of the neonatal rat. J Physiol 354, 173-183

Taccola G, Secchia L, Ballanyi K (2007) Anoxic persistence of lumbar respiratory bursts and block of lumbar locomotion in newborn rat brainstem spinal cords. J Physiol 585, 507-524

Takeda S, Eriksson LI, Yamamoto Y, Joensen H, Onimaru H, Lindahl SG (2001) Opioid action on respiratory neuron activity of the isolated respiratory network in newborn rats. Anesthesiology 95, 740-749

Tanabe A, Fujii T, Onimaru H (2005) Facilitation of respiratory rhythm by a mu-opioid agonist in newborn rat pons-medulla-spinal cord preparations. Neurosci Lett 375, 19-22

Tchekalarova J, Kubova H, Mares P (2007) Effects of postnatal caffeine exposure on seizure susceptibility in developing rats. Brain Res 1150, 32-39

Terenius L (1973) Stereospecific interaction between narcotic analgesics and a synaptic plasm a membrane fraction of rat cerebral cortex. Acta Pharmacol Toxicol 32, 317-320

Tryba AK, Peña F, Ramirez JM (2003) Stabilization of bursting in respiratory pacemaker neurons. J Neurosci 23, 3538-3546

Ukena D, Schudt C, Sybrecht GW (1993) Adenosine receptor-blocking xanthines as inhibitors of phosphodiesterase isozymes. Biochem Pharmacol 45, 847-851

Uneyama H, Harata N, Akaike N (1993) Caffeine and related compounds block inhibitory amino acid-gated Cl- currents in freshly dissociated rat hippocampal neurones. Br J Pharmacol 109, 459-65

Van Bockstaele EJ, Reyes BA, Valentino RJ (2010) The locus coeruleus: A key nucleus where stress and opioids intersect to mediate vulnerability to opiate abuse. Brain Res 1314, 162-174

Viemari JC, Bevengut M, Burnet H, Coulon P, Pequignot JM, Tiveron MC, Hilaire G (2004) Phox2a gene, A6 neurons, and noradrenaline are essential for development of normal respiratory rhythm in mice. J Neurosci 24, 928-937

Waldhoer M, Bartlett SE, Whistler JL (2004) Opioid receptors. Ann Rev Biochemistry 73, 953-990

Walter-Nicolet E, Annequin D, Biran V, Mitanchez D, Tourniaire B (2010) Pain management in newborns: from prevention to treatment. Paediatr Drugs 12, 353-365

Wang YY, Aghajanian GK (1990) Excitation of locus coeruleus neurons by vasoactive intestinal peptide: role of a cAMP and protein kinase A. J Neurosci 10, 3335-3343

Wang JL, Wu ZH, Pan BX, Li J (2005) Adenosine Al receptors modulate the discharge activities of inspiratory and biphasic expiratory neurons in the medial region of Nucleus Retrofacialis of neonatal rat in vitro. Neurosci Lett 379, 27-31

Wilken B, Ramirez JM, Hanefeld F, Richter DW (2000) Aminophylline modulation of the mouse respiratory network changes during postnatal maturation. J Appl Physiol 89, 2015-2022

Williams JT, Marshall KC (1987) Membrane properties and adrenergic responses in locus coeruleus neurons of young rats. J Neurosci 7, 3687-3694

Williams JT, Egan TM, North RA (1982) Enkephalin opens potassium channels on mammalian central neurones. Nature 299, 74-77

Williams JT, North RA, Shefner SA, Nishi S, Egan TM (1984) Membrane properties of rat locus coeruleus neurones. Neuroscience 13, 137-156

Williams JT, Christie MJ, Manzoni O (2001) Cellular and synaptic adaptations mediating opioid dependence. Physiol Rev 81, 299-343

Winter SM, Hirrlinger J, Kirchhoff F, Hülsmann S (2007) Transgenic expression of fluorescent proteins in respiratory neurons. Respir Physiol Neurobiol 159, 108-114

Winter SM, Fresemann J, Schnell C, Oku Y, Hirrlinger J, Hülsmann S (2009) Glycinergic interneurons are functionally integrated into the inspiratory network of mouse medullary slices. Eur J Physiol (Pflüger's Arch) 458, 459-469

Yoshikawa H (2007) First-line therapy for theophylline-associated seizures. Acta Neurol Scand Suppl 186, 57-61

Yuste R, Konnerth A, Masters B (2006) Imaging in neuroscience and development, a laboratory manual. J Biomed Opt 11, 19902

Zhao J, Gonzalez F, Mu D (2011) Apnea of prematurity: from cause to treatment. Eur J Pediatrics 170, 1097-1105

Zwicker JD, Rajani V, Hahn LB, Funk GD (2011) Purinergic modulation of preBötzinger complex inspiratory rhythm in rodents: the interaction between ATP and adenosine. J Physiol 589, 4583-4600

CHAPTER 2

Methods

Fragments of this chapter have been published as:

Kantor C^{+}, Panaitescu B^{+}, Kuribayashi J, Ruangkittisakul A, Lee TF, Cheung PY, MacTavish D, Jhamandas J, Ballanyi K (2012) Electrophysiological imaging of early network oscillations in brain slices from newborn rats and piglets. In Isolated Central Nervous System Circuits (Ed K Ballanyi), Neuromethods Series Vol 73 (Ed W Walz). Springer Science+Business Media, LLC, New York, NY, 315-356

Panaitescu B^{+}, Ruangkittisakul A^{+}, Ballanyi K (2009) Silencing by raised extracellular Ca^{2+} of pre-Bötzinger complex neurons in newborn rat brainstem slices without change of membrane potential or input resistance. Neurosci Lett 456, 25-29

Ruangkittisakul A, Secchia-Ballanyi L, Panaitescu B, Bobocea N, Kuribayashi J, Iizuka M, Kantor C, Ballanyi K (2012) Anatomically 'calibrated' isolated respiratory networks from newborn rodents. In Isolated Central Nervous System Circuits (Ed K Ballanyi), Neuromethods Series Vol 73 (Ed W Walz). Springer Science+Business Media, LLC, New York, NY, 61-124

$^{+}$Authors contributed equally to the study

2.1 Preparations and Solutions

The experiments were performed on *en bloc* brainstem-spinal cords, transverse brainstem slices or horizontal brain slices from P0-4 Sprague-Dawley or Wistar rats **(Figs. 1-11, 2-1)** (for more details see Kantor et al., 2012; Ruangkittisakul et al., 2012). All procedures were done in compliance with the guidelines of the Canadian Council for Animal Care and with approval of the University of Alberta Health Animal Care and Use Committee for Health Sciences. Because there was no apparent major difference between findings, data obtained from either rat strain were pooled. Animals were anesthetized with isoflurane vapor until disappearance of the paw withdrawal reflex. Following decerebration, the neuraxis (for respiratory models) or brain without spinal cord (for LC slices) were isolated at 18-21 ^{o}C in 'standard' solution containing (in mM) 120 NaCl, 3 KCl, 1 (or 1.2) $CaCl_2$, 2 $MgSO_4$, 26 $NaHCO_3$, 1.25 NaH_2PO_4, and 30 (for *en bloc* models), 20 (preBötC slices) or 10 (LC slices), D-glucose; pH was adjusted to 7.4 by gassing with 95% O_2, 5% CO_2. The same solution was used for studying the isolated brainstem models in the recording chambers for electrophysiology and imaging (see below) **(Fig. 2-2)**.

Importantly, this standard superfusate contains physiological concentrations of K^+ and Ca^{2+} which both have a major influence on biophysical plasma membrane properties of excitable cells (Hansen, 1985; Hille, 2002; Somjen, 2002). The latter three publications point out that K^+ in the extracellular space of mammalian central nervous tissues is regulated closely to 3 mM whereas interstitial Ca^{2+}

ranges between 1-1.2 mM, depending on the brain area and the method used for its determination. For further information in that regard, see Ruangkittisakul et al. (2007).

As outlined above (Chapter **1.4**), preBötC slices are typically studied in high (mostly 7-9 mM) K^+, which however affects some biophysical and pharmacological properties of isolated inspiratory networks. For these reasons, our group has developed calibrated preBötC slices with defined rostrocaudal boundaries that generate, at a thickness of ≥500 μm, inspiratory rhythm for several hours in solution with $3K^+/1Ca^{2+}$ (Chapter **1.3**) (Ruangkittisakul et al., 2006, 2008; Ballanyi & Ruangkittisakul, 2009). At the same time, our laboratory showed that preBötC bursting in newborn rat calibrated slices is very much depressed or even abolished upon raising Ca^{2+} from 1 to 1.5 mM and that this depression is countered by elevating K^+ to >6 mM (Ruangkittisakul et al., 2007). The latter study showed that this Ca^{2+}/K^+ antagonism also determines inspiratory rhythms in the newborn rat *en bloc* model if the preBötC is located close to the rostral brainstem section level **(Fig. 2-1)**.

For Project-1 of this thesis, I planned to firstly study the cellular mechanism underlying the depression of preBötC bursting by raised Ca^{2+}. For this, superfusate Ca^{2+} was raised from its 1 mM control level to up to 3 mM. Secondly, I wished to investigate the quantitative relationship between superfusate K^+ and Ca^{2+} that provides stable rhythm for several hours in the novel m-preBötC[400].

These slices were kept for at least 20 min in a solution containing a particular concentration of K^+ and Ca^{2+} to determine the steady-state characteristics of rate, duration and amplitude of preBötC (-driven) rhythms. In a further approach, these slices were kept right from the start in solution with 1 mM Ca^{2+} and 3-6 mM K^+ to determine the longevity of rhythms. For other projects, the μ-opioid receptor agonist DAMGO (Chapter **1.5**) and/or methylxanthines (Chapter **1.7**) were bath-applied, and their basic actions were assessed while these responses were also modulated by various other neuromodulators. Each of the agents was applied at least for 20 min, or until a steady-state of the effect was reached. Recovery from effects was tested after 20 min or longer time periods when the effect persisted for >20 min. Details regarding specific application protocols are described in the individual project chapters.

2.2 Agents

The following agents were used: rolipram (5 μM, 10 mM in dimethyl sulfoxide [DMSO]), theophylline (0.25-10 mM; added to superfusate), caffeine (0.25-10 mM; added to superfusate), [D-Ala^2,N-Me-Phe^4,Gly^5-ol]-Enkephalin (DAMGO, 0.01-1 μM; 10 mM in H_2O), (+)-bicuculline (10-25 μM; 25 mM in DMSO), muscimol (1-2.5 μM; 10 mM in H_2O), strychnine hydrochloride (5 μM; 5 mM in H_2O), isobuthylmethylxanthine (IBMX, 100μM; 100 mM in DMSO), forskolin (25 μM; 50 mM in DMSO), 8-Cyclopentyl-1,3-dipropylxanthine (DPCPX, 2 μM; 25 mM in DMSO), 3,7-Dimethyl-1-propargyl-xanthine (DMPX, 10 μM; 25 mM

in DMSO), naloxone (1 μM; 1 mM in H_2O), cyclopiazonic acid (CPA, 30 μM, 100 mM in DMSO), tetrodotoxin (TTX, 0.5 μM; 1 mM in H_2O), glutamate (1 mM; 1 M in H_2O), Fluo-4 acetoxy-methyl (Fluo-4 AM, stock 5 mM in pluronic acid, 20% in dimethyl sulfoxide further diluted to 0.5 mM in superfusate); fixation solution (4% paraformaldehyde in phosphate buffer, i.e. 1:2 mixture of 0.1 M NaH_2PO_4 + 0.1 M Na_2HPO_4 in H_2O, pH 7.2), staining solution (1% thionin acetate in 0.1 M sodium acetate trihydrate + 0.1 M acetic acid), sulforhodamine-101 (SR101, added to superfusate. Agents were obtained from Sigma-Aldrich (Canada) except salts for superfusate, sodium acetate trihydrate, acetic acid (Fisher Scientific, Ottawa, Ontario, Canada), theophylline, glutamate (ICN Biomedicals, Costa Mesa, California, USA), Fluo-4-AM (Invitrogen, Carlsbad, CA, USA).

2.3 Spontaneously Active Newborn Rat Brainstem *En Bloc* and Slice Models

Calibrated m-preBötC[400] slices were developed by me to study bursting in the preBötC and cranial XII inspiratory motor networks in the absence of major influences from rostrally and caudally adjacent (respiratory) structures while preserving a major portion of the often coronally oriented dendritic tree of preBötC neurons (Ballanyi & Ruangkittisakul, 2009) (Chapter **1.9**) **(Figs. 1-3, 2-1)**. Specifically, these slices were used for studying (*i*) preBötC modulation by Ca^{2+} (Project-1), (*ii*) countering of opioid depression of preBötC bursting by

methylxanthines (Project-2) and (*iii*) potential of methylxanthines to evoke seizure-like bursting in inspiratory networks (Project-3). For generating such slices, a brainstem block was glued rostral side down to a metal plate after removal of the cerebellum and transections just rostral to the caudal cerebellar artery and slightly rostral to C_1 **(Figs. 1-3, 2-1)** (Ruangkittisakul et al., 2006, 2012). Serial 100 μm sections were made in caudal-to-rostral direction using a vibratome (VT1000S, Leica Microsystems, Richmond Hill, ON, Canada). Sectioning was stopped, and a single m-preBötC[400] slice was cut, when 'online histology' revealed (respiratory) marker structures, particularly the inferior olive, with a specific distance to VII_c (Ruangkittisakul et al., 2006, 2008) **(Figs. 1-3, 2-1)**. For example, in 76 slices used for Project-3, the mean caudal and rostral slice margins were -0.71 ± 0.04 and -0.33 ± 0.75 mm caudal to VII_c. This value was very close to the optimal boundaries of -0.7 and -0.3 caudal to VII_c.

In addition to studying m-preBötC[400] slices, three different types of *en bloc* models were used in Project-3 for analyzing methylxanthine-evoked hyperexcitability in the preBötC and preBötC-driven spinal motor networks (**Fig. 2-1)**. Firstly, experiments were done on the 'Suzue' preparation (Suzue, 1984; Ballanyi et al., 1999; Ruangkittisakul et al., 2012) in which the preBötC interacts with pre/post-inspiratory active pFRG neurons (Chapter **1.2**) **(Figs. 1-1, 2-1)**. For generating this preparation, the isolated brainstem was transected rostrally at the caudal cerebellar artery and thus contained the VII motor nucleus ('*en bloc* [+VII] model') while the spinal cord was cut at the last cervical (C_8) or first thoracic (T_1)

level **(Fig. 2-1)**.

For investigating whether methylxanthines evoke hyperexcitability primarily in respiratory or non-respiratory motoneurons, *en bloc* [+VII] preparations with rostral and caudal boundaries identical to those in the Suzue model were isolated with the cervical and brachial plexuses for simultaneous suction electrode recording from the 4th cervical root (C_4) plus phrenic and musculocutaneous nerves **(Fig. 2-1)**. Inspiratory active ventral cervical nerve roots (C_1-C_8) contain axons from both inspiratory and non-respiratory motor neurons, whereas the phrenic nerve contains solely axons from inspiratory (phrenic) motoneurons, while musculocutaneous nerve contains motor axons innervating arm muscles (Ballanyi et al., 1999; Cho et al., 2007; Greene, 1935).

Finally, calibrated *en bloc* preparations were used **(Fig. 2-1)** in which brainstem transection exposed the preBötC more or less to the rostral cut surface (Ruangkittisakul et al., 2007). In newborn rats, the preBötC extends within the VRC between -0.4 and -0.6 mm caudal to VII_c (Chapter **1.4**), and spans the most anterior XII nerve root as a ventral brainstem surface landmark (Ruangkittisakul et al., 2006, 2007, 2008) **(Figs. 1-3, 2-1)**. In 7 such preparations, the mean rostral transection was located at -0.22 ± 0.10 mm caudal to VII_c. In this transected model, the RTN/pFRG complex does not seem to be active based on the absence of pre/post-inspiratory activity in lumbar nerves that normally drives abdominal expiratory muscles (Chapter **1.2**, **1.5**) (Janczewski et al., 2002; Ruangkittisakul et

al., 2007; Taccola et al., 2007). In these preparations, the cord was transected between T_2 to T_3 and suction electrodes were used for simultaneous recording of inspiratory rhythms from ventral spinal nerves and also in the ventrolateral aspect of the cut medullary surface containing the exposed preBötC **(Fig. 2-1)**.

For Project-4, LC slices of 400 μm thickness were generated using the same solutions and slicing procedures as described above for m-preBötC[400] slices (Kantor et al., 2012). However, for their generation, the brain, including the rostral pons and cerebellum, from P1-4 rats were isolated and glued ventral side down to the vise of the vibratome. Horizontal sections were cut from anterior to posterior direction to avoid tearing of the fourth ventricle. Initial sections were cut at 400-600 μm steps until the apex of the fourth ventricle appears. Slice thickness was then reduced to 100 μm when approaching the LC. Once the LC started to appear in the 100 μm thin section as a dark oval area located close to the lateral border of the fourth ventricle as inspected under a microscope, one 400 μm thick brain slice was cut. Either a complete or hemisected LC slice was used for some aspects of Project-4.

After immediate transfer to an acrylic recording chamber (volume ~2 ml), a LC slice, *en bloc* preparation or m-preBötC[400] slice (the latter with caudal side up) were mechanically fixed with insect pins inserted into the sylgard layer covering the bottom of the chamber **(Fig. 2-2)**. Two pins were positioned at the rostral and caudal ends of brainstem-spinal cords or at the dorsolateral slice margins (for m-

preBötC[400] slices) and further mechanical stabilization was achieved by suction electrode(s) positioned carefully on the slice surface. For imaging experiments, a titanium harp with threads was placed on top of the slice to hold it in place. Superfusate was applied at a flow rate of 5 ml/min via a peristaltic pump (Watson-Marlow Alitea-AB, Sin-Can, Calgary, AB, Canada) and kept at 25-27 ^{o}C in the recording chamber via a TC-324B heat control system (Harvard Apparatus, Saint-Laurent, QC, Canada) in conjunction with a circulating water bath (DC 10, Thermo-Haake, Fisher Scientific, Nepean, ON, Canada) **(Fig. 2-2)**. After experiments, preparations were chemically fixed in 4% paraformaldehyde and stained with thionin for photographing and histological documentation (Chapter **2.6**) (Ruangkittisakul et al., 2006, 2007, 2008) **(Fig. 2-1)**.

2.4 Electrophysiological Recording

In all *in vitro* models used for this thesis (Chapter **2.3**), synchronized rhythmic ('phasic') neuronal activities were recorded with suction electrodes. In the slices, such suction electrode recording was often combined with 'blind' whole-cell patch-clamp membrane potential recording (Blanton et al., 1989; Smith et al., 1991, 1992; Onimaru et al., 1996; Ruangkittisakul et al., 2012).

2.4.1 Suction Electrode Recording

Neuronal population discharge was recorded with suction electrodes (outer ø 80-250 μm) that were filled with standard superfusate (Chapter **2.1**). Extracellular

inspiratory or non-respiratory discharge in preBötC-driven spinal motoneurons was monitored from cervical roots or phrenic and musculocutaneous nerves (see above). In slices and *en bloc* preparations with rostrally exposed preBötC, suction electrodes were also used for recording 'VRC rhythm', i.e. inspiratory population activity in the ventrolateral slice or cut en bloc brainstem surface area containing the preBötC. In slices, a further suction electrode was positioned in the XII nucleus and, in ~30% of cases, also at the distal end of a XII nerve root for recording cranial inspiratory motor output (Ballanyi et al., 1999; Greer & Funk, 2005; Feldman & Del Negro, 2006; Ballanyi & Ruangkittisakul, 2009). In the LC slices, suction electrode recording revealed rhythmic bursting from populations of synchronized neurons (Christie et al., 1989; Christie, 1997) **(Fig. 1-11)**. Electrode signals were amplified (x10k) and band-pass filtered (0.3-3 kHz) using a Model-1700 differential amplifier (AM-Systems, Sequim, WA, USA) plus integrated (□: 10-50 ms) using an MA-821/RSP (CWE; www.cwe-inc.com) prior to digital recording at a rate of 1 kHz (Powerlab/8SP, ADInstruments, Colorado Springs, CO, USA). Based on such electronic signal processing, rhythmic activities appear as upward deflections in the illustrated traces. Importantly, a change in the baseline of these integrated ('moving average') signals may indicate a change in the activity of tonically active neurons, emergence of activity of quiescence neurons, or emergence of neuronal firing during expiratory phase (Ballanyi & Ruangkittisakul, 2009; Panaitescu et al., 2009).

2.4.2 Whole-cell Recording

For whole-cell recording, patch pipettes (outer tip Ø: 2-3 μm) were pulled from borosilicate glass capillaries (GC-150TF-10; 1.5 mm outer ø; 1.17 mm inner ø; Harvard Apparatus, Saint-Laurent, QC, Canada) and filled with (in mM): 140 K-gluconate, 1 NaCl, 0.5 $CaCl_2$, 1 $MgCl_2$, 1 K_4-BAPTA, 1 Na_2-ATP and 10 Hepes; pH was adjusted to 7.4 with KOH; dc resistance in superfusate was 4-9 MΩ. Using a motor-driven micromanipulator with display of recording depth (7600, Siskiyou Corporation, Grant Pass, OR, USA), patch electrodes were advanced perpendicularly into the preBötC region that was not used for VRC recording **(Fig. 2-2)**. Inspiratory neurons were identified by their rhythmic extracellular discharge which was in phase with contralateral VRC population bursting. 'Tonic' neurons were characterized by regular extracellular discharge of single action potentials at a rate of 1-10 Hz that was not changed during contralateral inspiratory VRC bursting. Augmentation by up to 300% of a voltage signal in response to repetitive injection of negative dc current pulses (1 nA, 20 ms) indicated that the electrode was close to a neuronal plasmalemmal membrane **(Fig. 2-3)**. Positive pressure (20 mmHg) was then released and negative pressure was applied for 'giga seal' (>1 GΩ) formation before the whole-cell configuration was established by abrupt suction (~100 mmHg) **(Fig. 2-3)**. At resting potential, which was not corrected for liquid junction potentials (Onimaru et al., 1996; Ruangkittisakul et al, 2012), input resistance was measured via repetitive (interval 5-15 s) injection of hyperpolarizing dc current pulses (40-250 pA, 0.5-0.7 s). Settings for series resistance compensation using the 'bridge' recording mode of

the ‘sample-and-hold’ single-electrode voltage-clamp amplifier (npi electronic, Tamm, Germany) were checked every 3-6 min and eventually corrected. Similar to suction electrode signals (Chapter **2.4.1**), intracellular recordings were sampled at 4 kHz into a different channel of the digital recorder. For identification of the location of the recorded presumptive preBötC neuron, the recording depth as indicated by the micromanipulator display was compared with the anatomical margins of the post-experiment thionin-stained slices (Chapter **2.3, 2.6**). The same electrophysiological approach was used for blind whole-cell recording from LC neurons in the 400 µm thick horizontal brainstem slices.

2.5 Multiphoton/Confocal Imaging

Like in other types of neurons, voltage-gated Ca^{2+} channels represent a feature of newborn rat VRC neurons (Onimaru et al., 1996, 2003). Thus, imaging of dynamic changes of free concentration of cytosolic Ca^{2+} (Chapter **1.2**, **1.3**) is an important tool to visualize the activity, morphology and distribution of neonatal inspiratory neurons and presumptive astrocytes in preBötC slices (Koshiya & Smith, 1999; Frermann et al., 1999; Yuste et al., 2006; Ruangkittisakul et al., 2006, 2008, 2009, 2012; Hayes & Del Negro, 2007; Härtel et al., 2008; Ballanyi et al., 2010; Huxtable et al., 2010). Similar to loading of neurons (and glia) for Ca^{2+} imaging in other (isolated) nervous tissues (Stosiek et al., 2003; Yuste et al., 2006), the membrane-permeable Ca^{2+} sensitive dye Fluo-4-AM (0.5 mM in superfusate) was backfilled into a broken patch pipette (outer ø 5-10 µm) and

pressure-injected (0.7-1.0 psi) for 10 min. Similar to our previous respiratory Ca^{2+} imaging studies (Ruangkittisakul et al., 2006, 2008, 2009, 2012; Bobocea et al., 2010), Fluo-4-AM was injected into the VRC/preBötC from the caudal surface while inspiratory activity was electrophysiologically monitored from the contralateral VRC/preBötC.

Fluorescence signals were measured using either a confocal microscope and software (20x XLUMPlanF1, numerical aperture 0.95, objective; Olympus FV300; Carsen group, Markham, ON, Canada) or a FV300 connected to a Ti:Sa laser (10 W Mira/Verdi; Coherent, Santa Clara, CA, USA) for multiphoton imaging (Stosiek et al., 2003; Yuste et al., 2006; Nikolenko et al., 2003). Within 10-20 min after injection, labelling in an area with a lateral diameter of 200-300 µm revealed neuronal somata and primary dendrites plus changes in fluorescence intensity that oscillated in phase with electrophysiological VRC/preBötC activity on the contralateral side **(Fig. 1-6)**. Spontaneous non-synchronized Ca^{2+} rises of robust amplitude originated from cells with a soma diameter of typically 10 µm, likely representing astrocytes (Ruangkittisakul et al., 2009, 2012; Ballanyi et al., 2010). Rhythmic Ca^{2+} rises, cell bodies, and primary dendrites could be resolved at tissue depths up to 60 µm for confocal and 90 µm for multiphoton microscopy (Ruangkittisakul et al., 2006, 2009, 2012). Respiratory neurons were typically imaged at tissue depths between 30 and 60 µm. Rhythmic Ca^{2+} rises were visualized in up to 10 cells (typically 3-6) in a single xy-image plane. The stained region was monitored using a 2-3x digital zoom at reduced settings for y-axis

scanning. To improve morphological reconstruction and 3D animation, slices were exposed to glutamate (0.5-1 mM; 5-10 min) after the experiments and 'z-stack' image series were acquired. Glutamate-induced fluorescence signals were 3-10 times larger than those associated with spontaneous or drug-induced inspiratory activity. An identical Fluo-4-AM loading protocol and other described procedures were used for Ca^{2+} imaging in the LC of horizontal slices for Project-4.

For live cell labelling of neurons and glia in LC, slices were incubated for 1-1.5 h in carbogenated standard solution with sulforhodamine 101 (SR-101, Sigma) at 165 μM 20-23 ^{o}C or 1 μM at 34 ^{o}C, respectively. Injection of Ca^{2+} dye or SR-101 into the LC reveals basic morphological features of several cell classes. Presumptive neurons have a soma diameter of 20-35 μm, whereas most cells with a soma diameter of ~10 μm most likely represent astrocytes. Bath-application at 20-23 ^{o}C of 165 μM of the morphological dye SR-101 improves the resolution of morphological details in LC, but does not appear to stain mainly neurons as in newborn rat hippocampal and cortical slices (Kantor et al., 2012). Conversely, 1 μM SR-101 at 34 ^{o}C results in (fainter) staining of all cell types, contrary to preferential labelling of astrocyte as in newborn rat hippocampus (Kantor et al., 2012).

For additional analysis of LC neuronal morphology, patch electrodes were filled with 0.5 % lucifer yellow (lithium salt, Sigma), which was dissolved in the

intracellular solution. Intracellular recordings of >30 min duration provided enough time to fill dendrites with lucifer yellow. At the end of the experiments, preparations were fixed for >24 h in 4% paraformaldehyde (see above). Lucifer yellow-stained neurons were visualized with a multiphoton microscope (excitation wavelength: 425 nm, emission wavelength: 525 nm) **(Fig. 6-3)**.

2.6 Histology

The brainstem and LC slices were transferred after the experiments to fixation solution (Chapter **2.2**). Slices were incubated in phosphate buffer for 2 min and immersed in thionin solution for 1.30 min and then immediately rinsed with phosphate buffer for 2 min, and consecutively 'washed' with 50% ethanol (4 min) followed by phosphate buffer (2 min). Slices were then transferred on a 'hanging drop' glass slide to a microscope (Standard 16, magnification x32, Carl Zeiss Jena, Germany) and photographed (PL-A642-1.3 Megapixel, PixeLINK, Ottawa, ON, Canada). Stained rhythmic brainstem slices were photographed in phosphate buffer (PL-A686-6.6 Megapixel, PixeLINK) under a stereo microscope (Zeiss-SR15, magnification x32). Resulting pictures were compared with the reference atlas of the neonatal rat brainstem and slices borders were evaluated as distance in mm to VII_c **(Fig. 1-3)** (Ruangkittisakul et al., 2006, 2008).

2.7 Data Analysis

For all extracellularly and intracellularly recorded neuronal activities, burst rate was averaged every 20 min over 2 min time windows. 'Longevity' of rhythm was defined as the time from start of recording until the time when the period between consecutive bursts exceeded 5 min. Burst duration was defined using ClampFit software (Molecular Devices, Chicago, IL, USA) as the time interval from when the signal increased above and decreased below a threshold set at 10% of the peak amplitude for that burst. Pharmacologically reactivated rhythms were described by averaging burst rates over a 2 min time period at steady state. Values are means ± SEM except for histological analyses (means ± SD). Statistical significance was determined using Student's t-test or one-way ANOVA with Tukey post-test as appropriate using Prism (GraphPad Software Inc., La Jolla, CA, USA) as * $p<0.05$ and ** $p<0.01$. For analysis of Ca^{2+} imaging experiments, regions of interests (ROIs) were drawn around cell somata using Fluoview software to generate plots of fluorescence intensity over time (Chapter **1.3**) **(Fig. 1-6)**. Data were then transferred to Excel for further computation and Adobe Illustrator (Adobe Systems, San Jose, CA, USA) for plotting of graphs.

2.8 Figures and Legends

Fig. 2-1

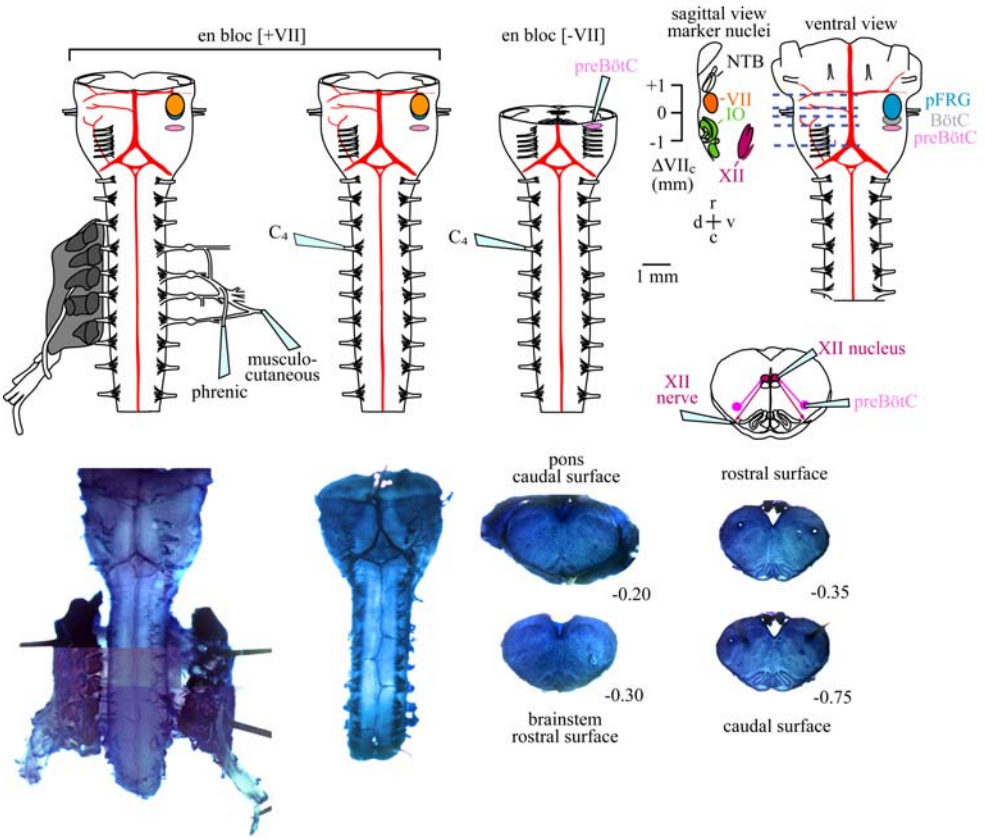

Fig. 2-1: Calibrated newborn rat 'respiratory networks in the dish'. The schema of a complete brainstem (rightmost) indicates in the ventral view the estimated rostrocaudal extents of inspiratory active preBötC and expiratory pre/post-inspiratory active pFRG neural networks that form a dual respiratory center. The region between these respiratory groups corresponds to the BötC which is primarily expiratory active in adults, but not yet studied in newborns. The sagittal view indicates mean values plus standard deviations of rostrocaudal extents of some respiratory brainstem marker nuclei included in a newborn rat brainstem atlas for generating anatomically defined ('calibrated') inspiratory active transversal preBötC slices (see **Fig. 1-3**). These nuclei are the inspiratory active XII motor nucleus, the nucleus of trapezoid body (NTB), and particularly the 'peri-inspiratory' active VII motor nucleus plus different subregions ('loops') of the inferior olive (IO). The respiratory groups and marker nuclei have a defined position relative to respiratory active nerve roots on the ventral brainstem surface. Specifically, these roots are from hypoglossal (XII), trigeminal (V), abducens (VI), glossopharyngeal (IX) and vagal (X) nerves. Importantly, the most rostral XII root corresponds to the location and rostrocaudal extent of the preBötC. **Leftmost**, schema (top) of the 'Suzue preparation' (Suzue, 1984) with complete

VII nucleus, isolated with or without intact cervical and brachial plexuses for recording from cervical (e.g. C_4) roots plus phrenic, brachial and/or musculocutaneous nerves. Both models were rostrally transected at the caudal cerebellar artery whereas the cord is typically cut at the last cervical (C_8) or first thoracic (T_1) level. For the brainstem model with intact cervical and brachial plexuses, the drawing on the left is based on an actual preparation, while the drawing on the right is derived from (Greene, 1935). **Middle,** schema of a 'calibrated' *en bloc* preparations with the manually cut rostral surface located -0.25 mm caudal to the caudal end of VII nucleus. This '*en bloc* [-VII]' model does not produce pFRG motor output and allows recording from the VRC/preBötC at the rostral surface and spinal (cervical) nerves. **Lower right,** schema of a 400 μm thick transversal slice with the preBötC in the middle ('m-preBötC[400] slice') with suction electrode positions for recording inspiratory-related rhythms. **Bottom row** showed corresponding preparations that were chemically fixed and thionin-stained after the experiment for better visualization of brainstem (surface) markers for histological analysis of their anatomical margins. For further details, see text or Ruangkittisakul et al., 2006, 2007, 2008, 2012 (modified from Ruangkittisakul et al., 2012).

Fig. 2-2

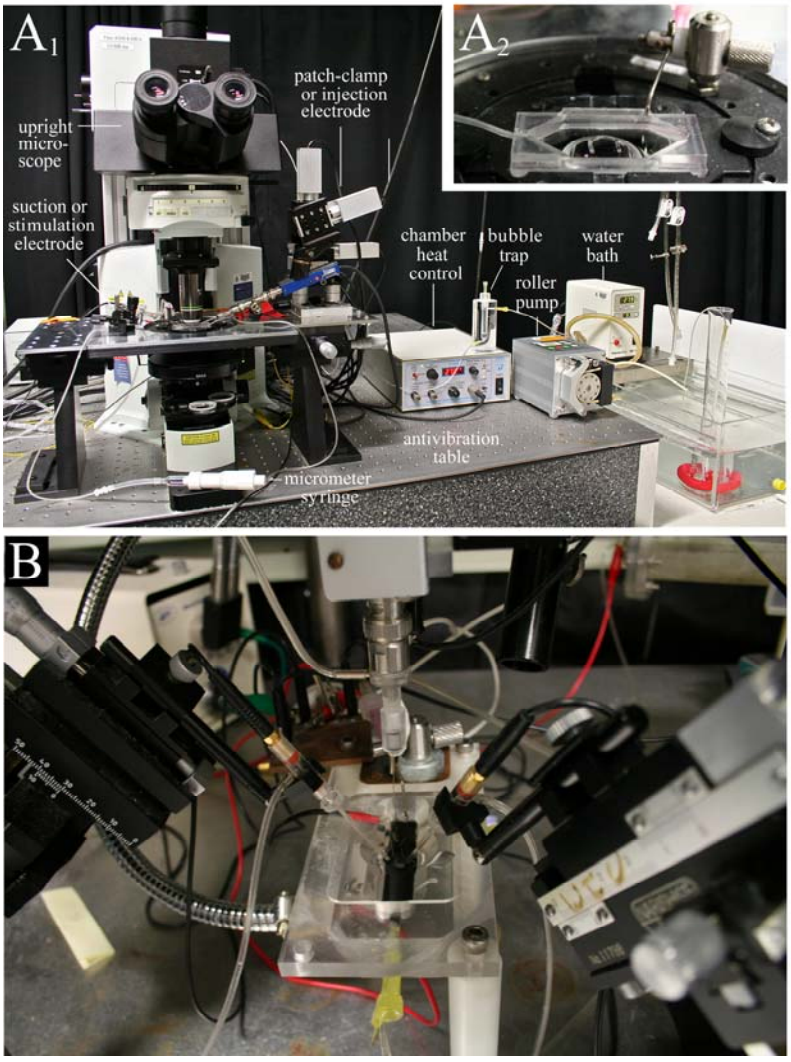

Fig. 2-2: Equipment for 'electrophysiological-imaging' in respiratory networks in the dish. A, an upright microscope (**A_1**) and a 'fixed' custom-made xy microscope stage are used for positioning and mechanical fixation of one calibrated preBötC slice or *en bloc* preparation with a 'harp' to the glass bottom of a 'Warner' submerged-type recording chamber (**A_2**), or with steel insect pins, if a layer of silicone ('sylgard-184®') has been added to cover the bottom of the chamber. Superfusate enters the chamber via a Tygon® or steel tube and is removed at the opposite end via a hypodermic cannula connected to a vacuum system (e.g. an aquarium pump). Superfusate is pre-warmed in a 'Haake' water bath while the temperature of superfusate in the recording chamber is kept constant by a 'Warner' temperature control system. Superfusate is transported via a 'Watson-Marlow' peristaltic ('roller') pump and passes an acrylic 'bubble trap' before entering the recording chamber. Cells in slices are visualized using a x20 objective which is part of a FV300 Olympus confocal laser scan imaging system.

Fluorescent dye is injected via a broken patch electrode positioned with a 'Siskiyou' step motor also used for patch recording using a HEKA 'patch-clamp' (HEKA headstage shown here) or npi 'single-electrode voltage-clamp' amplifier. Neuronal population activity is extracellularly recorded using suction electrodes positioned via a 'Micro-Narishige' manipulator and connected to a 'WPI' or 'AM-Systems' differential amplifier. The entire recording system is positioned on a 'Kinetic Systems' antivibration table. **B**, recording chamber and mechanical arrangement for combining suction electrode (and eventually ion- and/or gas-sensitive microelectrode recording) with 'blind' patch-clamp recording from the respiratory networks in the dish. Preparations are positioned and fixed in the silicone-covered submerged-type custom-made recording chamber using a stereo-microscope that can be combined with (or replaced by) a video camera. Superfusate system including inlet and outlet are identical with that in **A**. Intracellular recording is done using a 'Sikiyou' (see **A**) or 'Sutter' step motor while 'Märzhäuser' (left) or 'Narishige' (right) micromanipulators are stable enough for >10 h recording, e.g. of neuronal population activity. Suction and patch electrodes are conveniently placed in 'ALA Scientific' or 'Warner' holders. The latter models, shown here on the left and right sides, are not bulky, thus enabling positioning of up to 8 electrodes in this type of chamber in particular when using the slim Narishige manipulators. While extracellular electrodes are positioned at an angle, the patch-electrode (connected here to the headstage of an npi amplifier), advances perpendicularly through the tissue using digital readouts for the Siskiyou or Sutter motors for identifying the recording depth). (from Ruangkittisakul et al., 2012).

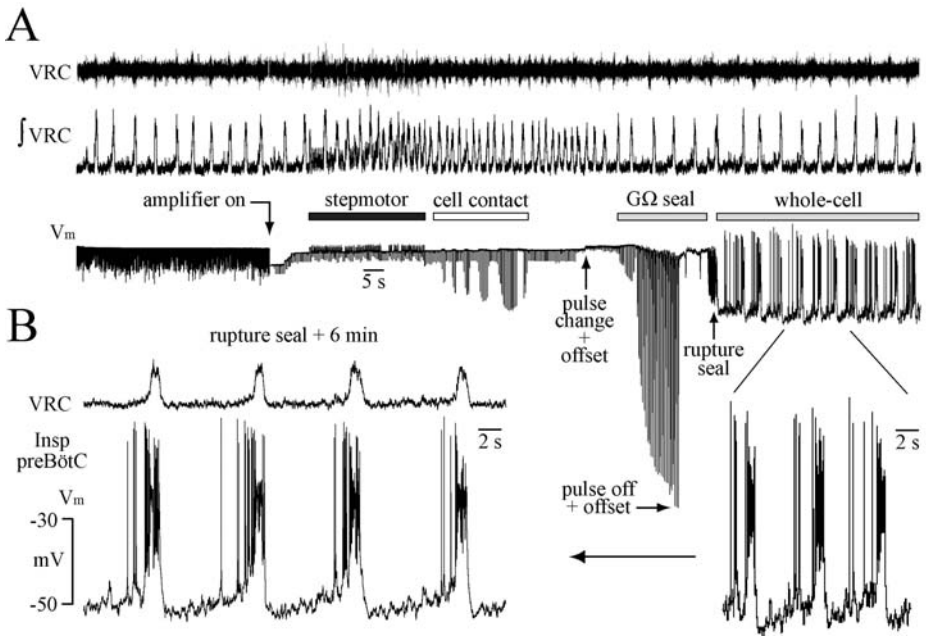

Fig. 2-3: 'Blind' whole-cell patch-clamp recording from respiratory neurons. **A**, procedures involved in establishing a membrane potential (V_m) recording in the 'whole-cell' patch-clamp configuration. **A**, in a m-preBötC[400]W-P3 slice inspiratory-related bursting is recorded with a suction electrode from the ventrolateral slice aspect containing the ventral respiratory column (VRC) with the preBötC extending rostrocaudally between 100-300 µm below the surface. Compared to the upper VRC trace showing the amplified (x10k) differentially-recorded and band-pass filtered (0.3-3 kHz) raw signal, the integrated (□: 50 ms) signal reveals the inspiratory bursts much better. After turning the intracellular npi amplifier on, the patch electrode is positioned in the contralateral VRC and forwarded through the tissue using a Siskiyou stepmotor (see **Fig. 2-2**). Close to the cell membrane, the amplitude of the electrode voltage change in response to a repetitively applied rectangular DC current (100 pA, 20 ms), increases and shows some flickering ('oscillations'). At this stage, the electrode is moved up and down by 1-5 µm until the oscillations during the test pulse are maximal and stable. Then, the amplitude of the test pulse is reduced to 10% and the positive pressure (20-30 mmHg) applied to the electrode is removed. In most cases, a Giga-Ohm seal establishes spontaneously while in the other cases slight suction is applied to facilitate this. Once a seal of at least 1 G□ is established, the pulse is switched off and the patch is ruptured by sudden suction, eventually combined with application of a short current pulse. In this example, the whole-cell configuration is established for an inspiratory ('Insp') preBötC neuron. The recording in **B** from the same neuron shows that the recording stabilized within some minutes after the rupture of the seal. It is difficult to determine resting V_m in this cell because of its rhythmic fluctuations. Specifically, V_m is slightly more negative than -50 mV during a hyperpolarization after termination of the inspiratory burst and subsequently shows a progressive depolarization until action potential ('spike')

discharge occurs in the pre-inspiratory phase preceding the onset of the inspiratory VRC population burst that is accompanied by a synaptic drive potential and further spike discharge in the neuron (from Ruangkittisakul et al., 2012).

2.9 References

Ballanyi K, Ruangkittisakul A (2009) Structure-function analysis of rhythmogenic inspiratory pre-Botzinger complex networks in "calibrated" newborn rat brainstem slices. Resp Physiol Neurobiol 168, 158-178

Ballanyi K, Onimaru H, Homma I (1999) Respiratory network function in the isolated brainstem-spinal cord of newborn rats. Progr Neurobiol 59, 583-634

Ballanyi K, Panaitescu B, Ruangkittisakul A (2010) Control of breathing by nerve glue. Sci Signal 3, pe41

Blanton MG, Lo Turco JJ, Kriegstein AR (1989) Whole cell recording from neurons in slices of reptilian and mammalian cerebral cortex. J Neurosci Methods 30, 203-210

Bobocea N, Ruangkittisakul A, Ballanyi K (2010) Multiphoton/confocal Ca^{2+} imaging of inspiratory pre-Bötzinger complex neurons at the caudal or rostral surface of newborn rat brainstem slices. Adv Exp Med Biol 669, 81-85

Cho YR, Pawela CP, Li R, Kao D, Schulte ML, Runquist ML, Yan JG, Matloub HS, Jaradeh SS, Hudetz AG, Hyde JS (2007) Refining the sensory and motor ratunculus of the rat upper extremity using fMRI and direct nerve stimulation. Magn Reson Med 58, 901-909

Christie MJ (1997) Generators of synchronous activity of the locus coeruleus during development. Semin Cell Dev Biol 8, 29-34

Christie MJ, Williams JT, North RA (1989) Electrical coupling synchronizes subthreshold activity in locus coeruleus neurons in vitro from neonatal rats. J Neurosci 9, 3584-3589

Feldman JL, Del Negro CA (2006) Looking for inspiration: new perspectives on respiratory rhythm. Nature Rev Neurosci 7, 232-242

Frermann D, Keller BU, Richter DW (1999). Calcium oscillations in rhythmically active respiratory neurones in the brainstem of the mouse. J Physiol 515, 119-131

Greene EC (1935) The anatomy of the rat. Camden, New Jersey, Haddon Craftsmen

Greer JJ, Funk GD (2005) Perinatal development of respiratory motoneurons. Respir Physiol Neurobiol 149, 43-61

Härtel K, Schnell C, Hülsmann S (2008) Astrocytic calcium signals induced by neuromodulators via functional metabotropic receptors in the ventral respiratory group of neonatal mice. Glia 57, 815-827

Hansen AJ (1985). Effect of anoxia on ion distribution in the brain. Physiol Rev 65, 101-148

Hayes JA, Del Negro CA (2007) Neurokinin receptor-expressing pre-botzinger complex neurons in neonatal mice studied in vitro. J Neurophysiol 97, 4215-4224

Hille B (2002) Ion channels of excitable membranes. Sunderland, MA: Sinauer Associates

Huxtable AG, Zwicker JD, Alvares TS, Ruangkittisakul A, Fang X, Hahn LB, Posse de Chaves E, Baker GB, Ballanyi K, Funk GD (2010) Glia contribute to the purinergic modulation of inspiratory rhythm generating networks. J Neurosci 30, 3947-3958

Janczewski WA, Onimaru H, Homma I, Feldman JL (2002) Opioid-resistant respiratory pathway from the preinspiratory neurones to abdominal muscles: In vivo and in vitro study in the newborn rat. J Physiol 545, 1017-1026

Kantor C, Panaitescu B, Kuribayashi J, Ruangkittisakul A, Lee TF, Cheung PY, MacTavish D, Jhamandas J, Ballanyi K (2012) Electrophysiological imaging of early network oscillations in brain slices from newborn rats and piglets. In Isolated Central Nervous System Circuits (Ed K Ballanyi), Neuromethods Series Vol 73 (Ed W Walz). Springer Science+Business Media, LLC, New York, NY, 315-356

Koshiya N, Smith JC (1999). Neuronal pacemaker for breathing visualized in vitro. Nature 400, 360-363

Nikolenko V, Nemet B, Yuste R (2003) A two-photon and second-harmonic

microscope. Methods 30, 3-15

Onimaru H, Ballanyi K, Richter DW (1996) Calcium-dependent responses in neurons of the isolated respiratory network of newborn rats. J Physiol 491, 677-695

Onimaru H, Ballanyi K, Homma I (2003) Contribution of Ca^{2+}-dependent conductances to membrane potential fluctuations of medullary respiratory neurons of newborn rats in vitro. J Physiol 552, 727-741

Panaitescu B, Ruangkittisakul A, Ballanyi K (2009) Silencing by raised extracellular Ca2+ of pre-Botzinger complex neurons in newborn rat brainstem slices without change of membrane potential or input resistance. Neurosci Lett 456, 25-29

Ruangkittisakul A, Schwarzacher SW, Ma Y, Poon B, Secchia L, Funk GD, Ballanyi K (2006) High sensitivity to neuromodulator-activated signalling pathways at physiological $[K^+]$ of confocally-imaged respiratory centre neurons in online-calibrated newborn rat brainstem slices. J Neurosci 26, 11870-11880

Ruangkittisakul A, Secchia L, Bornes TD, Palathinkal DM, Ballanyi K (2007) Dependence on extracellular Ca^{2+}/K^+ antagonism of inspiratory centre rhythms in slices and en bloc preparations of newborn rat brainstem. J Physiol 584, 489-508

Ruangkittisakul A, Schwarzacher SW, Secchia L, Ma Y, Bobocea N, Poon BY, Funk GD, Ballanyi K (2008) Generation of eupnea and sighs by a spatiochemically organized inspiratory network. J Neurosci 28, 2447-2458

Ruangkittisakul A, Okada Y, Oku Y, Koshiya N, Ballanyi K (2009) Fluorescence Imaging of active respiratory networks. Resp Physiol Neurobiol 168, 26-38

Ruangkittisakul A, Secchia-Ballanyi L, Panaitescu B, Bobocea N, Kuribayashi J, Iizuka M, Kantor C, Ballanyi K (2012) Anatomically ‘calibrated‘ isolated respiratory networks from newborn rodents. In Isolated Central Nervous System Circuits (Ed K Ballanyi), Neuromethods Series Vol 73 (Ed W Walz). Springer Science+Business Media, LLC, New York, NY, 61-124

Smith JC, Ellenberger HH, Ballanyi K, Richter DW, Feldman JL (1991) Pre-Botzinger complex: a brainstem region that may generate respiratory rhythm in mammals. Science 254, 726-729

Smith JC, Ballanyi K, Richter DW (1992) Whole-cell patch-clamp recordings from respiratory neurons in neonatal rat brainstem in vitro. Neurosci Lett 134, 153-156

Somjen GG (2002) Ion Regulation in the brain: implications for pathophysiology. Neuroscientist 8, 254-267

Stosiek C, Garaschuk O, Holthoff K, Konnerth A (2003) In vivo two-photon calcium imaging of neuronal networks. Proc Natl Acad Sci USA 100, 7319-7324

Suzue T (1984) Respiratory rhythm generation in the in vitro brain stem-spinal cord preparation of the neonatal rat. J Physiol 354, 173-183

Taccola G, Secchia L, Ballanyi K (2007) Anoxic persistence of lumbar respiratory bursts and block of lumbar locomotion in newborn rat brainstem spinal cords. J Physiol 585, 507-524

Yuste R, Konnerth A, Masters B (2006) Imaging in neuroscience and development, a laboratory manual. J Biomed Opt 11, 19902

CHAPTER 3

Ca^{2+}/K^{+} Antagonism of Isolated preBötC Bursting

Bogdan A. Panaitescu, Araya Ruangkittisakul, Klaus Ballanyi

Department of Physiology, 750 MSB, University of Alberta, Edmonton, Canada

Fragments of this chapter have been published as:

Panaitescu B^{+}, Ruangkittisakul A^{+}, Ballanyi K (2009) Silencing by raised extracellular Ca^{2+} of pre-Bötzinger complex neurons in newborn rat brainstem slices without change of membrane potential or input resistance. Neurosci Lett 456, 25-29

Panaitescu B, Ruangkittisakul A, Ballanyi K (2010) Depression by Ca^{2+} and stimulation by K^{+} of fictive inspiratory rhythm in newborn rat brainstem slices. Adv Exp Med Biol 669, 91-95

My contribution to this study consisted of the execution of all whole-cell recordings and the majority of extracellular recordings plus analysis and contribution to writing the manuscript which was finalized by Dr. Ballanyi. For the second part of this chapter, I did ~50% of recordings and contributed to analysis plus writing. The rest of the analysis was done by Dr. Ruangkittisakul and Dr. Ballanyi finalized the manuscript.

$^{+}$Authors contributed equally to the study

3.1 Silencing by Raised Extracellular Ca^{2+} of Pre-Bötzinger Complex Neurons in Newborn Rat Brainstem Slices Without Change of Membrane Potential or Input Resistance

3.1.1 Introduction

Breathing is controlled by inspiratory pre-Bötzinger complex (preBötC) networks that remain active in brainstem slices from perinatal rodents (Smith et al., 1991; Ramirez et al., 2004; Feldman & Del Negro, 2006). Raising superfusate Ca^{2+} in physiological (3 mM) K^+ from 1 to 1.5 mM, i.e., from the lower to the upper limit of the estimated physiological range in interstitial brain tissue (Nicholson et al., 1978; Richter & Acker, 1989; Puka-Sundvall et al., 1994; Somjen, 2002), severely depresses inspiratory-related bursting in 600 μm thick preBötC slices, but rhythm is restored by elevated K^+ (Ruangkittisakul et al., 2006). Similar slowing of rhythm in mouse slices by opioids has been attributed to K^+ channel-mediated hyperpolarization of preBötC neurons (Gray et al., 1999; Feldman & Del Negro, 2006) whereas others proposed a major contribution of presynaptic inhibition to opioid-evoked inspiratory depression *in vitro* (Chapter **1.5**) (Ballanyi et al., 1997, 1999; Ballanyi et al., 2009). Here, we studied whether block of inspiratory rhythm by high Ca^{2+} is typically associated with membrane hyperpolarization of preBötC neurons and neighbouring cells, or whether this phenomenon occurs in the absence of a postsynaptic change in neuronal membrane potential or input resistance.

The isolated preBötC should ideally be studied in thin slices to minimize modulation of its activity by adjacent (respiratory) brainstem structures (Ballanyi et al., 1997; Feldman & Del Negro, 2006; Ruangkittisakul et al., 2007, 2008). We showed recently that the newborn rat preBötC is centered 0.5 mm caudal to facial (VII) motor nucleus and extends by <200 μm (Ruangkittisakul et al., 2008). Slices of 200-250 μm thickness containing this kernel are capable of generating inspiratory activity in 3 mM K^+, but these rhythms (and more regular bursting in elevated K^+) appear to last for <2.5 h (Ruangkittisakul et al., 2008). This limited viability may be related to the fact that dendrites of newborn rat preBötC cells extend by ~400 μm (Ballanyi et al., 1999; Onimaru et al., 2003) and are thus partly cut in thin slices. Here, we used 400 μm thin newborn rat slices with the preBötC in the middle ('m-preBötC[400]' slices) and 'calibrated' margins (Ruangkittisakul et al., 2006) as a compromise between long term viability of rhythmogenic neurons and minimal preBötC modulation by adjacent tissue. We hypothesize that longevity of rhythm in 3 mM K^+ in such slices is sufficient for the planned intracellular analysis.

3.1.2 Methods

(see Chapter **2**)

3.1.3 Results

First, we tested whether longevity of inspiratory-related rhythm in solution with most common brain interstitial K^+ (3 mM) and Ca^{2+} (1.2 mM), i.e., '$3K^+$-$1.2Ca^{2+}$ solution', is sufficient for cellular analyses that require already extended time periods for cell tracking. Bursting in the VRC area at an initial rate of 6.6 ± 1.4 bursts/min was stable in 10 slices for 40 min, whereas in one slice rhythm arrested after 37 min **(Fig. 3.1-1)**. Such '*in vitro* apnea' (Ruangkittisakul et al., 2006, 2007, 2008) occurred in the other slices during the next hour, resulting in a mean longevity of rhythm in $3K^+$-$1.2Ca^{2+}$ of 67 ± 4 min. Next, we tested whether rhythm persists for longer time periods in solution with 1 mM Ca^{2+} as seen in m-preBötC[600] slices (Ruangkittisakul et al., 2007). Indeed, in seven slices longevity of rhythm in $3K^+$-$1Ca^{2+}$ was more pronounced (124 ± 24 min, $P< 0.05$). Specifically, rhythm at a rate similar to the initial value (7.6 ± 0.9 bursts/min) was still seen in five of these slices after 100 min of recording, when *in vitro* apnea had already occurred in all slices in $3K^+$-$1.2Ca^{2+}$ **(Fig. 3.1-1)**. In both slice groups, raising K^+ from 3 to 7 mM upon *in vitro* apnea restored rhythm at 9.1 ± 1.0 (1.2 mM Ca^{2+}) and 10.4 ± 0.7 (1 mM Ca^{2+}) bursts/min. Burst rate, amplitude and duration of restored rhythms remained stable for notably >3 h, similar to pre-BötC bursting in seven other slices, in which K^+ was raised from 3 to 7 mM immediately after transfer to the recording chamber **(Fig. 3.1-1)**. The reversibility of the effect of K^+ elevation on burst rate was investigated in other four slices. Raising K^+ to 7 mM after 20 min of recording in $3K^+$-$1.2Ca^{2+}$ increased burst rate

from 2.5 ± 0.3 to 7.5 ± 2.2 bursts/min, whereas rhythm slowed down again within <10 min to 1.0 ± 0.0 bursts/min upon return to $3K^+$-$1.2Ca^{2+}$.

Because of the limited longevity of rhythms in 3 mM K^+, intracellular recording was done in 7 mM K^+ and the most common estimated physiological Ca^{2+} value (1.2 mM). In initial experiments, Ca^{2+} was raised in $7K^+$-$1.2Ca^{2+}$ to 2 mM for inhibiting inspiratory rhythm. If burst rate was not severely depressed within ~5 min, Ca^{2+} was increased further to 2.5 and/or 3 mM, to avoid time-dependent deterioration of whole-cell-recording conditions. In subsequent experiments, slices were directly exposed to 3 mM Ca^{2+} for fast depression of rhythm and, eventually, for induction of more prominent intracellular effects. Rhythm in the latter nine slices was blocked in seven cases within ~5 min, while two slices remained active at <0.5 bursts/min for test periods of ~15 min **(Fig. 3.1-2)**. The mean values for inspiratory rates in 2 or 2.5 mM Ca^{2+} in **Fig. 3.1-2** may have been overestimated because superfusate was changed to higher Ca^{2+} values before steady-state of depressed bursting was reached. Independent on which Ca^{2+} concentration was used, cellular effects were quantified when rhythm was either blocked or its rate was depressed to <10% of control.

High Ca^{2+} decreased the baseline of the integrated VRC population signal which might be an indication of depressed tonic activity of non-respiratory neurons in the preBötC area **(Fig. 3.1-2)**. This high Ca^{2+} effect appeared to reflect indeed a depression of neuronal activity because four slices showed a similar block of

inspiratory-related bursting and a concomitant decrease of baseline in response to Cd^{2+} (250 μM), whereas tetrodotoxin (0.5 μM) was even more effective (n= 5). Combined application of both drugs (n= 9) reduced both baseline and width of VRC signals to levels monitored in superfusate above the slice **(Fig. 3.1-2)**.

Whole-cell-recordings were obtained from seven inspiratory neurons located 0.4-0.6 mm caudal to VII_c, thus within the preBötC (Ruangkittisakul et al., 2008), and also from five slightly more caudal inspiratory cells. None of these neurons showed ectopic bursts in response to current evoked depolarizing shifts of membrane potential (Smith et al., 1991; Ramirez et al., 2004; Feldman & Del Negro, 2006). High Ca^{2+} changed neither their resting potential (about -45 mV) nor their input resistance (about 250 MΩ), but block of VRC rhythm was accompanied by silencing of these inspiratory neurons **(Fig. 3.1-3)**. Though, their excitability was not impaired because action potentials with normal amplitude and duration could be evoked by depolarizing rectangular current pulses without a change in threshold potential (-34.4 ± 3.1 mV *versus* -34.8 ± 4.0 mV in control, n= 5) **(Fig. 3.1-3)**. Within ∼5 min after return to 1.2 mM Ca^{2+}, both inspiratory-related cellular bursting and contralaterally monitored VRC activity started to recover, but maximal recovery was reached only after 8–19 min **(Fig. 3.1-3)**. High Ca^{2+} also changed neither resting potential (about -45 mV) nor input resistance (about 380 MΩ) of tonic neurons (six within and four adjacent to the preBötC area) that may contribute to excitatory drive of inspiratory preBötC cells (Ballanyi et al., 1997, 1999; Ramirez et al., 2004) **(Fig. 3.1-3)**. Nevertheless, high Ca^{2+}

depressed their spontaneous tonic discharge within <5 min from 3.3 ± 0.61 to 0.09 ± 0.04 spikes/s (P< 0.01) as quantified in four of these neurons **(Fig. 3.1-3)**. However, similar to the inspiratory neurons, action potentials with normal amplitude and duration could be evoked without a change in threshold potential (-39.5 ± 1.6 mV *versus* -38.8 ± 2.5 mV in control, n= 4).

3.1.4 Discussion

As one major finding, longevity of inspiratory rhythm in m-preBötC[400] slices in physiological K^+ is less pronounced than in m-preBötC[500] slices (142 min) and, in particular, 600 µm or 700 µm thick m-preBötC slices (>3 h) (Ruangkittisakul et al., 2006, 2007, 2008). This implies that m-preBötC[400] slices are not suited for long term studies in 3 mM K^+, similar to 200-250 µm thin m-preBötC slices (Ruangkittisakul et al., 2008). Though, rhythm remained for >3 h in 7 mM K^+ and 1.2 mM Ca^{2+} at reasonably fast rates (6–8 bursts/min) and was stable for at least 9 h at 4-5 bursts/min. This indicates that m-preBötC[400] slices are a useful *in vitro* respiratory model because they represent a compromise between long term viability of neurons of the preBötC kernel and minimal modulation of this kernel by adjacent structures. The necessity to study m-preBötC[400] slices in elevated K^+ reverses already some of the depression of inspiratory rhythm in 1.2 mM compared to 1 mM Ca^{2+} **(Fig. 3.1-1)** according to the 'Ca^{2+}/K^+ antagonism' that determines bursting of the isolated preBötC (Ruangkittisakul et al., 2007). However, already increasing Ca^{2+} by 0.8 mM (from

1.2 mM in control) severely depressed the 7 mM K^+ rhythm. This shows that the isolated preBötC is still very sensitive to raised Ca^{2+} when it is subjected to unspecific drive that may, in some extent, mimic ongoing excitatory inputs *in vivo* (Ballanyi et al., 1997; Ramirez et al., 2004; Feldman & Del Negro, 2006). Similar to our *in vitro* findings, administration of Ca^{2+} to the brainstem *in vivo* inhibits breathing, and this inhibition is compensated by K^+ injection (Leusen, 1972). It is not known, how much Ca^{2+} is necessary to block preBötC activity *in vivo*, but it may be notably more than 2-3 mM because inspiratory rhythm is not abolished by such superfusate Ca^{2+} levels (at 5-6.2 mM K^+) in newborn rat brainstem-spinal cords with major amount of tissue adjacent to the preBötC (Kuwana et al., 1998; Ruangkittisakul et al., 2007).

High Ca^{2+} had no effect on resting potential and input resistance in all 22 recorded neurons. This suggests that Ca^{2+} does not primarily target postsynaptic K^+ channels of cells within or close to the preBötC area either directly or via (G protein-coupled) membrane receptors that presumably mediate the similarly severe depressing effects of opioids on slice rhythms (Gray et al., 1999; Feldman & Del Negro, 2006). Similarly, high Ca^{2+} does not seem to block postsynaptic TRPM7 cation channels (Wei et al., 2007) or activate Ca^{2+} sensitive K^+ channels (Weston et al., 2008), which both causes hyperpolarization in other tissues. Importantly, the apparent absence of an effect on resting potential or input resistance does not exclude saturation of surface charges as one possible postsynaptic target of Ca^{2+} because this would cause a highly local plasma

membrane hyperpolarization that is not revealed with whole-cell-recording (Kuwana et al., 1998; Somjen, 2002). Alternatively, high Ca^{2+} may affect postsynaptic conductances that are presumably important for intrinsic bursting of preBötC neurons, but do not contribute to resting potential. Examples are persistent Na^{+} channels or Ca^{2+} activated non-selective cation channels (Ballanyi et al., 1999; Feldman & Del Negro, 2006; Pace et al., 2007; Ramirez et al., 2004). Because none of the recorded 12 inspiratory neurons showed intrinsic bursting, it is possible that rhythmogenic (pacemaker) neurons in the vicinity of these cells are hyperpolarized by high Ca^{2+} which would explain the block of rhythm. As a further possibility, block of rhythm by high Ca^{2+} may be primarily due to presynaptic inhibition as proposed by us for opioid-evoked inspiratory depression *in vitro* (Ballanyi et al., 1997, 1999, 2009). For example, raised Ca^{2+} may modulate (presynaptic) $G_{i/o}$ protein-coupled Ca^{2+} sensing receptors that may decrease preBötC excitability, e.g., by affecting Ca^{2+} dependent K^{+} channels and metabotropic $GABA_B$ or glutamate receptors (Brown & MacLeod, 2001; Weston et al., 2008).

The observed depression of intracellular discharge of tonic cells by high Ca^{2+} was reflected by a baseline decrease of the integrated VRC population signal. This indicates that a substantial number of neurons are tonically active in the preBötC area. The finding of depressed tonic activity raises the possibility that inhibition of rhythmogenic neurons by high Ca^{2+} is caused by presynaptic block of excitatory drive from tonically active cells in the vicinity of preBötC neurons

(Ballanyi et al., 1997, 1999; Ramirez et al., 2004) and/or chemosensitive (serotonergic) raphe neurons (Richerson, 2004; Pace et al., 2007). Though, block of either drive should have some effects on resting potential (which typically shows spontaneous excitatory and inhibitory postsynaptic potentials), unless this drive specifically targets axon terminals of rhythmogenic pre-BötC neurons for facilitation of transmitter release. This scenario is principally possible, but not studied yet. Analysis of miniature postsynaptic potentials, which is beyond the format of this study, will likely provide information for discrimination between presynaptic and postsynaptic targets of inspiratory depression by raised Ca^{2+}.

3.1.5 Figures and Legends

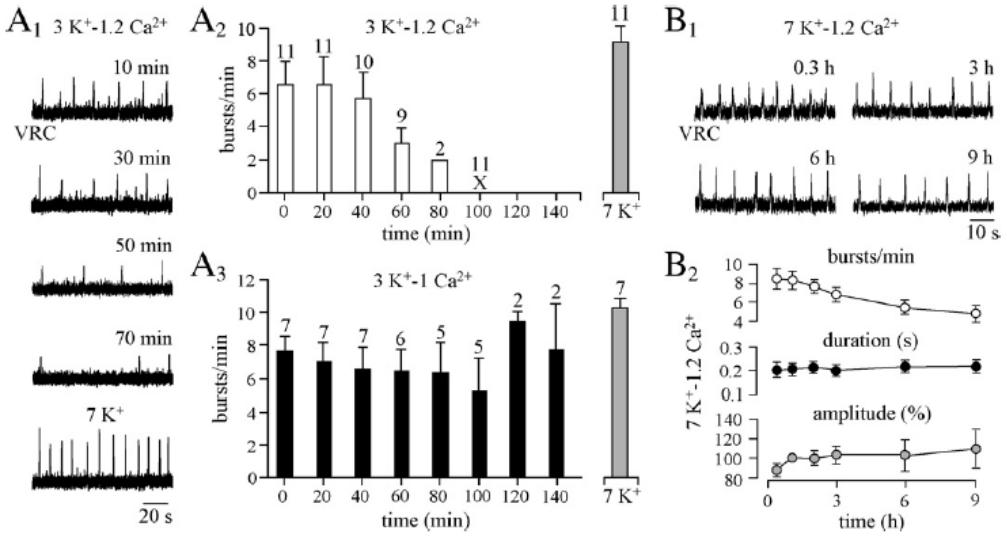

Fig. 3.1-1: Rhythmic activity of inspiratory pre-Bötzinger complex (preBötC) networks in 400 µm thin newborn rat brainstem slices. A_1, suction electrode recording from the ventrolateral slice area of a 400 µm thin slice containing the ventral respiratory column (VRC) with the preBötC in the middle ('m-preBötC[400]' slice) that was generated with 'online histology' (Ruangkittisakul et al., 2006). The differentially amplified, bandpass-filtered and integrated VRC recordings show that inspiratory-related rhythm in physiological K^+ (3 mM) and most common physiological Ca^{2+} (1.2 mM) ('$3K^+$-$1.2Ca^{2+}$') (Nicholson et al., 1978; Puka-Sundvall et al., 1994; Richter & Acker, 1989; Somjen 2002) arrested spontaneously after slightly more than 70 min ['in vitro apnea' (Ruangkittisakul et al., 2006, 2008)], but was restored by raising superfusate K^+ to 7 mM. **A_2**, the plot of the time dependence of burst rates shows that only 2 of 11 (slice numbers above bars) m-preBötC[400] slices were active for >1 h in $3K^+$-$1.2Ca^{2+}$. 'x' indicates the time for arrest of rhythm in all slices. **A_3**, rhythm was more robust in seven slices, that were both generated and studied in 3 mM K^+ and 1 mM Ca^{2+} solution ('$3K^+$-$1Ca^{2+}$') corresponding to the low end of the estimated physiological Ca^{2+} range (Nicholson et al., 1978; Puka-Sundvall et al., 1994; Richter & Acker, 1989; Somjen 2002). Bars represent means (± SEM) of burst rates in slices that were still active at indicated times. **B_1**, the original recording indicates that rhythm was stable for 9 h in slices generated in $3K^+$-$1.2Ca^{2+}$ and studied in $7K^+$-$1.2Ca^{2+}$. This was confirmed in the plots in **B_2** of burst rate, duration and amplitude in seven slices that did not significantly differ from control (20 min) at any time until 9 h of recording.

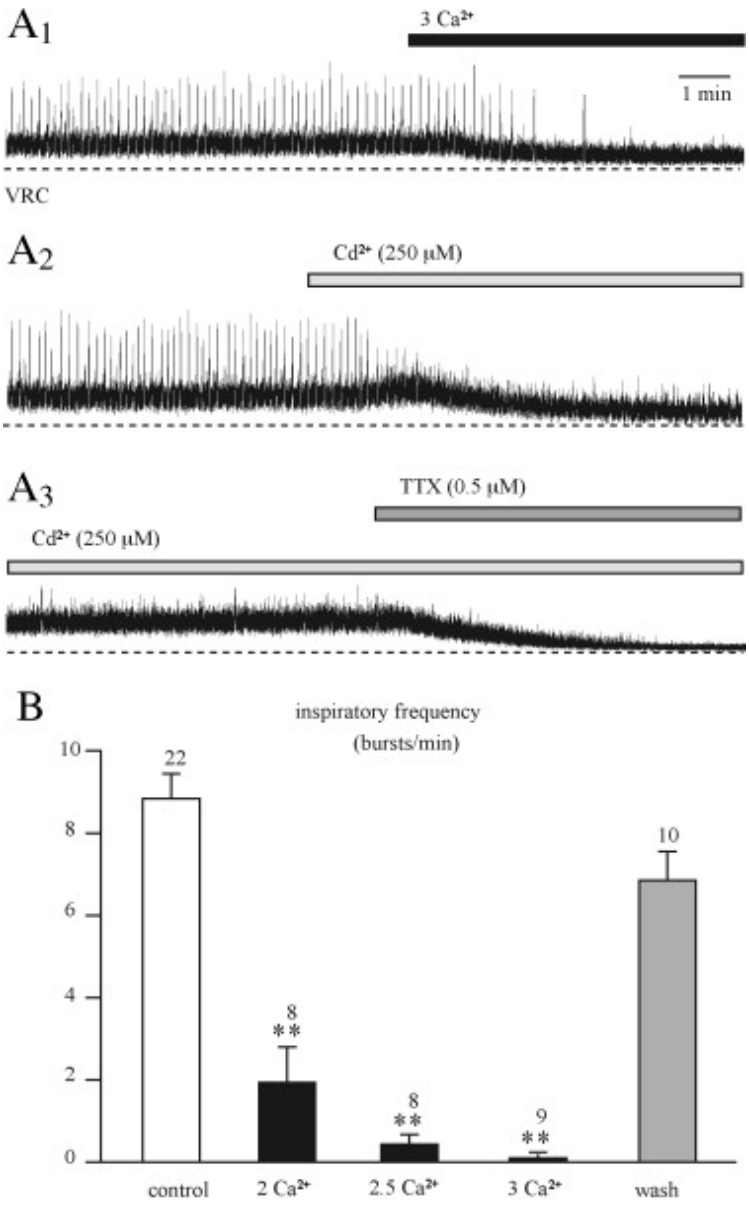

Fig. 3.1-2: Inhibition of inspiratory-related rhythm in m-preBötC[400] slices by raised superfusate Ca^{2+}. A_1, block of inspiratory-related VRC population bursting in $7K^+$-$1.2Ca^{2+}$ solution within <5 min following elevation of Ca^{2+} to 3 mM was accompanied by a modest fall of the baseline of the integrated suction electrode signal. **A_2**, following recovery of both VRC rhythm and baseline in this slice ~15 min after return to 1.2 mM Ca^{2+}, bath-application of the voltage-activated Ca^{2+} channel blocker Cd^{2+} evoked a similarly fast block of inspiratory rhythm and fall of baseline. **A_3**, with Cd^{2+} still present, addition of the voltage-activated Na^+ channel blocker tetrodotoxin (TTX) decreased VRC signal baseline further and also notably reduced its width. **B**, statistical analysis of Ca^{2+} block of VRC bursting in $7K^+$-$1.2Ca^{2+}$. Recovery values were determined 8-19 min after return to 1.2 mM Ca^{2+}.

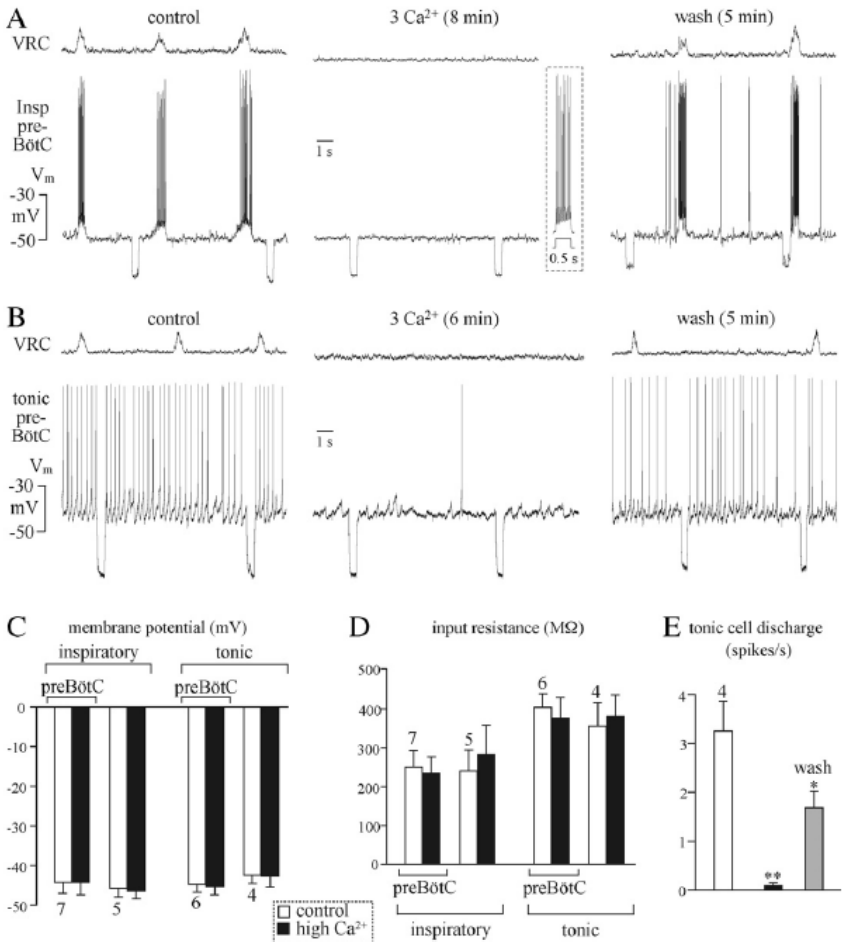

Fig. 3.1-3: Response of inspiratory and tonic (preBötC) neurons to Ca^{2+} block of inspiratory-related slice rhythm. A, an inspiratory neuron located 0.58 mm caudal to facial motor nucleus and thus within the preBötC, which extends between 0.4 and 0.6 mm caudal to this reference nucleus (Ruangkittisakul et al., 2006, 2007, 2008), showed a depolarizing drive potential and action potential discharge in synchrony with VRC population activity in 7 K^+-1.2Ca^{2+}. Despite blocking the rhythm, 3 mM Ca^{2+} changed neither membrane potential (V_m) nor input resistance, which was calculated from V_m deflections in response to injection via the patch electrode of depolarizing current pulses (100 pA, 0.5 s). The inset shows that normal action potentials were evoked by current injection. **B**, block of rhythm by 3 mM Ca^{2+} changed neither V_m nor input resistance in a tonically active neuron in the preBötC area 0.60 mm caudal to VII_c. **C**, **D**, analysis of neuronal responses of V_m (**C**) or input resistance (**D**) to block or major depression of preBötC rhythm by 2-3 mM Ca^{2+} revealed no significant effect in either preBötC or non-preBötC inspiratory or tonic neurons. **E**, high Ca^{2+} substantially reduced ($P< 0.01$) the rate of spontaneous spiking in tonic neurons, similar to findings in tonic cells of unknown location in newborn rat brainstem-spinal cords (Kuwana et al., 1998). Upon return to 1.2 mM Ca^{2+}, tonic discharge recovered significantly ($P< 0.05$) compared to the depression. Digits above bars indicate number of slices.

3.2 Optimization of Divalent Cation Ratios for Long-Term Inspiratory Rhythm in Newborn Rat Brainstem Slices

3.2.1 Introduction

The free extracellular concentrations of K^+, Ca^{2+} and Mg^{2+} greatly determine neuronal excitability (Hille, 2001; Somjen, 2002; Brown et al., 2004). For example, screening of surface charges at the outer face of the plasmalemmal membrane by Ca^{2+} and Mg^{2+} counteracts overexcitability during tetany (Hille et al., 1975; Somjen, 2002). These divalent cations also interact with neuronal membrane proteins as evidenced by the fact that Mg^{2+} blocks NMDA-type glutamate receptors and voltage-gated Ca^{2+} channels, thus attenuating synaptic processes when it is raised and enhancing them when it is lowered (Czéh & Somjen, 1989; Jefferys, 1995; Hille, 2001; Somjen, 2002). Conversely, transmission is often stimulated at central synapses by high Ca^{2+} and inhibited by low Ca^{2+} (Hille, 2001; Somjen, 2002).

In contrast, spontaneous activity of neural networks involved in respiratory control is depressed by Ca^{2+} injection *in vivo* into close to lower brainstem respiratory network areas (Berndt et al., 1969; Berkenbosch & Adan, 1974; Leusen, 1972). These studies also showed that Ca^{2+}-mediated depression of breathing does not occur if K^+ is injected at the same time as Ca^{2+}. Such a 'Ca^{2+}/K^+ antagonism' also determines rhythmic activity of isolated respiratory networks. Firstly, bursting of rhythmogenic inspiratory pre-Bötzinger complex

(preBötC) neural networks in newborn rat 'Suzue-type' brainstem-spinal cord preparations was found to be depressed by raising either extracellular Ca^{2+} or Mg^{2+} notably above physiological values (Kuwana et al., 1998). Subsequently, our group showed that the Ca^{2+} sensitivity of preBötC bursting is particularly high when rostral tissue is removed by defined sectioning from the *en bloc* model and also in transversal newborn rat preBötC slices (Ruangkittisakul et al., 2007). Similarly, Ca^{2+}/K^{+} antagonism determines preBötC rhythm in slices from C57/BL6 mice that are often the basis for genetic engineering (Del Negro et al., 2009; Ruangkittisakul et al., 2011). Finally, we presented evidence in 400 μm thick 'm-preBötC[400]' slices with centered preBötC that presynaptic inhibition might play a major role in Ca^{2+} block of inspiratory bursting (Panaitescu et al., 2009). In the latter study, we showed that rhythm arrests spontaneously in these slices after ~2 h in physiological K^{+} (3 mM) and Ca^{2+} (1-1.2 mM), whereas bursting persists in ≥600 μm thick m-preBötC slices for >4 h in this solution which is usually sufficiently long for studying inspiratory network properties (Ruangkittisakul et al., 2006, 2008, 2012; Ballanyi & Ruangkittisakul, 2009). In the latter reports, we also showed that Ca^{2+} depression of the isolated preBötC is countered by raised K^{+} which changes though its sensitivity to some neuromodulators.

It was one major aim of the present study to quantify how preBötC rhythm in the m-preBötC[400] slice model depends on the ratio of Ca^{2+} and K^{+} and also on Mg^{2+}. Another aim was to determine whether low Ca^{2+} and Mg^{2+} are capable of

evoking seizure-like hyperexcitability in line with the fact that solution of low content of these divalent cations is an established model for studying mechanisms of epilepsy in cortical brain slices (Konnerth et al., 1986; Jeffreys, 1995; Kilb et al., 2007). As a final aim, we investigated whether rhythm in these slices remains active beyond 5 h, which would thus be sufficient for most pharmacological or intracellular analyses, when the superfusate contains 5 or 6 mM K^+ at 1 or 0.75 mM Ca^{2+} right from the start of recording. Parts of the results have been published (Panaitescu et al., 2010).

3.2.2 Methods

(see Chapter **2**)

3.2.3 Results

In the present study, m-preBötC[400] slices generated inspiratory rhythms at 7-8 bursts/min in standard solution with 7 mM K^+, 1.2 mM Ca^{2+} and 1.0 mM Mg^{2+} ('$7K^+/1.2Ca^{2+}/1Mg^{2+}$') in the ventrolateral slice aspect containing the VRC with the preBöt and in preBötC-driven hypoglossal (XII) motoneurons whose activity was either monitored in the XII nucleus or nerve. We investigated here how different levels of Ca^{2+}, Mg^{2+} and K^+ affect these rhythms.

3.2.3.1 Ca^{2+} and Mg^{2+} Effects

In 21 slices, in which respiratory XII nerve or nucleus rhythm was monitored simultaneously with VRC bursting, variation of Ca^{2+} (between 0.75-3.0 mM) or Mg^{2+} (between 0.25-3.0 mM) induced very similar effects on both types of activities **(Figs. 3.2-1**, **3.2-2)**. In 5 slices, raising Mg^{2+} to 2.0 or 3.0 mM had a tendency to slow burst rate, but the effect was only significant for 3 mM. In 6 different slices, lowering Mg^{2+} to 0.25 mM showed an (also non-significant) trend for increased burst rate **(Fig. 3.2-1)**. Burst duration was not affected by changing Mg^{2+}, but its amplitude decreased slightly in response to both 2 and 3 mM Mg^{2+} **(Fig. 3.2-1)**. Raising Ca^{2+} to 1.5 mM and 2.0 mM depressed burst rate progressively, with block of rhythm occurring in 2 of 5 slices for 1.5 mM Ca^{2+} and 7 of 10 slices for 2.0 mM, whereas rhythm was abolished in 5 slices tested in 3.0 mM Ca^{2+} **(Fig. 3.2-2)**. Lowering Ca^{2+} to 1.0, 0.75 or 0.5 mM induced a progressively larger increase in burst rate. This was reflected by a progressive decrease in burst amplitude which was significant for 0.75 and 0.5 mM Ca^{2+} while burst duration did not change **(Fig. 3.2-2)**. In 19 of 23 slices, exposure to 0.25 mM Ca^{2+} reduced burst amplitude within 27.4 ± 2 min to <15% of control, i.e. below a level allowing for a quantitative analysis. In these cases, rhythm also became irregular although the frequency appeared to increase further compared to 0.5 mM Ca^{2+}. In the remaining 4 slices, rhythm stabilized after 25.3 ± 4.1 min at a rate of 18.3 ± 1.2 bursts/min with a trend for a decrease in burst amplitude, but not duration **(Figs. 3.2-2)**. Depression of rhythm was even more pronounced in

0.1 mM Ca^{2+}, thus not allowing a quantitative analysis. In 1 of 4 slices, burst rate increased from 4 in control to 27 bursts/min in 0.1 mM Ca^{2+} and remained elevated at 15 bursts/min at re-increased amplitude for ~15 min following return to standard solution. In ~30% of slices, rhythm was accelerated by up to 250% of control during the initial 5-15 min of return from Ca^{2+} <0.5 mM to standard solution **(Fig. 3.2-2)**. Exposure of 2 slices to nominally Ca^{2+}-free solution (n= 2) or Ca^{2+}-free solution containing 5 mM of the Ca^{2+} chelators EGTA **(**n= 6**)** or EDTA **(**n= 4**)** abolished VRC rhythm (see below).

3.2.3.2 Seizure-like Activities in Low Ca^{2+}

The stimulatory effect of 0.25 mM Ca^{2+} on the rate of VRC rhythm rhythm was stronger than that of 0.25 mM Mg^{2+}. As a further difference between these divalent cations at low extracellular concentrations, prominent discharge developed in both XII nerve and nucleus firstly in the initial phase of the responses to Ca^{2+} ≤0.75 mM. This tonic activity was much more pronounced in XII than VRC recordings and typically occluded inspiratory XII activity. Tonic activity with a similar time course, but reduced amplitude, was also revealed in the VRC **(Fig. 3.2-3A)**. After 4-15 min, the initial tonic activity turned into slow rhythmic bursting in response to 0.75 mM Ca^{2+} in 2 of 7 VRC and 4 of 7 XII recordings. Correspondingly, 0.5 mM Ca^{2+} initiated slow seizure-like activity in 3 of 7 VRC and 5 of 6 XII recordings, while such activity developed in 7 of 8 VRC and 5 of 5 XII recordings in response to 0.25 mM Ca^{2+}. Such rhythm was also

revealed in 5 of 5 VRC and 2 of 2 XII recordings in response to 0.1 mM Ca^{2+}, although the amplitude of seizure-like bursting seemed to be smaller in both the VRC and XII nerve or nucleus compared to 0.25-0.75 mM Ca^{2+}. Seizure-like activity was substantially larger in XII than VRC recordings, although VRC respiratory rhythm could be partially masked at the peak of the hyperexcitability episodes due to an increase in the baseline of the integrated signal **(Fig. 3.2-3B)**. Both, the duration of a single seizure activity and their frequency varied considerably, specifically single bursts could last 5-150 s while they occurred at intervals between 10 and 500 s **(Fig. 3.2-3)**. In 4 of 8 slices, XII bursts in low Ca^{2+} were due to unsynchronized tonic activity. In the other slices, the bursts consisted of 2-7 Hz oscillations whose amplitude showed a rhythmic variation indicating seizure-like activity when displayed at lower time resolution **(Fig. 3.2-3B)**.

Seizures in response to 0.1-0.5 mM Ca^{2+} were blocked by Ca^{2+}-free saline containing a Ca^{2+} chelator **(Fig. 3.2-3B)**. Ca^{2+}-free solution with 5 mM EDTA (n= 4) abolished XII and VRC signals and recovery was either absent (n= 1) or delayed (n= 3) with incomplete recovery of burst strength upon return to low Ca^{2+} saline. In contrast, seizure-like XII rhythm in low Ca^{2+} transformed into fast (0.5-2 Hz, n= 6) bursting in XII nerve or nucleus in Ca^{2+}-free solution with 5 mM EGTA (n= 6) **(Fig. 3.2-3B)**. Fast XII bursts in the latter solution were not affected by 250 μM Cd^{2+} (n= 3), but were blocked upon addition of tetrodotoxin (0.1 mM) to 250 μM Cd^{2+} solution.

3.2.3.3 Cd^{2+} Effects

Next, we tested whether the increase in VRC burst rate in response to low Ca^{2+} may be related to reduced Ca^{2+} influx through voltage-gated Ca^{2+} channels and subsequent reduced activation of Ca^{2+} activated K^{+} channels that are both a prominent feature of newborn rat VRC neurons (Onimaru et al., 1996, 2003). At 5 or 10 μM, the voltage-activated Ca^{2+} channel blocker Cd^{2+} had no significant effect on either burst rate or duration, but notably attenuated their amplitude **(Fig. 3.2-4)**. At 25 μM, Cd^{2+} abolished rhythm in 3 of 4 slices, but irregular non-respiratory bursts with an amplitude <15% of control persisted in all cases at a rate of 3-6 bursts/min. Such non-respiratory bursting was also resistant to 250 μM Cd^{2+}, whereas addition of tetrodotoxin (0.1 μM) to 250 μM Cd^{2+}-containing solution abolished that activity (n= 5) **(Fig. 3.2-4)**. Cd^{2+} decreased the baseline of the integrated suction electrode signal indicating depression of tonic neuronal activity within the VRC, although tetrodotoxin had a more pronounced depressing effect **(Fig. 3.2-4)**.

3.2.3.4 Ca^{2+} and Mg^{2+} Effects in 9 K^{+}

The above results show that preBötC rhythm is very sensitive to variations of Ca^{2+}, while Mg^{2+} has a principally similar, though notably more modest effect. Next, we studied whether the modulatory Ca^{2+} effects are also pronounced in

$9K^+/1.5Ca^{2+}/1Mg^{2+}$ solution used in a majority of studies on preBötC slices (Richter & Spyer, 2001; Feldman & Del Negro, 2006; Ballanyi & Ruangkittisakul, 2009). After arrest of rhythm within <1 h in $3K^+/1.5Ca^{2+}/1Mg^{2+}$, raising K^+ to 9 mM reactivated inspiratory rhythm at a mean rate of 9.1 ± 0.5 bursts/min (n= 4) **(Fig. 3.2-5)** very similar to that of slices in $7K^+/1Ca^{2+}/1Mg^{2+}$, i.e. 9.4 burst/min (see above and **(Figs. 3.2-1, 3.2-6)**). Raising Ca^{2+} to 2.0 mM abolished rhythm in 1 of these slices and decreased burst rate to <50% of control, whereas 3.0 mM abolished rhythm in 3 slices thus decreasing mean burst rate to <1 burst/min **(Fig. 3.2-5)**. In slices with persistent bursting, single burst amplitude and duration were not affected by raising Ca^{2+}. Lowering Ca^{2+} to 1.0 and 0.75 mM accelerated rhythm in these slices by 53 and 71%, respectively **(Fig. 3.2-5)**. In addition to these effects on VRC burst rate, both the width of the VRC trace and its baseline increased in response to lowering Ca^{2+} while raising it had opposite effects **(Fig. 3.2-5)**. This indicates that Ca^{2+} not only modulates the activity of inspiratory VRC/preBötC neurons, but also of tonic neurons in this area, as described above for Cd^{2+}. Corresponding baseline changes of electrophysiological traces were not seen in XII nerve or nucleus recordings. In further 4 slices, we showed that block of VRC bursting by raising Ca^{2+} in 7 mM K^+ from 1.2 to 2.0 mM is reversed to reactivate very similar bursting by raising K^+ to 9 mM **(Fig. 3.2-5)**.

Next, we studied depressing effects of high Ca^{2+} on rhythm in fresh slices kept in 5 or 7 mM K^+. For 4 experiments in 5 mM K^+, slices were initially kept in

$3K^+/1.2Ca^{2+}/1Mg^{2+}$. At the onset of *in vitro* apnea, K^+ was raised to 5 mM which restored rhythm at a rate of ~2 bursts/min. Subsequent lowering of Ca^{2+} to 1, 0.75, 0.5 and 0.25 mM notably increased burst rate, whereas increasing it to 1.5 mM abolished bursting **(Fig. 3.2-6A)**. The graph in **Fig. 3.2.-6B** shows that there is a similar (linear) relationship for burst rates in dependence on superfusate Ca^{2+} and K^+ levels.

3.2.3.5 Longevity of Rhythms in <7 K^+

In our initial study introducing the m-preBötC[400] calibrated slice model, we showed that rhythm in $3K^+/1Mg^{2+}$ with either 1 or 1.2 mM Ca^{2+} is not stable for >2 h, whereas rhythm at reasonable rates (6-8 bursts/min) in $7K^+/1.2Ca^{2+}/1Mg^{2+}$ is robust for >6 h (Panaitescu et al., 2009). In a final set of experiments for the present study, the longevity of inspiratory rhythms was determined for slices kept from the beginning of recording in 1Ca/1Mg solution with either 5 or 6 mM K^+. In both types of solution, rhythm persisted throughout the 8 h test period, except for 1 of 10 slices that stopped bursting after 3.5 hours in 5 mM K^+ **(Fig. 3.2-7)**. In 6 mM K^+, burst rate dropped slowly from initially ~8 to ~5 bursts/min at 8 h, whereas this drop was more pronounced for slices in 5 mM K^+, specifically from initially ~8 to ~4 bursts/min at 2 h and ~2.5 bursts/min at 8 h. Four slices, studied in $7K^+/1Mg^{2+}$ with 0.75 mM Ca^{2+} showed rates >10 bursts/min for the first 2 h of recording while burst rates dropped steeply between 2-5 h **(Fig. 3.2-7)**. Seven and 11 slices tested in $3K^+/1Mg^{2+}$ and either 1 or 2 mM Ca^{2+} showed a longevity of

rhythm of ~2 h, similar to our previous study (Panaitescu et al., 2009) and 7 slices studied in $7K^+/1Ca^{2+}/1Mg^{2+}$ showed stable rhythm at initially ~12 bursts/min which slowed to ~9 bursts/min during 8 h. In all slices studied at 3, 5 or 6 mM K^+, raising K^+ at the end of the 8 h test period accelerated bursting to values typical for high K^+ as tested after shorter time period of recording **(Fig. 3.2-7)**.

3.2.4 Discussion

Previous studies, including various reports from our laboratory, have already provided evidence for depressing effects of Ca^{2+} and Mg^{2+} on isolated inspiratory networks and discussed potential underlying mechanisms (Kuwana et al., 1998; Ruangkittisakul et al., 2007; Del Negro et al., 2009; Panaitescu et al., 2009; Ballanyi & Ruangkittisakul, 2009). Here, we focus the discussion on our main findings on effects of 'low Ca^{2+}' and systematic variation of Ca^{2+} and Mg^{2+} in solutions of different K^+ content for optimized bursting in m-preBötC[400] slices that represent a good compromise between long term viability of rhythmogenic neurons and minimal preBötC modulation by adjacent tissue (Panaitescu et al., 2009; Ballanyi & Ruangkittisakul, 2009).

3.2.4.1 Inspiratory Network Stimulation *versus* Perturbation by Low Ca^{2+}

It has been proposed already in 1996 by Rekling and colleagues (1996) that 'low Ca^{2+}' superfusate stimulates inspiratory rhythm in preBötC slices, but they did not provide experimental evidence for that hypothesis. By low, they mean 0.7-0.8

mM, as used in some of their *in vitro* studies (Rekling et al., 1996; Voituron et al., 2006; Meillerais et al., 2010), compared to 1.5 mM which is typical for one major group of investigators, while others use 2 mM or more for studying 'breathing' slices and other active *in vitro* respiratory models (McLean & Remmers, 1994; Herlenius et al., 2002; Pierrefiche et al., 2002; Iizuka, 2004; St. John et al., 2004; Kuwana et al. 2006; Onimaru et al. 2006). Similarly, 2-3 mM superfusate Ca^{2+} is routinely applied since several decades by the majority of laboratories studying slices of diverse brain regions (Somjen, 2002; Ballanyi, 1999, 2012). This is done despite the fact that the interstitial free Ca^{2+} concentration ranges between 1 to 1.2 mM, particularly in more recent studies using Ca^{2+} sensitive microelectrodes in different brain structures *in vivo* (Heinemann et al., 1977; Nicholson et al., 1978; Hansen, 1985; Richter & Acker, 1989; Trippenbach et al. 1990; Nilsson et al., 1993; Puka-Sundvall et al., 1994; Somjen, 2002; Brown et al. 2004).

Taking this into account, we showed that preBötC slices with anatomically defined margins and rostrocaudal thickness of ≥500 μm generate inspiratory rhythm for several hours in 1 mM Ca^{2+} and physiological K^+ (3 mM) (Ruangkittisakul et al., 2006, 2007, 2008, 2011, 2012; Ballanyi & Ruangkittisakul, 2009). In one of the latter studies (Ruangkittisakul et al., 2007), we revealed that even slightly higher than physiological superfusate Ca^{2+} levels, i.e. ≥1.5 mM *versus* 1 mM, block rhythm in 3 mM K^+ in preBötC slices and that raised K^+ counters this inhibition. Previously, it was thought that such slices need to be studied in high K^+ because depolarization of rhythmogenic preBötC neurons

by this cation mimics excitatory synaptic drive that these highly reduced networks are deprived of, contrary to multiple on-going inputs in intact animals (Richter & Spyer, 2001; Feldman & Del Negro, 2006). It has even been predicted by modelling that preBötC slices can not show stable rhythm in 3 mM K^+ (Rybak et al., 2003). Important to note, slice rhythm in $3K^+/1Ca^{2+}$ 'washes out' after several hours with a clear correlation between their thickness and the time of onset of *in vitro* apnea (Ruangkittisakul et al., 2006, 2007, 2008, 2011, 2012; Ballanyi & Ruangkittisakul, 2009). As explanations for this spontaneous arrest of slice rhythm in physiological Ca^{2+} and K^+, synaptic terminals may continue to release excitatory neurotransmitters, such as glutamate or neuromodulators like thyrotropin-releasing hormone or substance-P just for limited time periods and/or inhibitory transmitters may progressively accumulate in the extracellular space.

In conclusion of the above considerations, superfusate needs to contain <1 mM Ca^{2+} to test whether 'low Ca^{2+}' stimulates preBötC slice rhythm. We show here that 0.75 mM Ca^{2+} (in 7 mM K^+) indeed increases VRC burst rate, by ~50% compared with 1.2 mM Ca^{2+}, with no concomitant change in burst duration, but with a ~20% decrease in its amplitude. VRC rhythm speeds up further in 0.5 mM, at the expense of a more pronounced amplitude decrease, but again with no effect on burst duration, while 0.25 mM Ca^{2+} causes a major amplitude depression and block of typical inspiratory rhythm in the VRC of most slices. The acceleration of rhythm is likely not due to reduced Ca^{2+} influx that would possibly cause attenuated activation of Ca^{2+}-activated K^+ channels (Onimaru et al., 1996, 2003;

Crowder et al., 2007; Zavala-Tecuapetla et al., 2008; Krey et al., 2010) because partial blockade of such channels by Cd^{2+} did not accelerate rhythm. Importantly, already at 0.75 mM Ca^{2+}, inspiratory XII nucleus and nerve activity are perturbed in some slices by occurrence of seizure-like bursting. Similarly, seizure-like bursting occurs in 0.75 mM Ca^{2+} in spinal motor networks of fetal mouse brainstem-spinal cords (Meillerais et al., 2010) and, in the same model from fetal rats, even already at 1 mM (Ren et al., 2006). Accordingly, use of <1 mM Ca^{2+} is not recommended for preBötC slices particularly when XII motor networks are going to be studied (Schwarzacher et al., 2002; Greer & Funk, 2005; Ballanyi & Ruangkittisakul, 2009). Moreover, in slices kept right from the start in solution with modestly elevated (5 mM) K^+, the longevity of rhythm does not improve in 0.75 *versus* 1 mM Ca^{2+}. Finally, the initially higher VRC burst rate in 0.75 mM Ca^{2+} and 5 mM K^+ shows a steeper drop over time. This would make it more difficult to analyze effects of neuroactive agents on inspiratory networks in such slices.

Decreasing divalent cation levels in the superfusate is an established epilepsy model (Jefferys, 1995; Kilb et al., 2007). In contrast to *in vitro* findings on cortical brain structures (Derchanski et al., 2004; Abdelmalik et al., 2005), 0.25 mM Mg^{2+} did not induce hyperexcitability in preBötC slices. Conversely, similar to findings on cortical structures (Konnerth et al., 1986; Jefferys, 1995; Kilb et al., 2007), reducing Ca^{2+} to ≤0.75 mM evoked massive seizure-like activity occluding XII inspiratory rhythm. Such low Ca^{2+} seizures may originate in the XII motor

nucleus because similar synchronous activity was notably less pronounced in the VRC. Similarly, seizure-like hyperexcitability due to block of synaptic inhibition was found to be very pronounced in respiratory motor nuclei compared to VRC interneurons (Brockhaus & Ballanyi, 1998, 2000). Also our recent findings on effects of methylxanthine effects suggest that preBötC networks are rather insensitive to their epileptiform potential whereas they evoke major perturbations of both inspiratory spinal and cranial motor network activities (Chapter **5**) **(Fig. 5-1**, **5-4)**. In contrast to seizures in higher brain regions (Konnerth et al., 1986; Jefferys, 1995; Kilb et al., 2007) and robust XII bursting of fetal rat preBötC slices in Ca^{2+}-free saline (Ren et al., 2006), low Ca^{2+} seizure-like XII bursting in the newborn rat slices of the present study were blocked by Ca^{2+}-free solution. While Ca^{2+}-free solution containing the Ca^{2+} buffer EDTA abolished both preBötC and XII activities, EGTA-buffered solution transformed slow XII seizures into regular large-amplitude 0.3-1 Hz oscillations. This indicates that the XII nucleus contains neuronal circuitry capable of generating multiple types of rhythmic activity (Nistri et al., 2006; Ren et al., 2006). Findings using EGTA/EDTA as Ca^{2+} chelators need to be considered with caution as the agents can, e.g., inhibit glutamate binding to NMDA receptors (Chen et al., 2000) or act as Ca^{2+} ionophores causing membrane damage (Pitta et al., 1997).

The tolerance of the preBötC to low Ca^{2+} may be functionally important. Ongoing inspiratory bursting during the normal respiratory cycle or during exaggerated activity such as sighs may cause rhythmic decreases of Ca^{2+} by >0.5 mM as

shown for evoked responses in various brain regions including respiratory brainstem areas (Richter & Acker, 1989; Heinemann et al., 1977; Jefferys, 1995; Cohen & Fields, 2004). Yet, *in vitro* or *in vivo* studies have not provided evidence for respiratory-related decreases of extracellular Ca^{2+} contrary to various reports on rhythmic K^+ rises (Ballanyi et al., 1992, 1996; Brockhaus et al., 1993; Völker et al., 1995; Morawietz et al., 1995; Richter & Acker, 1989; Trippenbach et al., 1990).

3.2.4.2 Optimal Ratios for K^+, Ca^{2+} and Mg^{2+} for Long-Term preBötC Slice Rhythm

In our previous report (Ruangkittisakul et al. 2007), a comparison of m-preBötC[600] slices in $3K^+/1Ca^{2+}$ indicated that the longevity of rhythms in 1 *versus* 2 mM Mg^{2+} is similar, while there was a trend for a higher burst rate in lower Mg^{2+}. This trend was consolidated here because burst rate in m-preBötC[400] slices in $3K^+/1.2Ca^{2+}$ seemed to be lower in 2 compared to 1 mM Mg^{2+} and rhythm was significantly slower (~30% of control) in 3 *versus* 1 mM. For testing effects of lower Mg^{2+}, we started by using 0.25 mM. Similar to low Ca^{2+} (see above), 0.25 mM Mg^{2+} accelerated VRC rhythm, but did not evoke seizure-like bursting as seen with 0.25 mM Ca^{2+}. Because the (non-significant) stimulatory effect of Mg^{2+} was modest (~120 % of control), we did not study whether intermediate values between 0.25 and 1 mM would accelerate rhythm. We were not able to find consistent numbers regarding the free concentration of

Mg^{2+} in interstitial brain tissue. Anyway, we recommend to use 1 mM for studying preBötC slices because of the slightly stimulatory action. Accordingly, we propose that 1 mM Ca^{2+} and 1 mM Mg^{2+} in the superfusate may be the choice, if recording robust VRC rhythm at high rate is desired for a particular study. Several laboratories believe that whole-cell recordings are more stable in superfusate with elevated divalent cation content. However, in our previous studies using superfusate with 1.5 mM Ca^{2+} and 1 mM Mg^{2+}, >50% of several hundred whole-cell recordings were stable for at least 1 h, often for >2 h (Smith et al., 1991; Brockhaus & Ballanyi, 1998, 2000; Schwarzacher et al., 2002). Cell numbers are yet lower for our whole-cell recordings in calibrated preBötC slices in 1 mM Ca^{2+} and 1 mM Mg^{2+}, but recordings are on average stable for at least 0.5-1 h (Chapter **3.1**) (Panaitescu et al., 2009; Ballanyi & Ruangkittisakul, 2009; Ruangkittisakul & Ballanyi, 2012; Ruangkittisakul et al., 2012).

The graph in **Fig. 3.2-6** summarizes which rates of VRC rhythm can be expected in 7 and 9 mM K^+ depending on which Ca^{2+} value is chosen (in 1 mM Mg^{2+}). This analysis revealed, for example, that varying K^+ between 7 and 9 mM and Ca^{2+} between 1 and 1.5 mM results in frequency of VRC rhythm ranging from 8 to 16 bursts/min. The graph shows further that rhythm at ~5 bursts/min is observed in $5K^+/1Ca^{2+}/1Mg^{2+}$. However, the longevity graph in **Fig. 3.2-7** for slices kept in this solution from the start of recording illustrates that burst rate drops from initially ~8 to ~3 bursts/min within 5 h. This drop of 1 burst/min per hour is slow enough and 5 h are usually long enough for most pharmacological,

intracellular and optical imaging analyses. The disadvantage of the slow burst rate is countered by the fact that potential manipulation of pharmacological or burst properties of preBötC networks is notably lower compared to studying these slices in mostly used 9 mM K^+. For example, VRC rhythm in calibrated slices is blocked in 3 mM K^+ by 10-25 nM of the μ-opioid receptor agonist DAMGO, while this inhibition is reversed by raising K^+ to 9 mM and, consequently, DAMGO doses have to be raised to close to micromolar levels to attenuate bursting again (Ballanyi & Ruangkittisakul, 2009) (Chapter **1.3**) **(Fig. 1-6)**. As further examples, *in vivo*-like membrane potential oscillations in inspiratory preBötC neurons of calibrated newborn rat slices kept in 3 mM K^+ are 'flattened' in 9 mM K^+ and sigh-like inspiratory burst patterns in 3 mM K^+ are absent in 9 mM K^+ (Ballanyi & Ruangkittisakul, 2009) (Chapter **1.3**) **(Fig. 1-6)**. Several previous studies on preBötC slices were conducted in 5-6 mM K^+, but properties of VRC rhythms in these slices were not analyzed in much detail (Del Negro et al., 2001, 2002; Pierrefiche et al., 2002; Rybak et al., 2003). Our recent results indicate that calibrated preBötC slices from C57BL/6 mice show robust rhythm at a rate of 8-12 bursts/min for >6 h in $6K^+/1Ca^{2+}/1Mg^{2+}$ (Ruangkittisakul et al., 2011). Our future work will focus very much on optical imaging analyses of neuron-glia interactions in preBötC networks of calibrated slices (Ruangkittisakul et al., 2009, 2012). Our previous multipoton/confocal Ca^{2+} imaging approaches (Ruangkittisakul et al., 2006, 2008, 2009) revealed that the decay time of inspiratory-related Ca^{2+} rises can be as long as 2-4 s. Consequently, bursts rates notably higher than 10 bursts/min are not desirable for such imaging. Multiphoton

approaches have yet not enabled respiratory optical imaging at high spatial resolution in slice depths >100 μm (Ruangkittisakul et al., 2009). Accordingly, we currently use for such imaging calibrated 'r+preBötC[400]' slices in which the rhythmogenic inspiratory kernel is located close to the caudal boundary (Ruangkittisakul et al., 2008, 2009, 2012; Bobocea et al., 2010). We have not tested the sensitivity to Ca^{2+}, Mg^{2+} and K^{+} in detail in these slices, but assume that basic features of preBötC bursting such as burst rates and durations are similar to those revealed here for the m-preBötC[400] slices. Based on all these consideration, we propose to use $6K^{+}/1Ca^{2+}/1Mg^{2+}$ solution for studying preBötC[400] slices because (*i*) initial burst rates are higher than in 5 mM K^{+} solution of identical divalent cation content (~8 bursts/min) and (*ii*) these slices show bursts rate of ~5 bursts/min even after 8 h of recording indicating that the drop of initial rate is rather slow.

3.2.5 Figures and Legends

Fig. 3.2-1

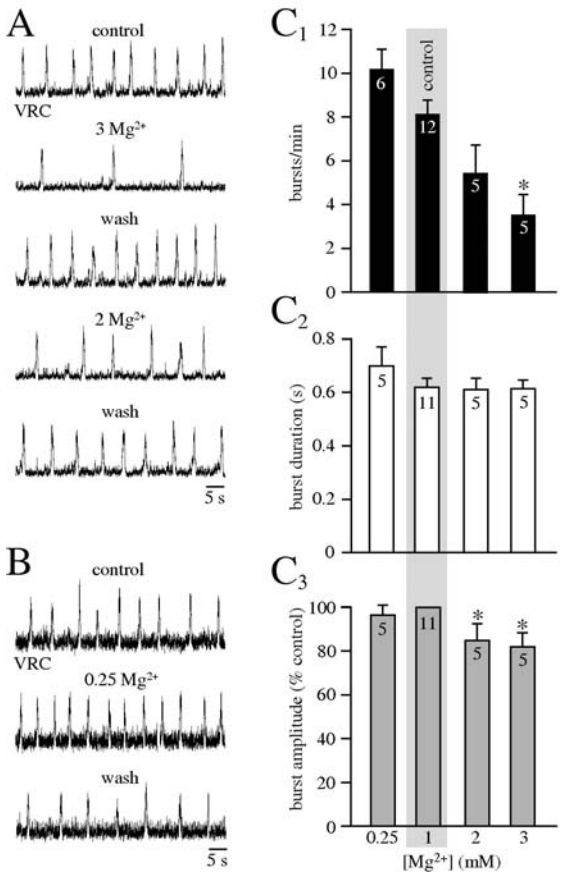

Fig. 3.2-1: Effects of superfusate Mg^{2+} on rhythmic activity inspiratory pre-Bötzinger complex (preBötC) networks in transversal newborn rat slices. A, inspiratory-related rhythm was measured as the integrated differential amplifier signal via a suction electrode positioned within the ventral respiratory column (VRC) at the caudal surface of a 400 μm thick transverse brainstem slice from a postnatal day (P) 1 Sprague-Dawley (SD) rat with the preBötC in the middle and the caudal boundary -0.68 mm caudal to the caudal end of the facial (VII) motor nucleus as reference (Ruangkittisakul et al., 2006; Panaitescu et al., 2009). In this m- preBötC[400/-0.68]SD-P1 slice superfused with saline containing 7 mM K^+, raising Mg^{2+} from 1.0 to 3.0 or 2.0 mM depressed inspiratory burst rate with no major effect on the amplitude or duration of single bursts. **B**, in a m-preBötC[400/-0.75]SD-P2 slice lowering Mg^{2+} to 0.25 mM reversibly increased burst rate. **C**, statistical analysis of Mg^{2+} effects on rate, duration and amplitude of inspiratory bursts in m-preBötC[400/-0.71]W/SD-P0/3 slices. Bars represent means ± SEM; digits indicate the number of preparations tested; asterisks indicate significant ($P< 0.05$) difference of bar value compared with control.

Fig. 3.2-2

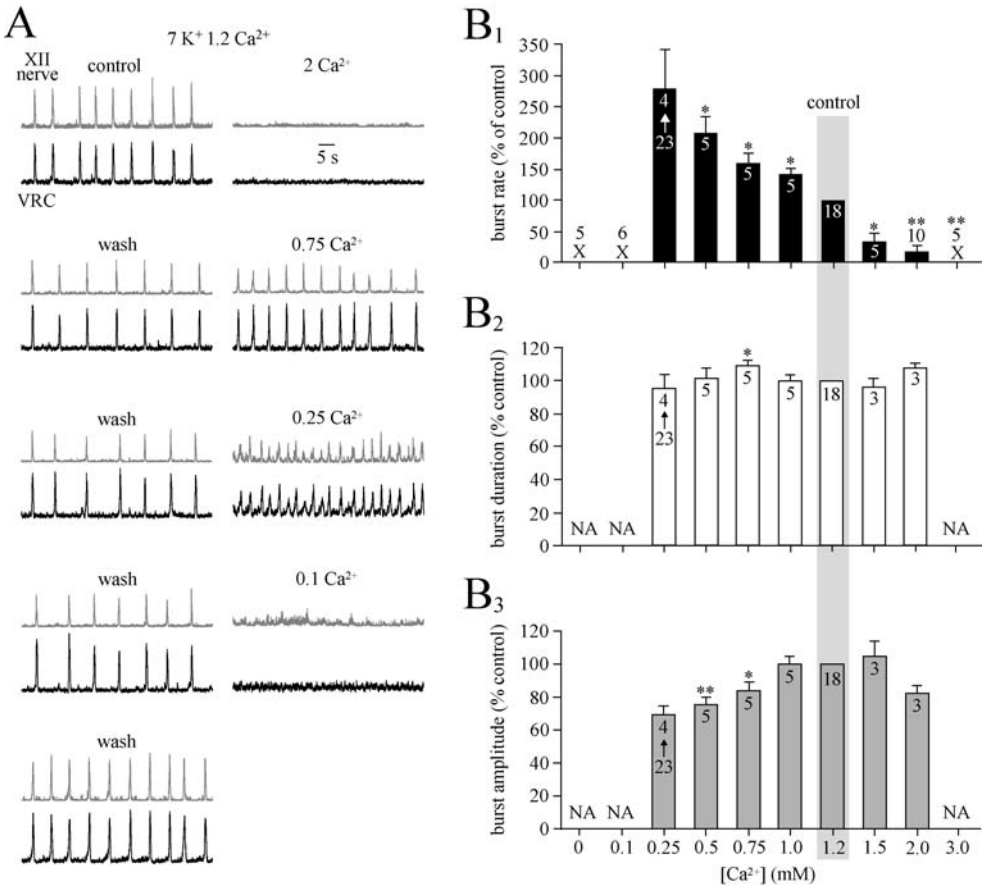

Fig. 3.2-2: Strong modulation of preBötC slice rhythm by superfusate Ca^{2+}. Inspiratory VRC rhythm in 7 mM K^+ and 1 mM Mg^{2+} was measured simultaneously with hypoglossal (XII) nerve activity in a m-preBötC[400/-0.68]W-P2 slice. Raising Ca^{2+} from 1.2 to 2 mM abolished rhythm while 0.25 mM Ca^{2+} increased burst rate, but depressed burst amplitude and rhythm was blocked in 0.1 mM Ca^{2+}. **B**, statistics of Ca^{2+} effects on preBötC rhythm. Effects of variation of Ca^{2+} in 7 K^+ are shown on the rate (**B_1**), duration (**B_2**) and amplitude (**B_3**) of inspiratory bursts in m-preBötC[400/-0.70]W/SD-P0/3 slices.

Fig. 3.2-3

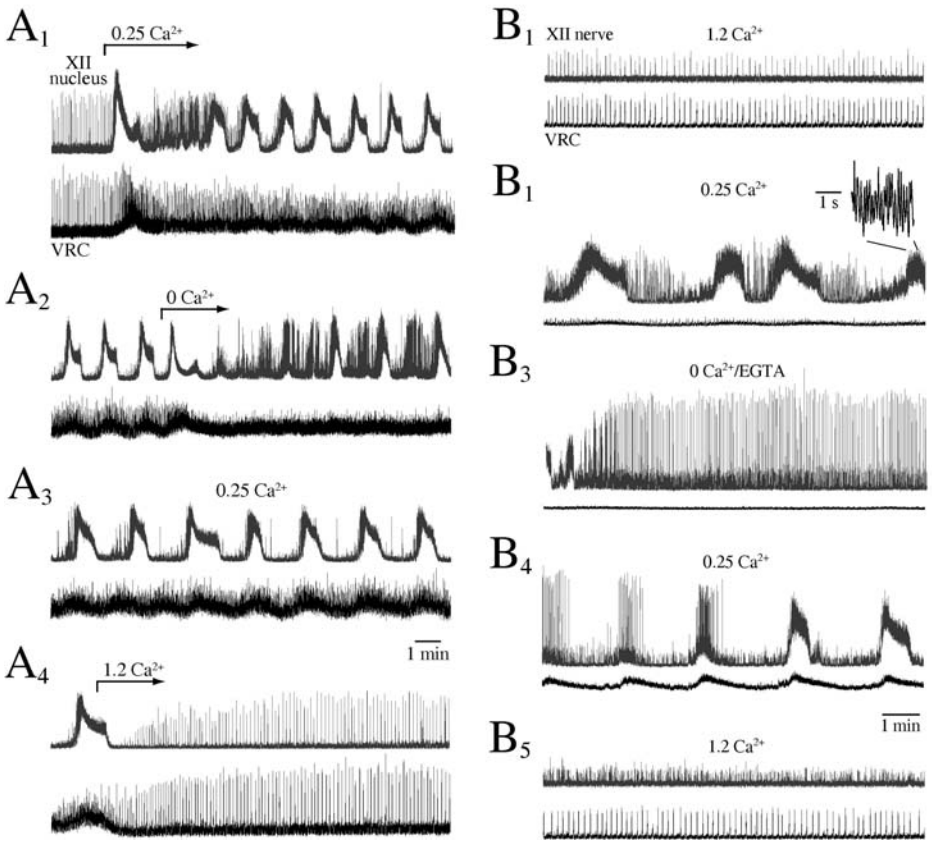

Fig. 3.2-3: Transformation of inspiratory rhythm into seizure-like activity by low Ca^{2+}. A, in a m-preBötC[400/-0.70]W-P1 slice in $7K^{+}/1Mg^{2+}$ lowering Ca^{2+} from 1.2 to 0.25 mM (**A_1**) depressed the amplitude of inspiratory XII nucleus discharge and evoked massive non-respiratory bursting. Such seizure-like activity was less pronounced in the VRC which showed inspiratory rhythm of greatly increased rate at reduced strength. **A_2**, application of nominally Ca^{2+}-free solution substituted inspiratory VRC rhythm with irregular low amplitude discharge, whereas seizure-like XII rhythm was intermingled with 1-5 Hz short duration bursts. **A_3**, return to 0.25 mM Ca^{2+} (3 min prior to onset of recording) reestablished rhythmic VRC and XII discharges as in **A_2**. **A_4**, within <3 min of return to standard (1.2 mM Ca^{2+}) solution, regular respiratory VRC and XII rhythm reappeared. **B**, transformation of low Ca^{2+} seizure-like XII rhythm into regular bursting. **B_1**, **B_2**, lowering Ca^{2+} to 0.25 mM in a m-preBötC[400/-075]SP-P1 slice greatly attenuated the amplitude of inspiratory VRC bursting but increased burst rate whereas seizure-like bursting developed in the XII nerve. **B_3**, Ca^{2+}-free saline with 5 mM of the Ca^{2+} chelator ethyleneglyco-tetraacetic acid (EGTA) abolished VRC activity and transformed seizure-like XII bursting into pacemaker-like activity that was already sporadically present in 0.25 mM Ca^{2+}. **B_4**, return to 0.25 mM Ca^{2+} 2 min prior to start of recording reestablished seizure-like XII rhythm and synchronous non-respiratory VRC oscillations. **B_5**, upon

washout of low Ca^{2+}, inspiratory rhythm reappeared in the VRC, but not the XII recording that showed irregular tonic bursting.

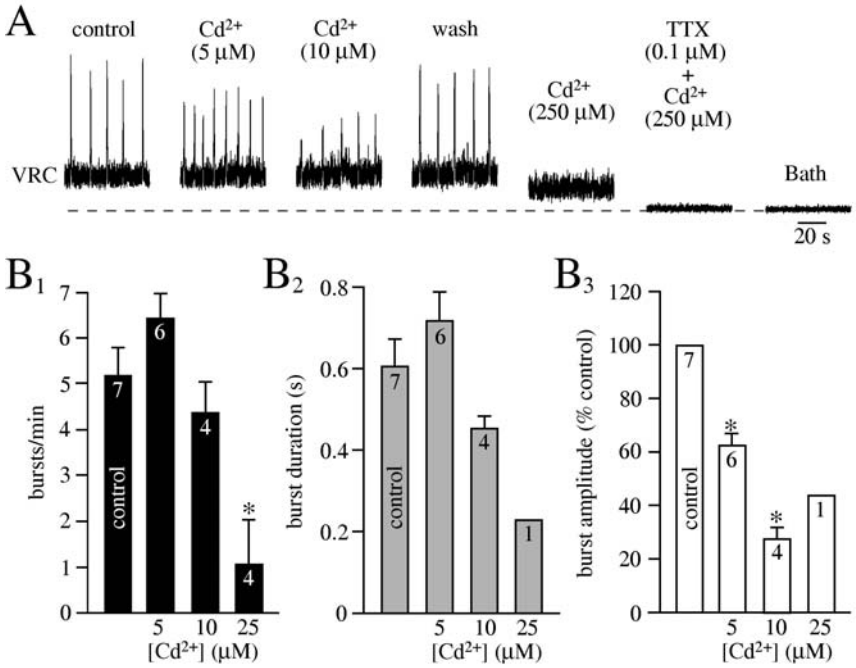

Fig. 3.2-4: Effects of Cd^{2+} on preBötC rhythm. A, bath-application of 5 µM Cd^{2+} in $7K^{+}/1Mg^{2+}$ increased the rate, but depressed the amplitude of inspiratory VRC bursting in a m-preBötC[400/-0.70] slice. 10 µM Cd^{2+} depressed inspiratory bursts further, but did not accelerate the rhythm which was blocked by subsequent administration of 250 µM Cd^{2+}. 250 µM Cd^{2+} decreased the baseline of the integrated VRC recording indicating depression of tonic neuronal population activity within the VRC. Addition of tetrodotoxin (TTX) abolished neuronal activity as indicated by the similarity of the VRC signal with that upon withdrawal of the suction electrode from the slice (Bath). **B_{1-3}**, statistics of Cd^{2+} effects on rate (**B_1**), duration (**B_2**) and amplitude (**B_3**) of inspiratory VRC bursts in m-preBötC[400/-0.70]W-P0/2 slices. Only one slice was evaluated for the effects of 25 µM Cd^{2+} on burst duration and amplitude because rhythm was blocked in the other slices.

Fig. 3.2-5

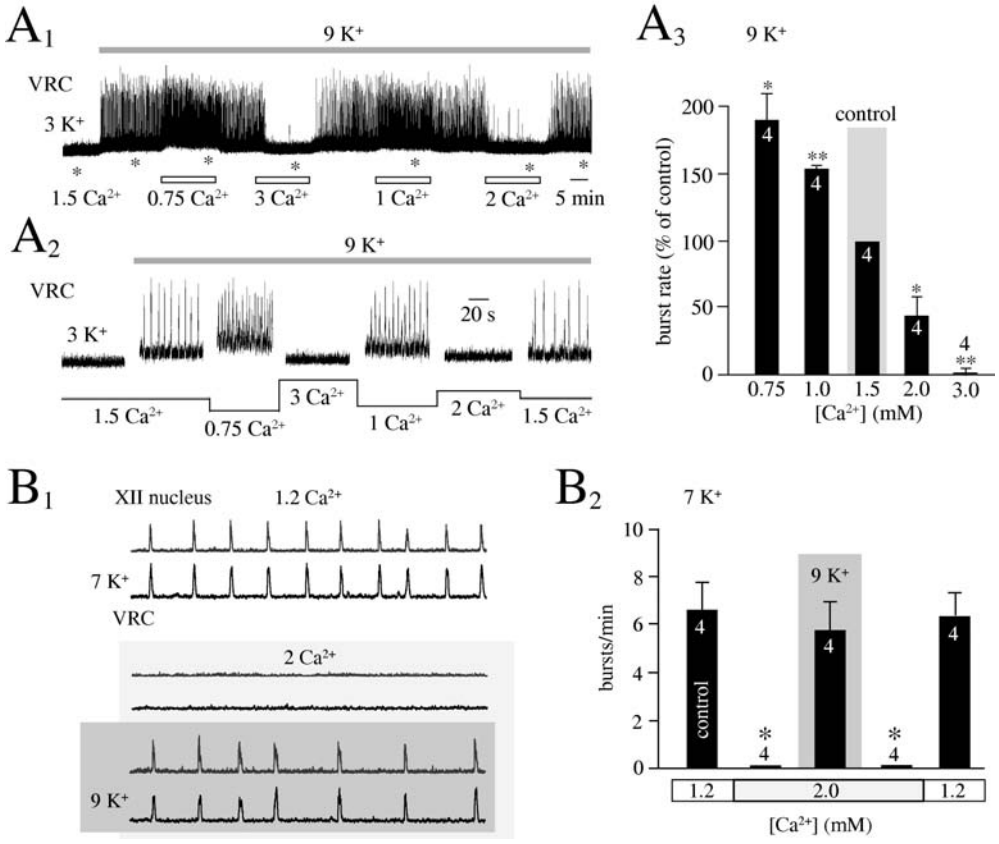

Fig. 3.2-5: Strong Ca^{2+} modulation of preBötC rhythm in 9 K^+. **A**, the recording of VRC activity in a m-preBötC[400/-0.75]SD-P2 slice in 1.5Ca^{2+}/1Mg^{2+} started when endogenous rhythm in 3 mM K^+ arrested spontaneously after 27 min. **A_1**, raising K^+ to 9 mM evoked regular VRC bursting shown for indicated time periods (asterisks) at higher time resolution in (**A_2**). Lowering Ca^{2+} increased burst rate and concomitantly raised the baseline of integrated recording indicating augmented tonic activity within the VRC. Increasing Ca^{2+} had opposite effects on both burst rate and tonic VRC activity. **A_3**, statistical analysis of the Ca^{2+} dependence of burst rates in m-preBötC[400/-0.75]W/SD-P1/3 slices in 9 mM K^+. Effects of Ca^{2+} on burst amplitude and duration were not significant, thus not shown. **B**, K^+ reversal of block of preBötC rhythm by 2 mM Ca^{2+}. **B_1**, raising Ca^{2+} from 1.2 to 2 mM in 7 mM K^+ abolished inspiratory rhythm in a m-preBötC[400/-0.68]W-P2 slice. Subsequent elevation of K^+ to 9 mM restored rhythm at a rate not significantly different from control rhythm in 7 mM K^+. **B_2**, statistical analysis of reversal by 9 mM K^+ of block of inspiratory rhythm in m-preBötC[400/-0.68]W/SD-P1/2 in 7 mM K^+. Effects of Ca^{2+} on burst amplitude and duration were not significant, thus not shown.

Fig. 3.2-6

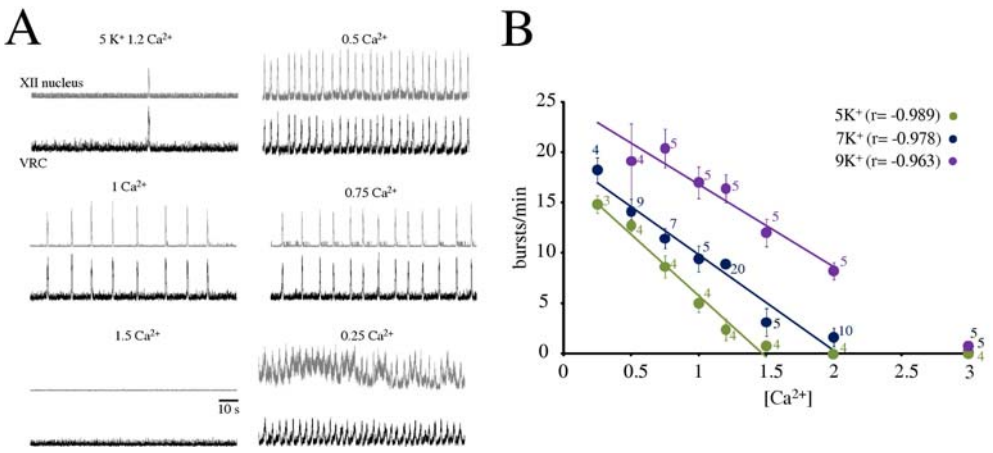

Fig. 3.2-6: Relationship between VRC burst rates, superfusate Ca^{2+} and superfusate K^+. **A**, the recording of VRC activity in a m-preBötC[400] slice shows that very slow synchronous VRC and XII nucleus bursting was induced after onset of *in vitro* apnea in $3K^+/1.2Ca^{2+}/1Mg^{2+}$ solution by raising K^+ to 5 mM. Bursting was very much accelerated by lowering Ca^{2+} from 1.2 to 0.5 mM and remained quite robust at lower rate after subsequent change to 1 and 0.75 mM Ca^{2+}. In 0.25 mM Ca^{2+} very fast VRC rhythm occurrd at greatly reduced amplitude while seizure-like discharge partially occluded inspiratory XII nucleus rhythm. **B**, Ca^{2+} dependence of preBötC burst rate at different superfusate K^+ levels. Linear regression analysis revealed a non-significant difference between slopes for the measurements in 5, 7, or 9 mM K^+.

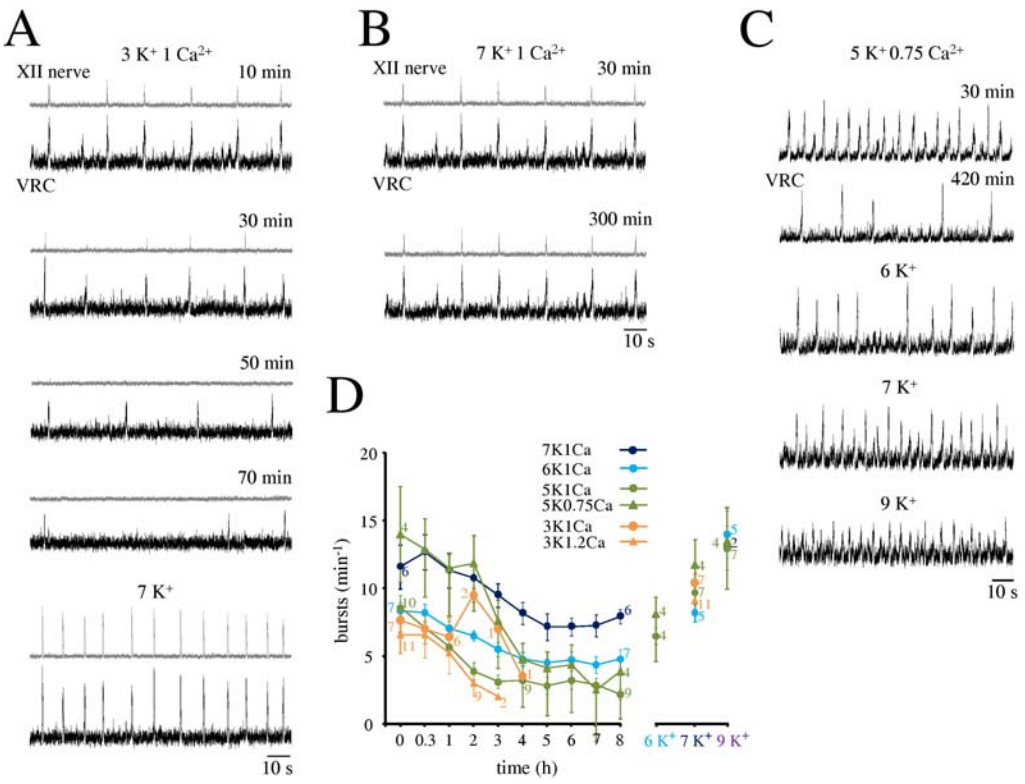

Fig. 3.2-7: Longevity of preBötC slice rhythm in superfusate with varying Ca^{2+}/K^{+} content. **A,** VRC and XII nerve rhythms were stable in $3K^{+}/1Ca^{2+}/1Mg^{2+}$ for 30 min, but XII bursting disappeared shortly afterwards while VRC bursting continued until 70 min of recording. 7 mM K^{+} reactivated rhythm at a faster rate than in the fresh slice in control. **B**, rhythm in another slice kept in $7K^{+}/1Ca^{2+}/1Mg^{2+}$ from the beginning of recording was stable for >5 h. **C**, in $5K^{+}/0.75Ca^{2+}$, a preBötC slice was active for >7 h although the rate of rhythm decreased notably. Subsequent elevation of K^{+} increased inspiratory burst rate to values higher than in control while burst amplitude was reduced in 9 mM K^{+}. **D**, the plot of time dependence of burst rates of preBötC slices studied in superfusate with varying Ca^{2+}/K^{+} content. The right portion of the graph shows steady-state burst rate in response to elevated K^{+} at the end of the 8 h recording period.

3.3 References

Abdelmalik PA, Burnham WM, Carlen PL (2005) Increased seizure susceptibility of the hippocampus compared with the neocortex of the immature mouse brain in vitro. Epilepsia 46, 356-366

Ballanyi K (1999) Isolated tissues. In Vitro Preparations, in Modern Techniques in Neuroscience Research, U. Windhorst and H. Johansson, Editors, Springer: Heidelberg 307-326

Ballanyi K (2012) Isolated Central Nervous System Circuits. Neuromethods Series (Ed. W. Walz). Springer Science-Business Media, LLC, New York, NY

Ballanyi K, Ruangkittisakul A (2009) Structure-function analysis of rhythmogenic inspiratory pre-Bötzinger complex networks in 'calibrated' newborn rat brainstem slices. Respir Physiol Neurobiol 168, 158-178

Ballanyi K, Kuwana S, Völker A, Morawietz G, Richter DW (1992) Developmental changes in the hypoxia tolerance of the in vitro respiratory network of rats. Neurosci Lett 148, 141-144

Ballanyi K, Völker A, Richter DW (1996) Functional relevance of anaerobic metabolism in the isolated respiratory network of newborn rats. Eur J Physiol (Pflüger's Arch) 432, 741-748

Ballanyi K, Lalley PM, Hoch B, Richter DW (1997) cAMP-dependent reversal of opioid- and prostaglandin-mediated depression of the isolated respiratory network in newborn rats. J Physiol 504, 127-134

Ballanyi K, Onimaru H, Homma I (1999) Respiratory network function in the isolated brainstem-spinal cord of newborn rats. Prog Neurobiol 59, 583-634

Ballanyi K, Ruangkittisakul A, Onimaru H (2009) Opioids prolong and anoxia shortens delay between onset of preinspiratory (pFRG) and inspiratory (preBötC) network bursting in newborn rat brainstems. Eur J Physiol (Pflüger's Arch) 458, 571-587

Berkenbosch A, Adan AJ (1974) Influence of CSF calcium concentration on the ventilatory response to CO_2 and O_2. Eur J Physiol (Pflüger's Arch) 348, 33-50

Berndt J, Fenner A, Berger K (1969) Influence of calcium and magnesium on the respiratory response to changes in CSF pH. Respir Physiol Neurobiol **7**, 216-229

Bobocea N, Ruangkittisakul A, Ballanyi K (2010) Multiphoton/confocal Ca^{2+} imaging of inspiratory pre-Bötzinger complex neurons at the caudal or rostral surface of newborn rat brainstem slices. Adv Exp Med Biol 669, 81-85

Brockhaus J, Ballanyi K (1998) Synaptic inhibition in the isolated respiratory network of neonatal rats. Eur J Neurosci 10, 3823-3839

Brockhaus J, Ballanyi K (2000) Anticonvulsant A_1 receptor-mediated adenosine action on neuronal networks in the brainstem-spinal cord of newborn rats. Neuroscience 96, 359-371

Brockhaus J, Ballanyi K, Smith JC, Richter DW (1993) Microenvironment of respiratory neurons in the *in vitro* brainstem-spinal cord of neonatal rats. J Physiol 462, 421-445

Brown EM, MacLeod RJ (2001) Extracellular calcium sensing and extracellular calcium signaling. Physiol Rev 81, 239-297

Brown PD, Davies SL, Speake T, Millar ID (2004) Molecular mechanisms of cerebrospinal fluid production. Neuroscience 129, 957-970

Chen N, Murphy TH, Raymond LA (2000) Competitive inhibition of NMDA receptor-mediated currents by extracellular calcium chelators. J Neurophysiol 84, 693-697

Cohen JE, Fields RD (2004) Extracellular calcium depletion in synaptic transmission. Neuroscientist 10, 12-17

Crowder EA, Saha MS, Pace RW, Zhang H, Prestwich GD, Del Negro CA (2007) Phosphatidylinositol 4,5-bisphosphate regulates inspiratory burst activity in the neonatal mouse preBötzinger complex. J Physiol 582, 1047-1058

Czeh G, Somjen GG (1989) Changes in extracellular calcium and magnesium and synaptic transmission in isolated mouse spinal cord. Brain Res 486, 274-285

Del Negro CA, Johnson SM, Butera RJ, Smith JC (2001) Models of respiratory rhythm generation in the pre-Bötzinger complex. III. Experimental tests of model predictions. J Neurophysiol 86, 59-74

Del Negro CA, Morgado-Valle C, Feldman JL (2002) Respiratory rhythm: an emergent network property? Neuron 30, 821-830

Del Negro CA, Kam K, Hayes JA, Feldman JL (2009) Asymmetric control of inspiratory and expiratory phases by excitability in the respiratory network of neonatal mice in vitro. J Physiol 587, 1217-1231

Derchansky M, Shahar E, Wennberg RA, Samoilova M, Jahromi SS, Abdelmalik PA, Zhang L, Carlen PL (2004) Model of frequent, recurrent, and spontaneous seizures in the intact mouse hippocampus. Hippocampus 14, 935-947

Feldman JL, Del Negro CA (2006) Looking for inspiration: new perspectives on respiratory rhythm. Nat Rev Neurosci 7, 232-242

Gray PA, Rekling JC, Bocchiaro CM, Feldman JL (1999) Modulation of respiratory frequency by peptidergic input to rhythmogenic neurons in the preBotzinger complex. Science 286, 1566-1568

Greer JJ, Funk GD (2005) Perinatal development of respiratory motoneurons. Respir Physiol Neurobiol 149, 43-61

Hansen AJ (1985) Effect of anoxia on ion distribution in the brain. Physiol Rev 65, 101-148

Heinemann U, Lux HD, Gutnick MJ (1977) Extracellular free calcium and potassium during paroxsmal activity in the cerebral cortex of the cat. Exp Brain Res 27, 237-243

Herlenius E, Aden U, Tang LQ, Lagercrantz H (2002) Perinatal respiratory control and its modulation by adenosine and caffeine in the rat. Pediatr Res 51, 4-12

Hille B (2001) Ion channels of excitable membranes. Sunderland, MA: Sinauer Associates

Hille B, Woodhull AM, Shapiro BI (1975) Negative surface charge near sodium channels of nerve: divalent ions, monovalent ions, and pH. Philos Trans R Soc Lond B Biol Sci 270, 301-318

Iizuka M (2004) Rostrocaudal distribution of spinal respiratory motor activity in an in vitro neonatal rat preparation. Neurosci Res 50, 263-269

Jefferys JG (1995) Nonsynaptic modulation of neuronal activity in the brain: electric currents and extracellular ions. Physiol Rev 75, 689-723

Kilb W, Sinning A, Luhmann HJ (2007) Model-specific effects of bumetanide on epileptiform activity in the in-vitro intact hippocampus of the newborn mouse. Neuropharmacology 53, 524-533

Konnerth A, Heinemann U, Yaari Y (1986) Nonsynaptic epileptogenesis in the mammalian hippocampus in vitro. I. Development of seizurelike activity in low extracellular calcium. J Neurophysiol 56, 409-423

Krey RA, Goodreau AM, Arnold TB, Del Negro CA (2010) Outward currents contributing to inspiratory burst termination in preBötzinger complex neurons of neonatal mice studied in vitro. Front Neural Circuits 29, 124

Kuwana S, Okada Y, Natsui T (1998) Effects of extracellular calcium and magnesium on central respiratory control in the brainstem-spinal cord of neonatal rat. Brain Res 786, 194-204

Kuwana S, Tsunekawa N, Yanagawa Y, Okada Y, Kuribayashi J, Obata K (2006) Electrophysiological and morphological characteristics of GABAergic respiratory neurons in the mouse pre-Bötzinger complex. Eur J Neurosci 23, 667-674

Leusen I (1972) Regulation of cerebrospinal fluid composition with reference to breathing. Physiol Rev 52, 1-56

McLean HA, Remmers JE (1994) Respiratory motor output of the sectioned medulla of the neonatal rat. Respir Physiol 96, 49-60

Meillerais A, Champagnat J, Morin-Surun MP (2010) Extracellular calcium induces quiescence of the low-frequency embryonic motor rhythm in the mouse isolated brainstem. J Neurosci Res 88, 3555-3565

Morawietz G, Ballanyi K, Kuwana S, Richter DW (1995) Oxygen supply and ion homeostasis of the respiratory network in the in vitro perfused brainstem of adult rats. Exp Brain Res 106, 265-274

Nicholson C, ten Bruggencate G, Stockle H, Steinberg R (1978) Calcium and potassium changes in extracellular microenvironment of cat cerebellar cortex. J Neurophysiol 41, 1026-1039

Nilsson P, Hillered L, Olsson Y, Sheardown MJ, Hansen AJ (1993). Regional changes in interstitial K^+ and Ca^{2+} levels following cortical compression contusion trauma in rats. J Cereb Blood Flow Metab 13, 183-192

Nistri A, Ostroumov K, Sharifullina E, Taccola G (2006) Tuning and playing a motor rhythm: how metabotropic glutamate receptors orchestrate generation of motor patterns in the mammalian central nervous system. J Physiol 572, 323-334

Onimaru H, Ballanyi K, Richter DW (1996) Calcium-dependent responses in neurons of the isolated respiratory network of newborn rats. J Physiol 491, 677-695

Onimaru H, Ballanyi K, Homma I (2003) Contribution of Ca^{2+}-dependent conductances to membrane potential fluctuations of medullary respiratory neurons of newborn rats in vitro. J Physiol 552, 727-741

Onimaru H, Kumagawa Y, Homma I (2006) Respiration-related rhythmic activity in the rostral medulla of newborn rats. J Neurophysiol 96, 55-61

Pace RW, Mackay DD, Feldman JL, Del Negro CA (2007) Role of persistent sodium current in mouse preBotzinger Complex neurons and respiratory rhythm generation. J Physiol 580, 485-496

Panaitescu B, Ruangkittisakul A, Ballanyi K (2009) Silencing by raised extracellular Ca2+ of pre-Botzinger complex neurons in newborn rat brainstem slices without change of membrane potential or input resistance. Neurosci Lett 456, 25-29

Panaitescu B, Ruangkittisakul A, Ballanyi K (2010) Depression by Ca^{2+} and stimulation by K^{+} of fictive inspiratory rhythm in newborn rat brainstem slices. Adv Exp Med Biol 669, 91-95

Pierrefiche O, Maniak F, Larnicol N (2002) Rhythmic activity from transverse brainstem slice of neonatal rat is modulated by nitric oxide. Neuropharmacology 43, 85-94

Pitta TP, Sherwood EE, Kobel AM, Berg HC (1997) Calcium is required for swimming by the nonflagellated cyanobacterium Synechococcus strain WH8113. J Bacteriol 179, 2524-2528

Puka-Sundvall M, Hagberg H, Andine P (1994) Changes in extracellular calcium concentration in the immature rat cerebral cortex during anoxia are not influenced by MK-801. Brain Res Dev Brain Res 77, 146-150

Ramirez JM, Tryba AK, Pena F (2004) Pacemaker neurons and neuronal networks: an integrative view. Curr Opin Neurobiol 14, 665-674

Rekling JC, Champagnat J, Denavit-Saubi M (1996) Electroresponsive properties and membrane potential trajectories of three types of inspiratory neurons in the newborn mouse brain stem in vitro. J Neurophysiol 75, 795-810

Ren J, Momose-Sato Y, Sato K, Greer JJ (2006) Rhythmic neuronal discharge in the medulla and spinal cord of fetal rats in the absence of synaptic transmission. J Neurophysiol 95, 527-534

Richerson GB (2004) Serotonergic neurons as carbon dioxide sensors that maintain pH homeostasis. Nat Rev Neurosci 5, 449-461

Richter DW, Acker H. (1989) Respiratory neuron behaviour during medullary hypoxia. In: Chemoreceptors and reflexes in breathing: cellular and molecular aspects (S. L, ed), pp 267-274. Oxford: Oxford University Press.

Richter DW, Spyer KM (2001) Studying rhythmogenesis of breathing: comparison of in vivo and in vitro models. Trends Neurosci 24, 464-472

Ruangkittisakul A, Ballanyi K (2012) Anoxia Response in Physiological Potassium of the Isolated Inspiratory Center in Calibrated Newborn Rat Brainstem Slices. Adv Exp Med Biol (*in press*)

Ruangkittisakul A, Schwarzacher SW, Secchia L, Poon BY, Ma Y, Funk GD, Ballanyi K (2006) High sensitivity to neuromodulator-activated signaling pathways at physiological [K^+] of confocally imaged respiratory center neurons in on-line-calibrated newborn rat brainstem slices. J Neurosci 26, 11870-11880

Ruangkittisakul A, Secchia L, Bornes TD, Palathinkal DM, Ballanyi K (2007) Dependence on extracellular Ca^{2+}/K^+ antagonism of inspiratory centre rhythms in slices and en bloc preparations of newborn rat brainstem. J Physiol 584, 489-508

Ruangkittisakul A, Schwarzacher SW, Secchia L, Ma Y, Bobocea N, Poon BY, Funk GD, Ballanyi K (2008) Generation of eupnea and sighs by a spatiochemically organized inspiratory network. J Neurosci 28, 2447-2458

Ruangkittisakul A, Okada Y, Oku Y, Koshiya N, Ballanyi K (2009) Fluorescence Imaging of active respiratory networks. Resp Physiol Neurobiol 168, 26-38

Ruangkittisakul A, Panaitescu B, Ballanyi K (2011) K^+ and Ca^{2+} dependence of inspiratory-related rhythm in novel 'calibrated' mouse brainstem slices. Resp Physiol Neurobiol 175, 37-48

Ruangkittisakul A, Secchia-Ballanyi L, Panaitescu B, Bobocea N, Kuribayashi J, Iizuka M, Kantor C, Ballanyi K (2012) Anatomically 'calibrated' isolated respiratory networks from newborn rodents. In Isolated Central Nervous System Circuits (Ed K Ballanyi), Neuromethods Series Vol 73 (Ed W Walz). Springer Science+Business Media, LLC, New York, NY, 61-124

Rybak IA, Shevtsova NA, St-John WM, Paton JF, Pierrefiche O (2003) Endogenous rhythm generation in the pre-Bötzinger complex and ionic currents: modelling and in vitro studies. Eur J Neurosci 18, 239-257

Schwarzacher S, Pestean A, Günther S, Ballanyi K (2002) Serotonergic modulation of respiratory motoneurons and interneurons in brainstem slices of perinatal rats. Neuroscience 115, 1247-1259

Smith JC, Ellenberger HH, Ballanyi K, Richter DW, Feldman JL (1991) Pre-Botzinger complex: a brainstem region that may generate respiratory rhythm in mammals. Science 254, 726-729

Somjen GG (2002) Ion regulation in the brain: implications for pathophysiology. Neuroscientist 8, 254-267

St-John WM, Paton JF, Leiter JC (2004) Uncoupling of rhythmic hypoglossal from phrenic activity in the rat. Exp Physiol 89, 727-737

Trippenbach T, Richter DW, Acker H (1990) Hypoxia and ion activities within the brain stem of newborn rabbits. J Appl Physiol 68, 2494-2503.

Voituron N, Frugière A, Champagnat J, Bodineau L (2006) Hypoxia-sensing properties of the newborn rat ventral medullary surface in vitro. J Physiol 577, 55-68

Völker A, Ballanyi K, Richter DW (1995) Anoxic disturbance of the isolated respiratory network of neonatal rats. Exp Brain Res 103, 9-19

Wei WL, Sun HS, Olah ME, Sun X, Czerwinska E, Czerwinski W, Mori Y, Orser BA, Xiong ZG, Jackson MF, Tymianski M, MacDonald JF (2007) TRPM7 channels in hippocampal neurons detect levels of extracellular divalent cations. Proc Natl Acad Sci USA 104, 16323-16328

Weston AH, Absi M, Harno E, Geraghty AR, Ward DT, Ruat M, Dodd RH, Dauban P, Edwards G (2008) The expression and function of Ca^{2+}-sensing receptors in rat mesenteric artery; comparative studies using a model of type II diabetes. Br J Pharmacol 154, 652-662

Zavala-Tecuapetla C, Aguileta MA, Lopez-Guerrero JJ, González-Marín MC, Peña F (2008) Calcium-activated potassium currents differentially modulate respiratory rhythm generation. Eur J Neurosci 27, 2871-2884

Chapter 4

Role of membrane potential and cytosolic Ca^{2+} in reversal by methylxanthines of opioid depression of newborn rat isolated rhythmogenic inspiratory networks

Bogdan A. Panaitescu, Araya Ruangkittisakul, Klaus Ballanyi

Department of Physiology, 750 MSB, University of Alberta, Edmonton, Canada

Parts of the results have already been published:

Ballanyi K, Panaitescu B, Ruangkittisakul A (2010) Indirect opioid actions on inspiratory pre-Bötzinger complex neurons in newborn rat brainstem slices. Adv Exp Med Biol 669, 75-79

My contribution to this study consisted of the execution of all whole-cell recordings and 40% of Ca^{2+} imaging studies and corresponding analyses and writing the manuscript; Dr. Araya Ruangkittisakul performed the rest of Ca^{2+} imaging and analyses. Dr. Klaus Ballanyi developed the concept for the work and revised the manuscript.

4.1 Introduction

Caffeine and theophylline are the gold standard for reversing often severe apnea of prematurity (Comer et al., 2001; Schmidt et al., 2006; Henderson-Smart & Steer, 2010). It is generally assumed that these and other methylxanthines have respiratory stimulating actions by blocking adenosine receptors that presumably exert a tonic inhibitory effect on respiratory networks in the lower brainstem (Eldridge et al., 1985; Hedner et al., 1985; Herlenius et al. 2002; Montandon et al., 2008). Among these networks, the pre-Bötzinger complex (preBötC) is of utmost importance because it generates inspiratory-related neuronal activities for normal breathing movements (Feldman & Del Negro, 2006). Using isolated *in vitro* models, we have provided evidence that adenosine does not endogenously inhibit rhythmogenic inspiratory networks and that methylxanthines counter opioid-evoked '*in vitro* apnea' starting at close to millimolar doses, at which they inhibit phosphodiesterase-4 (PDE4) (Ruangkittisakul & Ballanyi, 2010). The rise of cellular cyclic adenosine-monophosphate (cAMP) levels resulting from methylxanthine-induced PDE4 blockade may be similar to that evoked by several excitatory respiratory neuromodulators using this signalling pathway that seems to be important for bursting of rhythmogenic preBötC networks (Ballanyi et al., 1997, 1999; Richter et al., 1997; Manzke et al., 2003). Consequently, a PDE4-dependent respiratory stimulating methylxanthine action would probably counteract a cAMP decrease that is likely evoked by opioids in rhythmogenic preBötC neurons. There is evidence based on whole-cell recording in newborn rodent brainstem slice that opioids induce an activation of a postsynaptic K^+

conductance in preBötC neurons to shunt their rhythmic bursting (Gray et al., 1999; Mellen et al., 2003; Lorier et al., 2008; Montadon et al., 2011) **(Fig. 4-1A)**. Also others, including our group, found in the newborn rat *en bloc* model that some inspiratory VRC neurons are (modestly) hyperpolarized by opioids, while other neurons with similar burst characteristics are depressed by opioids without a postsynaptic effect (Ballanyi et al., 1997; Takeda et al., 2001) **(Fig. 4-1B)**. In a recent study from our group, histologically identified inspiratory neurons in the preBötC of the newborn rat *en bloc* model did not show a postsynaptic response during opioid blockade of rhythm (Ballanyi et al., 2009). Because rhythmogenic inspiratory preBötC have not yet been identified unambiguously, it is thus currently not clear whether presynaptic or postsynaptic mechanisms are more important for opioid-induced respiratory depression and its reversal by methylxanthines.

Here, we investigated in a first major aim of the present study whether the μ-opioid receptor agonist [D-Ala^2,N-Me-Phe^4,Gly^5-ol]-enkephalin (DAMGO) directly hyperpolarizes identified preBötC neurons in rhythmic slices and whether this postsynaptic effect is reversed by theophylline. For this, we performed 'blind' whole-cell patch-clamp recording in 400 μm thick 'm-preBötC[400]' transversal newborn rat brainstem slices with anatomically-defined rostrocaudal margins and centered preBötC (Smith et al., 1991, 1992; Ruangkittisakul et al., 2006; Panaitescu et al., 2009). To exclude the possibility that our findings of lack of opioid-induced hyperpolarization is due to experimental conditions, such as

superfusate composition or patch electrode solution, we compared our findings based on whole-cell recording from preBötC neurons under otherwise identical conditions with those in *locus coeruleus* (LC) neurons of horizontal brainstem slices that are an established model for postsynaptic hyperpolarization via opioid-activated K^+ channels (Williams & North, 1984; North & Williams, 1983; Alreja & Aghajanian, 1993).

In addition to PDE4 blockade, methylxanthines at low millimolar doses required for respiratory stimulating effects may act via releasing Ca^{2+} from intracellular stores (Nehlig et al., 1992; Fredholm et al., 1999; Blaustein & Golovina, 2001). Moreover, it is not known if preBötC glial cells also play a role in mediating methylxantine action. To test this, we monitored Ca^{2+} dynamics in neurons and presumptive astrocytes in 400 μm thick 'r+preBötC[400]' slices with the preBötC exposed to the caudal margin (Ruangkittisakul et al., 2008, 2009; Ballanyi & Ruangkittisakul, 2009) in response to opioids, methylxanthines and the PDE4 inhibitor, rolipram. To distinguish between neuronal and glial effects, different pharmacological strategies were employed, such as application of the Ca^{2+} store uptake blocker, cyclopiazonic acid (CPA), which showed distinct dynamic Ca^{2+} responses between neurons and glia. Preliminary findings were already published (Ballanyi et al., 2010).

4.2 Methods

(see Chapter **2**)

4.3 Results

A recent study from our group showed that low millimolar methylxanthine doses are necessary to antagonize DAMGO-evoked inhibition of preBötC bursting in newborn rat brainstem-spinal cords and m-preBötC[400] slices and that this reversal is mimicked by the PDE4 inhibitor rolipram (Chapters **2**, **3**) (Soderling & Beavo, 2000; Ruangkittisakul & Ballanyi, 2010) **(Fig. 4-1C)**. In the present study, we firstly used blind whole-cell patch-clamp recordings in m-preBötC[400] slices to demonstrate presumably antagonistic effects of DAMGO *versus* theophylline or rolipram on membrane potential of inspiratory and tonic neurons in the center of these slices that were thus mostly located in the preBötC (Chapters **2**, **3**) (Panaitescu et al., 2009). In a further approach, r+preBötC[400] slices with the preBötC exposed to the caudal margin were used for Ca^{2+} imaging using the fluorescent dye Fluo4-AM (Chapter **2.5**) (Ruangkittisakul et al., 2006, 2008, 2009) of responses to DAMGO, theophylline and a blocker of either PDE4 (rolipram) or Ca^{2+} uptake into endoplasmic reticulum (CPA) (Blaustein & Golovina, 2001). For long-term stability of inspiratory rhythm, both slice models were superfused with $7K^+/1Ca^{2+}$ solution (Chapter **2.1**) (Panaitescu et al., 2009; Ruangkittisakul & Ballanyi, 2010). Based on the attenuating effect of elevated K^+ on depression of the isolated preBötC by opioids (Chapter **1.3**) (Ballanyi &

Ruangkittisakul, 2009) **(Fig. 1-5)**, DAMGO was applied at 1 μM to assure that rhythm is blocked. This should have been sufficient for resolving potential membrane potential and Ca^{2+} responses to this opioid and theophylline plus rolipram that were applied at 2.5 mM and 5 μM, respectively, which is sufficient to recover robust preBötC bursting in DAMGO (Ruangkittisakul & Ballanyi, 2010) **(Fig. 4-1C)**. Drug effects on membrane properties or cytosolic Ca^{2+} were determined at steady-state, i.e. usually within 5-15 min after start of bath-application of the agents.

4.3.1 Membrane Characteristics of Inspiratory and Tonic preBötC Neurons

Stable whole-cell recordings were obtained from 27 inspiratory neurons, 19 of which were located in the preBötC, i.e. between 0.4 to 0.6 mm caudal to VII_c **(Fig. 1-3)** (Smith et al., 1991; Ruangkittisakul et al., 2008), while the remaining 8 cells were located between 0.61-0.66 mm caudal to VII_c. Resting potential reached a stable value within <2 min after rupturing the membrane patch for establishing the whole-cell configuration (Chapter **2.4.2**) **(Fig. 2-3)**. Inspiratory neurons showed a synaptically-mediated 'drive' potential with an amplitude of 5-25 mV leading to repetitive action potential discharge that was synchronous with suction electrode-recorded integrated extracellular population bursting in the contralateral VRC **(Fig. 4-2)**. During the initial ~5 min of whole-cell recording, membrane potential was changed by dc current injection via the patch electrode to test for conditional bursting (Smith et al., 1991; Feldman & Del Negro, 2006)

(Chapters **1.2**, **2.4.2**) **(Figs. 1-4, 4-2)**. This test revealed that 7 preBötC inspiratory neurons showed voltage-dependent ectopic bursting, i.e. periodic depolarization and concomitant action potential discharge that was not in phase with contralateral VRC rhythm **(Fig. 4-2A$_1$)**. In non-burster inspiratory neurons, spontaneous bursting occurred exclusively in synchrony with contralateral VRC discharge and current-evoked depolarization elicited only tonic single action potential discharge **(Fig. 4-2A$_2$)**. Following this initial test, negative dc current pulses (40-250 pA, 0.5-0.7 s) were injected at an interval of 5-15 s for monitoring neuronal input resistance (Chapter **2.4.2**) (Onimaru et al., 1996, 2003; Panaitescu et al., 2009). Potentially inhibitory effects of DAMGO, and reversal of this inhibition by theophylline and rolipram, were also analyzed in tonically active neurons within the VRC and preBötC that might provide a pivotal excitatory drive to rhythmogenic inspiratory networks (Ballanyi et al., 1997, 1999; Ballanyi & Ruangkittisakul, 2009). In 14 tonic neurons, 11 of which were located in the preBötC between 0.45-0.59 mm caudal to VII$_c$, membrane potential stabilized within <2 min after establishing the whole-cell configuration. Independent of their specific rostrocaudal location, these neurons showed 2 major types of spontaneous discharge. Specifically, 7 of these neurons showed very regular single action potential discharge and current-evoked change of resting potential evoked an apparently linear change in discharge rate which remained very regular even at quite depolarized levels **(Fig. 4-2B$_1$)**. In the other group of tonic cells, discharge rate was less regular at resting potential and depolarization typically increased this irregularity **(Fig. 4-2B$_2$)**.

In a first pharmacological test, we investigated whether VRC/preBötC neurons in this newborn rat slice model can principally respond with a G protein-coupled inward-rectifying K^+ (GIRK) channel-mediated hyperpolarization to the activation of B-type γ-aminobutyric acid ($GABA_B$) receptors with baclofen (1-5 μM), similar to unidentified newborn rat VRC neurons in the *en bloc* model in our previous study (Brockhaus & Ballanyi, 1998). Indeed, 4 out of 7 inspiratory neurons and 9 of 10 tonic cells showed a concomitant mean hyperpolarization by 1.57 ± 0.61 mV ($P< 0.05$) and 4.5 ± 1.1 mV ($P< 0.01$). Baclofen appeared to lower input resistance in both cell types, by 27.4 ± 24.4 and 53.0 ± 18.1 M□, but this was significant ($P <0.05$) only for tonic cells. The baclofen-evoked hyperpolarization was accompanied by *in vitro* apnea and a modest decrease of the baseline of the integrated suction electrode signal indicating possible inhibition of spontaneously active non-inspiratory neurons **(Fig. 4-3**, compare **Fig. 3.2-5)** (Chapters **2.4.1**, **3.1**) (Ballanyi & Ruangkittisakul, 2009; Panaitescu et al., 2009).

4.3.2 Inspiratory Neuron Responses to Theophylline and Rolipram in DAMGO

Bath-application of DAMGO abolished within <5 min VRC population bursting which was, similar to the responses to baclofen, in >80% of cases accompanied by a modest, sometimes substantial, decrease of the baseline of the integrated suction electrode signal **(Fig. 4-3)**. In an inspiratory preBötC neuron, rhythmic

bursting stopped with no effect on either membrane potential or input resistance when DAMGO had abolished VRC rhythm. Inspiratory cellular bursting recommenced in that neuron at the same time when VRC rhythm was reconstituted upon addition of theophylline (2.5 mM) to DAMGO-containing solution, again without postsynaptic effects **(Fig. 4-4A)**. Similarly, in another inspiratory preBötC neuron, membrane potential and input resistance were changed neither during DAMGO-evoked *in vitro* apnea nor upon reactivation of VRC and cellular bursting with rolipram (5 μM) **(Fig. 4-4B)**. Despite lack of a major hyperpolarization, statistical analysis in the 19 preBötC inspiratory neurons revealed that DAMGO caused a small hyperpolarization of 1.8 ± 0.61 mV, but no significant change in input resistance **(Fig. 4-4C$_1$)**. Reactivation of rhythm in 6 preBötC neurons by theophylline **(Fig. 4-4C$_2$)** and in 5 different preBötC neurons by rolipram **(Fig. 4-4C$_3$)** was not accompanied by a postsynaptic response. This analysis revealed further that mean values for resting potential, i.e. -42 mV *versus* -40 mV and input resistance, i.e. 175 *versus* 163 M□, were similar for preBötC *versus* the non-preBötC inspiratory neurons **(Fig. 4-4)**.

As described above (Chapter **4.3.1**), we tested at the beginning of every whole-cell recording if the preBötC inspiratory neuron studied is a conditional bursting, which was done in order to assess whether DAMGO has a preferential effect. In 6 of the 12 non-burster inspiratory neurons, DAMGO abolished all membrane potential fluctuations, including subthreshold depolarizations likely respresenting excitatory postsynaptic potentials. In further 4 of these 12 neurons, single action

potential discharge persisted at a rate of <5/min, with 1 cell also showing continued subthreshold potentials, also at low rate. Finally, 1 of these non-burster neurons showed persistent bursting at rates <3 events/min, whereas another neuron showed weak bursts with few action potentials. Contrary, 4 of the 7 burster inspiratory neurons continued to burst at a rate of between 0.5-3 events/min **(Fig. 4-5A)**. Another burster neuron showed only persistent low rate single action potential discharge whereas the remaining 2 cells were silenced by DAMGO.

In inspiratory neurons that stopped bursting in DAMGO, Na^+ action potentials could still be evoked by depolarizing dc current pulses, as tested in 3 burster versus 4 non-burster inspiratory preBötC neurons and their number was not changed (100 ± 13.3% *versus* 79 ± 6.4% of control). In 2 of the 4 non-burster inspiratory neurons, pulse-evoked action potentials were partially inactivated and this inactivation was removed in DAMGO resulting in a more uniform amplitude **(Fig. 4-5B)**. DAMGO did not affect steady-state membrane potential values in response to depolarizing or hyperpolarizing current pulses in these cells **(Fig. 4-5C)**.

4.3.3 Tonic Neuron Responses to Theophylline and Rolipram in DAMGO

As the most prominent effect of DAMGO effects on tonic neurons, their spontaneous discharge was inhibited **(Fig. 4-3),** while both theophylline **(Fig. 4-**

6A) and rolipram **(Fig. 4-6B)** appeared to counter this depression. Moreover, the recordings in the latter figures indicate that DAMGO, theophylline and rolipram do not have a notable effect on either membrane potential or input resistance. Statistical analysis in the 11 preBötC tonic neurons confirmed that DAMGO-evoked *in vitro* apnea occurred in absence of a postsynaptic response, whereas discharge rate dropped notably, from >3 Hz to <1 Hz **(Fig. 4-6C)**. Also reactivation of rhythm in 6 tonic neurons (4 preBötC *versus* 2 non-preBötC cells) by theophylline and in 5 different cells (4 preBötC cells *versus* 1 non-preBötC cell) by rolipram was not accompanied by a postsynaptic effect **(Fig. 4-6C)**. Burst rate showed a trend to reincrease after adding either theophylline or rolipram to DAMGO-containing solution, but these effects were not significant **(Fig. 4-6C)**. This contrasts with the finding that the decrease in the baseline of the integrated VRC trace recovered completely upon washout of DAMGO or during application of either theophylline or rolipram in DAMGO **(Fig. 4-6D)**.

This analysis revealed also that the mean resting potential and input resistance of either type of tonic neurons were very similar, regardless whether located within the preBötC or adjacent slice regions. Moreover, membrane potential values closely resembled those in inspiratory VRC/preBötC neurons whereas input resistance appeared to be higher in tonic neurons (330 *versus* 175 M□, compare **Figs. 4-4C**, **4-6C**).

4.3.4 Hyperpolarization of LC Neurons by DAMGO

The above findings indicate that a majority of inspiratory and tonic VRC/preBötC neurons is inhibited by DAMGO without postsynaptic effects. To test whether this lack of postsynaptic hyperpolarization is due to particular experimental conditions inhibiting responses to opioids, DAMGO effects were tested on membrane potential and input resistance of LC neurons in horizontal newborn rat brainstem slices (Williams & North, 1984; North & Williams, 1983; Alreja & Aghajanian, 1993) (Chapter **6**). In 19 LC neurons, resting potential stabilized within <2 min after establishing the whole-cell configuration. All cells were spontaneously active and showed either a regular tonic discharge at a rate of 0.3-3 Hz **(Fig. 4-7A)** or bursts of 2-10 action potentials that were followed by a hyperpolarization of 2-6 mV for 1-4 s before start of another burst cycle **(Fig. 4-7B)**. In $7K^+/1Ca^{2+}$ solution, used for these tests, mean resting potential and input resistance of these (pooled) cells were -41.7 ± 2.8 mV and 188 ± 120 MΩ **(Fig. 4-7C)**.

Bath-application of DAMGO (1 μM) hyperpolarized all LC neurons of both types in similar fashion to an average value of -49.6 ± 3.9 mV and input resistance decreased concomitantly to 108 ± 46.2 MΩ **(Fig. 4-7)**. Addition of the μ-opioid receptor antagonist naloxone (1 μM) to DAMGO-containing solution reversed the hyperpolarization and the countering effect on input resistance showed a trend towards recovery which was though not significant **(Fig. 4-7B,C)**. The recording in **Fig. 4-7B$_2$** shows a typical example for the kinetics of the onset of, and the

recovery from DAMGO-evoked hyperpolarization and input resistance decrease. Specifically, the hyperpolarization develops within <2 min after start of bath-application of DAMGO and reaches its peak within <3 min, whereas recovery starts within <2 min after start of return to standard solution and is complete within <5 min (Chapter **6**).

These findings clearly show that lack of postsynaptic opioid effect on preBötC neurons is not due to differences in experimental conditions compared to the above studies, demonstrating a hyperpolarizing action in such cells.

4.3.5 Discrimination of preBötC Neurons and astrocytes during Ca^{2+} Imaging

For the present study, Ca^{2+} imaging was performed in r+preBötC[400] in 13 slices. In a single confocal image plane in the ventrolateral slice aspect containing the (partially) exposed preBötC, typically 6-20 cells with a soma diameter of 15-25 μm showed rhythmic increases of cytosolic Ca^{2+} in phase with contralateral suction electrode-recorded preBötC bursting (Chapter **1.3**) **(Fig. 1-6) (Figs. 4-8** to **4-11)**. While these cells likely represent inspiratory preBötC neurons, neighboring cells of similar soma diameter and shape were not inspiratory active. In initial experiments, we used r+preBötC slices of 700 or 800 μm thickness to elucidate which pharmacological tools may be suitable to help discriminate neurons from (astrocytic) glia. This analysis revealed firstly that bath-application of excitatory neuromodulator glutamate (1 mM) evoked robust Ca^{2+} rises in inspiratory

neurons, while thyrotropin-releasing hormone (10-100 nM) or the neurokinin-1 receptor agonist GR73632 (5-50 nM) induced a modest baseline Ca^{2+} rise in neurons **(Fig. 4-8)**. In previous studies, we assumed that cells with a smaller (~10 μm) soma are astrocytes which did not show inspiratory Ca^{2+} rises (Ruangkittisakul et al., 2009, 2012; Ballanyi et al., 2010; Huxtable et al., 2010). While these presumptive astrocytes responded to glutamate in similar fashion as neurons, their Ca^{2+} baseline was only modestly, if at all, affected by thyrotropin-releasing hormone or GR73632 **(Fig. 4-8)**. Note that some astrocytes showed slow random non-inspiratory related Ca^{2+} rises. A major (oscillatory) rise of glial Ca^{2+} was revealed in response to phenylephrine (10-100 μM) or the metabotropic glutamate receptor agonist aminocyclopentane-*trans*-1,3-dicarboxylic acid (t-ACPD, 25 μM) **(Figs. 4-8, 4-9),** as well as to adenosine triphosphate (100 μM) (Huxtable et al., 2010). Moreover, we found that bath-application of Cd^{2+} (100 μM) firstly (within the initial 5-10 min) enters glia to interact with Fluo-4. Generation of z-stacks and 3D animation at this time reveals a network of brightly stained small cells with astrocyte-like morphology **(Fig. 4-9)**.

4.3.6 Neuronal and Glial Ca^{2+} Responses to DAMGO, Theophylline and Rolipram

As exemplified in **Fig. 4-10**, concomitant with block of preBötC rhythm by DAMGO, cytosolic Ca^{2+} decreased in inspiratory neurons, whereas Ca^{2+} baseline was unaffected in neighboring astrocytes. In one inspiratory neuron of this

experiment, rhythmic Ca^{2+} rises persisted, while other inspiratory active cells and bursting in the contralateral preBötC were silenced by DAMGO. Within ~1 min after start of theophylline application in DAMGO, synchronous Ca^{2+} rises in inspiratory neurons reappeared, in some cells even before recovery of preBötC bursting **(Fig. 4-10)**. Recovery of inspiratory neuron activity was accompanied in this example by a modest reincrease of Ca^{2+} baseline in some neurons and in 1 of 4 astrocytes. During washout of theophylline in DAMGO, the endoplasmic reticulum Ca^{2+} pump blocker CPA (100 μM) was applied. While CPA did not exert a notable effect on (decaying) preBötC bursting, it evoked a major rise of Ca^{2+} baseline in all 4 astrocytes, but only in 1 of 6 inspiratory neurons **(Fig. 4-10)**. The CPA-evoked Ca^{2+} rises did not recover by >30% upon washout of the agent for >30 min. Also rolipram reactivated Ca^{2+} in inspiratory neurons with no effect on Ca^{2+} baseline and the drug had no apparent effect on astrocytes. Statistical analysis in 153 inspiratory neurons of 13 slices and 70 astrocytes of 5 slices revealed that DAMGO decreased Ca^{2+} in both inspiratory active and silent neurons with no effect on astrocytes **(Fig. 4-11)**. Theophylline or rolipram in DAMGO did not affect Ca^{2+} baseline in either neurons or astrocytes, whereas CPA in DAMGO elevated Ca^{2+} in both types of cells, but the effect on astrocytes was >4-fold larger than on neurons **(Fig. 4-11)**.

4.4 Discussion

As major findings of the present study, DAMGO did not evoke a notable hyperpolarization and fall of R_i in either inspiratory or tonic preBötC neurons that would explain blockade of rhythm, while this inhibition of cellular plus VRC/preBötC population bursting was reversed by both theophylline and rolipram with no postsynaptic changes in V_m or R_i. DAMGO lowered Ca^{2+} in inspiratory preBötC neurons, but not in presumptive adjacent astrocytes, and reactivation of inspiratory neuronal Ca^{2+} rises and rhythmic motor activity by theophylline or rolipram occurred without effect on Ca^{2+} signal in presumptive glia.

4.4.1 Lack of Postsynaptic Opioid, Methylxanthine or Rolipram Effects

Most inspiratory neurons in the present study were recorded within the preBötC which extends by <200 μm in newborn rats (Ruangkittisakul et al., 2008; Ballanyi & Ruangkittisakul, 2009). The finding here that neither these cells nor neurons with similar spontaneous activities in neighboring VRC layers showed a major hyperpolarization or input resistance decrease in DAMGO shows that a direct K^+ channel-mediated hyperpolarization that presumably shunts rhythmic bursting (Gray et al., 1999; Mellen et al., 2003; Montandon et al., 2011) may not be a predominant mechanism. The fact that also inspiratory preBötC neurons in our previous study on the newborn rat *en bloc* model do not show DAMGO-evoked hyperpolarization and concomitant input resistance decrease (Ballanyi et al., 2009) proves that this phenomenon is independent of the respiratory *in vitro*

model. The 'negative' result in the slice model compared to reports on opioid-evoked hyperpolarization of preBötC neurons in other studies on neonatal rodent brainstem slices (Gray et al., 1999; Mellen et al., 2003; Montandon et al., 2011) is not caused by our specific experimental conditions because DAMGO hyperpolarized all LC neurons tested here with a concomitant decrease of input resistance. This hyperpolarization is in line with numerous earlier slice studies on these cells which have established the view that opioids often act inhibitory by activating (postsynaptic) GIRK channels (Williams & North, 1984; North & Williams, 1983; Alreja & Aghajanian, 1993).

It was not the aim of the present study to clarify whether potentially rhythmogenic inspiratory preBötC neurons are indeed hyperpolarized and shunted by opioids because there is yet no indication regarding identification of such cells in an acute slice, particularly for rats (Ballanyi & Ruangkittisakul, 2009). Rather, we used DAMGO here as a tool for testing whether methylxanthines have effects antagonistic to those of opioids on identified inspiratory neurons in the preBötC that may (or may not) be rhythmogenic. We included tonic neurons in this analysis because (some of) these cells may provide an excitatory drive to rhythmogenic preBötC neurons (Ballanyi & Ruangkittisakul, 2009). In line with that assumption, DAMGO depressed their tonic activity with a time course similar to that of its inhibitory action on inspiratory VRC bursting and, at the same time, the baseline of the integrated VRC signal decreased in a notable number of cases. We have hypothesized previously in our study on strong inhibition of the isolated

preBötC by modestly raised extracellular Ca^{2+} that this baseline decrease of the population activity signal might indicate inhibition of tonic neuronal activity within the VRC (Ballanyi & Ruangkittisakul, 2009; Panaitescu et al., 2009). In line with this idea, also opioids apparently silence a major number of tonic VRC/preBötC neurons. Similar to inspiratory neurons within and outside the preBötC, inhibition by DAMGO of spontaneous discharge in tonic neurons in both areas occurred without a notable hyperpolarization or input resistance decrease and also neither theophylline nor rolipram had a postsynaptic action. The latter agents failed to restore the initial level of tonic spiking in DAMGO contrary to a complete reincrease in the baseline of contralateral population activity. This indicates that cellular factor determining tonic activity is washed out upon whole-cell recording. Such potential washout does not seem to have a major effect on GIRK channels as possible explanation for lack of opioid-evoked hyperpolarizations because (*i*) the same patch electrodes and filling solution were used for recording from the LC neurons that were hyperpolarized by DAMGO, (*ii*) baclofen evoked a stable hyperpolarization in some inspiratory neurons and a larger number of tonic cells, similar to findings in our previous study on the *en bloc* model (Brockhaus & Ballanyi, 1998) and (*iii*) depression of preBötC rhythm in by anoxia is accompanied by a (likely K^+ channel-mediated) notable hyperpolarization, input resistance decrease and resulting shunting of bursting in a subpopulation of inspiratory preBötC neurons (Ruangkittisakul & Ballanyi, 2012). Finally, it is principally possible that postsynaptic effects are not seen because opioid receptors are located on distal dendrites and membrane potential

responses at such sites would not be detected by whole-cell-recording which are very likely obtained from the cell soma.

Our present findings support the idea that a cAMP decrease likely occurring in (rhythmogenic inspiratory and/or excitatory drive-providing tonic) preBötC neurons does not generally induce a substantial postsynaptic K^+ channel-mediated hyperpolarization and conductance increase to shunt inspiratory center bursting as explanation of inhibition of breathing by opioids. Rather, in a major number of both inspiratory and tonic preBötC neurons bursting arrests during opioids without postsynaptic effects, suggesting a possible involvement of presynaptic mechanisms. Opioids do not seem to have major depressing effects on conditional bursting based on our findings that ~25% of whole-cell-recorded inspiratory preBötC neurons continued to burst in DAMGO, as well as a comparable number of neurons during Ca^{2+} imaging (see below).

Recovery of rhythm by either theophylline or rolipram occurred also without postsynaptic effect, suggesting no direct involvement of postsynaptic ion channels, at least not of those located close to the soma. It is likely that the common respiratory stimulating action of low millimolar methylxanthine and rolipram is inhibition of PDE4 in rhythmogenic inspiratory networks (Fredholm et al., 1999; Soderling and Beavo, 2000; Ballanyi, 2004; Ruangkittisakul & Ballanyi, 2006, 2010; Ballanyi & Ruangkittisakul, 2009; Ruangkittisakul et al., 2006, 2008). Postsynaptic actions of rolipram on central mammalian neurons have

not been studied yet according to our knowledge. On the other hand, methylxanthines are known to block $GABA_A$ receptors, in addition to PDE4 inhibition (Lopez et al., 1989; Fredholm et al., 1999; Shi et al., 2003; Taketo et al., 2004). It is thus possible that tonic endogenous activity of $GABA_A$ receptors at presynaptic sites within preBötC networks is one target of their respiratory stimulating action. If that is the case, methylxanthines would possibly not act directly antagonistic on the signalling pathway induced in preBötC neurons by opioids. In that context, it is interesting to note that tonic activity of $GABA_A$ receptors is assumed to have a major contribution to the balance of central respiratory network activity in physiological conditions and, particularly, under the influence of anesthetics (Zuperku & McCrimmon, 2002; Stuth et al., 2008).

4.4.2 Lack of Ca^{2+} Role in Respiratory Stimulating Actions of Methylxanthine and Rolipram

Our first finding using multiphoton/confocal microscopy here was that DAMGO lowers cytosolic Ca^{2+} in inspiratory preBötC neurons. This fall may be related to the relatively low resting potential of between -40 to -50 mV for most of these neurons, particularly in elevated K^+ solution as used here and in numerous studies using the slice or *en bloc* models (Onimaru et al., 1996; 2003; Ballanyi et al., 1999; Brockhaus & Ballanyi 1998, 2000; Ballanyi & Ruangkittisakul, 2009; Ruangkittisakul et al., 2007). This may indicate that ongoing opening of somatic voltage-activated Ca^{2+} channels provides a steady elevated level of Ca^{2+} baseline,

as revealed in dorsal vagal neurons in juvenile rat brainstem slices (Ballanyi & Kulik, 1998). If that is the case, DAMGO possibly blocks these channels as one established action of opioids (North & Williams, 1983; Moises et al., 1994; Soldo & Moises, 1998; Connor et al., 1999). Alternatively, if some voltage-activated Ca^{2+} channels are open at resting potential, these channels would likely close during a DAMGO-evoked hyperpolarization similar to that in dorsal vagal neurons in response to anoxia or inhibitory neuromodulators (Ballanyi & Kulik, 1998). In a notable number of inspiratory preBötC neurons, non-synchronized rhythmic Ca^{2+} oscillations persisted throughout DAMGO application which is in line with persistence of cellular bursting in ~25% of inspiratory preBötC neurons. Similarly, a subpopulation of presumptive neurons in the preBötC continues to show rhythmic Ca^{2+} bursts after silencing of cervical nerve bursting by DAMGO in a newborn rat 'sagittal slab' *en bloc* model (Barnes et al., 2007). The authors discussed in this study that, for example, Pre-I neurons may be responsible because these neurons are insensitive to opioids (Janczewski et al., 2002; Mellen et al., 2003) including the subpopulation located within the preBötC (Ballanyi et al., 2009). This supports our above and previous (Ballanyi & Ruangkittisakul, 2009) hypothesis that Pre-I neurons transform into inspiratory neurons in preBötC slices, as in response to blockade of receptor-coupled anion channels in the newborn rat *en bloc* model (Brockhaus & Ballanyi, 1998).

The findings indicate that neither low millimolar methylxanthines nor rolipram reactivate rhythm by inducing a Ca^{2+} rise from cellular stores that may trigger

other excitatory processes. In this regard, evidence has been presented that activation of metabotropic glutamate receptors on dendrites of preBötC neurons causes Ca^{2+} release from stores (Mironov, 2008; Mironov & Skorova, 2011). Store-mediated Ca^{2+} release by methylxanthines may require concentrations higher than 2.5 mM used in the present study based on dose response curves in other tissues (Nehlig et al., 1992; Fredholm et al., 1999). Accordingly, mostly 5 mM or more theophylline or caffeine are applied in that regard including findings on preBötC networks (Mironov, 2008; Mironov & Skorova, 2011) and hypoglossal motoneurons (Ladewig et al., 2003), both studied in (cultured) slices from newborn mice. While 5 mM caffeine evoked a major Ca^{2+} release in the hypoglossal motoneurons of the latter study, blockade of the Ca^{2+} release store pump with thapsigargin in the former reports on the isolated preBötC led only to a modest rise of cytosolic Ca^{2+}. The thapsigargin-evoked minor Ca^{2+} increases were comparable to those in (inspiratory active) neurons of the present study in response to a very similar endoplasmic Ca^{2+} pump blocker, CPA. That the drug was active is indicated by the fact that neighboring astrocytes showed a very prominent Ca^{2+} rise. This is in line with the view the glial cells in the preBötC are capable of Ca^{2+} signalling via release from stores activated by neuromodulators such as tACPD, phenylephrine or adenosine-triphosphate (Härtel et al., 2008; Ballanyi & Ruangkittisakul, 2009; Ruangkittisakul, 2009; Ballanyi et al., 2010; Huxtable et al., 2010). However, the presumptive astrocytes did not respond with a change in cytosolic Ca^{2+} to DAMGO, theophylline or rolipram. This indicates that Ca^{2+} signalling in these cells does not play a major role in opioid depression

of the preBötC or in reactivation of rhythm via blockade of PDE4. Important to note, microglia and/or oligodendrocytes may have been recorded from instead of presumptive astrocytes. While a role of microglia in responses to opioids is currently the focus of intensive research (Milligan & Watkins, 2009; Bennaroch, 2010; Ballanyi et al., 2010), the lack effects of DAMGO, theophylline and rolipram on any small sized cell suggests that Ca^{2+} signals in these cells are not important in preBötC modulation by opioids or methylxanthines.

4.5 Figures and Legends

Fig. 4-1

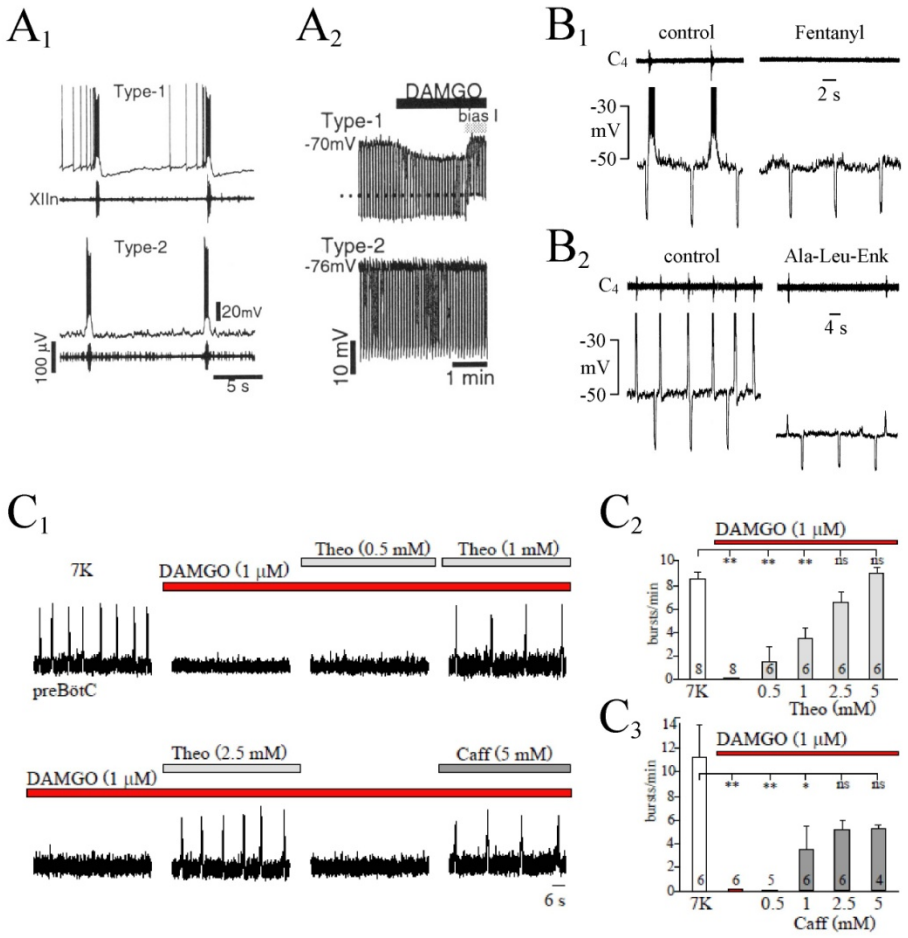

Fig. 4-1: Methylxanthine reversal of opioid depression of pre-Bötzinger complex (preBötC) inspiratory center bursting. A, the μ-opioid receptor agonist [D-Ala^2,N-Me-Phe^4,Gly^5-ol]-enkephalin (DAMGO, 5 μM) evoked a membrane potential hyperpolarization and input decrease in 'type-1', but not 'type-2' inspiratory preBötC neurons in newborn mouse brainstem slices. **B**, similarly, inspiratory ventral respiratory column (VRC) neurons in newborn rat brainstem-spinal cords were either hyperpolarized by, or did not show a postsynaptic response to other μ-agonists. **C**, DAMGO blocked inspiratory preBötC rhythm in 400 μm thick newborn rat 'm-preBötC[400]' slices with centered preBötC. The methylxanthine theophylline (Theo) countered DAMGO effects at low millimolar doses, similar to another methylxanthine, caffeine (Caff). The dose dependence of this respiratory stimulating effect by methylxanthines indicates blockade of cAMP-degrading phosphodiesterase-4 (PDE4) as the underlying mechanism. (**A** from Gray et al. 1999; **B** from Ballanyi et al., 1997; **C** from Ruangkittisakul & Ballanyi, 2010).

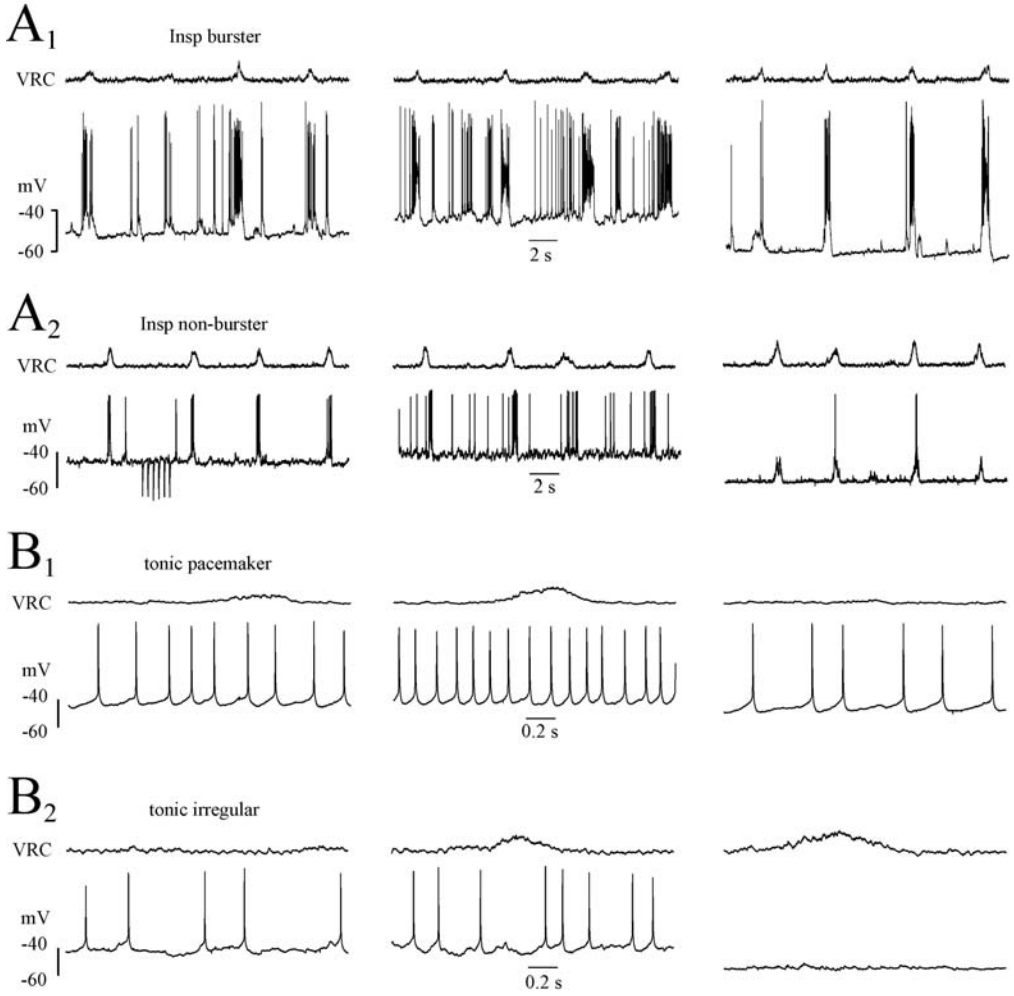

Fig. 4-2: Spontaneously active neuron types in preBötC of newborn rat m-preBötC[400] slices. A, inspiratory neurons. $\mathbf{A_1}$, in ~25% of inspiratory preBötC neurons depolarization due to dc current injection via the whole-cell recording patch electrode evoked bursts of action potential ('spike') discharge on top of rhythmic depolarizations mediated by intrinsic 'conditional burst' ion conductances. Such 'ectopic' bursts were not in phase with inspiratory-related synaptically-mediated bursts recorded with a suction electrode in the ventrolateral slices aspect containing the VRC (upper trace). $\mathbf{A_1}$, in a 'non-burster' inspiratory preBötC neuron depolarization evoked single spikes, but no ectopic bursting. **B**, tonic neurons. $\mathbf{B_1}$, in ~40% of tonic neurons spike discharge was regular and remained regular at varying rate upon changing of membrane potential. $\mathbf{B_1}$, in the remaining tonic cells spiking was irregular at various potentials. All neurons were located within the rostrocaudal area of the preBötC, i.e. between 0.4-0.6 mm caudal to the caudal end of facial (VII) motor nucleus, VII_c (Smith et al., 1991; Ruangkittisakul et al., 2008).

Fig. 4-3

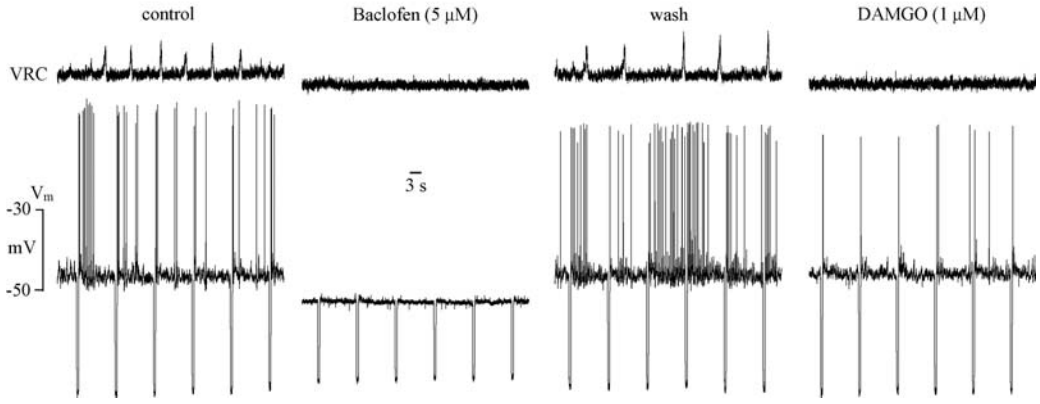

Fig. 4-3: Different mechanisms of block of inspiratory rhythm in m-preBötC[400] slices by agonists of inhibitory neuromodulators. In a tonic preBötC neuron located 0.55 mm caudal to VII_c, blockade of inspiratory VRC rhythm in response to bath-application of the B-type □-aminobutyric acid ($GABA_B$) receptor agonist baclofen (5 μM) was accompanied by postsynaptic G protein-coupled inward-rectifying K^+ ('GIRK') channel-mediated hyperpolarization and concomitant decrease of input resistance. The drop of the baseline of the integrated VRC signal indicates that spontaneous discharge is also blocked in a notable number of other tonic neurons within the VRC. Subsequent to recovery from baclofen, rhythm was blocked by DAMGO which induced a similar fall of the baseline of the VRC signal. However, the cell stopped firing (except a rebound spike at the end of the hyperpolarizing test pulse for input resistance determination) in the absence of an effect on membrane potential or resistance.

Fig. 4-4

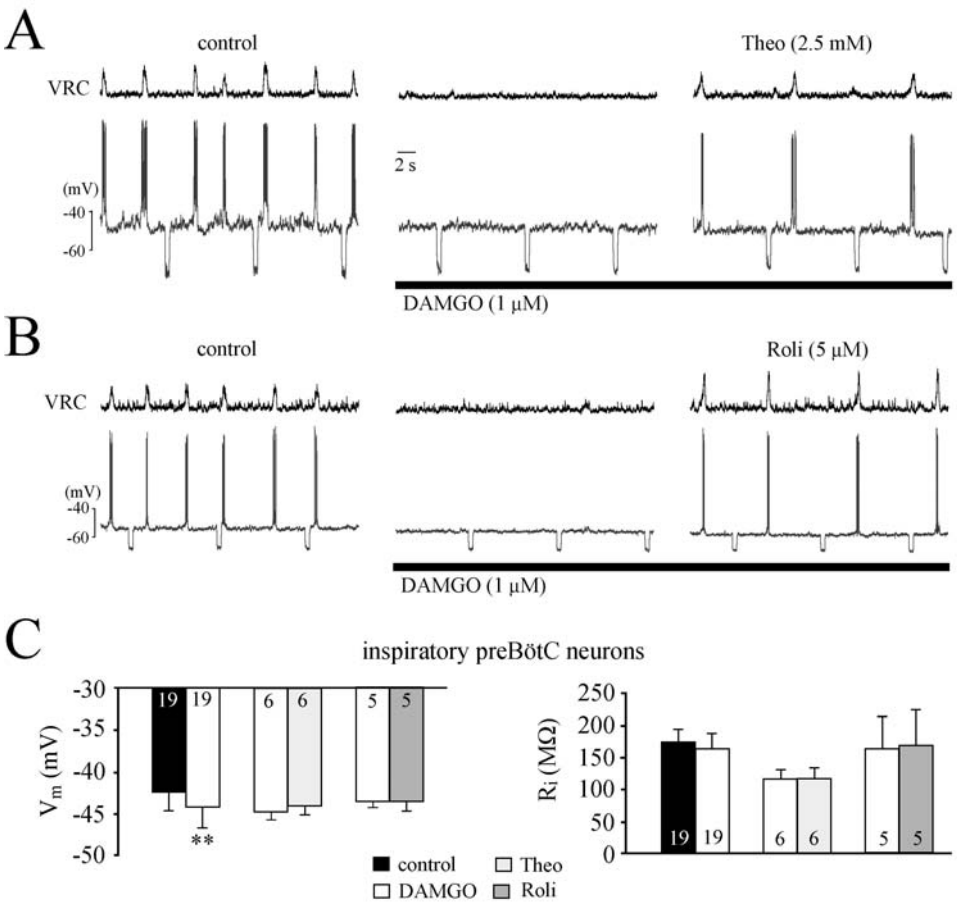

Fig. 4-4: Lack of major postsynaptic effects of DAMGO, theophylline and rolipram on inspiratory preBötC neurons. A, in this inspiratory preBötC neuron located 0.60 mm caudal to VII_c, blockade of rhythmic cellular and VRC population bursting by DAMGO was not accompanied by a change of either membrane potential or input resistance, similar to reactivation of cellular and VRC rhythms by theophylline in DAMGO. **B**, similarly, neither block of bursting by DAMGO nor its reactivation by rolipram (Roli) were accompanied by major postsynaptic effects in a different inspiratory preBötC neuron located 0.60 mm caudal to VII_c. **C**, statistical analysis revealed that DAMGO evoked a significant ($P< 0.01$), though minor (<2 mV), hyperpolarization without effect on input resistance, whereas reversal of opioid-induced *in vitro* apnea occurred in the absence of postsynaptic effects. Numbers in bars correspond to numbers of cells tested. Paired T-test was used for analyses (significance: * for $P<0.05$, ** for $P< 0.01$).

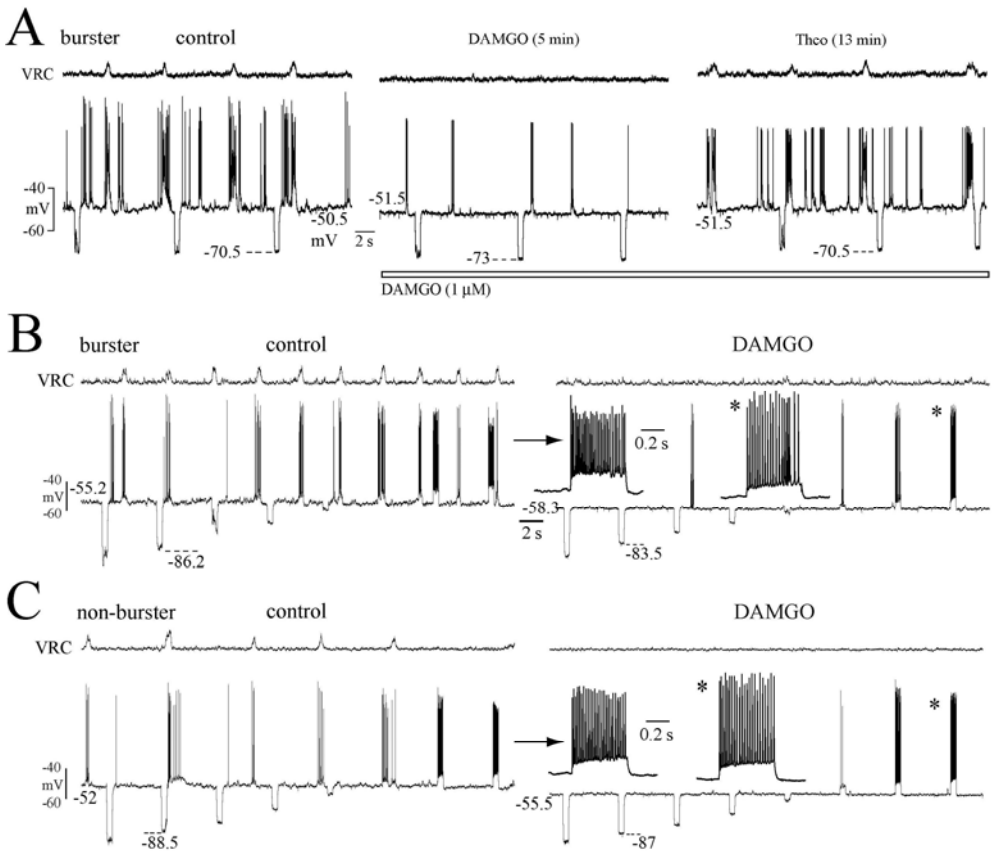

Fig. 4-5: Persistence of bursting in inspiratory preBötC neurons during DAMGO. A, in the inspiratory preBötC burster neuron of **Fig. 4-2** (0.60 mm caudal to VII_c), (shortened) ectopic bursts persisted during DAMGO-induced blockade of VRC bursting and its incidence increased again during theophylline in DAMGO. **B**, also in a different preBötC burster neuron (0.48 mm caudal to VII_c) some ectopic bursts persisted in DAMGO. Current pulse injection revealed that DAMGO had no major effect on either input resistance or on evoked spiking. Insets show the response to the largest depolarizing current pulse in control (left) *versus* DAMGO (right) at higher time resolution. **C**, in a non-burster preBötC cell (0.55 caudal to VII_c) DAMGO blocked spontaneous bursting, but evoked spiking was preserved. In both neurons of **B** and **C**, DAMGO removed some spikes inactivation resulting in slightly larger amplitudes.

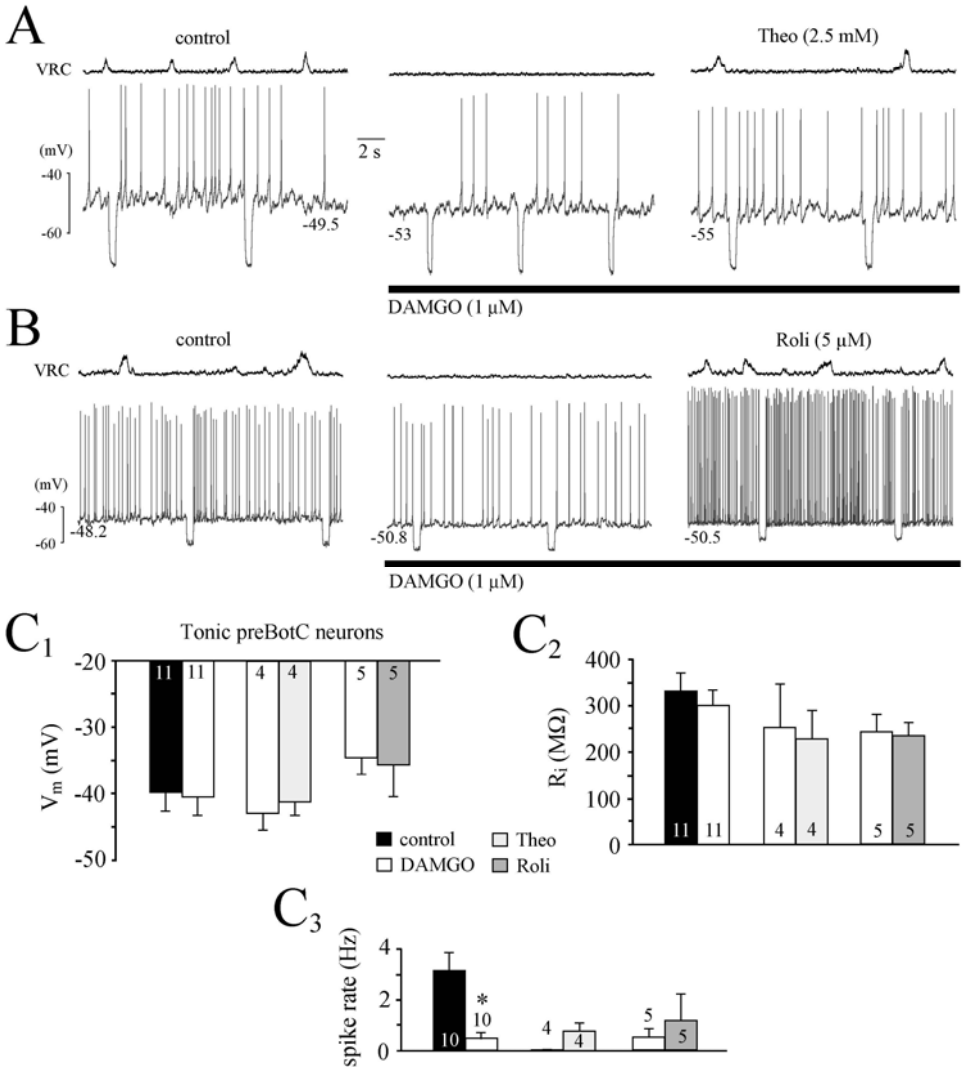

Fig. 4-6: Lack of postsynaptic effects of DAMGO, theophylline and rolipram on tonic preBötC neurons. A, in this preBötC neuron (0.50 mm caudal to VII_c), depression of tonic spiking by DAMGO was accompanied by a modest change of membrane potential with no change in input resistance. **B**, neither depression of spiking by DAMGO nor its reactivation by Roli were accompanied by major postsynaptic effects also in a different tonic preBötC neuron (0.45 mm caudal to VII_c). **C**, statistical analysis confirmed that DAMGO, theophylline or rolipram did not exert a significant postsynaptic response. Paired T-test was used for analyses.

Fig. 4-7

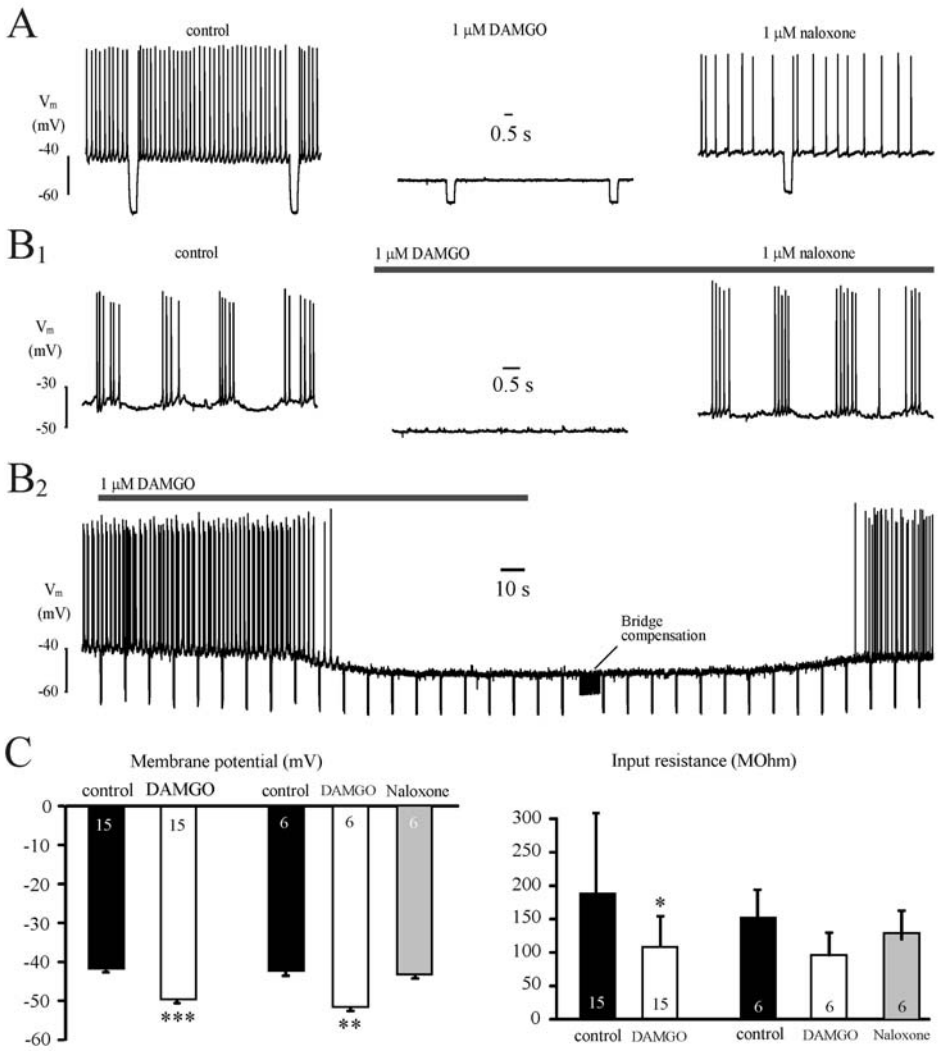

Fig. 4-7: Postsynaptic hyperpolarizing effect of DAMGO on spontaneously active LC neurons in 7 mM K^+ superfusate. A, this LC tonic neuron was hyperpolarized by DAMGO (1 μM) with a concomitant decrease of input resistance. Addition of the μ-opioid receptor antagonist naloxone (1 μM) reversed DAMGO-depression and restored membrane potential, resistance and tonic spiking. Similar effects were revealed in a different population of LC neurons, oscillatory type (**B_1**, **B_2**). **C**, statistical analysis showed the significant postsynaptic hyperpolarizing effect ($P< 0.05$) by DAMGO on LC neurons, with a simultaneous decrease of input resistance.

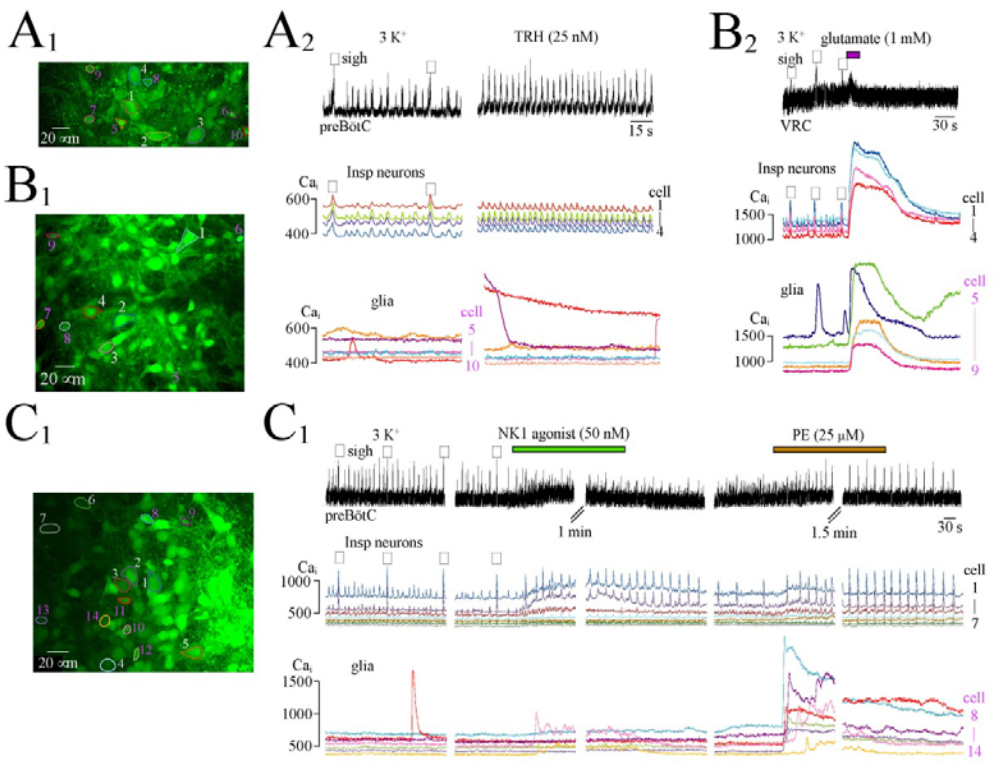

Fig. 4-8: Ca^{2+} rises in inspiratory neurons and glia of calibrated preBötC slices. A, in a r+preBötC[700/-0.60] slice, preBötC neurons located 25 µm caudal to the preBötC center (at -0.50) showed a 'sigh-eupnea' burst pattern in 3 mM K^+ and 1 mM Ca^{2+} solution. After spontaneous arrest of rhythm in 3 K^+, bath-application of thyrotropin-releasing hormone (TRH, 25 nM) evoked a regular eupnea burst pattern and rises of Fluo-4-monitored cytosolic Ca^{2+} (Ca_i) of regular rate and frequency indicating a reconfiguring preBötC (for details, see Ruangkittisakul et al., 2008). Note that TRH does not evoke a Ca_i rise in presumptive glial cells, which though, continued to show spontaneous rises lasting up to several minutes. Traces of neurons in **A_2** show activities in regions of interest (ROIs) in the image of **A_1**. **B**, in the ventral respiratory column (VRC) of a m-preBötC[800/-0.90] slice, spontaneous, but not inspiratory Ca_i oscillations were revealed in presumptive glial cells at -0.86 while bath-applied glutamate (20 s) caused a major increase of Ca_i in both glia and inspiratory neurons. Note that both components of the eupnea-sigh burst pattern are evident in inspiratory neurons, whereas only the peak of sighs is visible in the preBötC population recording because of high suction electrode noise. **C**, in a m-preBötC[700/-0.60] slice, the sigh-eupnea pattern of preBötC population and Ca_i responses in inspiratory neurons at -0.57 was not reflected by synchronous changes in Ca_i of 7 presumptive astrocytes, whereas one of the latter cells showed a spontaneous Ca_i transient. Bath-application of the neurokinin-1 (NK1) agonist GR73632 accelerated inspiratory bursts and Ca_i rises and elevated Ca_i baseline modestly in neurons, but not in the majority of presumptive astrocytes. In contrast, stimulation

of both the rate and amplitude of inspiratory preBötC bursting and neuronal Ca_i rises by the α_1-adrenergic agonist phenylephrine (PE) had a minor elevating effect on Ca_i baseline in neurons, but evoked major glial Ca_i rises (from Ruangkittisakul et al., 2009).

Fig 4-9

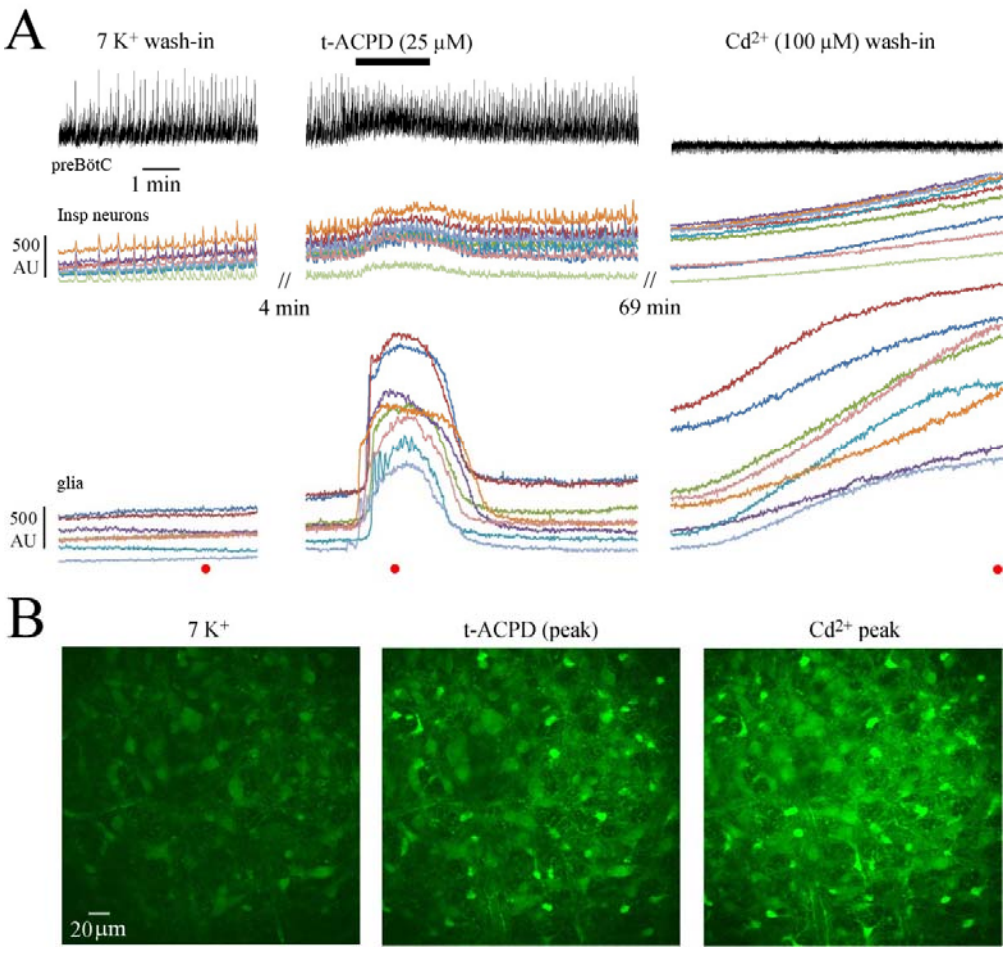

Fig. 4-9: Identification of preBötC astrocytes by the metabotropic glutamate receptor agonist aminocyclopentane-*trans*-1,3-dicarboxylic acid (t-ACPD) and Cd^{2+}. A, in a r+preBötC[400] slice, preBötC neurons showed an increase in Ca^{2+} baseline and inspiratory Ca^{2+} rises in response to countering of *in vitro* apnea in $3K^{+}/1Ca^{2+}$ solution by raising K^{+} to 7 mM (see Chapter **3** and Ruangkittisakul et al., 2007). Bath-application of t-ACPD accelerated preBötC rhythm notably and raised neuronal Ca^{2+} baseline modestly, whereas presumptive glial cells responded with a major Ca^{2+} rise. After recovery of rhythm and Ca^{2+} from t-ACPD, Cd^{2+} was added to the superfusate. This led to accumulation of this divalent cation in both neurons and glia, where it interacted with Fluo-4. This approach revealed glial cells that were not visible in control, probably because of a very low Ca^{2+} baseline. **B,** Ca^{2+} imaging aspects in the same slice while in 7 mM K^{+}, and after application of t-ACPD and Cd^{2+}, respectively.

Fig. 4-10

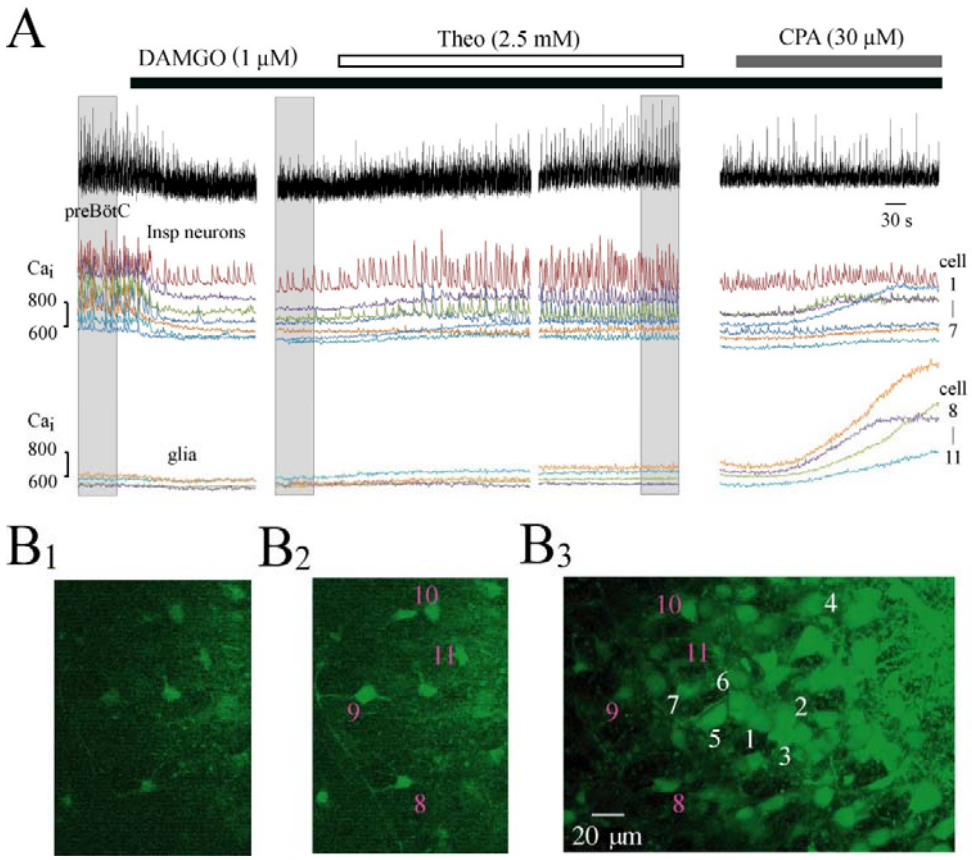

Fig. 4-10: DAMGO and theophylline effects on Ca^{2+} in preBötc neurons and glia. A, DAMGO blocked preBötC rhythm (top trace) and lowered the baseline of the integrated suction electrode signal, but small amplitude (likely nonrespiratory) activity persisted. Ca^{2+} rises (center traces) in most inspiratory active contralateral preBötC neurons were also inhibited, but some neurons continued to show random Ca^{2+} rises. Theophylline reactivated both preBötC rhythm and inspiratory Ca^{2+} rises without a major change in Ca^{2+} baseline in most neurons and glia. Contrary, the Ca^{2+} store blocker cyclopiazonic acid (CPA) evoked a major Ca^{2+} rise in glia, but only in 1 of 7 inspiratory neurons. The traces correspond to inspiratory and glial cells identified in **B**.

Fig. 4-11

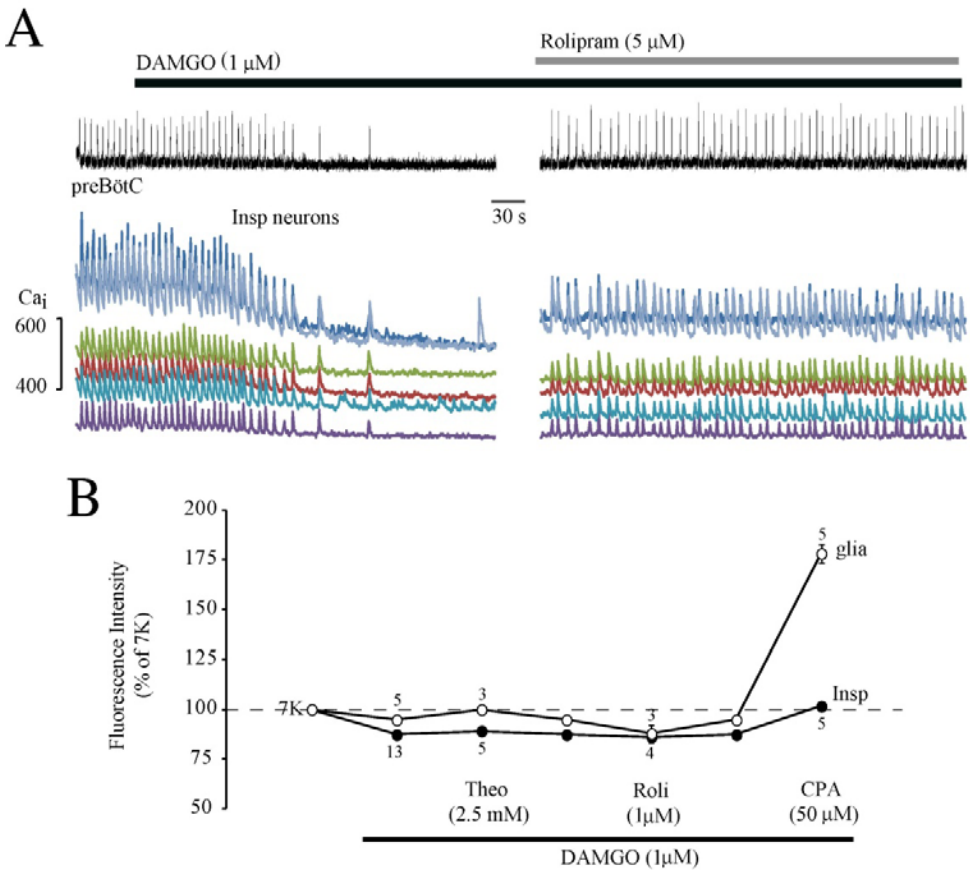

Fig. 4-11: Reversal of opioid-depressed preBötC rhythm by the PDE4 blocker rolipram without Ca^{2+} change in preBötc cells. A, bath-application of rolipram reversed DAMGO blockade of preBötC rhythm and associated Ca^{2+} rises in inspiratory preBötC neurons without a major change of neuronal Ca^{2+} baseline. **B**, the graphs show the percentage change of Ca^{2+} baseline in inspiratory preBötC neurons and neighboring glia in response to DAMGO, and theophylline, rolipram and CPA in DAMGO. The numbers indicate the number of slices tested; in each slice >4 neurons or astrocytes were analyzed.

4.6 References

Alreja M, Aghajanian GK (1993) Opiates suppress a resting sodium-dependent inward current and activate an outward potassium current in locus coeruleus neurons. J Neurosci 13, 3525-3532

Ballanyi K (2004) Neuromodulation of the perinatal respiratory network. Curr Neuropharmacol 2, 221-243

Ballanyi K, Kulik A (1998) Intracellular Ca^{2+} during metabolic activation of K_{ATP} channels in spontaneously active dorsal vagal neurons in medullary slices. Eur J Neurosci 10, 2574-2585

Ballanyi K, Ruangkittisakul A (2009) Structure-function analysis of rhythmogenic inspiratory pre-Botzinger complex networks in "calibrated" newborn rat brainstem slices. Resp Physiol Neurobiol 168, 158-178

Ballanyi K, Onimaru H, Homma I (1999) Respiratory network function in the isolated brainstem-spinal cord of newborn rats. Progr Neurobiol 59, 583-634

Ballanyi K, Ruangkittisakul A, Onimaru H (2009) Opioids prolong and anoxia shortens delay between onset of pre-inspiratory (pFRG) and inspiratory (preBötC) network bursting in newborn rat brainstems. Eur J Physiol (Pflüger's Archiv) 458, 571-587

Ballanyi K, Panaitescu B, Ruangkittisakul A (2010) Control of breathing by nerve glue. Sci Signal 3, pe41

Ballanyi K, Lalley PM, Hoch B, Richter DW (1997) cAMP-dependent reversal of opioid- and prostaglandin-mediated depression of the isolated respiratory network in newborn rats. J Physiol 504, 127-134

Barnes BJ, Tuong CM, Mellen NM (2007) Functional imaging reveals respiratory network activity during hypoxic and opioid challenge in the neonate rat tilted sagittal slab preparation. J Neurophysiol 97, 2283-2292

Benarroch EE (2010) Central neuron-glia interactions and neuropathic pain: overview of recent concepts and clinical implications. Neurology 75, 273-278

Blaustein MP, Golovina VA (2001) Structural complexity and functional diversity of endoplasmic reticulum Ca^{2+} stores. Trends Neurosci 24, 602-608

Brockhaus J, Ballanyi K (1998) Synaptic inhibition in the isolated respiratory network of neonatal rats. Eur J Neurosci 10, 3823-3839

Brockhaus J, Ballanyi K (2000) Anticonvulsant A_1 receptor-mediated adenosine action on neuronal networks in the brainstem-spinal cord of newborn rats. Neuroscience 96, 359-371

Comer AM, Perry CM, Figgitt DP (2001) Caffeine citrate: a review of its use in apnoea of prematurity. Paediatr Drugs 3, 61-79

Connor M, Schuller A, Pintar JE, Christie MJ (1999) Mu-opioid receptor modulation of calcium channel current in periaqueductal grey neurons from C57B16/J mice and mutant mice lacking MOR-1. Br J Pharmacol 126, 1553-1558

Del Negro CA, Hayes JA, Rekling JC (2011) Dendritic calcium activity precedes inspiratory bursts in preBotzinger complex neurons. J Neurosci 31, 1017-1022

Eldridge FL, Millhorn DE, Kiley JP (1985) Antagonism by theophylline of respiratory inhibition induced by adenosine. J Appl Physiol 59, 1428-1433

Feldman JL, Del Negro CA (2006) Looking for inspiration: new perspectives on respiratory rhythm. Nature Rev Neurosci 7, 232-242

Fredholm BB, Battig K, Holmen J, Nehlig A, Zvartau EE (1999) Actions of caffeine in the brain with special reference to factors that contribute to its widespread use. Pharmacol Rev 51, 83-133

Gray PA, Rekling JC, Bocchiaro CM, Feldman JL (1999) Modulation of respiratory frequency by peptidergic input to rhythmogenic neurons in the preBotzinger complex. Science 286, 1566-1568

Härtel K, Schnell C, Hülsmann S (2008) Astrocytic calcium signals induced by neuromodulators via functional metabotropic receptors in the ventral respiratory group of neonatal mice. Glia 57, 815-827

Hedner T, Hedner J, Bergman B, Mueller RA, Jonason J (1985) Characterization of adenosine-induced respiratory depression in the preterm rabbit. Biol Neonate 47, 323-332

Henderson-Smart DJ, Steer PA (2010) Caffeine versus theophylline for apnea in preterm infants. Cochrane Database Syst Rev, CD000273

Herlenius E, Adén U, Tang LQ, Lagercrantz H (2002) Perinatal respiratory control and its modulation by adenosine and caffeine in the rat. Pediatr Res 51, 4-12

Huxtable AG, Zwicker JD, Alvares TS, Ruangkittisakul A, Fang X, Hahn LB, Posse de Chaves E, Baker GB, Ballanyi K, Funk GD (2010) Glia contribute to the purinergic modulation of inspiratory rhythm generating networks. J Neurosci 30, 3947-3958

Janczewski WA, Onimaru H, Homma I, Feldman JL (2002) Opioid-resistant respiratory pathway from the preinspiratory neurones to abdominal muscles: In vivo and in vitro study in the newborn rat. J Physiol 545, 1017-1026

Ladewig T, Kloppenburg P, Lalley PM, Zipfel WR, Webb WW, Keller BU (2003) Spatial profiles of store-dependent calcium release in motoneurones of the nucleus hypoglossus from newborn mouse. J Physiol 547, 775-787

Lopez F, Miller LG, Greenblatt DJ, Kaplan GB, Shader RI (1989) Interaction of caffeine with the GABAA receptor complex: alterations in receptor function but not ligand binding. Eur J Pharmacol 172, 453-9

Lorier AR, Lipski J, Housley GD, Greer JJ, Funk GD (2008) ATP sensitivity of preBötzinger complex neurones in neonatal rat in vitro: mechanism underlying a P2 receptor-mediated increase in inspiratory frequency. J Physiol 586, 1429-1446

Manzke T, Guenther U, Ponimaskin EG, Haller M, Dutschmann M, Schwarzacher S, Richter DW (2003) 5-$HT_{4(a)}$ receptors avert opioid-induced breathing depression without loss of analgesia. Science 301, 226-229

Mellen NM, Janczewski WA, Bocchiaro CM, Feldman JL (2003) Opioid-induced quantal slowing reveals dual networks for respiratory rhythm generation. Neuron 37, 821-826

Milligan ED, Watkins LR (2009) Pathological and protective roles of glia in chronic pain. Nat Rev Neurosci 10, 23-36

Mironov SL (2008) Metabotropic glutamate receptors activate dendritic calcium waves and TRPM channels which drive rhythmic respiratory patterns in mice. J Physiol 586, 2277-2291

Mironov SL, Skorova EY (2011) Stimulation of bursting in pre-Bötzinger neurons by Epac through calcium release and modulation of TRPM4 and K-ATP channels. J Neurochem 117, 295-308

Moises HC, Rusin KI, Macdonald RL (1994) Mu- and kappa-opioid receptors selectively reduce the same transient components of high-threshold calcium current in rat dorsal root ganglion sensory neurons. J Neurosci 14, 5903-5916

Montandon G, Kinkead R, Bairam A (2008) Adenosinergic modulation of respiratory activity: developmental plasticity induced by perinatal caffeine administration. Resp Physiol Neurobiol 164, 87-95

Montandon G, Qin W, Liu H, Ren J, Greer JJ, Horner RL (2011) PreBotzinger complex neurokinin-1 receptor-expressing neurons mediate opioid-induced respiratory depression. J Neurosci 31, 1292-1301

Nehlig A, Daval JL, Debry G (1992) Caffeine and the central nervous system: mechanisms of action, biochemical, metabolic and psychostimulant effects. Brain Res Rev 17, 139-170

North RA, Williams JT (1983) Opiate activation of potassium conductance inhibits calcium action potentials in rat locus coeruleus neurones. Br J Pharmacol 80, 225-228

Onimaru H, Ballanyi K, Homma I (2003) Contribution of Ca^{2+}-dependent conductances to membrane potential fluctuations of medullary respiratory neurons of newborn rats *in vitro*. J Physiol 552, 727-741

Onimaru H, Ballanyi K, Richter DW (1996) Calcium-dependent responses in neurons of the isolated respiratory network of newborn rats. J Physiol 491, 677-695

Panaitescu B, Ruangkittisakul A, Ballanyi K (2009) Silencing by raised extracellular Ca2+ of pre-Bötzinger complex neurons in newborn rat brainstem slices without change of membrane potential or input resistance. Neurosci Lett 29, 456, 25-29

Richter DW, Lalley PM, Pierrefiche O, Haji A, Bischoff AM, Wilken B, Hanefeld F (1997) Intracellular signal pathways controlling respiratory neurons. Respir Physiol Neurobiol 110, 113-123

Ruangkittisakul A, Ballanyi K (2006) Reversal by phosphodiesterase-4 blockers of in vitro apnea in the isolated brainstem-spinal cord preparation from newborn rats. Neurosci Lett 401, 194-198

Ruangkittisakul A, Schwarzacher SW, Ma Y, Poon B, Secchia L, Funk GD, Ballanyi K (2006) High sensitivity to neuromodulator-activated signalling pathways at physiological [K^+] of confocally-imaged respiratory centre neurons in online-calibrated newborn rat brainstem slices. J Neurosci 26, 11870-11880

Ruangkittisakul A, Secchia L, Bornes TD, Palathinkal DM, Ballanyi K (2007) Dependence on extracellular Ca^{2+}/K^+ antagonism of inspiratory centre rhythms in slices and en bloc preparations of newborn rat brainstem. J Physiol 584, 489-508

Ruangkittisakul A, Schwarzacher SW, Secchia L, Ma Y, Bobocea N, Poon BY, Funk GD, Ballanyi K (2008) Generation of eupnea and sighs by a spatiochemically organized inspiratory network. J Neurosci 28, 2447-2458

Ruangkittisakul A, Okada Y, Oku Y, Koshiya N, Ballanyi K (2009) Fluorescence Imaging of active respiratory networks. Resp Physiol Neurobiol 168, 26-38

Ruangkittisakul A, Ballanyi K (2010) Methylxanthine reversal of opioid-evoked inspiratory depression via phosphodiesterase-4 blockade. Resp Physiology Neurobiol 172, 94-105

Ruangkittisakul A, Secchia-Ballanyi L, Panaitescu B, Bobocea N, Kuribayashi J, Iizuka M, Kantor C, Ballanyi K (2012) Anatomically ‘calibrated‘ isolated respiratory networks from newborn rodents. In Isolated Central Nervous System Circuits (Ed K Ballanyi), Neuromethods Series Vol 73 (Ed W Walz). Springer Science+Business Media, LLC, New York, NY, 61-124

Schmidt B, Roberts RS, Davis P, Doyle LW, Barrington KJ, Ohlsson A, Solimano A, Tin W (2006) Caffeine therapy for apnea of prematurity. N Engl J Med 354, 2112-2121

Shi D, Padgett WL, Daly JW (2003) Caffeine analogs: effects on ryanodine-sensitive calcium-release channels and GABAA receptors. Cell Mol Neurobiol 23, 331-47

Smith JC, Ellenberger HH, Ballanyi K, Richter DW, Feldman JL (1991) Pre-Botzinger complex: a brainstem region that may generate respiratory rhythm in mammals. Science 254, 726-729

Smith JC, Ballanyi K, Richter DW (1992) Whole-cell patch-clamp recordings from respiratory neurons in neonatal rat brainstem in vitro. Neurosci Lett 134, 153-156

Soderling SH, Beavo JA (2000) Regulation of cAMP and cGMP signaling: new phosphodiesterases and new functions. Curr Opin Cell Biol 12, 174-179

Soldo BL, Moises HC (1998) mu-opioid receptor activation inhibits N- and P-type Ca^{2+} channel currents in magnocellular neurones of the rat supraoptic nucleus. J Physiol 513, 787-804

Stuth EA, Stucke AG, Brandes IF, Zuperku EJ (2008) Anesthetic effects on synaptic transmission and gain control in respiratory control. Respir Physiol Neurobiol 164, 151-159

Takeda S, Eriksson LI, Yamamoto Y, Joensen H, Onimaru H, Lindahl SG (2001) Opioid action on respiratory neuron activity of the isolated respiratory network in newborn rats. Anesthesiology 95, 740-749

Taketo M, Matsuda H, Yoshioka T (2004) Calcium-independent inhibition of $GABA_A$ current by caffeine in hippocampal slices. Brain Res 1016, 229-239

Williams JT, North RA (1984) Opiate-receptor interactions on single locus coeruleus neurones. Mol Pharmacol 26, 489-497

Zuperku EJ, McCrimmon DR (2002) Gain modulation of respiratory neurons. Respir Physiol Neurobiol 131, 121-133

Chapter-5

$GABA_A$ receptor involvement in methylxanthine-evoked hyperexcitability of isolated spinal but not medullary inspiratory motor networks in newborn rats

Bogdan A. Panaitescu[1+], Junya Kuribayashi[1+], Araya Ruangkittisakul[1], Victoria Leung[1], Makito Iizuka[2], Klaus Ballanyi[1]

[+]Authors contributed equally to the study

[1]Department of Physiology, 750 MSB, University of Alberta, Edmonton, Canada

[2]Center for Medical Sciences, Ibaraki University of Health Sciences, Ami, Japan

I performed ~65% of all the experiments and analyzed the data together with Dr. Junya Kuribayashi, Dr. Araya Ruangkittisakul and Victoria Leung. The rest of the experiments were performed by Drs. Junya Kuribayashi and Araya Ruangkittisakul. Dr. Makito Iizuka did the experiments involving the recording from phrenic and musculocutaneous nerves in the '*en bloc* [+VII]' preparation.

5.1 Introduction

Tonic-clonic convulsions are commonly accompanied by ictal respiratory changes (IRCs) that likely play a major role in sudden unexplained death in epilepsy patients (SUDEP) (Navalet et al., 1989; Blum, 2009; Surges et al., 2009). Whether IRCs manifest as accelerated or depressed breathing depends on various factors such as (cortical) regions from which seizures originate or the animal species studied (Blum, 2009; Surges et al., 2009; Boison, 2011). Using penicilin or A-type γ-aminobutyric ($GABA_A$) receptor blockers such as bicuculline for inducing seizures in animal models, it was revealed that potentially lethal arrest of lung ventilation ('apnea') in IRCs can include both central nervous and obstructed airway components (Paydarfar et al., 1991; Terndrup et al., 1996, 1999; Johnston et al., 1997; Leaming et al., 1999; Budzinska, 2004; St. John et al., 2006). Inhibition of neural respiratory networks in the lower brainstem, the medulla oblongata, seems to be responsible for centrally depressed breathing in IRCs (St. John et al., 2006). Of utmost importance in that regard is the pre-Bötzinger complex (preBötC) inspiratory center whose cellular functions are studied in medullary slices or '*en bloc*' brainstem-spinal cord preparations from perinatal rodents (Ballanyi et al., 1999; Feldman & Del Negro, 2006; Ballanyi & Ruangkittisakul, 2009). Using the *en bloc* model, we found that bicuculline-evoked seizure-like bursting in cervical nerves originates from spinal motor networks and not from medullary inspiratory interneurons (Brockhaus & Ballanyi, 1998, 2000). This shows that the bicuculline seizure model evokes hyperexcitability similar to that in cortical networks in some components of the

respiratory control system.

Convulsive seizures and associated IRCs can occur in patients treated with caffeine or theophylline for countering central apneas of prematurity in preterm infants or obstructive impairment of breathing in acute bronchial asthma and chronic obstructive pulmonary disease (Barnes, 2003; Rottier & Duiverman, 2009; Henderson-Smart & De Paoli, 2010; Mathew, 2011). Moreover, seizures can develop in healthy individuals upon abuse of 'energy' drinks containing methylxanthines (Stavric, 1988; Sawynok, 1995; Magkos & Kavouras, 2005; Iyadurai & Chung, 2007; Mortelmas et al., 2008; Duchan et al., 2010). It is not known whether such IRCs are secondary to hyperexcitability in cortical circuits that can, in turn, influence respiratory networks, or rather also originate directly from the latter structures.

It was one aim of this study to investigate methylxanthine effects on isolated inspiratory networks of newborn rats. For this, we used suction electrodes for simultaneous recording of population bursting of preBötC interneurons and preBötC-driven spinal motor networks in anatomically 'calibrated' *en bloc* preparations (Ruangkittisakul et al., 2007). In calibrated slices (Ballanyi & Ruangkittisakul, 2009), we performed suction electrode recording from preBötC-driven hypoglossal (XII) cranial motoneurons and the ventral respiratory column (VRC) containing the preBötC. Moreover, we used 'blind' whole-cell patch-clamp recording (Smith et al., 1991, 1992) for analyzing membrane potential

responses of inspiratory and tonically active neurons within the preBötC.

In line with our recent findings (Ruangkittisakul & Ballanyi, 2010) that low millimolar methylxanthine is needed for countering opioid depression of the isolated newborn rat preBötC, we hypothesize here that such doses are also necessary for evoking seizure-like activity. In other nervous tissues, such methylxanthine doses block $GABA_A$ receptors, cAMP-elevating phosphodiesterase-4 (PDE4) and Ca^{2+} uptake into cellular stores (Fredholm et al., 1999; Blaustein & Golovina, 2001; Francis et al., 2011; Guerreiro et al., 2011). For investigating the contribution of these mechanisms to presumptive methylxanthine-evoked perturbation of inspiratory networks, we studied whether bicuculline, the PDE4 blocker rolipram or the Ca^{2+} uptake inhibitor cyclopiazonic acid (CPA) mimic methylxanthine effects and/or counter $GABA_A$ receptor-evoked *in vitro* apnea.

5.2 Methods

(see Chapter **2**)

5.3 Results

It was investigated here if methylxanthines evoke seizure-like activity and, if so, whether that activity is associated with depression of inspiratory bursting in

rhythmogenic preBötC interneuronal networks or preBötC-driven spinal cervical (phrenic) and cranial (XII) motor networks. This was studied in different types of (anatomically calibrated) *en bloc* brainstem-spinal cord preparations and 400 μm thick transversal brainstem slices.

5.3.1 Methylxanthine-Evoked Seizure-Like Spinal Discharge in *En Bloc* Preparations

Firstly, it was tested whether methylxanthines affect cervical nerve root bursting in the *en bloc* [+VII] model in which the preBötC interacts with RTN/pFRG networks (Chapter **2**) **(Fig. 5-1)**. In 16 preparations, inspiratory rhythm occurred at a rate of 10.6 ± 0.7 bursts/min in control. At 0.1 or 0.25 mM, neither caffeine nor theophylline perturbed this rhythm substantially, except for occurrence of 1-3 non-respiratory single peak discharges lasting <1 min during the 20 min application period **(Fig. 5-1)**. At >0.25 mM, the rate of occurrence, amplitude and duration of the latter events increased, while 5-10 mM methylxanthine evoked rhythmic multipeak non-respiratory activity with amplitudes that were larger than those of inspiratory bursts. These seizure-like bursts followed initial massive tonic discharge during 1-8 min after start of methylxanthine administration **(Fig. 5-1)**. Both types of spinal hyperexcitability could occlude inspiratory rhythm and often increased the baseline of integrated suction electrode signals indicating sustained activity of motoneurons. Inspiratory rhythm persisted during 0.5-3 min periods between seizure-like activities at a rate, amplitude and duration similar to those in control **(Fig. 5-2)**. As quantified for 10 mM theophylline (n= 4), single burst rate

increased to 121.9 ± 7.7 % of control (7.5 ± 0.7 bursts/min) while single burst amplitude and duration were 90.0 ± 7.8 % and 105.0 ± 9.8 % of control. None of these values differed significantly from control **(Fig. 5-1)**. Non-respiratory activities seemed to be principally similar for both methylxanthines, although caffeine actions appeared to be more modest. Quantitative analysis of methylxanthine-evoked hyperexcitability was not possible because of the variability of responses. However, the classification scheme in **Fig. 5-1** indicates that the extent of perturbation of inspiratory cervical bursts depended on the methylxanthine concentration.

Next, an *en bloc* [+VII] model was used in which phrenic and musculocutaneous nerves were isolated **(Fig. 2-1)** for studying whether seizure-like activity occurs primarily in non-respiratory or inspiratory (phrenic) motoneurons (Chapter **2**). Musculocutaneous nerve was not spontaneously active, whereas inspiratory phrenic nerve bursting at a rate of 8.4 ± 0.9 bursts/min (n= 6) was synchronous with that in contralateral C_4 nerve roots and both burst types had a similar shape **(Fig. 5-2)**. Administration of 10 mM theophylline, which reliably evoked massive non-respiratory activity in the above experiments, initially evoked tonic activity which turned into synchronous seizure-like non-respiratory discharge in all three recordings. In the 6 preparations, theophylline-evoked seizure-like phrenic bursts were smaller than inspiratory phrenic bursts, whereas seizure-like bursts were larger than inspiratory bursts in C_4 roots. Theophylline also decreased the amplitude ($P< 0.05$) and increased the duration ($P< 0.01$) of phrenic inspiratory

bursts, but did not change C_4 burst characteristics **(Fig. 5-2)**. Inspiratory rate did not change during theophylline, but fell to 74.7 ± 3.8 % of control ($P< 0.01$) after 90 min washout **(Fig. 5-2)**.

In a further approach, 10 mM methylxanthine was applied to calibrated *en bloc* preparations with the preBötC exposed to the rostral brainstem surface (Chapter **2**). This model allows the study of methylxanthine effects in the absence of (respiratory) brainstem structures rostral to the preBötC while monitoring VRC/preBötC neuronal population activity directly from the ventrolateral aspect of the cut brainstem surface **(Fig. 2-1)**. In 7 such *en bloc* [-VII] preparations, rhythm in control occurred at 8.1 ± 0.5 bursts/min. Theophylline or caffeine evoked initially tonic, subsequently periodic, seizure-like activity in cervical nerves, whereas inspiratory VRC rhythm was less perturbed. The baseline of integrated VRC signals increased modestly and sometimes, but not always, synchronously with perturbed spinal nerve bursting. However, VRC/preBötC bursts could still be resolved well, contrary to often occluded cervical inspiratory bursts **(Fig. 5-3)**. Similar to effects on phrenic nerve bursting, 10 mM theophylline appeared to reversibly decrease the amplitude and increase the duration of VRC signals **(Fig. 5-3)**. After transecting these preparations between C_1 and C_2 in presence of methylxanthine, VRC rhythm persisted at reduced amplitude in the brainstem aspect. In the spinal aspect, inspiratory rhythm was abolished but seizure-like bursting persisted, also at reduced amplitude **(Fig. 5-3)**. The reduction of the amplitude of these signals may be (partly) due to the fact that

suction electrodes needed to be repositioned following the cut.

5.3.2 Methylxanthine-Evoked Fast Oscillations in XII Nucleus of Brainstem Slices

Next, it was studied in m-preBötC[400] slices **(Fig. 2-1)**, containing a centered (<200 μm thin) preBötC and only a minor rostrocaudal amount of non-preBötC tissue (Chapter **2**), whether methylxanthines evoke seizure-like nerve activity in cranial inspiratory XII motor networks contrary to less pronounced effects on bursting of inspiratory preBötC interneurons.

At <1 mM, neither methylxanthine affected inspiratory VRC or XII rhythms which occurred at a rate of 14.4 ± 0.8 bursts/min (n= 17) in control. As quantified in 6 slices for 1, 2.5 and 5 mM theophylline, neither VRC burst amplitude nor duration were affected, except 1 mM theophylline which increased burst duration to 117.0 ± 6.5 % ($P< 0.05$) of control. Inspiratory VRC rates did not change in response to 1-5 mM caffeine and 1-2.5 mM theophylline, whereas rhythm was accelerated to rates of 183 ± 38.4, 196.2 ± 28.8 and 221.5 ± 31.4 % of control by 10 mM caffeine (n= 8) and 5 mM (n= 9) or 10 mM theophylline (n= 10), respectively **(Fig. 5-4)**. At 10 mM, theophylline depressed VRC burst amplitude to 64.4 ± 5.6 % of control ($P< 0.05$), and decreased burst duration to 61.0 ± 4.3 % of control ($P< 0.01$). In no case did the methylxanthines induce seizure-like perturbations of VRC rhythm. Inspiratory activity occurred in XII nucleus *vs* XII nerve in >80% *vs* ~50% of slices. In ~40% of slices, inspiratory burst amplitudes

in XII nucleus were smaller and less uniform than corresponding VRC signals while <100 ms long small amplitude non-respiratory events could occur at irregular rates **(Fig. 5-4)**. Inspiratory XII nucleus burst amplitudes appeared to increase 1.5-fold at methylxanthine doses <1 mM at steady-state, and 2-2.5-fold early during application of 1-5 mM, but these effects were not significant.

At >1 mM, both methylxanthines evoked synchronized 1-10 Hz oscillations in XII nucleus that were maintained throughout the application period. In particular at 2.5-10 mM, the amplitude of these oscillations could be several-fold larger than that of inspiratory bursts, thus occluding them reversibly **(Figs. 5-4, 5-5)**. Similar to the variability of methylxanthine effects on spinal nerve bursts, it was not possible to quantify the dose dependence for non-respiratory rhythms in XII nucleus. However, the classification scheme in **(Fig. 5-4)** indicates that their extent depended on methylxanthine dose in 10 slices tested for each drug. The amplitude of fast oscillations in XII nucleus depended also very much on the time constant settings for integrated population activity recording, and this activity typically increased the baseline of that signal indicating sustained neuronal activity **(Fig. 5-5)**. In 4 slices, simultaneous recordings were done from the VRC/preBötC area, XII nucleus and XII nerve during 10 mM theophylline. This revealed the above described (lack of) effects on inspiratory rhythms in the VRC/preBötC and XII nucleus regions. However, fast oscillations were either absent (n= 3) or much less pronounced (n= 1) in XII nerve recordings, whereas inspiratory XII nerve rhythm was reversibly abolished within 5-10 min after start

of theophylline administration **(Fig. 5-5)**.

5.3.3 Comparison of Motoneuron Hyperexcitability due to Methylxanthines and Bicuculline

We showed previously in the newborn rat *en bloc* [+VII] model that the $GABA_A$ receptor blocker bicuculline elicits seizure-like discharge in spinal motoneurons, contrary to minor effects on medullary inspiratory neuron activity (Brockhaus & Ballanyi, 1998, 2000). These studies were done under different experimental conditions because ether was used for anesthesia and the superfusate contained 1.5 instead of 1 mM Ca^{2+} which notably depresses preBötC rhythm (Ruangkittisakul et al., 2007, 2010; Panaitescu et al., 2009). Accordingly, we compared next methylxanthine effects on inspiratory networks with those of bicuculline under conditions of the present study.

In 5 *en bloc* [+VII] preparations, 5-25 µM bicuculline evoked rhythmic seizure-like non-respiratory cervical activity with a single burst duration lasting between 10 s and several minutes **(Fig. 5-6)**. The rate of these bursts varied from several, typically single-peaked, events per minute to one event per 5 min and neither rate of intermittent inspiratory cervical bursts **(Fig. 5-6)** nor their amplitude or duration were affected. While 5 µM bicuculline was sufficient to evoke seizure-like bursts, 10 and 25 µM increased seizure rates and sometimes also single burst duration. Bicuculline also evoked seizure-like discharge in 5 *en bloc* [+VII] preparations that were previously treated with methylxanthines **(Fig. 5-6)**. In

~50% of preparations, bicuculline-evoked cervical discharge resembled that caused by methylxanthine, whereas bicuculline effects appeared to be more pronounced in the remaining cases **(Fig. 5-6)**. In 10 slices, 25 μM bicucculline did not perturb VRC rhythm, but increased its rate to 132.7 ± 11.6 % ($P< 0.05$) of control with no effect on VRC burst amplitude or duration **(Fig. 5-6)**. As analyzed in 4 of the latter slices, 25 μM bicuculline irreversibly increased inspiratory burst amplitude in XII nucleus to 190.3 ±16.8 % ($P< 0.01$), whereas an apparent increase of XII nerve burst amplitude to 112.3 ± 10.8 % of control was not significant. In 3 of these 4 XII nucleus recordings, bicuculline (25 μM) did not evoke fast oscillations, instead it induced modest seizure-like activity with amplitudes smaller than those of inspiratory bursts. Such activity was either absent (n= 3) or less pronounced (n= 1) in XII nerve **(Fig. 5-6)**.

5.3.4 Blockade by Methylxanthines of $GABA_A$ Receptors in Inspiratory Networks

To investigate further whether methylxanthines act on $GABA_A$ receptors in inspiratory networks, we depressed rhythm with $GABA_A$ receptor agonist (muscimol, 1-2.5 μM). At >1 mM, theophylline countered muscimol-evoked *in vitro* apnea in 8 *en bloc* [+VII] preparations and similar results were obtained in 7 slices **(Fig. 5-7)**. Restoration by theophylline of inspiratory cervical bursting was accompanied in >50% of cases by seizure-like discharge, whereas the agent evoked fast oscillations in XII nucleus of slices **(Fig. 5-7)**. In both models, bicuculline application following testing of methylxanthine also restored

muscimol-blocked inspiratory rhythm, but this time with concomitant (modest) seizure-like discharge **(Fig. 5-7)**. Cervical bursting recovered to rates of 45 % and 67 % and VRC bursting to 131 % and 68 % of control in response to 10 mM theophylline and 25 μM bicuculline, respectively **(Fig. 5-7)**.

These findings indicate that methylxanthines are capable of reversing the $GABA_A$-induced depression of inspiratory networks. For analyzing the underlying cellular mechanism, V_m and R_i were monitored in inspiratory preBötC neurons and tonically active preBötC neurons that may provide excitatory drive to rhythmogenic inspiratory neurons (Ballanyi & Ruangkittisakul, 2009; Panaitescu et al., 2009) (Chapter **2**). The recording from an inspiratory preBötC neuron in **Fig. 5-8** shows that muscimol-evoked *in vitro* apnea is accompanied by hyperpolarization and concomitant decrease of R_i and that 10 mM theophylline counters both cellular effects and reactivates VRC rhythm. Very similar results were obtained in 9 other inspiratory and 4 tonic preBötC neurons. Specifically in 10 inspiratory and 4 tonic preBötC neurons, muscimol caused a hyperpolarization by 5.4 ± 0.7 and 7.5 ± 1.8 mV and a concomitant fall of R_i by 128.0 ± 24.5 and 117.1 ± 23.4 MΩ, respectively. Application of 10 mM theophylline reversed all muscimol effects to control values except recovery of V_m in inspiratory neurons, which nevertheless showed a clear trend of recovery **(Fig. 5-8)**.

5.3.5 Lack of role of PDE4 or Ca^{2+} release in Methylxanthine - Evoked Hyperexcitability

Besides inhibiting $GABA_A$ receptors, low millimolar methylxanthine doses block cAMP-dependent PDE4 or endoplasmatic reticulum Ca^{2+} pumps causing Ca^{2+} release from this type of store (Fredholm et al., 1999; Blaustein & Golovina, 2001). We tested a possible contribution of these processes to methylxanthine-evoked hyperexcitability of inspiratory motor networks by using the PDE4 blocker rolipram and the Ca^{2+} pump blocker CPA. In 3 *en bloc* [+VII] preparations, rolipram (5 μM) did not evoke spinal hyperexcitability, whereas in further 2 such preparations it elicited several low amplitude non-respiratory cervical bursts. These events were similar to those in about 10% of control preparations, in particular during the first hour of recording **(Figs. 5-6, 5-9)**. Similarly, in 4 slices rolipram did not change burst characteristics or induced hyperexcitability in the VRC, XII nucleus or XII nerve. Also CPA did not affect cervical bursting in 4 *en bloc* [+VII] preparations except for occurrence of modest spinal hyperexcitability **(Fig. 5-9)**. Similarly, in 4 slices CPA did not perturb VRC rhythm and had no effect on XII bursting in 3 of these cases. In 1 slice, CPA reversibly increased the amplitude and rate of non-respiratory discharge in XII nucleus.

Neither CPA nor rolipram were capable of countering muscimol-evoked *in vitro* apnea in the *en bloc* [+VII] or slice models contrary to subsequently applied 10 mM theophylline **(Fig. 5-9)**. Lack of a countering effect of rolipram on VRC bursting in slices was reflected by lack of an effect of the drug on V_m or R_i on 6 inspiratory preBötC neurons **(Fig. 5-10)**.

5.4 Discussion

We studied here whether methylxanthines, which can elicit seizures, perturb bursting of preBötC interneurons and preBötC-driven spinal and cranial motor networks and may thus directly cause IRCs typically associated with seizures. We found that <5 mM methylxanthine does not affect preBötC bursting in brainstem slices. Contrary to this, >1 mM initiates synchronized 1-10 Hz oscillations of unknown mechanism in the inspiratory active XII motor nucleus and evokes notably slower rhythmic seizure-like discharge in spinal motor networks. The results are discussed in context of underlying cellular mechanisms and clinical relevance.

5.4.1 Lack of Methylxanthine Effects on Isolated preBötC

As summarized in an excellent review by Fredholm and colleagues (1999), methylxanthines exert a variety of cellular effects. Specifically, between 0.1-10 mM they block in the order of increasing doses (*i*) A-type adenosine receptors at 0.05-0.2 mM, (*ii*) cAMP-dependent PDE4 at high submillimolar to low millimolar doses, (*iii*) $GABA_A$ receptors at slightly higher low millimolar doses and (*iv*) up to 10 mM are required for blocking Ca^{2+} uptake into endoplasmic reticulum. Our recordings in the VRC area of slices reflect preBötC neuron bursting which ultimately drives inspiratory muscle contractions (Smith et al., 1991; Feldman & Del Negro, 2006). The findings that up to 10 mM caffeine or theophylline did not induce non-respiratory VRC discharge shows that preBötC networks are intrinsically resistant to the tendency of these agents to evoke

seizures (Stavric, 1988; Sawynok, 1995; Barnes, 2003; Magkos & Kavouras, 2005; Iyadurai & Chung, 2007; Mortelmas et al., 2008; Rottier & Duiverman, 2009; Duchan et al., 2010; Henderson-Smart & De Paoli, 2010; Mathew, 2011). In line with a low intrinsic susceptibility of the preBötC to seizure-like perturbations, even combined application of bicuculline and the glycine receptor blocker strychnine does not affect VRC rhythm in rhythmic slices from newborn rodents (Lieske et al., 2000; Ballanyi & Ruangkittisakul, 2009). The finding here that the rate, amplitude and burst duration of VRC slice rhythm are not changed by methylxanthine <5 mM supports conclusions from our recent study (Ruangkittisakul & Ballanyi, 2010) that A_1 or A_2 receptors are not endogenously active in newborn rat preBötC slices. The latter report discusses in detail such lack of a major adenosinergic modulation of isolated preBötC networks in the context of other *in vitro* and *in vivo* work, some of which proposed ongoing tonic adenosinergic depression of preBötC function, with interspecies and developmental differences (Wessberg et al., 1984; Schmidt et al., 1995; Herlenius et al., 2002; Ballanyi, 2004a,b; Montandon et al., 2008; Huxtable et al., 2009; Zwicker et al., 2011).

The observation that 5-10 mM methylxanthine accelerates VRC rhythm and concomitantly depresses its amplitude indicates a direct action on preBötC networks. The methylxanthine-evoked stimulation of inspiratory rate is in agreement with our previous findings that low millimolar methylxanthine restores or accelerates both endogenously and opioid/prostaglandin-depressed preBötC

rhythms in fetal/newborn rat *en bloc* and slice models (Ballanyi, 2004a,b; Ruangkittisakul et al., 2006, 2007, 2008, 2010; Ruangkittisakul & Ballanyi, 2010). The observation in these studies that respirogenic effects of low millimolar methylxanthine are mimicked by rolipram substantiates the hypothesis that cAMP is a major stimulus for bursting in rhythmogenic preBötC neurons or (tonic) neurons driving these cells (Ballanyi et al., 1997, 1999; Richter et al., 1997). In the present study, rolipram did not stimulate inspiratory rhythm in control solution in the *en bloc* or slice model. This confirms previous assumptions that stimulatory effects of cAMP-raising drugs are only evident when (*in vitro*) respiratory networks are (endogenously) depressed (Arata et al., 1993; Ballanyi et al., 1999; Ballanyi, 2004a) similar to respiratory stimulating effects of ampakines (Ren et al., 2006; Greer & Ren, 2009). Acceleration of inspiratory rhythm by high methylxanthine is also unlikely related to block of $GABA_A$ receptors or store-mediated Ca^{2+} signaling because of the lack of effects on inspiratory burst rate of bicuculline and CPA, respectively. Because these drugs and also rolipram did not affect VRC burst amplitude, the attenuated strength of preBötC rhythm at 10 mM methylxanthine is likely also caused by yet unknown mechanisms.

Theophylline, in a concentration >1 mM reversed respiratory depression due to $GABA_A$ receptor activation, while rolipram and CPA were ineffective. This reversing effect might be due to an effect on $GABA_A$ receptors because 10 mM theophylline also reversed the muscimol-evoked fall of input resistance in both inspiratory and tonic neurons in the preBötC. Lack of network and cellular

stimulatory effects of rolipram in this regard indicates that PDE4 blockade may not reverse inspiratory depression unless related to lowered cellular cAMP. In summary, our findings on VRC rhythms in slices suggest that methyxanthines do not affect preBötC networks directly as a possible cause for IRC associated with methylxanthine application. However, as outlined in the following, these drugs perturb inspiratory motor output substantially, at both cranial and spinal levels.

5.4.2 Methylxanthine-Evoked Seizure-Like Spinal Hyperexcitability

In the *en bloc* model, already 0.1-0.25 mM methylxanthine evoked (minor) non-respiratory cervical nerve activities which might thus be due to blockade of A-type adenosine receptors (see above). Perturbation of cervical rhythm became gradually more severe upon increasing methylxanthine doses to 0.5-10 mM. At >2.5 mM, non-respiratory activities often resembled slow rhythmic seizure-like discharge evoked by bicuculline, which is an established model for studying mechanisms of epilepsy, or more general, disinhibited neural network bursting, both *in vivo* and *in vitro* (Jefferys, 1994; Bracci et al., 1996; Brockhaus & Ballanyi, 1998, 2000; Kilb et al., 2007). Involvement of $GABA_A$ receptor inhibition in methylxanthine-evoked seizure-like spinal bursting is also indicated by the finding in our present study that muscimol-evoked blockade of inspiratory cervical rhythm is countered by >1 mM of either agent which can be associated with seizure-like bursting. However, compared to methylxanthines bicuculline often evoked here a more regular pattern of spinal non-respiratory activity like in our previous studies (Brockhaus & Ballanyi, 1998, 2000). This suggests that

blockade of $GABA_A$ receptors is not the only target for methylxanthine-evoked seizure-like bursting in spinal motor networks. Contribution of blockade of PDE4 or store-related Ca^{2+} signaling is not likely because neither rolipram nor CPA caused a major perturbation of spinal cervical bursts. Other possible mechanisms of action that might explain the effect of methylxanthines are: inhibition of glycinergic receptors (Uneyama et al., 1993; Duan et al., 2009) or TREK-1 channels (Harinath & Sikdar, 2005) or enhancement of NMDA receptor transmission (Amabeoku et al., 1999).

Contrary to the lack of non-respiratory VRC activity in slices, inspiratory VRC activity in rostrally transected *en bloc* preparations with exposed preBötC was perturbed by methylxanthines. This methylxanthine-evoked non-respiratory VRC activity was often, but not always, synchronous with notably larger seizure-like perturbation of inspiratory rhythm recorded from cervical roots. Also, seizure-like activity in high methylxanthine persisted in the cord upon transection at C_2, whereas perturbation of VRC rhythm in the brainstem aspect seemed attenuated. This is in line with our previous observation in the newborn rat *en bloc* model that bicuculline-evoked seizure-like XII nerve bursting was greatly attenuated upon removal of the cord, whereas inspiratory rhythm was not affected (Brockhaus & Ballanyi, 2000). Simultaneous recording of phrenic, musculocutaneous nerves and cervical roots revealed that perturbation of spinal inspiratory motor networks is more modest compared to adjacent non-respiratory motor circuits, but not absent. However, it is possible that non-respiratory networks have a larger

motoneuron pool which has the potential to generate larger amplitude signals.

In summary, the findings in the different *en bloc* models indicate that spinal motor networks of different function respond in a similar fashion with seizure-like activity already to >0.1 mM methylxanthine and, at least at close to millimolar concentrations, this hyperexcitability is similar to the one produced by blocking of $GABA_A$ receptors.

5.4.3 Methylxanthine-Evoked Fast Oscillations in XII Networks

As opposed to lack of occurrence of non-respiratory activity in the VRC region of slices, >1 mM methylxanthine induced a novel type of synchronized 1-10 Hz oscillation in the XII nucleus which was maintained throughout the application period and could completely occlude inspiratory bursting in this area. Because bicuculline evoked only modest seizure-like discharge in XII nucleus, whereas rolipram and CPA did not induce notable non-respiratory discharge, it is unlikely that these oscillations are mediated by methylxanthine-evoked block of $GABA_A$ receptors, PDE4 or store-mediated Ca^{2+} signaling. It has been demonstrated previously that XII motoneurons are capable of showing high frequency oscillations of their membrane potential either generated by premotor networks during inspiratory activity (reviewed by Funk & Parkis, 2002) or evoked by activation of metabotropic glutamate receptors (Cifra et al., 2009). Unexpectedly, simultaneous recording in the VRC, XII nucleus and XII nerve revealed in the present study that the massive oscillatory activity in XII nucleus was only

reflected by a modest initial, if at all, fast oscillatory activity in XII nerve, whereas inspiratory XII nerve rhythm, but not VRC rhythm was blocked within several minutes into application of 10 mM theophylline. This indicates that not all rhythmic activities in XII nucleus originate from (inspiratory) motoneurons whose axons project via XII nerve. Because XII nucleus contains a small number of interneurons, it is possible that glial cells such as astrocytes or immunoreactive microglia contribute to these pronounced oscillations by providing excitatory neuromodulators to the neighboring neurons.

5.4.4 Functional Consequences of Methylxanthine - Evoked Motoneuronal Hyperexcitability

While spinal motor networks could show already seizure-like hyperexcitability at >0.1 mM methylxanthine, the incidence of its occurrence and the severity of perturbation of inspiratory rhythm were most pronounced at >0.5 mM. This concentration range fits well with the countering effect of methylxanthines on opioid-evoked severe depression of isolated newborn rat bursting in our recent study (Ruangkittisakul et al., 2010). However, as discussed already above, the respiratory stimulating effect of methylxanthine is mimicked by rolipram and is thus likely related to blockade of PDE4. In contrast, spinal activity may not be due to PDE4 inhibition, but, at least partly, caused by $GABA_A$ receptor blockade, whereas the mechanism involved in XII motor network oscillations at >1 mM methylxanthine is not clear yet. In the latter study, we discuss in detail reasons that might explain why millimolar methylxanthine is necessary to stimulate

depressed preBötC rhythm while methylxanthine levels >0.1 mM in the plasma are considered as toxic. One reason for this paradox might be that the absence of supramedullary structures in both the *en bloc* and slice model removes a possibly indirect tonic inhibitory influence on the preBötC of A-type adenosine receptors that are blocked by <0.2 mM methylxanthine (Fredholm et al., 1999). It is also possible that some *in vitro* conditions attenuate the sensitivity of isolated preBötC networks to these agents. That this may be indeed the case is indicated by our preliminary findings that low millimolar methylxanthine is also necessary for evoking seizure-like perturbation of early network oscillations in the areas of the hippocampus, entorhinal cortex and neocortex of newborn rat brain slices (Kantor et al., 2012). However, one study on newborn mouse preBötC slices showed an accelerating effect on inspiratory rhythm of methylxanthine at a dose as low as 0.05 mM (Wilken et al., 2000). This indicates that there may be also differences between species and humans may be most sensitive in responding to these agents. Whatever the reason is for the low sensitivity of isolated newborn rat inspiratory networks and motor networks to methylxanthines, it remains remarkable that the same low millimolar doses exert the respiratory stimulating effect and the hyperexcitability of motor networks. This explains that the therapeutic range, particularly of theophylline, is narrow and that slightly higher doses can evoke side effects, including seizures. Finally, the present findings indicate that perturbation of breathing by methylxanthines does not originate from the inspiratory center but rather from spinal and cranial motor networks.

5.5 Figures and Legends

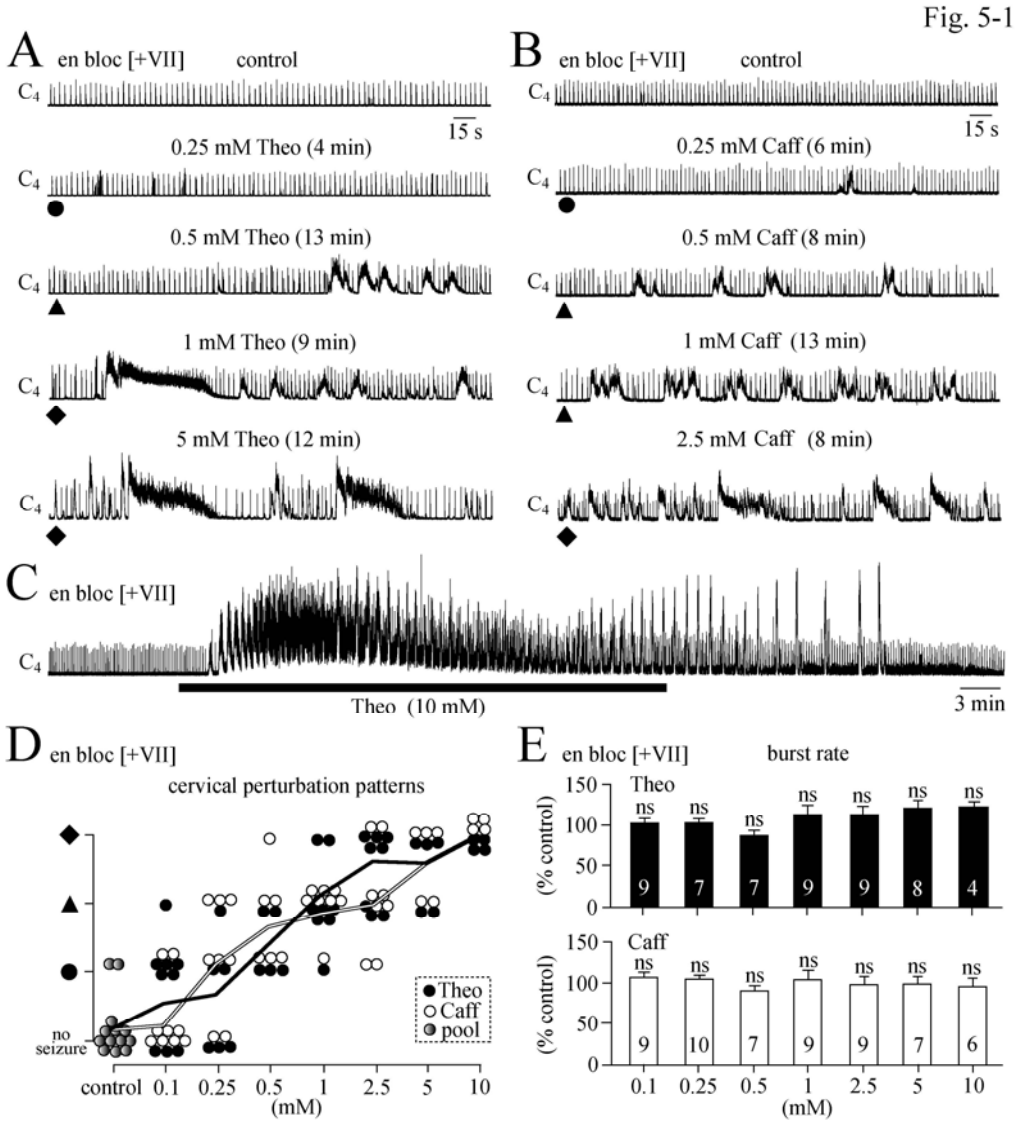

Fig. 5-1: Methylxanthine-evoked seizure-like activities in *en bloc* [+VII] model with functional pFRG. Amplified (10k), bandpass-filtered (0.3-3 kHz) and integrated (τ: 50 ms) inspiratory C_4 suction electrode signals were monitored during methylxanthines actions. **A**, theophylline (Theo) was bath-applied at different concentrations with intermittent 20-60 min 'wash' periods. At 0.25 mM, Theo only caused minor perturbation of inspiratory rhythm, whereas 0.5, 1 and 5 mM evoked seizure-like C_4 discharge lasting between 15 s and >1 min with amplitudes that could exceed that of inspiratory bursting. Consequently, such discharge could mask inspiratory rhythm which though persisted between 'seizure' episodes. **B**, similar seizure-like bursting was seen in a different *en bloc* [+VII] preparation during caffeine (Caff). **C**, in a further *en bloc* [+VII] preparation, continuous C_4 recording exemplifies that >1 mM methylxanthine evoked tonic C_4 discharge during the first 1-8 min of administration which

subsequently turned into periodic non-respiratory bursting. **D**, methylxanthine responses partly varied notably between preparations and could thus not be quantified. Instead, response patterns were classified as minor (●), moderate (▲), and major (♦) disturbance as exemplified with symbols below C_4 recordings in **A** and **B**. Scatter plot indicates that most severe perturbation of C_4 rhythm occurred mostly at >0.5 mM methylxanthine (each circle represents an individual preparation). **E**, bar graph shows that, despite occurrence of seizure-like discharge, the rate of intermittent inspiratory cervical rhythm was not changed by methylxanthines. Also inspiratory burst amplitude and duration were not affected (not shown). Numbers in bars correspond to number of preparations tested; 'ns' means not significant.

Fig. 5-2

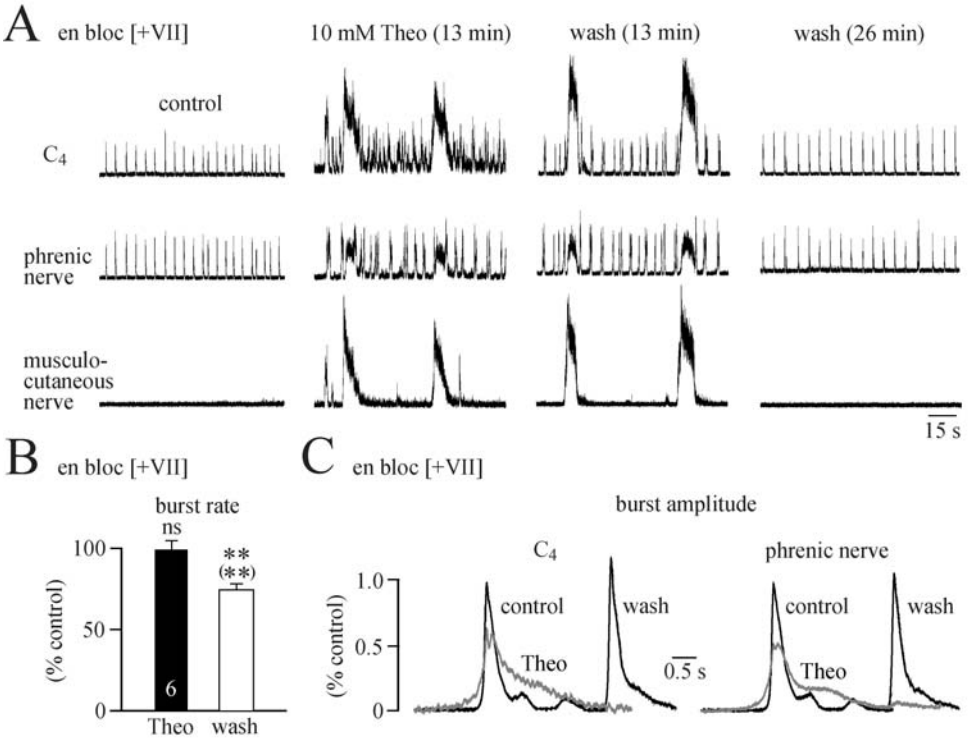

Fig. 5-2: Theophylline-evoked seizure-like bursting in phrenic and musculocutanous nerves in *en bloc* [+VII] model. Effects of 10 mM Theo were tested on 6 *en bloc* [+VII] preparations with intact phrenic nerve (solely containing axons from inspiratory active motoneurons innervating the diaphragm) and musculocutaneous nerve (containing no respiratory motor axons) (see Chapter **2** and **Fig. 2-1**). **A**, synchronous inspiratory bursting was seen in C_4 nerve roots containing axons from both inspiratory plus non-respiratory motoneurons and contralateral phrenic nerve whereas musculocutaneous nerve was not spontaneously active. During Theo application, all nerves showed synchronous seizure-like discharge that obscured C_4 inspiratory rhythm more than phrenic nerve bursts. **B**, during Theo (analyzed at 15-20 min after start of application), inspiratory rate was not changed, but rhythm slowed down after >30 min following start of Theo washout. Asterisks denote comparison to control, while asterisks in bracket refer to comparison against rate in Theo. **C**, in 6 preparations, Theo appeared to decrease amplitude and concomitantly increase inspiratory C_4 and phrenic burst durations, but these effects were only significant for phrenic nerve (see Results). Traces represent averaged overlays of >15 bursts in a 2-4 min analysis period, each from 6 preparations. Average trace for recovery (after 90 min of Theo wash) is displayed to the right of overlaid control and Theo bursts for higher clarity.

Fig. 5-3

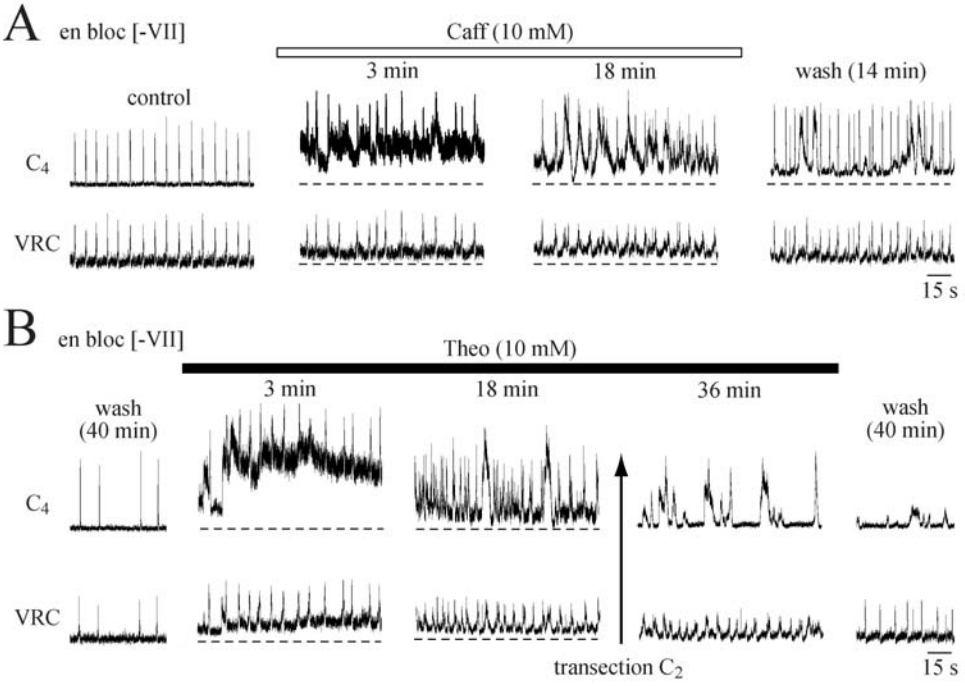

Fig. 5-3: Methylxanthine-evoked seizure-like bursting in *en bloc* [-VII] preparations with exposed preBötC. In 7 experiments, *en bloc* preparations were transected close to the rostral preBötC boundary, specifically -0.22 ± 0.1 mm caudal to VII_c, and did thus contain neither VII nucleus nor a major portion of pFRG/RTN complex (see Chapter **2** and **Fig. 2-1**). **A**, 10 mM Caff evoked typical major perturbations of C_4 nerve root bursting, whereas inspiratory rhythm in ventrolateral area of the cut rostral surface (-0.30 mm caudal to VII_c) containing the VRC including the exposed preBötC was less affected, except for an apparent though nonsignificant decrease in burst amplitude (see Results). Both C_4 and VRC rhythms recovered at >10 min into Caff wash, but inspiratory slowed down after 40 min of wash (**B**). Slowing of rhythm was due to the fact that the exposed preBötC remains active in solution of physiological K^+ (3 mM) only for several hours before it arrests spontaneously ('*in vitro* apnea') (Ruangkittisakul et al., 2006, 2007). In this situation, 10 mM Theo accelerated inspiratory rhythms and also evoked non-respiratory C_4 discharge. At 19 min of Theo application, the spinal cord was transected at C_2. Consequently, inspiratory rhythm in C_4 rootlet was abolished but persisted in the VRC recording from rostral aspect of the preparation, whereas seizure-like discharge persisted in the cord. The methylxanthine-evoked decrease in VRC burst amplitude was partly reversible 40 min after start of Theo wash.

Fig. 5-4

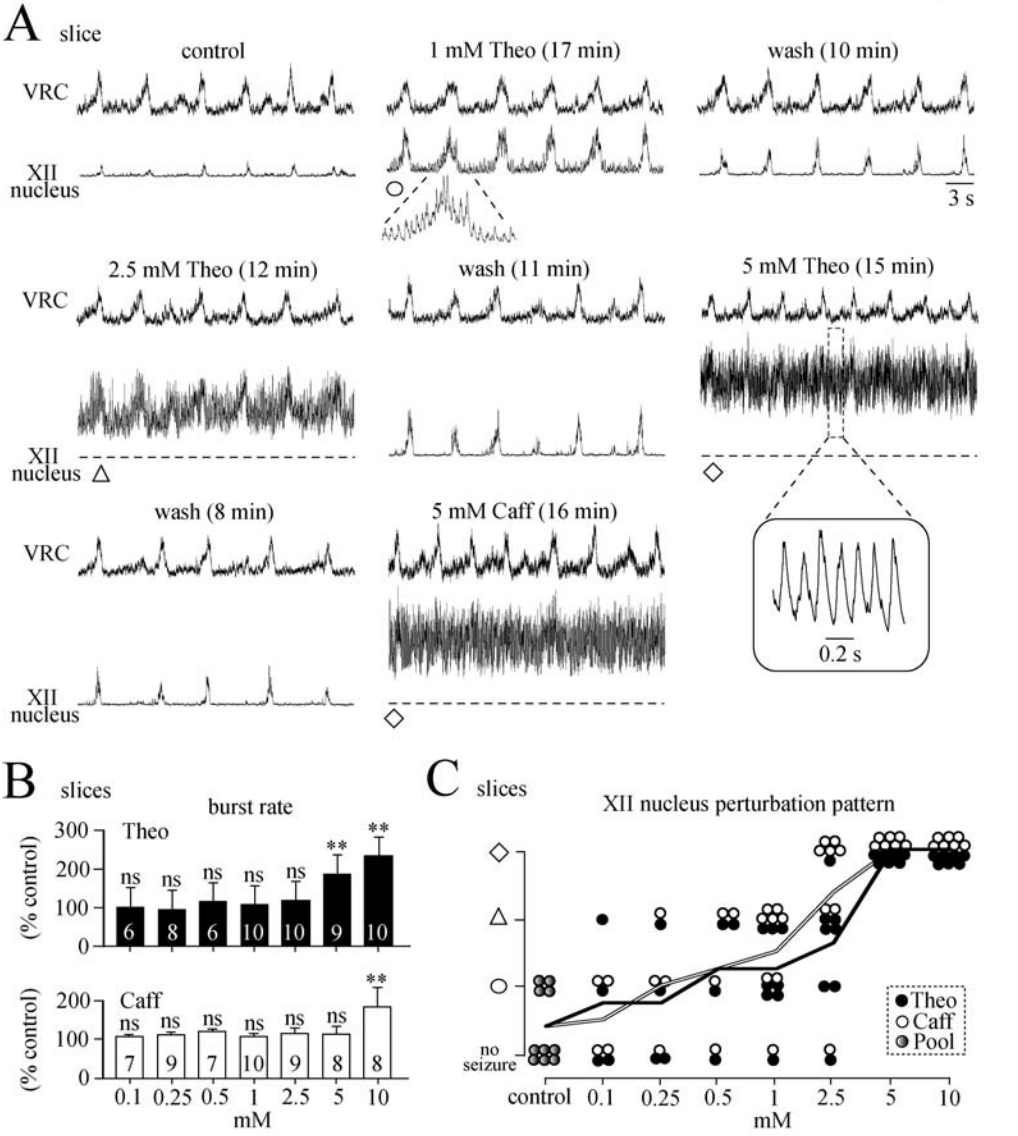

Fig. 5-4: Methylxanthine-evoked fast rhythm in XII nucleus of preBötC-containing 'calibrated' newborn rat brainstem slices. Inspiratory rhythms were monitored with suction electrodes in 400 μm thick transversal brainstem slices (n= 76) with mean caudal and rostral boundaries located -0.71 ± 0.04 mm and -0.33 ± 0.07 mm caudal to VII_c, respectively, and which thus contained a centered preBötC (see Chapter **2** and **Fig. 2-1**). As exemplified in **A** for such a 'm-preBötC[400] slice' with caudal and rostral boundaries located -0.70 and -0.35 mm caudal to VII_c, respectively, inspiratory VRC rhythm was not perturbed by Theo or Caff. In contrast, 1 mM Theo augmented amplitude of inspiratory bursting in XII nucleus with concomitant occurrence of rhythmic discharge at a rate of ~3 Hz. In response to 2.5 and 5 mM Theo or 5 mM Caff, baseline of integrated XII nucleus signal showed upward shift as indication of massive neural activity, while amplitude of fast oscillations increased. Inset shows XII nucleus

oscillations at higher time resolution. **B**, bar graphs show that rate of VRC rhythm is not affected by methylxanthines except for accelerating effect of 5 and 10 mM Theo and 10 mM Caff. **C**, similar to perturbation of inspiratory bursting in *en bloc* models (**Fig. 5-1**), patterns of perturbation of inspiratory rhythm in XII nucleus could be categorized into minor (●), moderate (▲), and major (♦) oscillations as exemplified with symbols below XII nucleus recordings in **A**. This indicates that large amplitude fast oscillations occurred primarily in response to >1 mM of either methylxanthine.

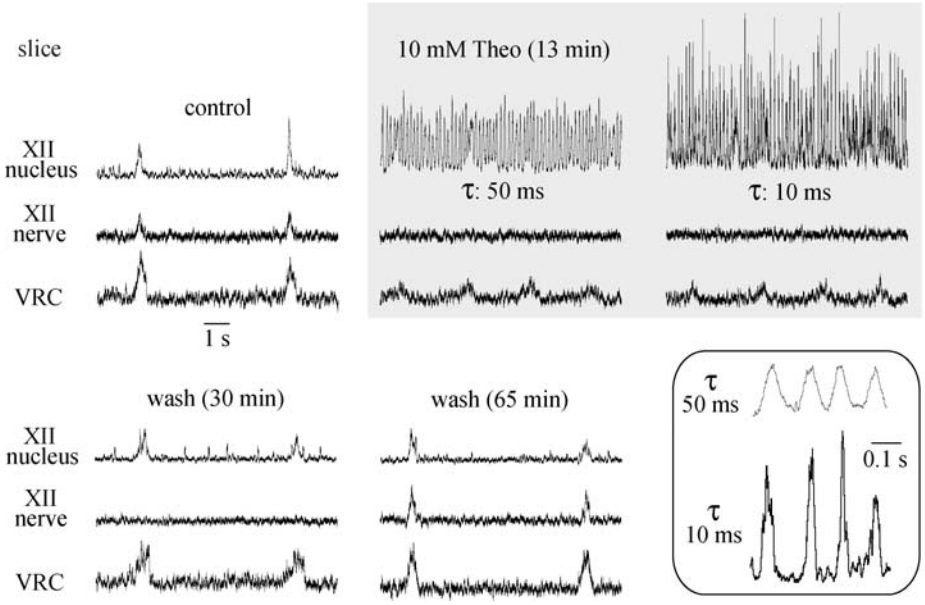

Fig. 5-5: Methylxanthine depression of XII nerve activity in m-preBötC[400] slices. In m-preBötC[400] slices (n=4), mean caudal and rostral boundaries located -0.75 ± 0.05 and -0.33 ± 0.09 caudal to VII_c, respectively, three suction electrodes were used for simultaneous recording of inspiratory rhythm in the VRC, XII nucleus and XII nerve in response to 10 mM Theo. **A**, in a slice with rostral and caudal boundaries located -0.80 and -0.45 mm caudal to VII_c, respectively, Theo accelerated VRC rhythm (compare **Fig. 5-4**) and decreased its amplitude. At the same time, Theo reversibly evoked fast oscillations in XII nucleus (compare **Fig. 5-4**) and reversibly abolished XII nerve root bursting. Changing the time constant for integrated XII nucleus signal from 50 to 10 ms during 10 mM Theo notably increased its amplitude as evidence of profound neural activity in this slice region. Traces in inset show latter XII nucleus signals at higher time resolution.

Fig. 5-6

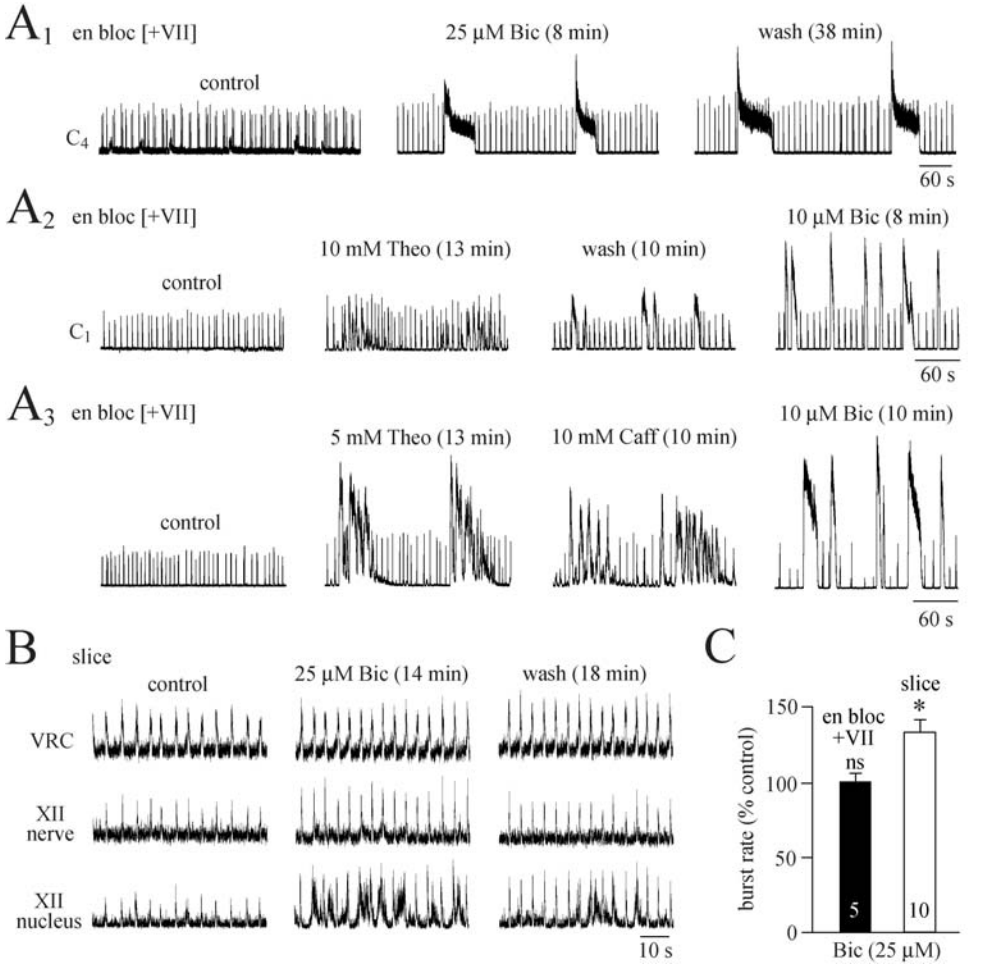

Fig. 5-6: Bicuculline-evoked hyperexcitability in *en bloc* [+VII] and slice models. A, effects of the A-type □-aminobutyric acid ($GABA_A$) receptor blocker bicuculline (Bic) (in comparison with effects of methylxanthine) in *en bloc* [+VII] preparations. Similar to methylxanthines, Bic evoked a spectrum of responses with one common feature that inspiratory C_4 rhythm was perturbed and/or obscured. **B**, in a m-preBötC[400] slice with caudal and rostral boundaries located -0.75 and -0.35 mm caudal to VII_c, respectively, 25 µM Bic evoked modest seizure-like bursting in XII nucleus that was reflected by very minor perturbation of XII nerve inspiratory rhythm, with neither fast XII oscillations nor disturbance of VRC bursting. **C**, Bic did not change rate of C_4 rhythm in the *en bloc* model, but accelerated slice rhythm to 132.7 ± 11.6 % of control.

Fig. 5-7

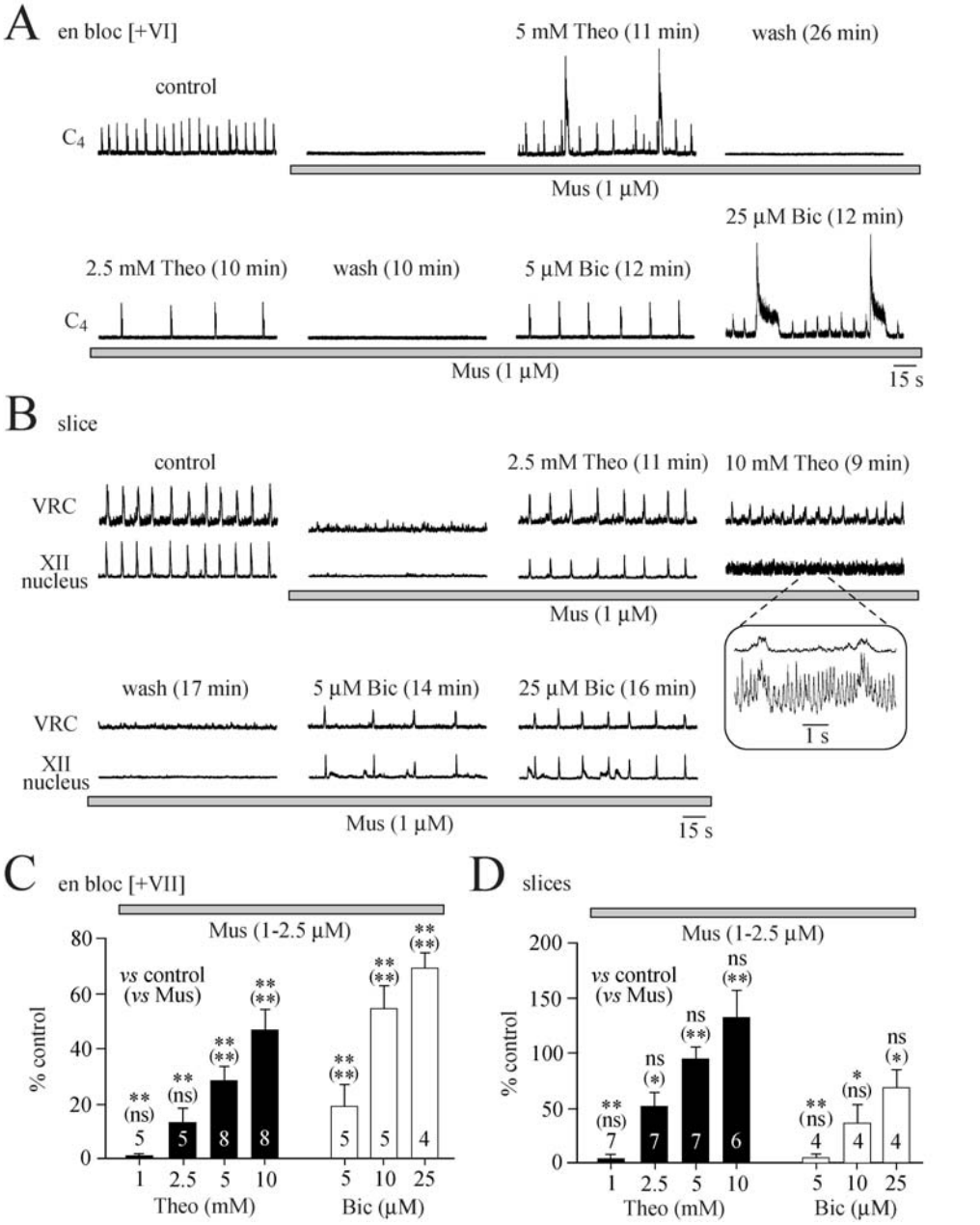

Fig. 5-7: Countering by methylxanthines of $GABA_A$ receptor-evoked *in vitro* apnea in *en bloc* [+VII] and slice models. To test whether low millimolar methylxanthine blocks $GABA_A$ receptors in inspiratory networks, cervical rhythm in *en bloc* [+VII] preparations and VRC bursting in m-preBötC[400] slices was blocked by bath-application of 1-2.5 µM of the $GABA_A$ receptor agonist muscimol (Mus). Theo or Bic were applied to counter such *in vitro* apnea. **A**, 2.5 and 5 mM Theo reactivated inspiratory C_4 rhythm and induced seizure-like bursting (at 5 mM) following *in vitro* apnea due to 1 µM Mus. After Theo washout in continuous presence of Mus, Bic also restored rhythm at 5 µM, whereas 25 µM accelerated inspiratory bursting and evoked seizure-like activity.

Decrease in the amplitude of the C_4 signal in 25 μM Bic may be due to loss of suction. **B**, both Theo and Bic were also able, in the continuous presence of 1 μM Mus, to restore VRC rhythm in m-preBötC[400] slice with caudal and rostral boundaries located -0.70 and -0.30 mm caudal to VII_c, respectively. Note that 10 mM Theo depressed amplitude of VRC rhythm and induced fast oscillations in XII nucleus in the presence of Mus (compare **Figs. 5-4, 5-5**). **C**, **D** statistical analysis of countering actions of Theo and Bic on rates of Mus-depressed inspiratory VRC rhythm in *en bloc* [+VII] (**C**) and slice model (**D**). Note difference in ordinate scale between **C** and **D** and that bicuculline was more effective in the *en bloc* model, whereas Theo was more potent in slices.

Fig. 5-8

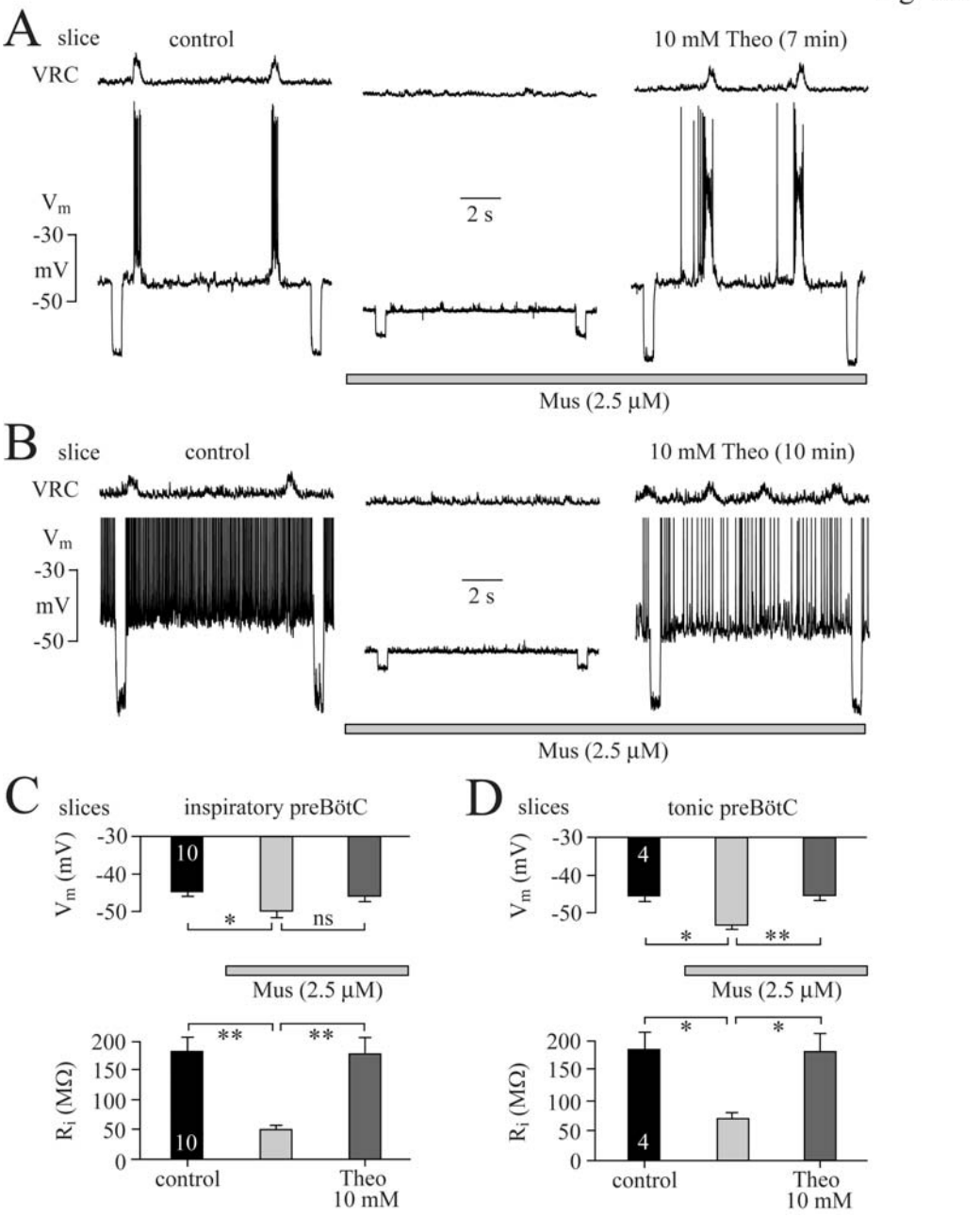

Fig. 5-8: Involvement of postsynaptic methylxanthine effects in countering $GABA_A$ receptor-evoked depression of preBötC neuron activity. 'Blind' whole-cell patch-clamp recording techniques were used to record membrane potential (V_m) and input resistance (R_i) in inspiratory and non-respiratory, tonically active neurons in the preBötC area. **A**, in m-preBötC[400] slice with the caudal and rostral boundaries located -0.65 and -0.25 mm caudal to VII_c, respectively, an inspiratory preBötC neuron located -0.53 mm caudal to VII_c showed synaptic drive potentials and concomitant action potential discharge during inspiratory activity in the contralateral VRC/preBötC area. Silencing of VRC rhythm and rhythmic bursting of this cell by 2.5 µM Mus was accompanied

by hyperpolarization of V_m and concomitant decrease of R_i measured in response to regular application of hyperpolarizing dc current pulses of pA amplitude. Both, V_m and R_i were restored within 7 min following start of application of 10 mM Theo in the continuous presence of Mus. **B**, similar effects of Mus and Theo were revealed in different slice **C**, **D**, statistical analysis of effects of Mus and Theo in Mus on V_m and R_i in inspiratory (**C**) and tonic (**D**) preBötC neurons.

Fig. 5-9

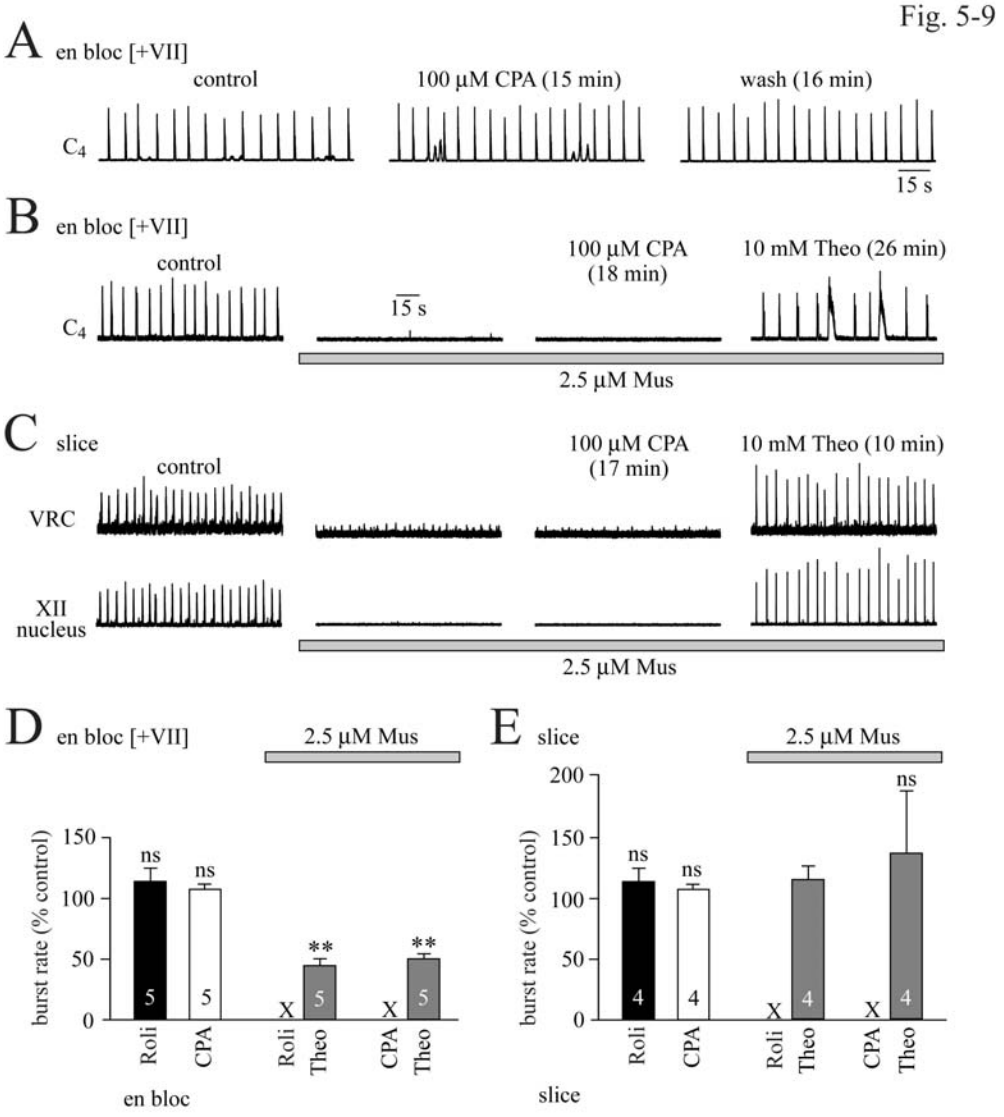

Fig. 5-9: Countering by methylxanthines of $GABA_A$ receptor-evoked depression of inspiratory rhythm in the *en bloc* [+VII] and slice models. To investigate other possible methylxanthine mechanisms, it was tested whether blockade of endoplasmic reticulum Ca^{2+} pumps with 100 µM cyclopiazonic acid (CPA) or of cAMP-dependent phosphodiesterase-4 with 5 µM rolipram (Roli) mimics methylxanthine effects. **A**, in an *en bloc* [+VII] preparation, CPA slightly augmented low amplitude non-respiratory bursting in C_4 roots while such discharge completely disappeared after washout of CPA. **B**, in a different *en bloc* [+VII] preparation CPA was not capable of countering Mus-evoked *in vitro* apnea contrary to 10 mM Theo which was applied 16 min after washout of CPA. **C**, also in m-preBötC[400] slice with caudal and rostral boundaries located -0.70 and -0.33 mm caudal to VII_c, Theo but not CPA countered Mus-evoked blockade of inspiratory VRC and XII nucleus rhythms. Very similar lack of effects was seen in response to Roli (not shown). **D**, **E**, statistical analysis of CPA and Roli effects on burst rates in en bloc [+VII] preparations and m-preBötC[400] slices. Note that

CPA and Roli did not affect the rate of inspiratory rhythm either in the *en bloc* or slice models and that they also did not counter Mus-induced *in vitro* apnea, contrary to Theo.

Fig. 5-10

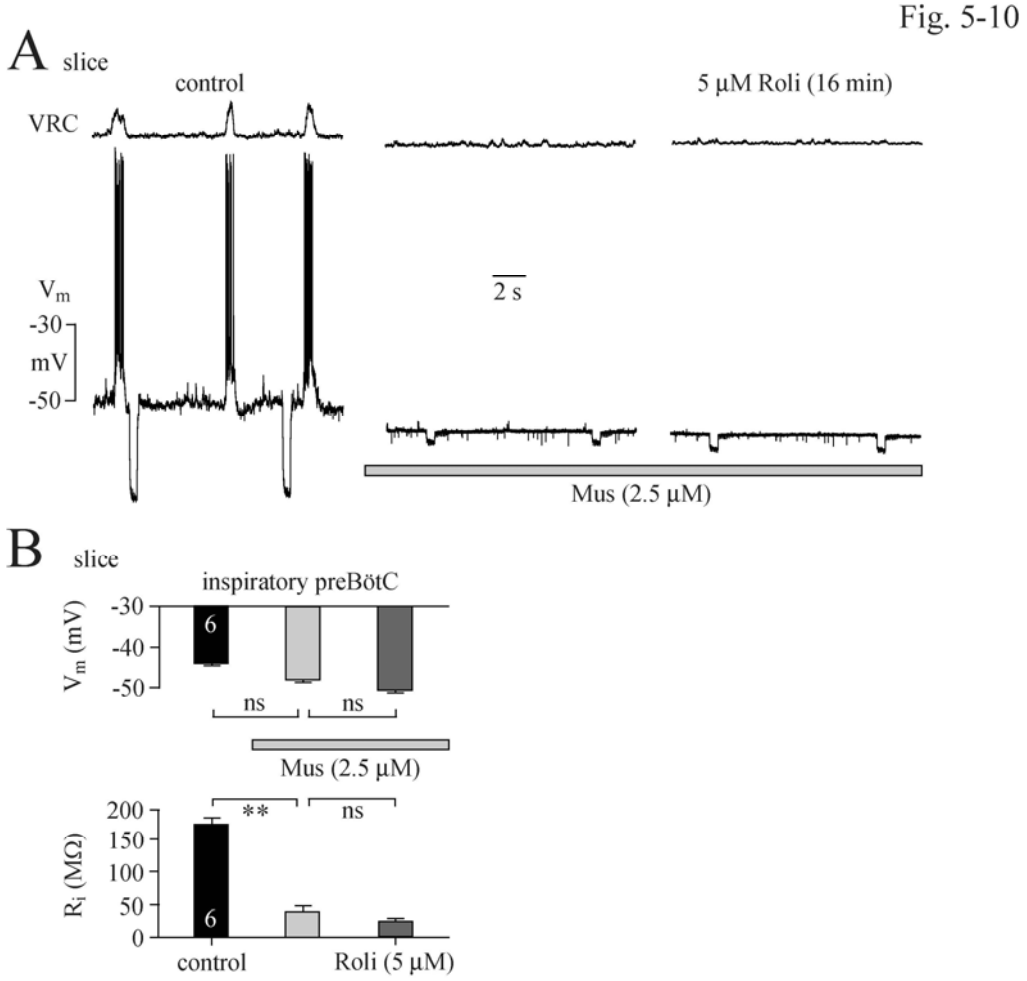

Fig. 5-10: Lack of postsynaptic effects of rolipram on $GABA_A$ receptor depressed preBötC neuron activity. A, in inspiratory preBötC neuron located -0.57 mm caudal to VII_c in m-preBötC[400] slice with caudal and rostral boundaries located -0.65 and -0.30 mm caudal to VII_c, respectively, 5 µM Roli did not reverse either V_m hyperpolarization, R_i decrease or concomitant silencing of spontaneous inspiratory-related bursting evoked by 2.5 µM Mus. **B**, statistical analysis of lack of reversal effects of Roli on Mus-evoked hyperpolarization and R_i decrease.

5.6 References

Amabeoku GJ (1999) Gamma-aminobutyric acid and glutamic acid receptors may mediate theophylline-induced seizures in mice. Gen Pharmacol 32, 365-372

Arata A, Onimaru H, Homma I (1993) Effects of cAMP on respiratory rhythm generation in brainstem-spinal cord preparation from newborn rat. Brain Res 605, 193-199

Ballanyi K (2004a) Neuromodulation of the perinatal respiratory network. Curr Neuropharmac 2, 221-243

Ballanyi K (2004b) Protective role of neuronal K_{ATP} channels in brain hypoxia. J Exp Biol 207, 3201-3212

Ballanyi K, Ruangkittisakul A (2009) Structure-function analysis of rhythmogenic inspiratory pre-Bötzinger complex networks in "calibrated" newborn rat brainstem slices. Respiratory Physiology Neurobiology 168, 158-178

Ballanyi K, Lalley PM, Hoch B, Richter DW (1997) cAMP-dependent reversal of opioid- and prostaglandin-mediated depression of the isolated respiratory network in newborn rats. J Physiol 504, 127-134

Ballanyi K, Onimaru H, Homma I (1999) Respiratory network function in the isolated brainstem-spinal cord of newborn rats. Progr Neurobiol 59, 583-634

Barnes PJ (2003) Theophylline: new perspectives for an old drug. Am J Respir Crit Care Med 167, 813-818

Blaustein MP, Golovina VA (2001) Structural complexity and functional diversity of endoplasmic reticulum Ca^{2+} stores. Trends Neurosci 24, 602-608

Blum AS (2009) Respiratory physiology of seizures. J Clin Neurophysiol 26, 309-315

Boison D (2011) Methylxanthines, seizures, and excitotoxicity. Handb Exp Pharmacol 200, 251-266

Bracci E, Ballerini L, Nistri A (1996) Localization of rhythmogenic networks responsible for spontaneous bursts induced by strychnine and bicuculline in the rat isolated spinal cord. J Neurosci 16, 7063-7076

Brockhaus J, Ballanyi K (1998) Synaptic inhibition in the isolated respiratory network of neonatal rats. Europ J Neurosci 10, 3823-3839

Brockhaus J, Ballanyi K (2000) Anticonvulsant A_1 receptor-mediated adenosine action on neuronal networks in the brainstem-spinal cord of newborn rats. Neuroscience 96, 359-371

Budzińska K (2004) Hypoglossal and phrenic nerve responses to changes in oxygen tension during picrotoxin-induced seizures in the rat. J Physiol Pharmacol 55, 31-39

Cifra A, Nani F, Sharifullina E, Nistri A (2009) A repertoire of rhythmic bursting produced by hypoglossal motoneurons in physiological and pathological conditions. Philos Trans R Soc Lond B Biol Sci 364, 2493-2500

Duan L, Yang J, Slaughter MM (2009) Caffeine inhibition of ionotropic glycine receptors. J Physiol 587, 4063-4075

Duchan E, Patel ND, Feucht C (2010) Energy drinks: a review of use and safety for athletes. Phys Sportsmed. 38, 171-179

Feldman JL, Del Negro CA (2006) Looking for inspiration: new perspectives on respiratory rhythm. Nat Rev Neurosci 7, 232-242

Francis SH, Sekhar KR, Ke H, Corbin JD (2011) Inhibition of cyclic nucleotide phosphodiesterases by methylxanthines and related compounds. Handb Exp Pharmacol, 93-133

Fredholm BB, Bättig K, Holmén J, Nehlig A, Zvartau EE (1999) Actions of caffeine in the brain with special reference to factors that contribute to its widespread use. Pharmacol Rev 51, 83-133

Funk GD, Parkis MA (2002) High frequency oscillations in respiratory networks: functionally significant or phenomenological? Respir Physiol Neurobiol 131, 101-120

Guerreiro S, Marien M, Michel PP. Methylxanthines and ryanodine receptor channels (2011) Handb Exp Pharmacol. 200, 135-150

Greer JJ, Ren J (2009) Ampakine therapy to counter fentanyl-induced respiratory depression. Respir Physiol Neurobiol 168, 153-157

Harinath S, Sikdar SK (2005) Inhibition of human TREK-1 channels by caffeine and theophylline. Epilepsy Res 64, 127-135

Henderson-Smart DJ, De Paoli AG (2010) Methylxanthine treatment for apnoea in preterm infants. Cochrane Database Syst Rev 12, CD000140

Herlenius E, Adén U, Tang LQ, Lagercrantz H (2002) Perinatal respiratory control and its modulation by adenosine and caffeine in the rat. Pediatr Res 51, 4-12

Huxtable AG, Zwicker JD, Poon BY, Pagliardini S, Vrouwe SQ, Greer JJ, Funk GD (2009) Tripartite purinergic modulation of central respiratory networks during perinatal development: the influence of ATP, ectonucleotidases, and ATP metabolites. J Neurosci 29, 14713-14725

Iyadurai SJ, Chung SS (2007) New-onset seizures in adults: possible association with consumption of popular energy drinks. Epilepsy Behav. 10, 504-508

Jefferys JG (1994) Experimental neurobiology of epilepsies. Curr Opin Neurol 7, 113-122

Kantor C, Panaitescu B, Kuribayashi J, Ruangkittisakul A, Lee TF, Cheung PY, MacTavish D, Jhamandas J, Ballanyi K (2012) Electrophysiological imaging of early network oscillations in brain slices from newborn rats and piglets. In Isolated Central Nervous System Circuits (Ed K Ballanyi), Neuromethods Series Vol 73 (Ed W Walz). Springer Science+Business Media, LLC, New York, NY, 315-356

Kilb W, Sinning A, Luhmann HJ (2007) Model-specific effects of bumetanide on epileptiform activity in the in-vitro intact hippocampus of the newborn mouse. Neuropharmacology 53, 524-533

Leaming JM, Terndrup TE, Ognibene S (1999) Glottal patency during experimental cortical seizures in piglets. Acad Emerg Med 6, 682-687

Lieske SP, Thoby-Brisson M, Telgkamp P, Ramirez JM. (2000) Reconfiguration of the neural network controlling multiple breathing patterns: eupnea, sighs and gasps. Nat Neurosci 3, 600-607

Magkos F, Kavouras SA (2005) Caffeine use in sports, pharmacokinetics in man, and cellular mechanisms of action. Crit Rev Food Sci Nutr 45, 535-562

Mathew OP (2011) Apnea of prematurity: pathogenesis and management strategies. J Perinatol 31, 302-310

Montandon G, Kinkead R, Bairam A (2008) Adenosinergic modulation of respiratory activity: developmental plasticity induced by perinatal caffeine administration. Resp Physiol Neurobiol 164, 87-95

Mortelmans LJ, Van Loo M, De Cauwer HG, Merlevede K (2008) Seizures and hyponatremia after excessive intake of diet coke. Eur J Emerg Med 15, 51

Navelet Y, Wood C, Robieux I, Tardieu M (1989) Seizures presenting as apnoea. Arch Dis Child 64, 357-359

Paydarfar D, Eldridge FL, Scott SC, Dowell RT, Wagner PG (1991) Respiratory responses to focal and generalized seizures in cats. Am J Physiol 260, R934-R940

Ren J, Poon BY, Tang Y, Funk GD, Greer JJ (2006) Ampakines alleviate respiratory depression in rats. Am J Respir Crit Care Med. 174, 1384-1391

Richter DW, Lalley PM, Pierrefiche O, Haji A, Bischoff AM, Wilken B, Hanefeld F (1997) Intracellular signal pathways controlling respiratory neurons. Respir Physiol 110, 113-123

Rottier BL, Duiverman EJ (2009) Anti-inflammatory drug therapy in asthma Paediatr Respir Rev 10, 214-219

Ruangkittisakul A, Ballanyi K (2010) Methylxanthine reversal of opioid-evoked inspiratory depression via phosphodiesterase-4 blockade. Resp Physiol Neurobiol 172, 94-105

Ruangkittisakul A., Schwarzacher SW, Ma Y, Poon B, Secchia L, Funk GD, Ballanyi K (2006) High sensitivity to neuromodulator-activated signalling pathways at physiological [K^+] of confocally-imaged respiratory centre neurons in online-calibrated newborn rat brainstem slices. J Neurosci 26, 11870-11880

Ruangkittisakul A, Secchia L, Bornes TD, Palathinkal DM, Ballanyi K (2007) Dependence on extracellular Ca^{2+}/K^+ antagonism of inspiratory centre rhythms in slices and en bloc preparations of newborn rat brainstem. J Physiol 584, 489-508

Ruangkittisakul A, Schwarzacher SW, Secchia L, Ma Y, Bobocea N, Poon BY, Funk GD, Ballanyi K (2008) Generation of eupnea and sighs by a spatiochemically organized inspiratory network. J Neurosci 28, 2447-2458

Ruangkittisakul A, Panaitescu B, Kuribayashi J, Ballanyi K (2010) Caffeine reversal of opioid-evoked and endogenous inspiratory depression in perinatal rat en bloc medullas and slices. Adv Exp Med Biol 669, 123-127

Sawynok J (1995) Pharmacological rationale for the clinical use of caffeine. Drugs 49, 37-50

Schmidt C, Bellingham MC, Richter DW (1995) Adenosinergic modulation of respiratory neurones and hypoxic responses in the anaesthetized cat. J Physiol 483, 769-781

Smith JC, Ellenberger HH, Ballanyi K, Richter DW, Feldman JL (1991) Pre-Bötzinger complex: a brainstem region that may generate respiratory rhythm in mammals. Science 254, 726-729

Smith JC, Ballanyi K, Richter DW (1992) Whole-cell patch-clamp recordings from respiratory neurons in neonatal rat brainstem in vitro. Neurosci Lett 134, 153-156

Stavric B (1988) Methylxanthines: toxicity to humans. 2. Caffeine. Food Chem Toxicol 26, 645-662

St-John WM, Rudkin AH, Homes GL, Leiter JC (2006) Changes in respiratory-modulated neural activities, consistent with obstructive and central apnea, during fictive seizures in an in situ anaesthetized rat preparation. Epilepsy Res ;70, 218-228

Surges R, Thijs RD, Tan HL, Sander JW (2009) Sudden unexpected death in epilepsy: risk factors and potential pathomechanisms. Nat Rev Neurol 5, 492-504

Terndrup TE, Knuth SL, Gdovin MJ, Darnall R, Bartlett D Jr (1996) Respiratory motor nerve activities during experimental seizures in cats. J Appl Physiol 80, 924-930

Terndrup TE, Darnall R, Knuth SL, Bartlett D Jr (1999) Effects of experimental cortical seizures on respiratory motor nerve activities in piglets. J Appl Physiol 86, 2052-2058

Uneyama H, Harata N, Akaike N (1993) Caffeine and related compounds block inhibitory amino acid-gated Cl- currents in freshly dissociated rat hippocampal neurones. Br J Pharmacol 109, 459-465

Wessberg P, Hedner J, Hedner T, Persson B, Jonason J (1984) Adenosine mechanisms in the regulation of breathing in the rat. Eur J Pharmacol 106, 59-67

Wilken B, Ramirez JM, Hanefeld F, Richter DW (2000) Aminophylline modulation of the mouse respiratory network changes during postnatal maturation. J Appl Physiol 89, 2015-2022

Zwicker JD, Rajani V, Hahn LB, Funk GD (2011) Purinergic modulation of preBötzinger complex inspiratory rhythm in rodents: the interaction between ATP and adenosine. J Physiol 589, 4583-4600

Chapter 6

Methylxanthine countering of opioid-evoked depression of spontaneous *locus coeruleus* network oscillations in newborn rat brain slices

Bogdan A. Panaitescu, Klaus Ballanyi

Department of Physiology, 750 MSB, University of Alberta, Edmonton, Canada

I performed all the experiments, analyzed them and wrote the manuscript together with Dr. Klaus Ballanyi.

6.1 Introduction

Caffeine and theophylline effectively counter apnea of prematurity (Martin & Abu-Shaweesh, 2005; Bancalari, 2006; Schmidt et al., 2007). These methylxanthines exert this stimulatory effect on breathing in (preterm) infants at plasma levels of 50-400 μM which are sufficient to block adenosine receptors (Lee et al., 1996; Fredholm et al., 1999; Leon et al., 2007; Charles et al., 2008). This led to the view that methylxanthines depress tonic inhibitory actions of adenosine on lower brainstem respiratory networks, among which the preBötzinger complex (preBötC) is pivotal for normal breathing (Eldridge et al., 1985; Herlenius et al., 2002; Feldman & Del Negro, 2006; Montandon et al., 2008; Zwicker et al., 2011; Huxtable et al., 2009, 2010). Our findings using *in vitro* brainstem models from newborn rats suggest that this scenario is more complex. Firstly, inspiratory-related bursting of the isolated preBötC was not inhibited by adenosine and low millimolar methylxanthine doses were necessary for reversing opioid-induced '*in vitro* apnea' (Ruangkittisakul & Ballanyi, 2010). Secondly, low millimolar methylxanthine was also needed for stimulating endogenously depressed preBötC rhythm in fetal rat brainstems (Ballanyi, 2004; Ruangkittisakul et al., 2010). Based on this dose dependence and a similar excitatory effect of the selective inhibitor rolipram on preBötC bursting, we proposed that methylxanthines can also enhance breathing via blockade of phosphodiesterase-4. Specifically, we hypothesized that this inhibition raises cyclic adenosine monophosphate (cAMP) in preBötC neurons whose rhythmic bursting seems to depend critically on this second-messenger (Ballanyi et al.,

1997, 1999; Richter et al., 1997). Besides respiratory networks, neural circuits in the neocortex and hippocampus are spontaneously active in newborns (Garaschuk et al., 2000; Ben-Ari et al., 2007; Sipilä & Kaila, 2008). Our findings in newborn rat brain slices indicated that low millimolar methylxanthine perturbs rhythmic bursting in these cortical areas by seizure-like discharges (Kantor et al., 2012) and that such hyperexcitability occurs also in inspiratory motor networks of newborn rat spinal cords (Ruangkittisakul et al., 2010) (Chapter **5**) **(Fig. 5-2)**. These results relate to the clinical observation that methylxanthines can evoke seizures in infants during treatment of bronchospasm and also in normal adults, e.g. upon consumption of energy drinks (Kaufman & Sachdeo, 2003; Iyadurai & Chung, 2007; Yoshikawa, 2007; Korematsu et al., 2008; Boison, 2011).

It was the aim of this study to investigate whether methylxanthines also hamper spontaneous activity, and thus eventually the maturation, of other nervous structures during the neonatal period. For this, we investigated the *locus coeruleus* (LC) in the dorsal pons. The LC is not fully functional in newborns and regulates in adults multiple nervous functions including arousal, attention, stress, locomotion, pain and is also involved in opioid dependence and withdrawal (Berridge & Waterhouse, 2003; Samuels & Szabadi, 2008a,b). Using newborn rat brain slices in which LC neurons show synchronized bursting (Christie et al., 1989; Oyamada et al., 1998; Maubecin & Williams, 1999), we firstly determined dose-response relationships for methylxanthine effects. We investigated next whether they reverse opioid-induced inhibition of neuronal activity which is due

to postsynaptic hyperpolarization mediated by G protein-coupled inward-rectifying K^+ channels (Williams et al., 1982; Alreja & Aghajanian, 1993). For these analyses, we combined novel suction electrode-based field potential recording at the LC edge with 'blind' whole-cell recording from single neurons in the same LC aspect. Moreover, we performed for the first time Ca^{2+} imaging in the LC to determine in both neurons and astrocytes effects of methylxanthines and opioids on this important cellular second-messenger.

6.2 Methods

(see Chapter **2**)

6.3 Results

Newborn rat brain slices were used to study how synchronized population bursting and underlying neuronal membrane potential oscillations in the LC are affected by theophylline and caffeine and whether these methylxanthines are capable of countering opioid inhibition of these activities. These electrophysiological analyses were complemented by multiphoton imaging of methylxanthine and opioid actions on cytosolic Ca^{2+} in LC neurons and adjacent astrocytes.

6.3.1 Electrophysiological Properties of LC Population and Neuronal Activities

Each aspect of the bilaterally-organized neonatal rodent LC spans 200-400 µm in all dimensions (Ballantyne et al., 2004). Accordingly, per animal typically only one horizontal 400 µm thick slice was obtained and directly transferred to a submerged-type experimental chamber **(Fig. 1-11)**. LC population bursting was immediately evident after activating the superfusion system. But, signal amplitude reached steady-state only within 0.5-1 h after start of recording (Kantor et al., 2012) **(Fig. 6-1A$_1$)**. In a complete slice, typically both LC aspects showed regular bursting of uniform amplitude while in ~10% of cases activity in one aspect was less pronounced and/or regular **(Fig. 6-1A$_1$)**. Bilateral LC bursting was not synchronous in twenty-five slices tested indicating lack of coupling between both LC aspects in this *in vitro* model **(Fig. 6-1A$_2$)**. Burst rates and single burst durations, respectively, ranged between 0.5-3 Hz and 0.2-0.5 s (means: 101.3 ± 12.3 bursts/min and 0.33 ± 0.05 s, n= 7). The longevity of LC population bursting was not determined here, but robust regular rhythm persists certainly for >5 h.

According to previous *in vitro* reports, rhythmically bursting 'type-1' and 'type-2' neurons showing tonic action potential discharge are spontaneously active in the isolated newborn rodent LC (Oyamada et al., 1998; Christie et al., 1989; Ballantyne et al., 2004). In an initial approach, we combined suction electrode recording from the edge of one LC aspect with whole-cell recording from adjacent neurons. This test aimed at determining phase relationships of type-1 neurons with LC population bursting as well as their relative numbers. If a major population of tonic type-2 neurons was active in the LC, this would likely raise

the baseline of the integrated suction electrode signal. Consequently, the signal-to-noise ratio of extracellular rhythmic bursting of type-1 neurons would be lowered similar to the scenario in the isolated newborn rat preBötC (Panaitescu et al., 2009; Ballanyi & Ruangkittisakul, 2009). Indeed, administration of agents that inhibited LC bursting, resulted in >50% of cases in a modest decrease in the integrated signal trace indicating a contribution of tonic neurons to the extracellular field potential.

While advancing the patch electrode for tracking for neurons, LC population bursting was notably perturbed as indication of a tight coupling between (single) cellular and network bursting **(Fig. 6-1B)**. Consecutive whole-cell recording for at least 5 min indicated that type-1 neurons notably outnumber type-2 cells. In the example of **Fig. 6-2A**, recordings were obtained from five type-1 neurons, but no type-2 cells. Type-1 neurons showed periodic membrane potential depolarizations by 5-10 mV that gave rise to bursts of 1-5 action potentials. These 'spike trains' occurred mostly during LC population bursting, but in ~30% of cases also slightly before onset of the field potential representing the summated activity of groups of LC neurons **(Fig. 6-2)**. In total, stable whole-cell recordings were obtained from twenty type-1 and six type-2 neurons.

Hyperpolarizing type-1 neurons via current injection through the patch electrode revealed subthreshold membrane potential oscillations that were in phase with LC population bursting **(Fig. 6-2B)**. In contrast, current-evoked depolarization

increased the number of non-phasic action potentials which could more or less mask their rhythmic bursting **(Fig. 6-2B)**. In some cases, depolarization-evoked tonic spiking in type-1 neurons resembled that in type-2 neurons at resting potential **(Fig. 6-2C)**. But, hyperpolarizing type-2 neurons via current injection did not reveal rhythmic subthreshold depolarizations typical for type-1 cells instead of decreasing the rate of tonic discharge until spiking stopped at membrane potential values of about -50 mV. Mean resting potentials and input resistances for 20 type-1 and 6 type-2 neurons were similar (-42.9 ± 2.2 *versus* -45.0 ± 3.0 mV). Input resistance in these type-1 neurons was slightly lower than that in type-2 cells, specifically 214.3 ± 61.6 *versus* 293.0 ± 84.0 MΩ ($P< 0.05$). There was no apparent difference between these neuron types regarding action potential amplitude (46.0 ± 15.1 *versus* 48.8 ± 8.5 mV) and access resistance (49.8 ± 10.5 *versus* 45.9 ± 8.6 MΩ) as determined within 5-10 min after establishing whole-cell recording.

Labeling of these neurons with lucifer-yellow (0.5%) via the patch electrode unraveled their morphology using fluorescence microscopy in chemically-fixed slices (Chapter **2.5**). Because multiple neurons were recorded per slice, their morphology could not be attributed to an individual cell with a specific activity pattern. However, basic morphological features of both cell types appeared to be similar, i.e. 2-6 primary dendrites originated from a round soma of 20-35 µm diameter **(Fig. 6-3A)**. In a different fluorescence imaging approach for visualizing cell types in the LC, aiming at discriminating neurons from astrocytic glia, we

incubated fresh slices with the morphological red fluorescent dye sulforhodamine-101 (SR-101) (Kjaerulff et al., 1994; Kafitz et al., 2008; Nimmerjahn et al., 2004). In our recent study on active neural networks in hippocampus and entorhinal cortex of newborn rat brain slices, we found that either neurons or astrocytes are primarily labelled with SR-101 depending on the incubation protocol (Kantor et al., 2012). Similar to that study, incubation of 4 hemislices for 1-1.5 h with 165 μM SR-101 at 20-23 ^{o}C revealed primarily morphological details of presumptive neurons including a 'rat's nest'-like connectivity **(Fig. 6-3B)**. However, also incubation of 5 different hemislices for 1 h in 1 μM SR-101 at 34 ^{o}C stained large cells **(Fig. 6-3C)** and not preferentially astrocytes as in cortical areas of neonatal rat slices (Kantor et al., 2012).

6.3.2 Methylxanthine Effects on LC Activities

In our previous studies on modulation of bursting in the isolated preBötC by methylxanthines, theophylline had a tendency to exert stronger effects than caffeine (Ruangkittisakul & Ballanyi, 2010; Ruangkittisakul et al., 2010). Accordingly, we initially assessed theophylline effects on LC population signals in the above seven slices that were rhythmically active at ~100 bursts/min **(Fig. 6-4)**. Initially, theophylline was bath-applied for 20 min at 0.25 mM which is sufficient to block adenosine receptors (Fredholm et al., 1999). The rate of LC bursting increased to 118.8% of control at this dose, but this effect became significant only at 0.5 mM theophylline (136.5% of control) **(Fig. 6-4)**. LC

rhythm accelerated further upon subsequent exposure to 1 mM theophylline and was by 169.4% faster than in control during 2.5 mM. At 5 and 10 mM theophylline, burst rate did not increase further, but discharge pattern transformed due to occurrence of 0.5-2 s periods of arrest of bursting at time intervals of 2-5 s, while single burst amplitude decreased in four of six slices **(Fig. 6-4)**. Within 10-20 min after start of washout of 10 mM theophylline, both the rate and amplitude of LC population bursting recovered to control values and silent periods disappeared **(Fig. 6-4A)**. In response to subsequent bath-application of 10 mM caffeine, burst rate increased again to values similar to those in 10 mM theophylline, pauses reoccurred and burst amplitude decreased in 15 slices tested **(Fig. 6-4)**.

In a further series of experiments, slices were initially exposed to 10 mM theophylline followed by washout and subsequent reapplication at increasing doses starting again at 0.25 mM. This comparison aimed at elucidating whether stepwise elevation of the theophylline dose in the previous experiments eventually desensitized LC networks as explanation for lack of seizure-like bursting at low millimolar doses. However, also initial application of 10 mM theophylline did not evoke hyperexcitability instead of accelerating burst rate and inducing silent periods. As summarized in **Figs. 6-4C_1, C_2**, stimulation of burst rate was similar, but slightly less pronounced than in the initial series of experiments. In both cases, there was also a non-significant trend for a decrease in burst amplitude in response to millimolar theophylline **(Fig. 6-4C_1, C_2)**. Simultaneous intracellular

and extracellular recording in five type-1 and two type-2 neurons showed that the transformation of population burst pattern upon bath-application of 10 mM theophylline was not accompanied by a change in resting potential (-42.1 ± 2.7 *versus* -44.3 ± 2.4 mV) or input resistance (219.9 ± 51.6 *versus* 267.1 ± 66.6 MΩ).

6.3.3 Effects of Blockers of Fast Synaptic Inhibition on LC Activities

Millimolar methylxanthine blocks A-type γ-aminobutyric acid ($GABA_A$) receptors (Lopez et al., 1989; Fredholm et al., 1999; Uneyama et al., 1993; Shi et al., 2003). Accordingly, we hypothesized that this effect may contribute to seizure-like bursting in newborn rat hippocampal and cortical circuits (Kantor et al., 2012) plus spinal motor networks (Ruangkittisakul et al., 2010) (Chapter **5**) **(Fig. 5-2)**. Thus, we studied next whether seizure-like LC bursting is evoked by inhibition of $GABA_A$ or glycine receptors that are coupled to similar anion channels. In six slices, bath-application of the $GABA_A$ receptor blocker bicuculline (25 μM) did not affect the rate of LC rhythm, but increased burst amplitude **(Fig. 6-5A**,**B)**. The same results were obtained upon addition of the glycine receptor blocker strychnine (5 μM) to the bicuculline-containing superfusate **(Fig. 6-5A**,**B)**. Nevertheless, both receptors are functional because the $GABA_A$ receptor agonist muscimol (2.5 μM) abolished LC bursting in six slices and bicuculline countered this inhibition while subsequent bath-application of

glycine blocked rhythm in bicuculline-containing solution and this inhibition was reversed by strychnine **(Fig. 6-5C**,**D)**.

6.3.4 Methylxanthine Reversal of Opioid Depression of LC bursting

It was analyzed next whether methylxanthines reverse depressing opioid effects on LC bursting (Nestler et al., 1999; Williams et al., 1982, 2001; Alreja & Aghajanian, 1993). In seven slices, bath-application of 10 nM of the μ-opioid receptor agonist [D-Ala^2,N-Me-Phe^4,Gly^5-ol]-enkephalin (DAMGO) slowed LC oscillations within <5 min by ~25% **(Fig. 6-6A**,**B)**. Subsequent application of 25 nM DAMGO changed burst pattern from regular single peak events to groups of bursts that were interrupted by a pause of 0.75-3 s duration **(Fig. 6-6A**,**B)**. In five of these slices, burst interval and single burst duration appeared to increase in 50 nM DAMGO and bursts with several peaks occurred. In the other two slices, such multipeak bursting was blocked to unravel small amplitude 'spikes' of <100 ms single event duration. Spike discharge was also seen in five slices during 100 nM DAMGO, whereas all activities were abolished in the other two slices. Rhythm in the remaining five slices was abolished by 250 nM DAMGO **(Fig. 6-6A**,**B)**. Within 6-7 min after start of application in 250 nM DAMGO, 0.5 mM theophylline restored spike discharge in six slices **(Fig. 6-6A)**, whereas multipeak rhythm was reactivated in the remaining slice. Theophylline restored the latter type of bursting in all slices at 1 mM, whereas 2.5-10 mM reactivated fast LC oscillations in all cases. These oscillations looked very similar to control bursts,

except for occurrence of silent periods in five slices during 10 mM theophylline **(Fig. 6-6A**,**B)**. Recovery of fast bursting after blockade by 250 nM DAMGO was significant for 2.5, 5 and 10 mM theophylline, although burst rate remained below control values for these three doses contrary to full recovery of burst amplitude **(Fig. 6-6B**,**C)**.

6.3.5 Effects of cAMP, and Blockers of Adenosine or $GABA_A$ Receptors on Opioid-Depressed LC Rhythm

We hypothesized that methylxanthine-evoked elevation of cellular cAMP levels due to blockade of phosphodiesterase-4 is responsible for the antagonizing methylxanthine effect on opioid inhibition of bursting of the isolated preBötC (Ruangkittisakul & Ballanyi, 2010; Ruangkittisakul et al., 2010). To investigate involvement of this mechanism in similar reversal of opioid inhibition in LC networks by methylxanthines, the selective phosphodiesterase-4 blocker rolipram (O'Donnell & Zhang, 2004) was bath-applied after LC rhythm had been abolished within <5 min by 250 nM DAMGO. Because rolipram (5 μM) did not restore DAMGO-depressed LC rhythm in five slices **(Fig. 6-7A)**, we tested effects of two other cAMP-elevating agents, specifically forskolin (50 μM) and isobutylmethylxanthine (100 μM). In two of six slices, forskolin reactivated bursting, but at rates that were notably lower than in control and also isobutylmethylxanthine restored some bursts in four of five slices **(Fig. 6-7B)**. Adding forskolin to isobutylmethylxanthine-containing solution, or application of

the agents in reverse order, reactivated modest slow and/or low amplitude bursting rhythm in further five slices **(Fig. 6-7B)** whereas this was ineffective in four of thirteen slices. Next, the antagonists 8-cyclopentyl-1,3-dipropylxanthine (2 μM, DPCPX) and 3,7-dimethyl-1-propargyl-xanthine (10 μM, DMPX) were used to investigate whether blockade of A_1 or A_{2A} adenosine receptors, respectively, contributes to methylxanthine countering of opioid depression of LC bursting. However, neither application of each agent to eight slices nor combined use in ten cases restored LC rhythm in DAMGO **(Fig. 6-7C)**. At the end of most of experiments, 5-10 mM caffeine or theophylline was applied, which reactivated robust LC bursting in DAMGO **(Fig. 6-7A**,**C)**.

6.3.6 Methylxanthine Reversal of $GABA_A$- and DAMGO-Mediated Hyperpolarizations

Next, it was tested whether a blocking methylxanthine effect on $GABA_A$ receptors (Lopez et al., 1989; Fredholm et al., 1999; Uneyama et al., 1993; Shi et al., 2003) is involved in their countering action on DAMGO-depressed LC rhythm. In eight slices, bicuculline (25 μM) failed to reverse arrest of LC rhythm by 250 nM DAMGO, whereas subsequent application of 5-10 mM theophylline (n= 6) or caffeine (n= 2) was effective **(Fig. 6-8A)**. But, methylxanthines appear to antagonize effects of $GABA_A$ receptor activation in LC neurons because a muscimol-evoked hyperpolarization by >10 mV and a concomitant >50% fall of input resistance in five type-1 neurons were reversed by 10 mM theophylline

(Fig. 6-8B). Muscimol-depressed LC rhythm in these experiments was also restored by theophylline to rates higher than in control, specifically 151.8 ± 16.55 *versus* 91.3 ± 19.4 bursts/min ($P< 0.001$; paired t-test) **(Fig. 6-8B)**. Silencing of five different type-1 neurons and three type-2 cells by 250 nM DAMGO was associated with a mean hyperpolarization from -44.2 ± 2.5 to -62.0 ± 5.0 mV and an apparent, but non-significant, ~15% fall of input resistance **(Fig. 6-9A**,**B)**. Theophylline (10 mM) in DAMGO recovered membrane potential to control values -43.0 ± 2.8 mV in conjunction with a trend for reincreasing input resistance **(Fig. 6-9A**,**B)**. Theophylline washout restored the DAMGO-evoked hyperpolarization (-51.4 ± 4.9 mV), which was then reversed in four neurons tested to -43.9 ± 1.9 mV ($P< 0.05$, paired t-test) by the opioid receptor antagonist naloxone (1 μM) **(Fig. 6-9A)**. At 1 μM, DAMGO caused a similar hyperpolarization in four other type-1 and one type-2 neurons. This hyperpolarization was blocked by 10 mM theophylline, while the effect on input resistance showed the same trend as in lower DAMGO **(Fig. 6-9C)**.

6.3.7 Methylxanthine and Opioid Actions on Cellular Ca^{2+} in LC

Injection of the green fluorescent Ca^{2+} dye Fluo-4 (0.5 mM, 50 mmHg, 10 min) (Chapter **2.5**) into the LC of 24 slices, respectively, resulted in labeling of both neurons and astrocytes **(Fig. 6-10)**. As shown above **(Fig. 6-3B)**, incubation of LC slices with the morphological dye SR-101 did not enable discrimination between both cell types. For this, effects of adenosine triphosphate (100 μM, 2 min) and the metabotropic glutamate receptor agonist 1-aminocyclopentane-trans-1,3-

dicarboxylic acid (25 μM, 2 min) were analyzed. This is based on our previous observations that these agents caused a notable Ca^{2+} rise in presumptive preBötC and cortical astrocytes of newborn rat slices (Ruangkittisakul et al., 2006, 2009, 2012; Ballanyi et al., 2010; Kantor et al., 2012). In four slices, 80% of 237 cells with a soma diameter of 5-15 μm responded with a prominent Ca^{2+} rise to both agents whereas 75 cells with a soma diameter >20 μm, similar to those in whole-cell-recorded LC neurons **(Fig. 6-3)** showed a notably smaller response **(Fig. 6-10)**. In contrast, both 233 small and 111 large cells in four slices responded with a robust Ca^{2+} rise to bath-applied glutamate (0.5 mM, 30 s) **(Fig. 6-10)**. In control solution, small amplitude fluctuations of Ca^{2+} baseline were seen in 95 large cells, presumptive neurons, in 19 of 21 slices, while synchronized oscillations in >4 neurons were seen in 14 of these slices. Contrary, Ca^{2+} baseline was unchanged in presumptive astrocytes, as analyzed in 120 small cells (20 slices).

Bath-application of methylxanthines in control solution evoked a Ca^{2+} rise in ~85 % of neurons. In thirty-five responding neurons of seven slices, theophylline (10 mM) increased Fluo-4 fluorescence intensity by (17.8 ± 17.4%, $P< 0.001$, paired t-test), whereas the response to caffeine (10 mM) was notably larger in 20 neurons in 4 slices (86 ± 28%, $P< 0.05$) **(Fig. 6-11)**. In fifty of fifty-five neurons in eleven slices, bath-application of either methylxanthine at 10 mM evoked (synchronous) Ca^{2+} rises. Upon bath-application of 25 or 50 nM DAMGO, fast LC oscillations transformed into slower and longer multipeak bursts **(**compare **Fig. 6-5)** that were accompanied by synchronized neuronal Ca^{2+} rises **(Fig. 6-11)**. While these low

DAMGO doses decreased neuronal Ca^{2+} baseline by ~10%, blockade of LC bursting at 250 nM lowered Ca^{2+} baseline by 16.0 ± 4.9% in thirty-five neurons of seven slices **(Figs. 6-11)**. In this situation, 10 mM theophylline restored LC rhythm and concomitant (synchronous) Ca^{2+} oscillation in >50% of neurons **(Fig. 6-12)**. Neither methylxanthine, DAMGO nor their combined application affected Ca^{2+} baseline in astrocytes as analyzed in 5-10 small cells of the same slices used for the analysis of the neuronal responses **(Figs. 6-11**, **6-12)**.

6.4 Discussion

Using simultaneous suction electrode and whole-cell recording, we report here for the first time spontaneous LC field potentials due to synchronized type-1 neuron bursting. Methylxanthines, the gold standard for treatment of apneas of prematurity, accelerated such synchronous LC rhythm at low millimolar doses without evoking seizure-like discharge and also countered depression of bursting by the μ-opioid DAMGO. Using Ca^{2+} imaging for the first time, we found that 25-50 nM DAMGO slowed rhythmic neuronal Ca^{2+} rises, while methylxanthines raised their Ca^{2+} in control and during countering of DAMGO-evoked arrest of LC bursting by 250 nM DAMGO. Neither methylxanthines nor DAMGO affected astrocytic Ca^{2+}, which increased more in these cells than in neurons in response to agents known to evoke glial Ca^{2+} signalling.

6.4.1 Modulation of LC Bursting by Methylxanthines

Previous studies established that newborn rodent LC neurons are spontaneously active *in vitro* (Williams & Marshall, 1987; Christie et al., 1989; Christie & Jelinek, 1993; Oyamada et al., 1998; Maubecin & Williams 1999; Ballantyne et al., 2004; Bennett & Zukin, 2004). Specifically, 'oscillatory' type-1 neurons show rhythmic bursting in contrast to tonic single spike discharge in type-2 neurons. Here, we revealed that synchronized type-1 neuron bursting generates a robust rhythmic field potential that is likely stable for >5 h. The incidence of whole-cell recordings suggests that type-1 neurons outnumber type-2 cells by a factor of ~3. The activity of type-2 neurons has a (minor) contribution to the LC field potential as evident from a modest drop of the baseline of the integrated electrode signal in response to inhibitory neuromodulators **(Fig. 6-7**, **6-8)**. Apart from lack of synchronicity of bursting in both LC aspects of the horizontal slices, the physical dimensions and bilateral anatomical organization of the LC, and its robust discharge of oscillatory neurons that likely cooperate with tonic neurons closely resemble features of the isolated preBötC inspiratory center (Feldman & Del Negro, 2006; Ballanyi & Ruangkittisakul, 2009). Moreover, both systems interact functionally because, on the one hand, bursting of LC neurons is modulated by phasic inputs from the preBötC (Oyamada et al., 1998; Ballantyne et al., 2004). On the other hand, the LC influences respiratory networks already at birth by producing norepinephrine, which seems to have a crucial role in the maturation and function of respiratory neurons (Viemari et al., 2004; Hilaire, 2006). In addition, the neonatal LC interact with the serotonergic system through dorsal

raphe or raphe magnus nuclei and might also indirectly regulate respiratory networks (Cedarbaum & Aghajanian, 1978; Peyron et al., 1996).

This mutual interaction between the pivotal inspiratory center and the LC and the fact that the LC influences multiple brain functions, some already during the early postnatal period, were major reasons for focusing on this network in the present study. Particularly, we wished to analyze whether methylxanthines, that are often applied for several weeks to (preterm) infants, hamper LC activity, which may have a negative influence on brain development (Hoecker et al., 2002; Kang et al., 2002; Desfrere et al., 2007; Black et al., 2008; Montadon et al., 2008). However, we found that methylxanthine effects on LC bursting occurred only at doses that are higher than those administered *in vivo* to reach therapeutic plasma levels of 50-400 µM (Chapter **1**) (Lee et al., 1996; Fredholm et al., 1999; Leon et al., 2007; Charles et al., 2008). In line with this, it was shown that systemic caffeine administration at doses of 1-70 mg/kg, corresponding to a plasma level of 2-100 µM, stimulates LC neurons as evidenced by c-Fos expression (Bennett & Semba, 1998; Deurveilher et al., 2006). Here, 0.5 mM theophylline was sufficient to accelerate LC rhythm, whereas 5-10 mM was needed to increase the rate of isolated preBötC bursting (Chapter **5**) **(Fig. 5-4)**. Both values are higher than <100 µM methylxanthine that is typically sufficient for blocking adenosine receptors (Ukena et al., 1993; Fredholm et al., 1999; Francis et al., 2011), suggesting that this concentration might be involved in countering a possible tonic inhibitory effect of adenosine on LC neurons (Shefner & Chiu, 1986).

As a further similarity with the preBötC, LC bursting was not perturbed by seizure-like discharge in response to low millimolar methylxanthine. This contrasts with ocurrence of large amplitude seizure-like discharges that occlude bursting of preBötC-driven of cranial hypoglossal and spinal inspiratory motor networks (Chapter **5**) **(Fig. 5-1)** and of hippocampal and entorhinal cortex networks (Kantor et al., 2012) in newborn rat *en bloc* models and brain slices, respectively. These observations and our present finding that also blockade of fast synaptic inhibition by bicuculline and/or strychnine does not hamper either type of bursting indicate that neither preBötC nor LC networks are capable of generating such excessive hyperexcitability. This view supports the previous view based on lack of excitatory bicuculline effects that local GABAergic and glycinergic interneurons are not capable of dampening potentially excessive activity of (glutamatergic) neurons in (neonatal *in vitro*) LC networks (Olpe et al., 1988). This is in contrast with a major role of such inhibitory interneurons in other brain regions including spinal (loco)motor networks, hippocampus, cortex or cerebellum (Jefferys, 1995; Brockhaus & Ballanyi, 1998; Huang et al., 2007; Gosgnach, 2011; Kullmann, 2011). As another example for similar pharmacological properties of preBötC and LC networks, 5-10 mM methylxantine evoked a trend for depressing single burst amplitude. Mechanisms for this depression and the above described frequency stimulation need to be analyzed in future studies. Glial Ca^{2+} signalling may not be involved because neither caffeine nor theophylline affected Ca^{2+} baseline in presumptive LC astrocytes.

6.4.2 Methylxanthine Reversal of Opioid-Evoked LC Depression

As a further similarity between preBötC and LC networks, the μ-opioid receptor agonist DAMGO abolished their rhythmic bursting. In physiological K^+, DAMGO already abolishes preBötC bursting at 25 nM, whereas this dose transforms LC bursting from fast oscillations into slower and longer-lasting multipeak events. According to our knowledge, this transformation of burst pattern has not been reported for *in vitro* LC models yet, while similar findings were obtained upon intracerebroventricular morphine injection *in vivo* (Zhu & Zhou, 2001). At 50-100 nM, DAMGO revealed small amplitude spike-like LC events that resemble non-respiratory small amplitude activities in preBötC slices (Figs. 1 and 2 in Ruangkittisakul & Ballanyi, 2010) (Chapter **4**) **(Fig. 4-10)**. A discussion of mechanisms for this transformation of LC bursting by opioids is beyond the scope of this study. Again in analogy with isolated preBötC properties, methylxanthines countered DAMGO-evoked depression of fast LC bursting at comparable similar low millimolar doses (compare **Fig. 6-6** with Figs 4 and 7 in Ruangkittisakul & Ballanyi, 2010). This dose-response relationship, in accordance with the finding that the specific blocker rolipram mimicked their effects, led to the conclusion in the latter study that countering methylxanthine effects on rhythmogenic inspiratory networks are due to raised cellular cAMP levels secondary to phosphodiesterase-4 blockade. This mechanism seems to play a minor role, if at all, for the antagonizing methylxanthine effects on opioid-evoked blockade of LC rhythm, because rolipram was not effective, while the

other cAMP-raising agents, forskolin and isobutylmethylxanthine, had inconsistent effects. A basic stimulatory effect of this class of neuromodulators on the excitability of LC neurons in slices led to the hypothesis that raised cAMP activates a nonspecific cation current (Alreja & Aghajanian, 1993, 1995; Wang & Aghajanian, 1987; Nestler et al., 1999). Also inhibition of adenosine receptors does not seem to be involved in countering of opioid depression of LC bursting by methylxanthine because the effect was not mimicked by A_1 and A_2 receptor blockers. An indirect effect via increasing network excitability due to blockade of $GABA_A$ receptors by methylxanthines (Lopez et al., 1989; Uneyama et al., 1993; Fredholm et al., 1999; Shi et al., 2003) is also unlikely because bicuculline did not reverse DAMGO-evoked blockade of LC rhythm. However, methylxanthines seem to be capable of blocking $GABA_A$ receptors in the LC because theophylline antagonized the notable mucimol-evoked neuronal hyperpolarization and input resistance decrease. While methylxanthines did not affect membrane potential and resistance in control solution, it cannot be excluded though that their countering effect on the muscimol inhibition is due to an excitatory effect on other conductances which becomes only evident at hyperpolarizations and concomitant resistance decreases in these cells.

Similarly, theophylline reversed the prominent DAMGO-evoked naloxone-sensitive hyperpolarization of LC neurons that is mediated by G protein-coupled inward-rectifying K^+ channels (Williams et al., 1982; Williams & Marshall, 1987; Alreja & Aghajanian, 1993; Travagli et al., 1995; Williams et al., 2001; Torecilla et al., 2002). While our results indicate that the antagonizing methylxanthine

effect on DAMGO-evoked depression of LC population bursting is caused by blockade of this hyperpolarization, the underlying cellular mechanism is not clear yet as outlined above. Despite intense research over the past decades, it is not clear yet whether opioid receptor activation in LC neurons involves inhibition of a cAMP-dependent Na^+-dependent conductance or is mostly due to activation of the metabolically regulated inward-rectifying K^+ channels (Wang & Aghajanian, 1987; Williams & Marshall, 1987; Alreja & Aghajanian, 1993, 1995; Nestler et al., 1999; Torecilla et al., 2002).

6.4.3 Imaging of Ca^{2+} Dynamics in LC neurons and Astrocytes

The majority of large LC cells, likely representing neurons, showed partly synchronized fluctuations of cytosolic Ca^{2+} at a rate corresponding to the lower range of rhythmic LC population and type-1 neuron bursting. This suggests that Ca^{2+} oscillations in faster bursting neurons cannot be resolved due to the slow Ca^{2+} binding/release properties of the Ca^{2+} dye Fluo-4, which would also explain the small amplitude of these fluctuations. Accordingly, more pronounced (synchronous) Ca^{2+} rises were seen when fast electrical neuronal oscillations transformed into slower and multipeak bursting in response to 25-50 nM DAMGO and during re-occurrence of such longer-lasting discharges in the initial phase of methylxanthine-evoked recovery of LC rhythm from blockade by DAMGO. The observed fall of neuronal Ca^{2+} baseline in response to DAMGO may partly be due to slowing of bursting which may attenuate a potentially steady

influx of Ca^{2+} via voltage-gated Ca^{2+} channels. This mechanism was revealed during pharmacological or metabolic blockade of tonic spiking in dorsal vagal neurons that have a low resting potential similar to LC neurons, i.e. -40 to -45 mV (Ballanyi & Kulik, 1998). In line with this assumption, recovery of DAMGO-depressed rhythm by methylxanthine was accompanied by a reincrease of Ca^{2+} baseline although this did not occur in all large cells. Reasons for these differences in neuronal behavior remain to be elucidated. This is also the case for the question, why subsets of neurons responded with a notable Ca^{2+} increase to application of 10 mM methylxanthines in control solution, whereas Ca^{2+} baseline did not change in other large cells. The Ca^{2+} rise in large cells in response to high methylxanthine indicates that neurons have Ca^{2+} stores that are typically depleted by this treatment (Fredholm et al., 1999; Blaustein & Golovina, 2001; Verkhratsky, 2005). However, neurons did not respond with a major Ca^{2+} increase to adenosine triphosphate or the metabotropic glutamate receptor agonist which both evoked a robust Ca^{2+} rise in the presumptive astrocytes that is likely store-mediated, as in presumptive astrocytes in the preBötC and cortex (Porter et al., 1997; Ruangkittisakul et al., 2009; Ballanyi et al., 2010; Kantor et al., 2012; Agulhon et al., 2008). In contrast, Ca^{2+} in these small cells was not affected either by (10 mM) methylxanthine or μ-opioid suggesting that glial Ca^{2+} signalling does not contribute to stimulation of LC rhythm by methylxanthines or its depression by opioids.

6.5 Figures and Legends

Fig. 6-1

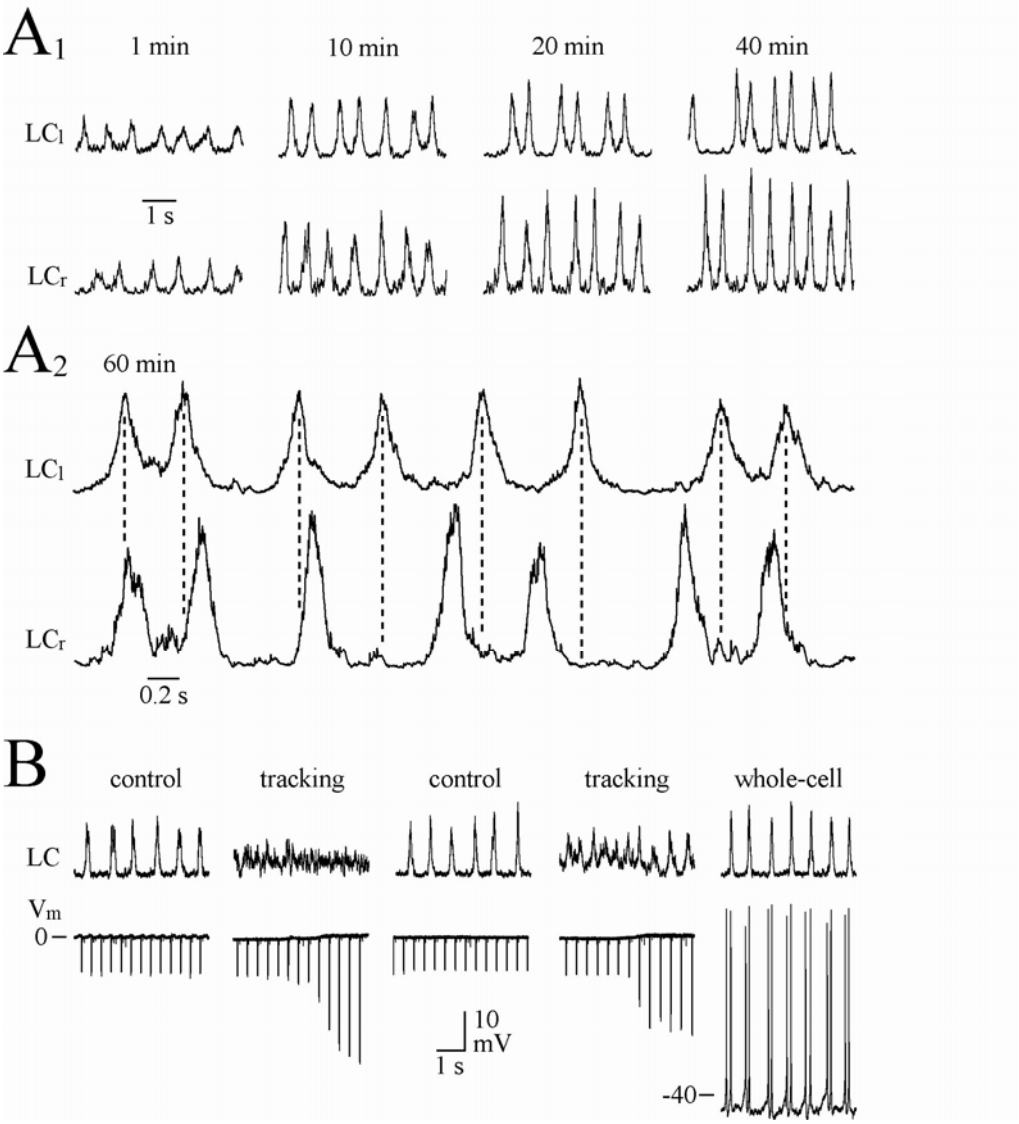

Fig. 6-1: Spontaneous activity in neural networks of the *locus coeruleus* (LC) in newborn rat brain slices. A, a 400 µm thick complete horizontal brain slice containing the bilaterally-organized LC is transferred immediately after cutting to a submerged-type acrylic recording chamber and mechanically fixed with a 'harp' or insect pins. Suction electrodes are positioned on the slice surface above or at the edge of one of the ~300 µm spanning LC aspects for recording spontaneous rhythmic extracellular activity that is differentially recorded, amplified (10k), bandpass-filtered (0.3-3 kHz) and integrated ('moving-average', τ: 20-100 ms). From the start of recording, burst amplitude increases until steady-state is reached after 30-60 min while burst rate (0.5-3 Hz) is stable right from the beginning (**A_1**).

In a total of 25 slices, bursting was not synchronous between the ipsi- and contralateral LC aspect (**A_2**). **B**, LC population bursting is sensitive to mechanical perturbation. This example shows that rhythm is depressed during positioning a patch electrode within the LC to obtain a gigaohm seal for 'blind' whole-cell membrane potential (V_m) recording, in this case from a rhythmically active 'type-1' cell (compare **Fig. 6-2**). This phenomenon indicates that LC neurons are tightly coupled (via gap-junctions).

Fig. 6-2

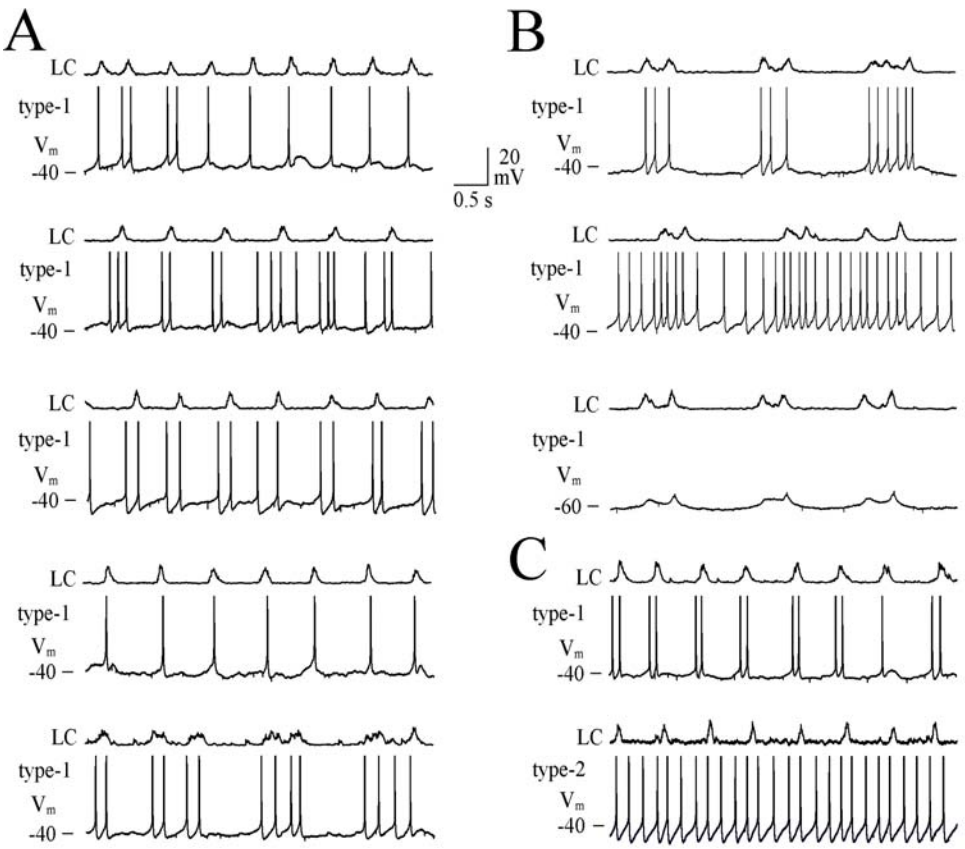

Fig. 6-2: Two types of spontaneously active LC neurons. A, whole-cell V_m recordings were consecutively performed in 5 different neurons within the same LC aspect of a single slice. These type-1 neurons were characterized by a similar resting V_m (about -40 mV) and (bursts of) spontaneous action potential discharge that was mostly in phase with LC population activity recorded from the edge of the same LC aspect. **B**, depolarization of a type-1 neuron in a different slice by <10 mV in response to current injection via the patch electrode transformed periodic phase-locked action potential discharge into 'tonic spiking', whereas subsequent hyperpolarization revealed phase-locked subtheshold V_m oscillations. **C**, in a different slice consecutive recordings were obtained from a type-1 neuron and a type-2 cell, the latter showing characteristic regular tonic spike discharge at resting V_m. Scale bars for V_m, time and cell size apply to all parts of the figure. The illustrated and further recordings (see Results section) indicate that type-1 neurons notably outnumber type-2 cells in neonatal rat LC.

Fig. 6-3

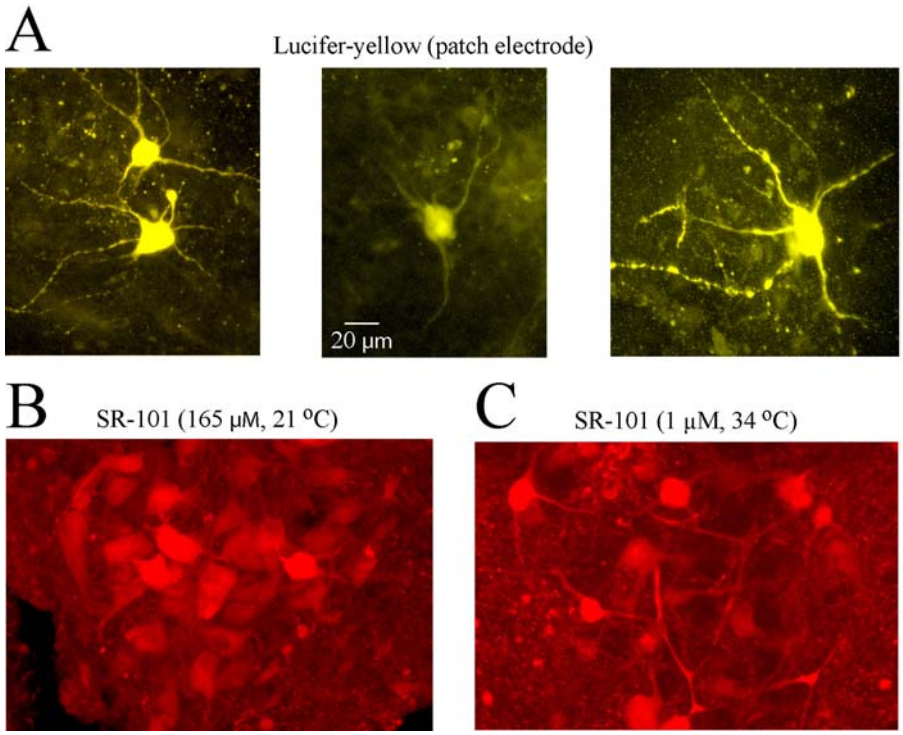

Fig. 6-3: Labeling of individual LC neurons with lucifer-yellow and groups of cells with sulforhodamine-101 (SR-101). Fluorescence imaging was done using a multiphoton system based on an Olympus FV300 laser-scanning confocal microscope connected to a Coherent infrared ti:sa laser system (Chapter **2**) **(Fig. 2-2)**. **A**, images in the left, middle and right part show the morphology of neurons in the slices from which V_m recordings were shown in **Fig. 6-2A**, **Fig. 6-2B** and **Fig. 6-2C**, respectively. Because several neurons were consecutively recorded in these slices, it is not clear which specific cell was successfully labeled. But, the morphology of all these cells is quite similar. **B**, incubation of a brainstem slice for 1 h with 165 µM of the membrane-permeant red fluorescent dye SR-101 at 22 ^{o}C primarily labeled large cells likely representing neurons and some smaller cells, likely astrocytes. Contrary to preferential labeling of astrocytes in hippocampus or cortex of newborn rat brain slices (Kantor et al., 2012), incubation of a different LC slice for 1 h with 1 µM SR-101 at 34 ^{o}C also labeled primarily neurons and not astrocytes. Both types of SR-101 labeling indicate that LC neurons are interconnected in 'rat's nest' fashion.

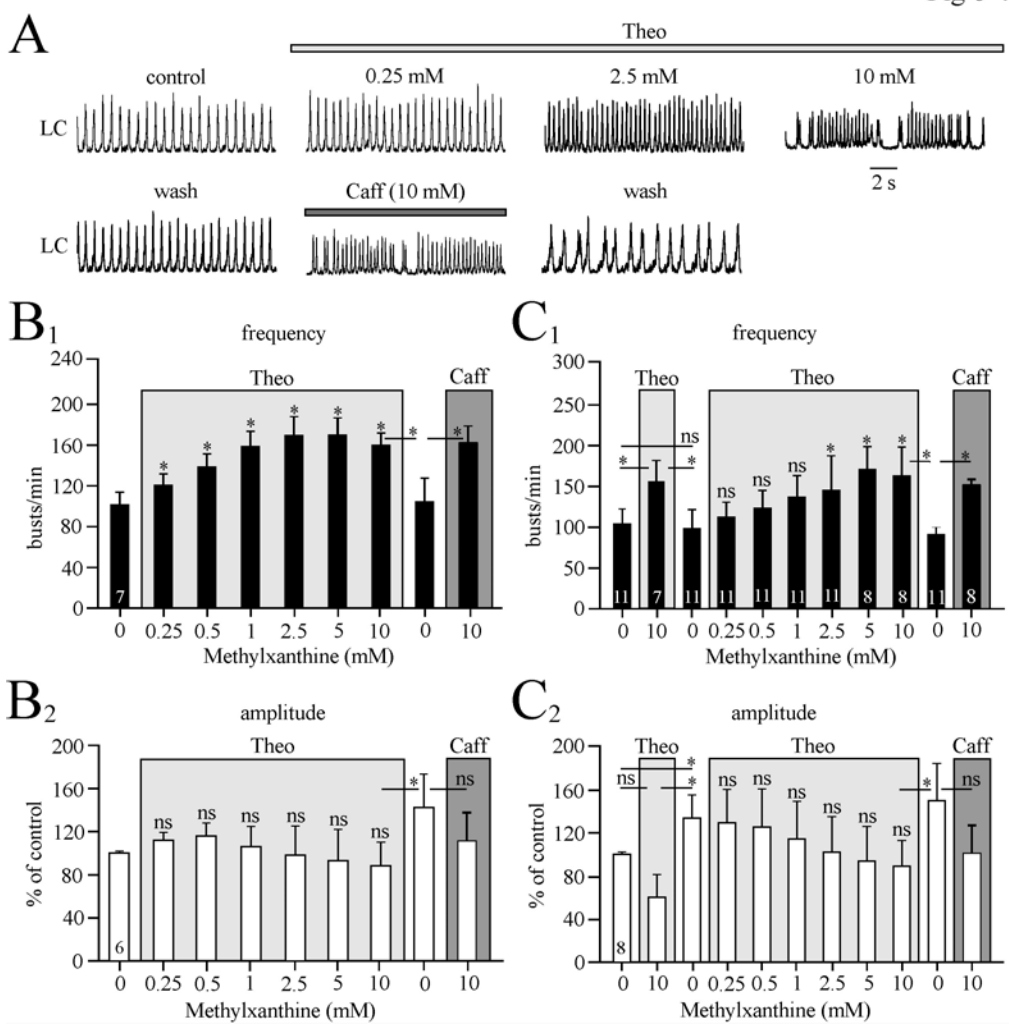

Fig. 6-4: Effects of the methylxanthines theophylline (Theo) and caffeine (Caff) on LC population bursting. A, a consecutive concentration increase in bath-applied Theo starting at 0.25 mM resulted in acceleration of the rate of regular LC oscillations. At 10 mM, Theo depressed the amplitude of LC bursting and transformed its pattern by causing pauses of activity for up to several seconds. After washout of Theo, 10 mM bath-applied Caff exerted a very similar effect on both LC burst rate and amplitude. Important for this study, even the high methylxathine doses did not evoke seizure-like bursting. **B**, statistical anlysis using one-way ANOVA revealed that the methylxanthine-evoked acceleration of rhythm is significant (*****: $P< 0.05$) (**B_1**) contrary to a non-significant attenuating effect on amplitude (**B_2**). Graphs in **C** summarize findings from a different group of experiments, in which firstly 10 mM Theo was applied to exclude that desensitization in other series may have occurred to explain lack of occurrence of seizure-like bursting. The findings were very similar including a trend for depression of LC burst amplitude by ≥2.5 mM methylxanthine. Numbers in bars correspond to numbers of slices tested.

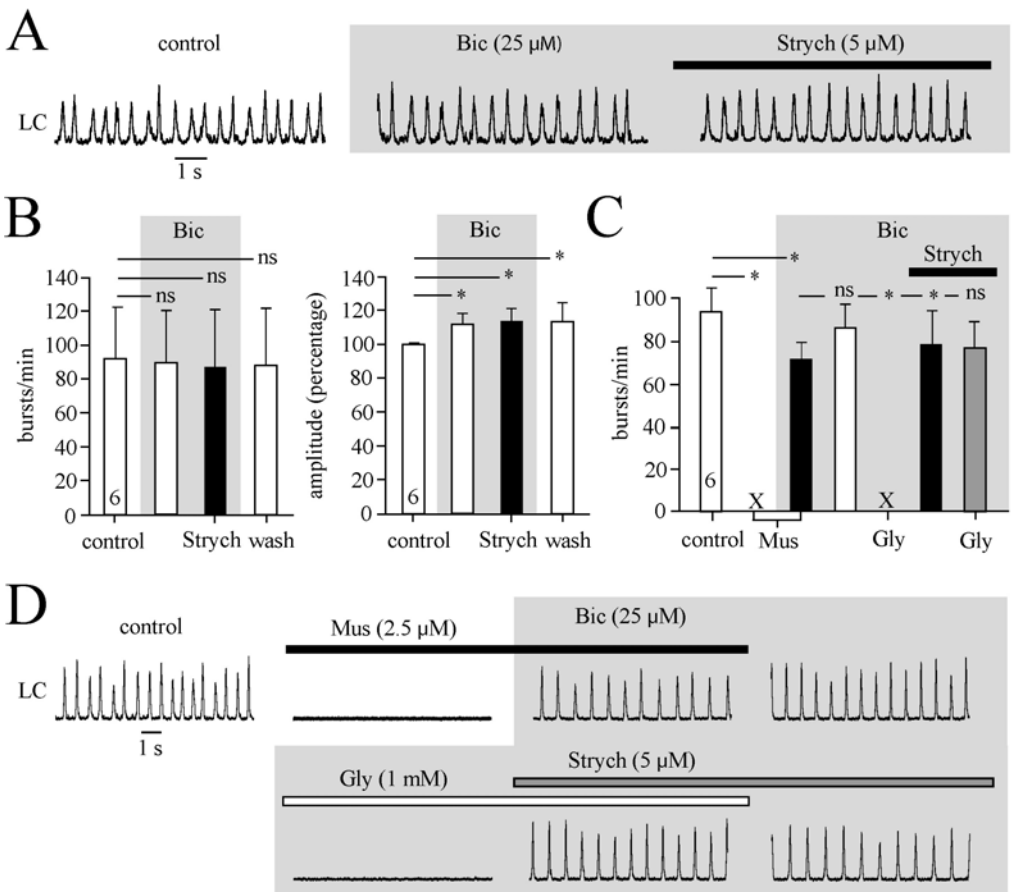

Fig. 6-5: Lack of seizure-like hyperexcitability in LC upon blockade of fast synaptic inhibition. A, bath-application of bicuculline (Bic), a blocker of A-type γ-aminobutyric acid ($GABA_A$) receptors had no effect on LC population bursting and even addition of the glycine (Gly) receptor blocker strychnine (Strych) did not perturb rhythm. **B**, statistical analysis (one-way ANOVA) of effects of Bic and Strych on the rate and amplitude of LC population bursting. **C**, summary (one-way ANOVA) of a series of experiments exemplified in **D** showing that the neonatal rat LC has functional $GABA_A$ and glycine receptors. Specifically, the $GABA_A$ receptor agonist muscimol (Mus, 2.5 µM) abolished LC rhythm which was restored by adding Bic to Mus-containing solution. Subsequent bath-application of Gly (1 mM) in Bic-containing solution abolished rhythm which was reactivated by Strych.

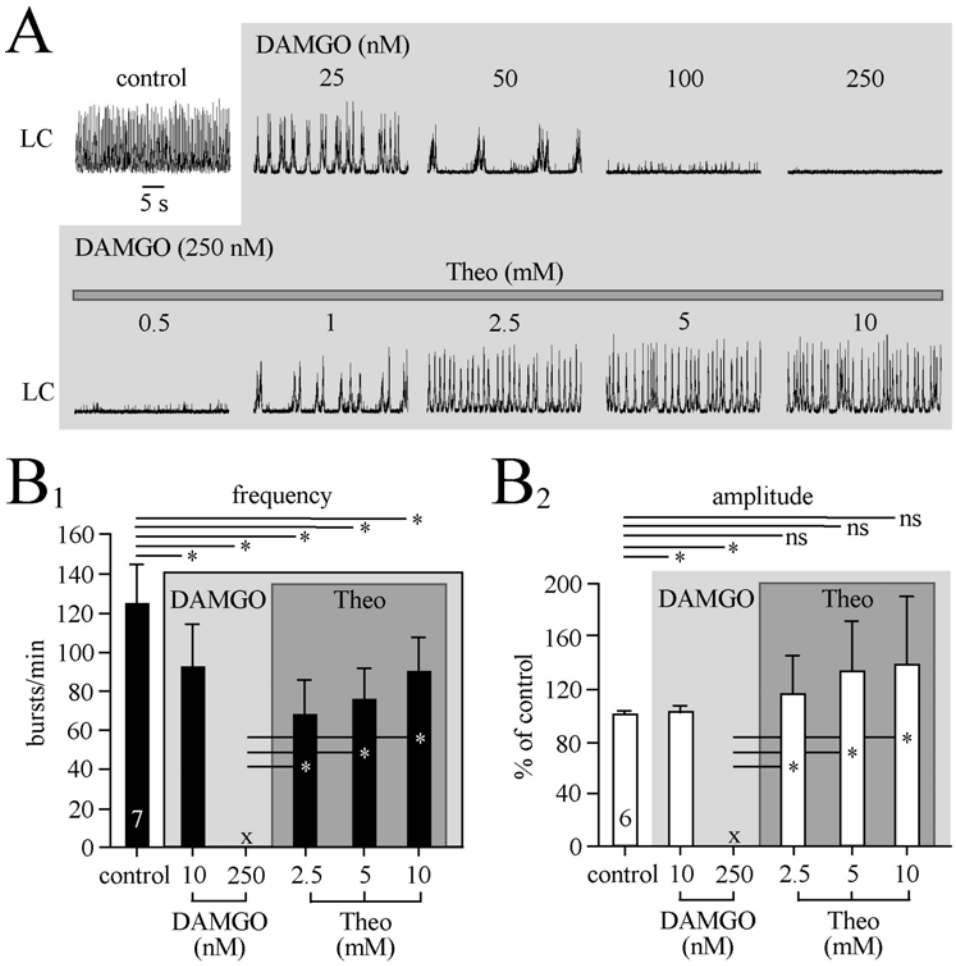

Fig. 6-6: Countering by methylxanthines of opioid depression of LC bursting. **A**, bath-application of increasing doses of the μ-opioid receptor agonist [D-Ala^2,N-Me-Phe^4,Gly^5-ol]-enkephalin (DAMGO) transformed LC bursting from fast regular oscillations into longer multipeak bursts (at 25-50 nM) and then into small amplitude 'spikes' (at 100 nM) before rhythm was abolished (at 250 nM). Spike rhythm recovered upon addition of 0.5 mM Theo to 250 nM DAMGO-containing solution, 1 mM reactivated periodic bursts and 2.5-10 mM Theo restored almost normal bursting. **B**, summarizes DAMGO effects on rate (**B_1**) and amplitude (**B_2**) of fast LC bursts (one-way ANOVA). Note that LC bursting was already slowed by 10 nM DAMGO.

Fig. 6-7

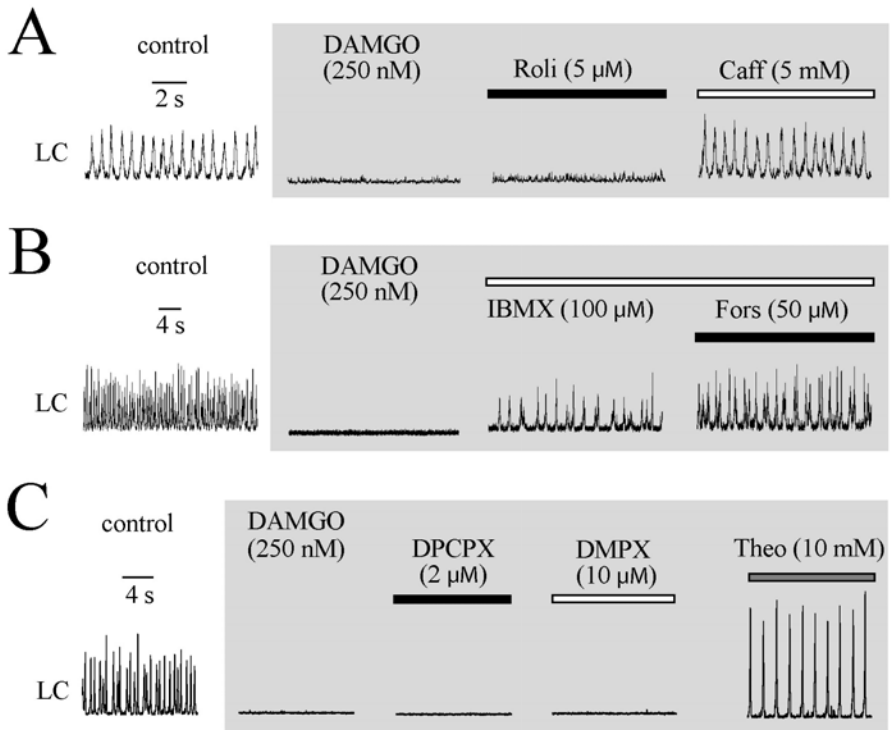

Fig. 6-7: Lack of countering effects of cyclic adenosine monophosphate (cAMP)-elevating drugs and adenosine receptor blockers on opioid depression of LC bursting. **A**, bath-application of the cAMP-dependent phosphodiesterase-4 blocker rolipram did not restore DAMGO-depressed LC bursting contrary to subsequent application of Caff. **B**, in a different slice the phosphodiesterase-4 blocker isobutylmethylxanthine (IBMX) reactivated some bursts after depression of rhythm by DAMGO and addition of the stimulator of cAMP-generating adenylyl cyclase forkolin (Fors) had an additional stimulatory effect. However, important to note, neither the individual drugs nor their combined application were effective in other slices, thus resulting in an overall non-significant effect (see text for details). **C**, in a further slice rhythm was not restored from DAMGO-evoked blockade by application of 8-Cyclopentyl-1,3-dipropylxanthine (DPCPX) or, after washout of DPCPX, by 3,7-Dimethyl-1-propargyl-xanthine (DMPX) which block A_1- or A_2-type adenosine receptors, respectively, whereas Theo was effective.

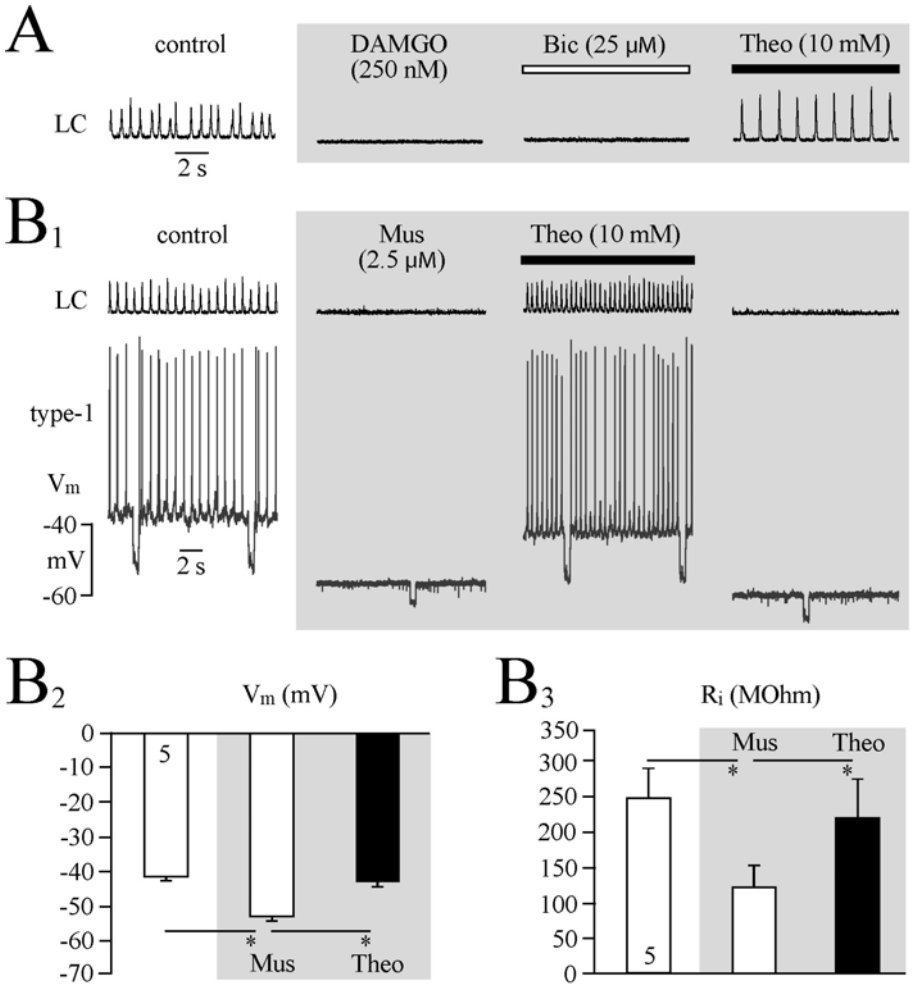

Fig. 6-8: Lack of countering effects of $GABA_A$ receptor blockade on opioid depression of LC bursting and effective $GABA_A$ receptor blockade by methylxanthine. A, bath-application of Bic did not counter DAMGO-evoked blockade of LC rhythm contrary to a pronounced stimulatory effect of Theo. **B**, in a type-2 neuron arrest of LC bursting by Mus was accompanied by a substantial hyperpolarization and decrease of input resistance (R_i), measured by injection of hyperpolarizing current pulses at regular intervals (**B_1**). Both, cellular and LC population effects of Mus were reversibly countered by Theo. **$B_{2,3}$**, statistical analysis (one-way ANOVA) of Mus and Theo effects on V_m (**B_1**) and R_i (**B_2**).

Fig. 6-9

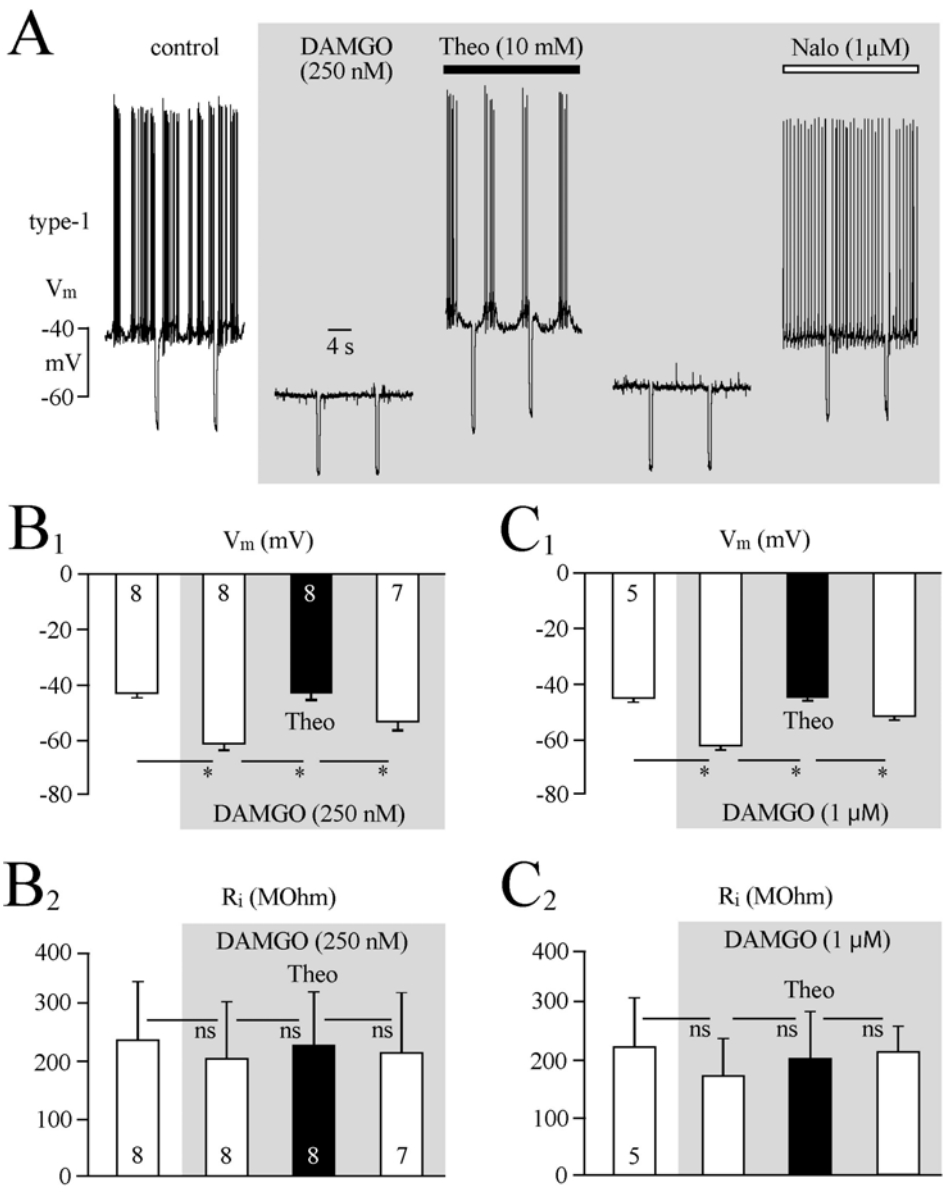

Fig. 6-9: Postsynaptic mechanism of methylxanthine-evoked reversal of opioid depression of LC bursting. A, bath-application of Theo reversed a prominent DAMGO-evoked hyperpolarization and also restored rhythmic bursting in this type-1 neuron. After restoration of DAMGO-evoked hyperpolarization upon washout of DAMGO, the opioid receptor antagonist naloxone (Nalo) antagonized the postsynaptic response while turning the activity pattern into that typical for type-2 neurons (compare **Fig. 6-2**). **B**,**C**, statistical analysis (one-way ANOVA) revealed that effects of 10 mM Theo in 250 nM (**B_1**, **B_2**) and 1 µM DAMGO (**C_1, C_2**) were significant on V_m, but not R_i.

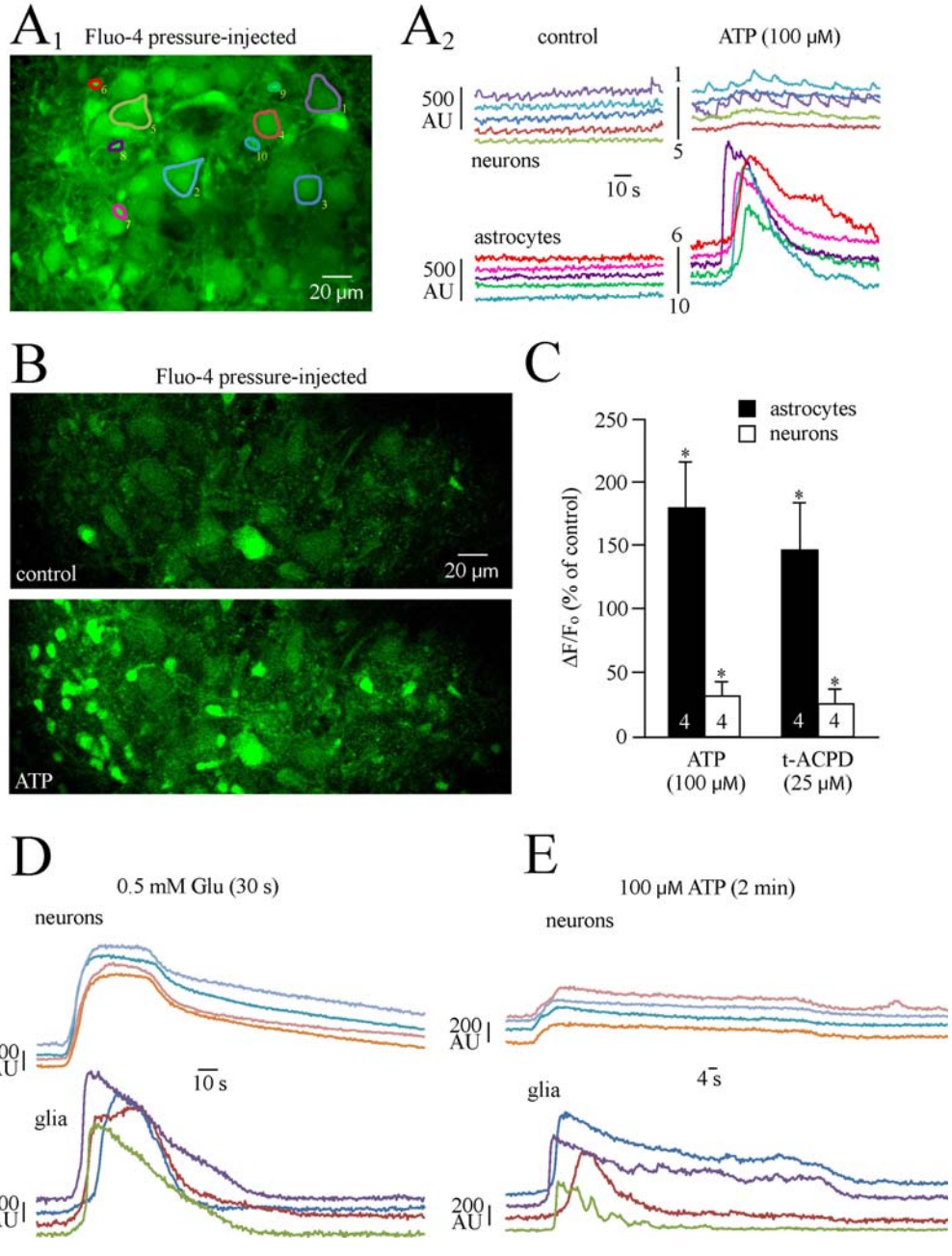

Fig. 6-10: Pharmacological discrimination of LC neurons from neighboring glia likely representing astrocytes. A, both neurons and astrocytes were labelled with the green Ca^{2+} sensitive fluorescent dye Fluo-4 via pressure injection (0.5 mM, 50 mm Hg, 10 min) into the LC (**A_1**). For optimizing visualization of morphological features, the slice was incubated after the experiment shown in **A_2** (and in **A** in **Fig. 6-10A**) in glutamate (1 mM) which evoked a sustained increase

in Fluo-4 fluorescence due to a major rise in neuronal and glial Ca^{2+}. Shown is the image after application of glutamate. The left panel of **A_2** shows synchronous low amplitude Ca^{2+} rises (evident as increases in Fluo-4 fluorescence intensity labeled in arbitrary units (AU) in 5 presumptive neurons outlined in **A_1** by large color-coded regions of interest (ROIs), whereas Ca^{2+} baseline was stable in 5 putative astrocytes outlined by small ROIs. The right panel shows that bath-application of adenosine-triphosphate (ATP) notably raised Ca^{2+} in the astrocytes, whereas Ca^{2+} baseline increased only modestly in neurons, two of which showed additional rhythmic asynchronous Ca^{2+} increases. **B**, shows in a different Fluo-4-labeled slice large neurons and small astrocytes in control solution (upper image) and during the peak of the Ca^{2+} response to ATP (lower image). **C**, statistical analysis (one-way ANOVA) of the differential neuronal and glial (20 neurons and 20 astrocytes in 4 slices) responses to ATP and the metabotropic glutamate receptor agonist 1-aminocyclopentane-trans-1,3-dicarboxylic acid (t-ACPD) (20 neurons and 20 astrocytes in 4 slices). **D** and **E** show neuronal and glial Ca^{2+} traces after application of glutamate (30 s) and ATP (2 min), respectively.

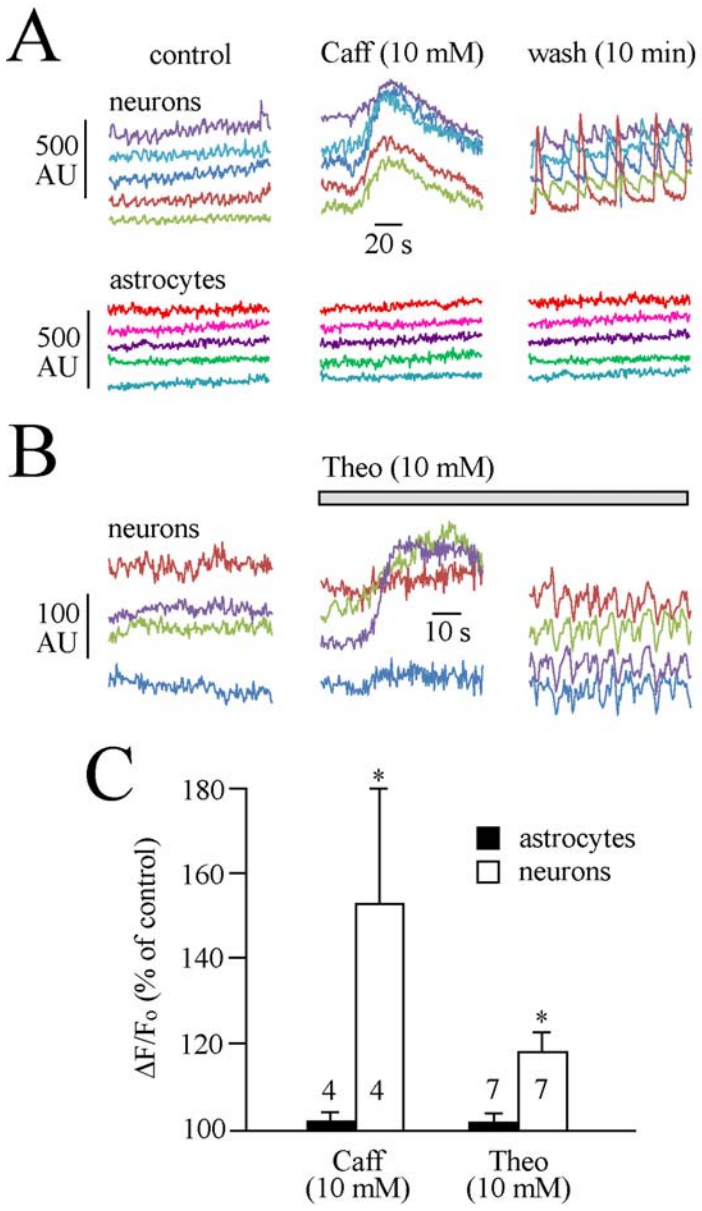

Fig. 6-11: Methylxanthine effects on neuronal and glial Ca^{2+}. **A**, bath-application of Caff evokes a Ca^{2+} rise in all neurons, whereas Ca^{2+} was not affected in astrocytes of the same slice. **B**, shows neuronal responses to Theo in a different slice. Note the occurrence of synchronized Ca^{2+} rises 10 min after start of washout (**A**) or during methylxanthine application (**B**).

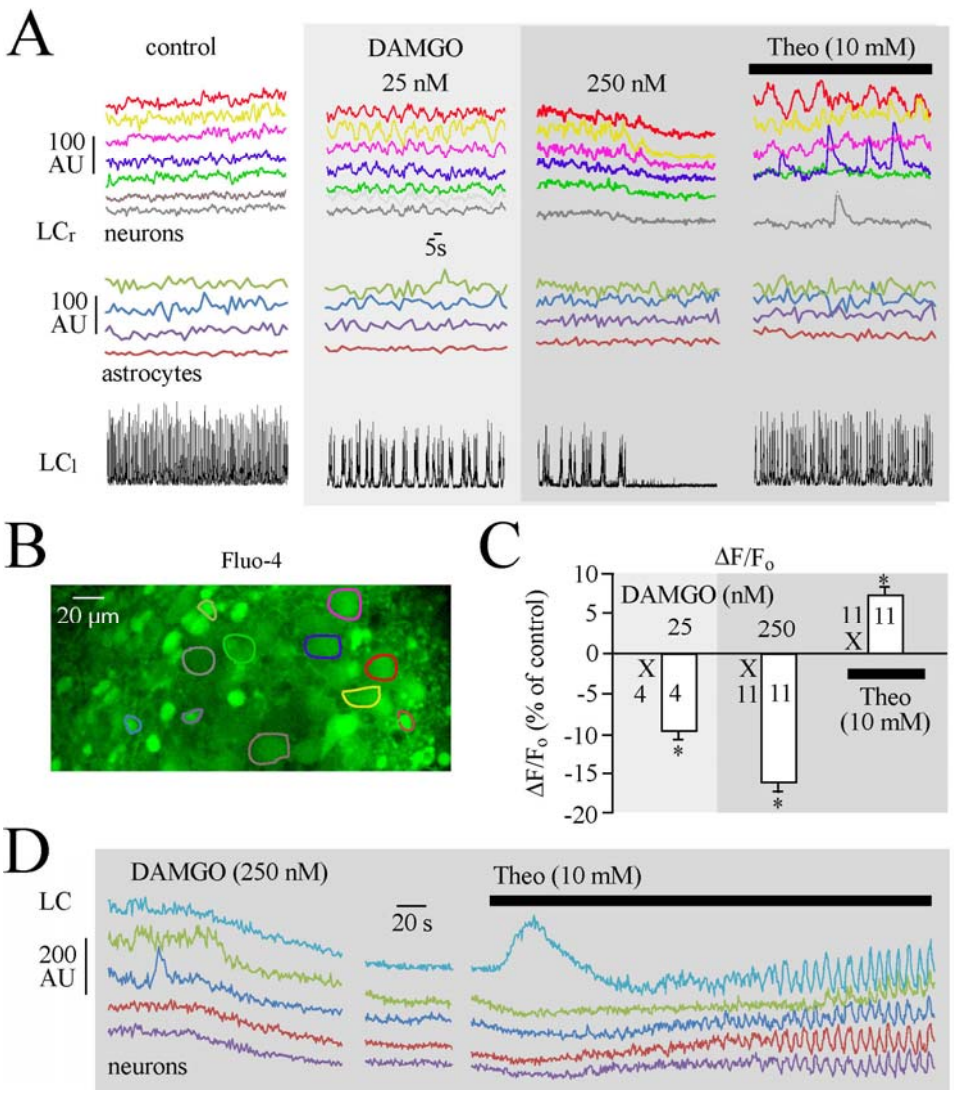

Fig. 6-12: Effects of opioids and methylxanthines on neuronal Ca^{2+} in LC neurons and astrocytes. A, at 25 nM DAMGO decreased Ca^{2+} baseline in 7 neurons (corresponding to color-coded large ROIs in **B**) and transformed fast regular LC oscillations, recorded with a suction electrode in the contralateral LC, into periodic bursts that were reflected by synchronous neuronal Ca^{2+} rises. Subsequent blockade of LC rhythm by 250 nM DAMGO lowered Ca^{2+} further, whereas reactivation by Theo of LC rhythm and concomitant Ca^{2+} rises in some neurons were accompanied by a modest reincrease of Ca^{2+} baseline in some cells. Neither DAMGO nor Theo affected Ca^{2+} baseline in 4 astrocytes (color-coded ROIs are shown in **B**). **C**, shows analysis of DAMGO effects on Ca^{2+} in neurons (white bars) *versus* (lack of effect) in astrocytes (X). ($P< 0.05$, paired t-test; n=

number of slices tested with >5 cells analyzed per slice). **D**, example for a notable fall of neuronal Ca^{2+} in response to direct exposure of a LC slice to 250 nM DAMGO and the reactivating effect of Theo (which includes synchronous Ca^{2+} oscillations in all neurons. Note that Theo can initially either raise or lower Ca^{2+} baseline or have no effect in some neurons.

6.6 References

Agulhon C, Petravicz J, McMullen AB, Sweger EJ, Minton SK, Taves SR, Casper KB, Fiacco T A, McCarthy KD (2008) What is the role of astrocyte calcium in neurophysiology? Neuron 59, 932-946

Alreja M, Aghajanian GK (1993) Opiates suppress a resting sodium-dependent inward current and activate an outward potassium current in locus coeruleus neurons. J Neurosci 13, 3525-3532

Alreja M, Aghajanian GK (1995) Use of the whole-cell patch-clamp method in studies on the role of cAMP in regulating the spontaneous firing of locus coeruleus neurons. J Neurosci Methods 59, 67-75

Ballantyne D, Andrzejewski M, Muckenhoff K, Scheid P (2004) Rhythms, synchrony and electrical coupling in the Locus coeruleus. Respir Physiol Neurobiol 143, 199-214

Ballanyi K, Ruangkittisakul A (2009) Structure-function analysis of rhythmogenic inspiratory pre-Bötzinger complex networks in "calibrated" newborn rat brainstem slices. Respir Physiol Neurobiol 168, 158-78

Ballanyi K, Kulik A (1998) Intracellular Ca2+ during metabolic activation of KATP channels in spontaneously active dorsal vagal neurons in medullary slices. Eur J Neurosci 10, 2574-85

Ballanyi K, Lalley PM, Hoch B, Richter DW (1997) cAMP-dependent reversal of opioid- and prostaglandin-mediated depression of the isolated respiratory network in newborn rats. J Physiol 504, 127-134

Ballanyi K, Onimaru H, Homma I (1999) Respiratory network function in the isolated brainstem-spinal cord of newborn rats. Progr Neurobiol 59, 583-634

Ballanyi K, Panaitescu B, Ruangkittisakul A (2010) Control of breathing by ‘nerve glue’. Sci Signal 3, pe41

Bancalari E (2006) Caffeine for apnea of prematurity. N Engl J Med 354, 2179-2181

Ben-Ari Y, Gaiarsa JL, Tyzio R, Khazipov R (2007) GABA: a pioneer transmitter that excites immature neurons and generates primitive oscillations. Physiol Rev 87, 1215-1284

Bennett HJ, Semba K (1998) Immunohistochemical localization of caffeine-induced c-Fos protein expression in the rat brain. J Comp Neurol 401, 89-108

Bennett MV, Zukin RS (2004) Electrical coupling and neuronal synchronization in the Mammalian brain. Neuron 41, 495-511

Berridge CW, Waterhouse BD (2003) The locus coeruleus-noradrenergic system: modulation of behavioral state and state-dependent cognitive processes. Brain Res Rev 42, 33-84

Black AM, Pandya S, Clark D, Armstrong EA, Yager JY (2008) Effect of caffeine and morphine on the developing pre-mature brain. Brain Res 1219, 136-142

Blaustein MP, Golovina VA (2001) Structural complexity and functional diversity of endoplasmic reticulum Ca^{2+} stores. Trends Neurosci 24, 602-8

Boison D (2011) Methylxanthines, seizures, and excitotoxicity. Handb Exp Pharmacol, 251-266

Brockhaus J, Ballanyi K (1998) Synaptic inhibition in the isolated respiratory network of neonatal rats. Eur J Neurosci 10, 3823-39

Cedarbaum JM, Aghajanian GK (1978) Afferent projections to the rat locus coeruleus as determined by a retrograde tracing technique. J Comp Neurol 178, 1-16

Charles BG, Townsend SR, Steer PA, Flenady VJ, Gray PH, Shearman A (2008) Caffeine citrate treatment for extremely premature infants with apnea: population pharmacokinetics, absolute bioavailability, and implications for therapeutic drug monitoring. Ther Drug Monit 30, 709-716

Christie MJ, Williams JT, North RA (1989) Electrical coupling synchronizes subthreshold activity in locus coeruleus neurons in vitro from neonatal rats. J Neurosci 9, 3584-3589

Christie MJ, Jelinek HF (1993) Dye-coupling among neurons of the rat locus coeruleus during postnatal development. Neuroscience 56, 129-137

Desfrere L, Olivier P, Schwendimann L, Verney C, Gressens P (2007) Transient inhibition of astrocytogenesis in developing mouse brain following postnatal caffeine exposure. Pediatr Res 62, 604-609

Deurveilher S, Lo H, Murphy JA, Burns J, Semba K (2006) Differential c-Fos immunoreactivity in arousal-promoting cell groups following systemic administration of caffeine in rats. J Comp Neurol 498, 667-689

Eldridge FL, Millhorn DE, Kiley JP (1985) Antagonism by theophylline of respiratory inhibition induced by adenosine. J Appl Physiol 59, 1428-1433

Feldman JL, Del Negro CA (2006) Looking for inspiration: new perspectives on respiratory rhythm. Nat Rev Neurosci 7, 232-242

Francis SH, Sekhar KR, Ke H, Corbin JD (2011) Inhibition of cyclic nucleotide phosphodiesterases by methylxanthines and related compounds. Handb Exp Pharmacol, 93-133

Fredholm BB, Battig K, Holmen J, Nehlig A, Zvartau EE (1999) Actions of caffeine in the brain with special reference to factors that contribute to its widespread use. Pharmacol Rev 51, 83-133

Garaschuk O, Linn J, Eilers J, Konnerth A (2000) Large-scale oscillatory calcium waves in the immature cortex. Nat Neurosci 3, 452-459

Gosgnach S (2011) The role of genetically-defined interneurons in generating the mammalian locomotor rhythm. Integr Comp Biol 51, 903-12

Herlenius E, Aden U, Tang LQ, Lagercrantz H (2002) Perinatal respiratory control and its modulation by adenosine and caffeine in the rat. Pediatr Res 51, 4-12

Hilaire G (2006) Endogenous noradrenaline affects the maturation and function of the respiratory network: possible implication for SIDS. Auton Neurosci 126-127, 320-331

Hoecker C, Nelle M, Poeschl J, Beedgen B, Linderkamp O (2002) Caffeine impairs cerebral and intestinal blood flow velocity in preterm infants. Pediatrics 109, 784-787

Huang ZJ, Di Cristo G, Ango F (2007) Development of GABA innervation in the cerebral and cerebellar cortices. Nat Rev Neurosci 8, 673-86

Huxtable AG, Zwicker JD, Poon BY, Pagliardini S, Vrouwe SQ, Greer JJ, Funk GD (2009) Tripartite purinergic modulation of central respiratory networks during perinatal development: the influence of ATP, ectonucleotidases, and ATP metabolites. J Neurosci 29, 14713-14725

Huxtable AG, Zwicker JD, Alvares TS, Ruangkittisakul A, Fang X, Hahn LB, Posse de Chaves E, Baker GB, Ballanyi K, Funk GD (2010) Glia contribute to the purinergic modulation of inspiratory rhythm generating networks. J Neurosci 30, 3947-3958

Iyadurai SJ, Chung SS (2007) New-onset seizures in adults: possible association with consumption of popular energy drinks. Epilepsy Behav. 10, 504-508

Jefferys JG (1995) Nonsynaptic modulation of neuronal activity in the brain: electric currents and extracellular ions. Physiol Rev 75, 689-723

Kafitz KW, Meier SD, Stephan J, Rose CR (2008) Developmental profile and properties of sulforhodamine 101--Labeled glial cells in acute brain slices of rat hippocampus. J Neurosci Methods 169, 84-92

Kang SH, Lee YA, Won SJ, Rhee KH, Gwag BJ (2002) Caffeine-induced neuronal death in neonatal rat brain and cortical cell cultures. Neuroreport 13, 1945-1950

Kantor C, Panaitescu B, Kuribayashi J, Ruangkittisakul A, Lee TF, Cheung PY, MacTavish D, Jhamandas J, Ballanyi K (2012) Electrophysiological imaging of early network oscillations in brain slices from newborn rats and piglets. In Isolated Central Nervous System Circuits (Ed K Ballanyi), Neuromethods Series

Vol 73 (Ed W Walz). Springer Science+Business Media, LLC, New York, NY, 315-356

Kaufman KR, Sachdeo RC (2003) Caffeinated beverages and decreased seizure control. Seizure 12, 519-521

Kjaerulff O, Barajon I, Kiehn O (1994) Sulphorhodamine-labelled cells in the neonatal rat spinal cord following chemically induced locomotor activity in vitro. J Physiol 478, 265-73

Korematsu S, Miyahara H, Nagakura T, Suenobu S, Izumi T (2008) Theophylline-associated seizures and their clinical characterizations. Pediatr Int 50, 95-98

Kullmann DM (2011) Interneuron networks in the hippocampus. Curr Opin Neurobiol 21, 709-16

Lee TC, Charles BG, Steer PA, Flenady VJ (1996) Saliva as a valid alternative to serum in monitoring intravenous caffeine treatment for apnea of prematurity. Ther Drug Monit 18, 288-293

Leon AE, Michienzi K, Ma CX, Hutchison AA (2007) Serum caffeine concentrations in preterm neonates. Am J Perinatol 24, 39-47

Lopez F, Miller LG, Greenblatt DJ, Kaplan GB, Shader RI (1989) Interaction of caffeine with the GABAA receptor complex: alterations in receptor function but not ligand binding. Eur J Pharmacol 172, 453-9

Martin RJ, Abu-Shaweesh JM (2005) Control of breathing and neonatal apnea. Biol Neonate 87, 288-295

Maubecin VA, Williams JT (1999) Developmental changes that regulate the activity of locus coeruleus neurons. Tokai J Exp Clin Med 24, 41-51

Montandon G, Kinkead R, Bairam A (2008) Adenosinergic modulation of respiratory activity: developmental plasticity induced by perinatal caffeine administration. Resp Physiol Neurobiol 164, 87-95

Nestler EJ, Alreja M, Aghajanian GK (1999) Molecular control of locus coeruleus neurotransmission. Biol Psychiatry 46, 1131-1139

Nimmerjahn A, Kirchhoff F, Kerr JN, Helmchen F (2004) Sulforhodamine 101 as a specific marker of astroglia in the neocortex in vivo. Nat Methods 1, 31-7

O'Donnell JM, Zhang HT (2004) Antidepressant effects of inhibitors of cAMP phosphodiesterase (PDE4). Trends Pharmacol Sci 25, 158-163

Olpe HR, Steinmann MW, Hall RG, Brugger F, Pozza MF (1988) $GABA_A$ and $GABA_B$ receptors in locus coeruleus: effects of blockers. Eur J Pharmacol 149, 183-185

Oyamada Y, Ballantyne D, Mückenhoff K, Scheid P (1998) Respiration-modulated membrane potential and chemosensitivity of locus coeruleus neurones in the in vitro brainstem-spinal cord of the neonatal rat. J Physiol 513, 381-398

Panaitescu B, Ruangkittisakul A, Ballanyi K (2009) Silencing by raised extracellular Ca^{2+} of pre-Bötzinger complex neurons in newborn rat brainstem slices without change of membrane potential or input resistance. Neurosci Lett 456, 25-9

Peyron C, Luppi PH, Fort P, Rampon C, Jouvet M (1996) Lower brainstem catecholamine afferents to the rat dorsal raphe nucleus. J Comp Neurol 364, 402-413

Porter JT, McCarthy KD (1997) Astrocytic neurotransmitter receptors in situ and in vivo. Progr Neurobiol 51, 439-455

Richter DW, Lalley PM, Pierrefiche O, Haji A, Bischoff AM, Wilken B, Hanefeld F (1997) Intracellular signal pathways controlling respiratory neurons. Respir Physiol Neurobiol 110, 113-123

Ruangkittisakul A, Ballanyi K (2010) Methylxanthine reversal of opioid-evoked inspiratory depression via phosphodiesterase-4 blockade. Resp Physiology Neurobiol 172, 94-105

Ruangkittisakul A, Schwarzacher SW, Ma Y, Poon B, Secchia L, Funk GD, Ballanyi K (2006) High sensitivity to neuromodulator-activated signalling pathways at physiological [K^+] of confocally-imaged respiratory centre neurons in online-calibrated newborn rat brainstem slices. J Neurosci 26, 11870-11880

Ruangkittisakul A, Okada Y, Oku Y, Koshiya N, Ballanyi K (2009) Fluorescence imaging of active respiratory networks. Respir Physiol Neurobiol 168, 26-38

Ruangkittisakul A, Panaitescu B, Kuribayashi J, Ballanyi K (2010) Caffeine reversal of opioid-evoked and endogenous inspiratory depression in perinatal rat en bloc medullas and slices. Adv Exp Med Biol 669, 123-7

Ruangkittisakul A, Secchia-Ballanyi L, Panaitescu B, Bobocea N, Kuribayashi J, Iizuka M, Kantor C, Ballanyi K (2012) Anatomically 'calibrated' isolated respiratory networks from newborn rodents. In Isolated Central Nervous System Circuits (Ed K Ballanyi), Neuromethods Series Vol 73 (Ed W Walz). Springer Science+Business Media, LLC, New York, NY, 61-124

Samuels ER, Szabadi E (2008a) Functional neuroanatomy of the noradrenergic locus coeruleus: its roles in the regulation of arousal and autonomic function part I: principles of functional organisation. Curr Neuropharmacol 6, 235-253

Samuels ER, Szabadi E (2008b) Functional neuroanatomy of the noradrenergic locus coeruleus: its roles in the regulation of arousal and autonomic function part II: physiological and pharmacological manipulations and pathological alterations of locus coeruleus activity in humans. Curr Neuropharmacol 6, 254-285

Schmidt B, Roberts RS, Davis P, Doyle LW, Barrington KJ, Ohlsson A, Solimano A, Tin W (2007) Long-term effects of caffeine therapy for apnea of prematurity. N Engl J Med 357, 1893-1902

Shefner SA, Chiu TH (1986) Adenosine inhibits locus coeruleus neurons: an intracellular study in a rat brain slice preparation. Brain Res 366, 364-368

Shi D, Padgett WL, Daly JW (2003) Caffeine analogs: effects on ryanodine-sensitive calcium-release channels and GABAA receptors. Cell Mol Neurobiol 23, 331-47

Sipilä ST, Kaila K (2008) GABAergic control of CA3-driven network events in the developing hippocampus. Results Probl Cell Differ 44, 99-121

Torrecilla M, Marker CL, Cintora SC, Stoffel M, Williams JT, Wickman K (2002) G-protein-gated potassium channels containing Kir3.2 and Kir3.3 subunits mediate the acute inhibitory effects of opioids on locus ceruleus neurons. J Neurosci 22, 4328-4334

Travagli RA, Dunwiddie TV, Williams JT (1995) Opioid inhibition in locus coeruleus. J Neurophysiol 74, 518-528

Ukena D, Schudt C, Sybrecht GW (1993) Adenosine receptor-blocking xanthines as inhibitors of phosphodiesterase isozymes. Biochem Pharmacol 45, 847-851

Uneyama H, Harata N, Akaike N (1993) Caffeine and related compounds block inhibitory amino acid-gated Cl- currents in freshly dissociated rat hippocampal neurones. Br J Pharmacol 109, 459-65

Verkhratsky A (2005) Physiology and pathophysiology of the calcium store in the endoplasmic reticulum of neurons. Physiol Rev 85, 201-279

Viemari JC, Bevengut M, Burnet H, Coulon P, Pequignot JM, Tiveron MC, Hilaire G (2004) Phox2a gene, A6 neurons, and noradrenaline are essential for development of normal respiratory rhythm in mice. J Neurosci 24, 928-937

Wang YY, Aghajanian GK (1987) Excitation of locus coeruleus neurons by an adenosine 3',5'-cyclic monophosphate-activated inward current: extracellular and intracellular studies in rat brain slices. Synapse 1, 481-487

Williams JT, Marshall KC (1987) Membrane properties and adrenergic responses in locus coeruleus neurons of young rats. J Neurosci 7, 3687-3694

Williams JT, Egan TM, North RA (1982) Enkephalin opens potassium channels on mammalian central neurones. Nature 299, 74-77

Williams JT, Christie MJ, Manzoni O (2001) Cellular and synaptic adaptations mediating opioid dependence. Physiol Rev 81, 299-343

Yoshikawa H (2007) First-line therapy for theophylline-associated seizures. Acta Neurol Scand 115, 57-61

Zhu H, Zhou W (2001) Morphine induces synchronous oscillatory discharges in the rat locus coeruleus. J Neurosci 21, RC179

Zwicker JD, Rajani V, Hahn LB, Funk GD (2011) Purinergic modulation of preBötzinger complex inspiratory rhythm in rodents: the interaction between ATP and adenosine. J Physiol 589, 4583-4600

Chapter 7

General Discussion

7.1 Introduction

Premature infants present with numerous medical conditions and often require multiple pharmacological strategies in order to survive. Most premature infants have apneic episodes lasting for more than 20 seconds (apnea of prematurity) and, if prolonged, might lead to hypoxemia, affecting many other brain areas (Miller & Martin, 1992; Martin & Abu-Shaweesh, 2005; Bancalari, 2006; Zhao et al., 2011). These apneas are usually treated with long-term respiratory stimulating drugs, such as methylxanthines (Miller & Martin, 1992; Bancalari, 2006). Methylxanthines have potent respiratory stimulating effects and their site of action is presumably within the CNS, targeting respiratory networks which might be incompletely developed in premature infants (Martin & Abu-Shaweesh, 2005; Conde et al., 2006). One particular target may be rhythmogenic inspiratory networks within the preBötC, comprising a brainstem region of utmost importance for normal breathing that is primarily mediating rhythmic contraction of the diaphragm (Bianchi et al., 1995; Martin & Abu-Shaweesh, 2005; Feldman & Del Negro, 2006). Also opioids are frequently administered to preterm infants for pain treatment and this can depress breathing, contrary to methylxanthine actions (Dahan et al., 2010; Law et al., 2000). Our recent study showed using newborn rat *en bloc* and slice preparations that low millimolar doses of methylxanthines reverse opioid-induced depression of the isolated newborn rat preBötC and that this may involve inhibition of PDE4 (Ruangkittisakul & Ballanyi, 2010; Ruangkittisakul et al., 2010). However, it was not studied until

now at the cellular level how methylxanthines exert that stimulatory action on the isolated preBötC networks. Similarly, it is unclear whether they also have a counteracting effect on the established inhibition by opioids of spontaneously active *locus coeruleus* (LC) neural networks in the pontine brainstem area. It is important to study the neonatal LC because it is actively involved in supporting the development of other brain areas through release of norepinephrine and has also reciprocal connections with respiratory networks (Hilaire et al., 2004; Oyamada et al., 1998; Gargaglioni et al., 2010). In that regard, it was studied here whether one particular central nervous side effect of methylxanthines, namely induction of cortical and hippocampal seizures (Moraidis & Bingmann, 1994; Dzhala et al., 1999; Kantor et al., 2012), might also perturb the neural networks in the preBötC and LC.

7.2 Modulation of preBötC Rhythm by extracellular Ca^{2+} and Mg^{2+}

Recent work from our group has established that the normal activity of the isolated preBötC and also the severity of responses to pathophysiological perturbations of inspiratory rhythm by opioids and anoxia depend, on the one hand, greatly on the K^+ and Ca^{2+} concentrations of superfusate used for its study (Ruangkittisakul et al., 2006, 2007, 2008, 2012). On the other hand, our group showed that brainstem tissue rostrally adjacent to the preBötC modulates its burst patterns (Ruangkittisakul et al., 2008) in addition to other influences from the more rostrally located pFRG expiratory center (Onimaru & Homma, 2003; Feldman & Del Negro, 2006). For these reasons, it was the first aim of this

thesis, dealt with in Chapter 3, to reduce such modulatory influences by developing 400 μm thin m-preBötC[400] slices, in which the dendritic tree of neurons within the ~200 μm spanning preBötC (Smith et al., 1991; Ruangkittisakul et al., 2008) is mostly intact to enable recordings of membrane potential responses to opioids or methylxanthines. It was revealed in Chapter 3 that rhythm in these slices in physiological K^+ (3 mM) and Ca^{2+} (1-1.2 mM) arrests spontaneously after ~2 h and that it is thus necessary to raise K^+ for long-term (pharmacological) preBötC analyses in these slices. Specifically, it was recommended to use 5-6 mM K^+ and 1-1.2 mM Ca^{2+} for new projects. However, during the experiments for that chapter, responses of these slices to opioids and methylxanthines were already studied in $7K^+/1.2Ca^{2+}$ and this solution was therefore used to finish the projects dealt with in Chapters 3 and 4. As one aspect of the analysis of properties of the novel m-preBötC[400] slices, the dependence of inspiratory rhythm on larger variations of Ca^{2+} and Mg^{2+} was studied. One rationale for this was to test whether <1 mM Ca^{2+} would increase the rate of preBötC rhythm as hypothesized by Rekling and colleagues (1996a,b) to justify use of 0.8 mM Ca^{2+} in their standard superfusate. It was found here that <0.75 mM Ca^{2+} evokes seizure-like preBötC discharges that are similar to hyperexcitability in cortical brain slices, which in fact established low Ca^{2+} as an *in vitro* model for epilepsy (Konnerth et al., 1986; Jefferys, 1995; Kilb et al., 2007). Accordingly, it is not recommended to use superfusate with <0.8 mM Ca^{2+} to study the isolated preBötC. As summarized in the latter studies, also ≤0.5 mM extracellular Mg^{2+} is an effective epilepsy model in cortical brain slices. In

contrast, preBötC rhythm was not perturbed even by 0.25 mM Mg^{2+}. Similarly, 2-3 mM Mg^{2+} had a notably less pronounced inhibitory effect on preBötC rhythm, compared to similar levels of raised Ca^{2+}. This may indicate that screening of negative surface charges is not a prominent mechanism of the inhibitory Ca^{2+} effect on the isolated preBötC as previously proposed (Kuwana et al., 1998; Ruangkittisakul et al. 2007). Other possible mechanisms of this inhibition may include a low expression of Ca^{2+} buffering proteins such as parvalbumin, calretinin or calbindin in the area of the preBötC (Alheid et al., 2002; Feldman & Del Negro, 2006). The potent inhibitory action of Ca^{2+} increases within physiological limits is likely not related to presynaptic Ca^{2+} influx, which should rather be enhanced due to an increased driving force (Hille, 2001; Somjen, 2002). That transmitter release is not primarily affected is also indicated by the finding that neither the amplitude nor duration of individual inspiratory bursts was reduced. Conversely, raised Ca^{2+} decreased the baseline of VRC recordings and low Ca^{2+} had the opposite effect. As one explanation for this phenomenon, spontaneously active (tonic) neurons, which possibly provide excitatory drive to rhythmogenic preBötC neurons (Richter et al., 1992; Richter & Spyer, 2001; Feldman & Del Negro, 2006) may be postsynaptically depressed by high Ca^{2+} via a decrease of their input resistance, as shown for other types of (mammalian) neurons (Jefferys, 1995; Hille, 2001; Somjen, 2002). Alternatively, raised Ca^{2+} may exert a relatively stronger inhibitory effect on such tonic neurons and/or preBötC cells due to a more pronounced stimulatory effect on (tonic) inhibitory than excitatory synapses (Jefferys, 1995). In line with the latter

assumption, inspiratory burst rate in isolated newborn rat brainstems is decreased by application of GABA or glycine (Feldman et al., 1990; Onimaru et al., 1990; Brockhaus & Ballanyi, 1998). In such a scenario, modest lowering of Ca^{2+} should increase burst rate due to relative depression of inhibition. However, blockade of $GABA_A$, $GABA_B$ and glycine receptors does not greatly increase inspiratory frequency *in vitro* (Feldman et al., 1990; Onimaru et al., 1990; Brockhaus & Ballanyi, 1998, 2000).

As a further possible explanation, high Ca^{2+} may depress postsynaptic excitability via a Ca^{2+}-sensing receptor that is expressed in various brain regions (Brown & MacLeod, 2001). As reviewed in the latter report, this receptor can be coupled to $G_{i/o}$ proteins. Receptor-coupled $G_{i/o}$ proteins strongly depress inspiratory networks, likely by decreasing cAMP in rhythmogenic preBötC neurons and/or neurons driving these cells (Richter et al., 1997; Ballanyi et al., 1997, 1999; Ruangkittisakul & Ballanyi, 2006; Ruangkittisakul et al., 2006). The Ca^{2+}-sensing receptor could hypothetically decrease preBötC excitability by stimulating Ca^{2+}-dependent K^+ channels (Zhao et al., 2006; Brown & MacLeod, 2001; Onimaru et al., 2003). Due to the structural similarity with the Ca^{2+}-sensing receptor, elevated Ca^{2+} might activate metabotropic $GABA_B$ or group-I glutamate receptors (Brown & MacLeod, 2001). However, as discussed above, raising Ca^{2+} unlikely decreases inspiratory burst rate substantially by stimulating $GABA_B$ receptors, while activation of group-I metabotropic glutamate receptors

with the agonist DHPG does strongly stimulate, and not inhibit, preBötC slice rhythm (Ruangkittisakul et al., 2006).

The modest depressing action of elevated Mg^{2+} could be due to presynaptic inhibition of ionotropic glutamatergic synapses that proposedly initiate inspiratory bursts via recurrent excitation within the preBötC interneuronal network (Del Negro et al., 2005, 2010; Feldman & Del Negro, 2006). However, as discussed above for Ca^{2+}, the lack of effect of elevated Mg^{2+} on single burst amplitude and duration rather suggests that the depression of inspiratory burst rate involves a relative augmentation of synaptic inhibition due to a more prominent depressing effect on excitatory than inhibitory synapses. Alternatively, Mg^{2+} may activate the Ca^{2+}-sensing receptors, though less effectively than Ca^{2+} (Brown & MacLeod, 2001), which is in line with its more moderate respiratory inhibitory action. Principally, Mg^{2+} can also exert neuronal inhibition by blocking subclasses of inward-rectifying K^+ channels (Nichols & Lopatin, 1997) that are possibly selectively expressed in inhibitory neurons. Finally, high Mg^{2+} may depress preBötC rhythm via activation of metabotropic group-I glutamate receptors (Kubo et al., 1998), although it is unlikely that Mg^{2+} acts only on such receptors in inhibitory interneurons.

It is not clear whether some of the above mentioned mechanisms operate primarily at presynaptic or postsynaptic sites. To study this, whole-cell recording was done in the m-preBötC[400] slices in identified inspiratory and tonic neurons located approximately in the center of the ~200 μm spanning preBötC (Smith et al., 1991; Ruangkittisakul et al., 2008). It turned out that rhythm was

abolished by high Ca^{2+} in both neuron classes without occurrence of a postsynaptic hyperpolarization or input resistance change. While this suggests that the blocking action of Ca^{2+} targets primarily presynaptic processes, this is not conclusive because of several methodological limitations. Firstly, it is possible that a postsynaptic blocking action via a hyperpolarization and input resistance decrease occurs primarily on distal dendrites which may be an important site for communication of rhythmogenic inspiratory preBötC neurons via recurrent (glutamatergic) excitation (Feldman & Del Negro, 2006; Del Negro et al., 2010). If that is the case, 'blind' whole-cell recording from most likely the soma of cells may not reveal the distal hyperpolarizations because of electrotonic attenuation of such signals during their propagation toward the soma. Secondly, it is also possible that whole-cell recordings in Chapter 3 were exclusively done in inspiratory preBötC neurons that are not important for generation of rhythm (similar to recordings for Chapters 4 and 5). However, it is important to note that it is currently not clear which preBötC neurons are rhythmogenic and how they can be easily identified in acute newborn rodent brainstem slices (Ballanyi & Ruangkittisakul, 2009). Candidate cells in that regard are recently discovered glutamatergic inspiratory neurons that express the transcription factor Dbx1 and are fluorescent labeled in transgenic mice (Bouvier et al., 2010; Gray et al., 2010). Of particular interest would be to study the subpopulation of Dbx1 neurons that is located within the 'sufficient' and 'necessary' anatomical boundaries of the preBötC (Ruangkittisakul et al., 2008) which are, however, not yet determined for Dbx1 (or other) mice. To enhance the probability of recording

from rhythmogenic Dbx1 neurons, a subpopulation of these cells that are expressing NK1 receptors in yet to be generated 'calibrated' preBötC slices from this species should be studied. NK1 and somatostatin receptors together with direct excitatory responses to thyrotropin-releasing hormone represent further characteristics of rhythmogenic inspiratory neurons (Rekling et al., 1996a,b; Gray et al., 1999; Pagliardini et al., 2005). It will take quite some time to establish all these technical preconditions for increasing the probability to record from likely rhythmogenic double- or triple fluorescent labeled Dbx1 neurons in the anatomically identified mouse preBötC. A further factor that hampers a defined strategy for targeting the right neurons is related to the fact that different neuron types may be important for generation of rhythm in rats *versus* mice. Specifically, in newborn rats, only 'Onimaru type-1' neurons receive excitatory synaptic input from the pFRG (Onimaru et al., 1992; Ballanyi et al., 1999). Because the opioid-insensitive pFRG is proposed to stimulate rhythmogenic preBötC neurons while they are inhibited by such drugs to cause 'quantal' slowing of rhythm (Mellen et al., 2003; Feldman & Del Negro, 2006), a subclass of such newborn rat type-1 neurons must be the rhythmogenic cells. However, for newborn rats it is not clear whether these neurons express Dbx1 and respond directly to thyrotropin-releasing hormone or NK1 agonists. Conversely, in mouse slices 'Rekling type-1' neurons were functionally defined by responding directly to μ-opioids, substance-P and thyrotropin-releasing hormone and with the onset of phasic EPSPs and discharge before the start of XII bursting (Rekling et al., 1996a,b; Gray et al., 1999; Feldman & Del Negro, 2006). However, it has not

been determined yet whether these mouse neurons are directly excited by the pFRG to keep them active in quantal fashion during opioid inhibition as further indication of an important role for generation of rhythm. Moreover, it has not yet been reported that any type of inspiratory neuron shows pre-inspiratory EPSPs in newborn rat slices in 7-9 mM K^+ which is necessary for long-term rhythm in thin preBötC slices. But, preliminary findings from our group show that newborn rat inspiratory neurons display in 3 mM K^+ activity patterns that resemble those in type-1 mouse neurons in high K^+ (Ballanyi & Ruangkittisakul, 2009). The increased evidence that astrocytes and other glial cells contribute to modulation of the preBötC like in other brain areas (Ballanyi et al., 2010; Huxtable et al., 2010; Schnell et al., 2010; Okada et al., 2012) raises the possibility that they are also involved in inhibition of inspiratory rhythm by high Ca^{2+}. Finally, in the experiments for Chapter 3, high Ca^{2+} was applied via the superfusate. Accordingly, its inhibitory action may primarily target areas other than the preBötC contained in the m-preBötC[400] slices. The obvious targets are neurons (and/or glia) in the *raphé obscurus* that presumably provide strong excitatory drive to the preBötC (Ptak et al., 2009). In line with a modulatory role of the *raphé obscurus* that is located in the midline of rhythmic slices are findings that injection of blockers of persistent Na^+ channels into this structure abolishes rhythm, whereas direct injection into the preBötC has no effect (Pace et al., 2007). This raises concern about the previously established view that this conductance is important for (rhythmogenic) preBötC neurons (Feldman & Del Negro, 2006; Ballanyi & Ruangkittisakul, 2009; Del Negro et al., 2010).

Consequently, future studies on elucidating the (sub)cellular targets and mechanisms of preBötC inhibition by high Ca^{2+} or other drugs require focal application into the preBötC to exclude a direct effect of activating neuronal cell bodies in other slice areas via bath-application. However, also this approach has a caveat because injection into the preBötC may nevertheless target the presynaptic terminals of axons from other slice areas or even from cut axons of brain region not contained in preBötC slices. As an example based on research from our group, electrically evoked norepinephrine release from cut axons of remote LC neurons raised glial Ca^{2+} in cerebellar slices from juvenile mice (Kulik et al., 1999). To discriminate between presynaptic influences from such sources and postsynaptic actions, e.g. of high Ca^{2+}, miniature postsynaptic potentials ('minis') should be analyzed in future studies (Capogna, 1998; Zucker, 2005).

The above discussion of mechanisms and sites of preBötC inhibition by high extracellular Ca^{2+} indicates that it is still a long way to go until rhythmogenic preBötC neurons and the exact (presynaptic versus postsynaptic) site of drug actions can be unambiguously targeted. Importantly, most of the above raised issues also apply to the discussion of cellular sites and mechanisms of opioid and methylxanthine effects as dealt with in the following.

7.3 Modulation of preBötC and LC Rhythm by Opioids and Methylxanthines

The main aim of Chapter 4 was to elucidate cellular mechanisms of respiratory stimulating actions of methylxanthines on the preBötC in the novel m-preBötC[400] slices. One assumption was that methylxanthines antagonize the depressing action of the μ-opioid DAMGO by a similar mechanism. It was in fact revealed that DAMGO did not exert a notable (i.e. <3 mV) postsynaptic hyperpolarization in anatomically identified inspiratory preBötC neurons and there was no concomitant fall of input resistance. Similarly, tonic preBötC neurons were not hyperpolarized by DAMGO and their input resistance was not changed. Also, methylxanthines did not change membrane potential or input resistance in either class of preBötC neurons. These findings regarding DAMGO consolidate previous observations from our group based on recordings from 'Onimary type-1' (Chapter **7.1**) inspiratory preBötC neurons in the newborn rat *en bloc* model showing that opioids do not exert a major hyperpolarizing action. While this indicates that lack of hyperpolarization in the preBötC of the en bloc model *versus* hyperpolarization in slices revealed by other groups (Gray et al., 1999; Montadon et al., 2011) is not due to the specific type of *in vitro* model, it does not allow the conclusion that blockade of preBötC slice rhythm is mainly due to presynaptic inhibition. As discussed in detail in the previous section for preBötC inhibition by high Ca^{2+}, it is possible that only a small subpopulation of glutamatergic Dbx1, NK1, thyrotropin-releasing hormone and somatostatin (receptor) expressing inspiratory preBötC neurons is notably hyperpolarized by opioids and that this hyperpolarization causes depression of rhythm. However, as

it was discussed above, there is currently no means of unambiguously targeting such presumably rhythmogenic neurons. A further potential limitation was that our experimental conditions, e.g. use of different types of patch electrode solutions, differ from those in other studies. However, it was found here that this does not impair activation of G protein-coupled K^+ conductances because some preBötC neurons hyperpolarized in response to the $GABA_B$ receptor agonist baclofen. Moreover, under identical experimental conditions all LC neurons tested in the experiments for Chapters 4 and 6 showed a prominent hyperpolarization in response to DAMGO. Nevertheless, it is possible that the opioid hyperpolarization of rhythmogenic preBötC neurons occurs mainly in distal dendrites and that this signal does not propagate electrotonically to the likely somatic whole-cell recording site. But, this argument is not fully valid because others reported hyperpolarizations that should also not have been revealed if strong electrotonic attenuation is a characteristic feature of opioid actions on rhythmogenic preBötC neurons. Based on these considerations, it cannot be concluded here that opioids depress the preBötC mainly via presynaptic mechanisms. However, it should be noted that there is also no proof yet based on studies by others that hyperpolarization of some preBötC neurons causes the depression or it is just a coincident phenomenon in some cells. Because also methylxanthines did not have a postsynaptic action on inspiratory or tonic preBötC neurons during DAMGO, it is possible that they target the same cells and sites as opioids. But, similar to the discussion for opioids it cannot be decided currently whether this is indeed the case and if the effect is presynaptic

or postsynaptic. The findings in the preBötC neurons differ from those in LC cells in which a clear postsynaptic hyperpolarization was reversed by low millimolar methylxanthine. However, also this does not unambiguously prove that methylxanthines act via PDE4 inhibition in these cells. It can well be that methylxanthines reverse the DAMGO depression via other postsynaptic mechanisms, although it is important to note that they did not affect membrane potential or input resistance of LC neurons in control solution.

For the LC, Ca^{2+} imaging was applied for the first time according to my knowledge. This imaging revealed that opioids decrease cytosolic Ca^{2+} in the large LC neurons and that this is reversed by methylxanthines which can evoke a Ca^{2+} rise in control solutions in some neurons. Notably smaller cells responded with a larger Ca^{2+} rise to bath-applied ATP or t-ACPD than larger cells. This may be a pharmacological tool for discriminating astrocytes from neurons, although additional anatomical characterization, particularly via fluorescent glial proteins (Schnell et al., 2010; Okada et al., 2012) is necessary in addition. But, if the small cells are mostly astrocytes, they did not respond with a Ca^{2+} change to opioids or methylxanthines. While this imaging approach in the LC was the initial step in elucidating potential roles of glia in inhibition of LC population bursting by opioids and its reversal by methylxanthines, a substantial amount of further work is necessary in that regard. For example, blockers of voltage-gated Ca^{2+} channels need to be applied to study the origin of the DAMGO-evoked fall of neuronal Ca^{2+}. The same holds true for Ca^{2+} imaging in the preBötC during

DAMGO and methylxanthines. While the basic findings were very similar compared to those in the LC, key points are to determine methods for discriminating neurons from astrocytes in the living slices. One possible means was to apply fluorescent SR-101 which presumably labels astrocytes. However, while our group succeeded to label astrocytes versus neurons selectively in the entorhinal cortex and hippocampus of newborn rat brain slices via distinct application protocols (Kantor et al., 2012), this approach was not successful in either LC or preBötC.

7.4 Epileptogenic Potential of Methylxanthines

In Chapter 5, it was studied whether methylxanthines have the potential to evoke seizure-like hyperexcitability like *in vivo* and in cortical or hippocampal brain slices (Chapter **7.1**). Indeed, it was revealed that spinal motor networks show such hyperpexcitability in response to low millimolar methylxanthine. These doses are identical to those that are necessary to reverse preBötC inhibition by opioids (compare Chapter **4**). Opposed to its antagonizing effect on opioid depression of the preBötC, rolipram did not mimic the methylxanthine-evoked spinal hyperexcitability, in contrast to bicuculline. This suggests that this hyperexcitability does not involve blockade of PDE4 (which is evoked by rolipram), but is rather due to inhibition of $GABA_A$ receptors (blocked by bicuculline). This assumption is supported by the findings in the LC neurons that both the hyperpolarization and input resistance decrease evoked by the $GABA_A$ receptor agonist muscimol were reversed by methylxanthine while similar

findings were obtained in the spinal cord based on ventral root recording. However, these results are not conclusive because methylxanthines may stimulate other pathways that indirectly overcome inhibition of bursting in the spinal cord or LC by the $GABA_A$ receptor agonist. In the literature there are described other possible mechanisms of action of methylxanthines, such as inhibition of glycinergic receptors or TREK-1 channels (Uneyama et al., 1993; Duan et al., 2009; Harinath & Sikdar, 2005) or enhancement of NMDA receptor transmission (Amabeoku et al., 1999). To determine whether methylxanthines indeed cause hyperpexcitability in spinal and LC neural networks, these cells would have to be dissociated for single channel recordings. While the methylxanthine-evoked spinal hyperexcitability resembled seizure-like discharges in brain slices (Moraidis & Bingmann, 1994; Dzhala et al., 1999; Kilb et al., 2007), they induced high frequency (~1 Hz) extracellular oscillations in the XII motor nucleus. This thesis did not provide evidence whether these oscillations originate from synchronized bursting of XII motoneurons or whether they originate from XII premotoneurons which then transmit that activity to the motor neurons (Funk & Parkis, 2002). Finally, it cannot be excluded at present whether astrocytes, that are capable of high frequency oscillations (MacVicar et al., 1987) or other glia play a role in these oscillations.

In contrast to the spinal and cranial motor networks, neither preBötC nor LC population bursting showed a major seizure-like perturbation in response to up to 10 mM methylxanthine. However, at >2.5 mM there was a trend for modest

acceleration of burst rate and a decrease of burst amplitude. Similarly, neither bicuculline nor strychnine was able to perturb rhythm in the preBötC and LC or mimic responses to methylxanthines in the XII nucleus. This is on the one hand an indication that perturbation of spinal networks by methylxanthines may involve blockade of $GABA_A$ (or glycine) receptors and that lack of similar discharge particularly in the preBötC and LC is due to only a minor role of ongoing tonic inhibition by GABA and glycine for normal bursting in these rhythmogenic networks contrary to cortical networks (Jefferys, 1995; Kilb et al., 2007; Kantor et al., 2012).

7.5 Doses for Methylxanthine Effects

Methylxanthines are used routinely for the clinical management of apnea of prematurity. The recommended doses for theophylline and caffeine in newborn infants are 4-15 mg/kg and 5-30 mg/kg, respectively. Caffeine and theophylline are administered orally or intravenously and the treatment often lasts for several weeks until the episodes of apnea have subsided. Pharmacological studies showed that caffeine or theophylline administered to premature infants have long half-lives, reflecting the immaturity of the enzymatic hepatic system to metabolize these drugs (Arnaud, 2011; Aranda et al., 1979). Plasma half-life range for theophylline and caffeine is 20-30 h and 40-230 h, respectively (Aranda et al., 1979). Half-life of caffeine decreases with postnatal age to 14.4 h and 2.6 h in 3-5 and 5-6 month old infants, respectively (Fredholm et al., 1999). Monitoring

plasma levels of caffeine or theophylline after therapeutic administration is recommended in order to prevent side-effects associated with their use (Pesce et al., 1998). Lee et al. (1996) reported that the mean caffeine plasma level in premature infants was 29.9 mg/l (corresponding to 154 μM), with a range from 0.28 to 93.3 mg/l (1.5-480 μM). Others reported levels of 19-80 mg/l (98-412 μM) (Charles et al., 2008) and 11-33 mg/l (57-170 μM) (Leon et al., 2007). In addition, it has been reported a serum concentration of 217.5 mg/l (1.1 mM) in a case of theophylline intoxication on a premature infant (Anderson et al., 1999). A question arises from these observations: is it possible that caffeine or theophylline levels are higher in the brain than in plasma? Previous *in vivo* and *in vitro* studies suggested that caffeine passes easily through blood-brain barrier and cerebrospinal fluid levels are directly correlated to plasma levels (Somani et al., 1980; Turmen et al., 1979). Other studies showed that acute caffeine administered orally to rodents results in higher caffeine and lower theophylline concentration in the rat brain (Ståhle et al., 1991), while after chronic consumption, theophylline levels are higher than caffeine (Johansson et al., 1996). This might suggest that chronic caffeine exposure results in accumulation of theophylline in the brain.

As discussed in Chapter 1.7, methylxanthines have various pharmacological actions which are dependent on their concentrations. Theophylline has IC_{50} values (half maximal inhibitory concentration) for adenosine antagonism, PDE inhibition, and $GABA_A$ receptors binding of approximately 10 μM, 150-650 μM, and 800 μM, respectively (Ukena et al., 1993; Shi et al., 2003; Daly, 2000).

Caffeine has IC_{50} values for adenosine receptor antagonism of about 40-50 μM, and for inhibition of PDE isozymes and $GABA_A$ receptors binding values of approximately 500 μM (Daly, 2000; Shi et al., 2003). All this suggests that methylxanthines administered to preterm infants might have a predominant effect on adenosine receptors while inhibition of PDE4 or other PDE isozymes is also plausible.

Caffeine is metabolized in the liver into other methylxanthines, such as paraxanthines, theobromine, and theophylline (Kennedy et al., 1987; Berthou et al., 1992; Arnaud, 2011). For premature infants, it was described an additional metabolic pathway, in which theophylline administered clinically can be converted to caffeine (Bory et al., 1979). Paraxanthine is the major metabolite in humans, accounting for approximately 80% of caffeine metabolism (Fredholm et al., 1999; Arnaud, 2011). There are ample evidences that paraxanthine and other metabolites are biologically active and have mechanisms of action similar to other xanthine derivatives (Ferré et al., 1990; Benowitz et al., 1995; Howell et al., 1997; Fredholm et al., 1999; Hawke et al., 2000; Daly, 2007; Guerreiro et al., 2008; Mitchell et al., 2011). Studies that distinguish the effects of *in vivo* methylxanthines should consider all these metabolites because they might act synergistically on the same cellular sites. It is thus possible that chronic exposure to these methylxanthines and the resulting metabolites have additive effects that might account for the stimulatory respiratory effects seen *in vitro* at higher concentrations. Future studies should address the role played by these metabolites

on respiratory system and to elucidate if they have an additive effect which might explain the *in vitro* effects on phosphodiesterases. Also, further studies are needed to clarify whether phosphodiesterases purified from preBötC neurons can be inhibited by methylxanthines at concentrations reported in the literature (Daly, 2000). Moreover, future *in vitro* experiments should be complemented by *in vivo* experiments to elucidate if PDE4 inhibition can stimulate breathing (Chapter **7.2**). There are already *in vivo* studies documenting PDE4 inhibition as a way to stimulate breathing. One study reported that rolipram administration to adult monkeys had a respiratory stimulatory effect, while adenosine receptor blocker CGS 15943 administration had only a behavior effect (Howell, 1993). Another study documented the respiratory stimulant role of rolipram in adult rats (Kajana & Goshgarian, 2008). Specifically, the results showed that after spinal cord lesion at the level of C2, ipsilateral phrenic nerve activity can be restored either by the antagonism of A_1 receptors or PDE4 inhibition. Moreover, contralateral phrenic nerve respiratory frequency was increased only after PDE4 blockade with rolipram, and not by the antagonism of A_1 receptors (Kajana & Goshgarian, 2008).

The above discussions indicate that it is not clear yet, which mechanism has the major contribution to stimulation of the isolated preBötC by methylxanthines. However, if future studies elucidate that concentrations of <0.5 mM are rarely reaching the extracellular/intracellular milieu of preBötC neurons, it is possible that this presumptive inspiratory center is not the primary target of stimulatory

actions of these agents, unless preBötC neurons are more sensitive to them in intact animals, including humans.

7.6 References

Alheid GF, Gray PA, Jiang MC, Feldman JL, McCrimmon DR (2002) Parvalbumin in respiratory neurons of the ventrolateral medulla of the adult rat. J Neurocytol 31, 693-717

Amabeoku GJ (1999) Gamma-aminobutyric acid and glutamic acid receptors may mediate theophylline-induced seizures in mice. Gen Pharmacol 32, 365-372

Anderson BJ, Gunn TR, Holford NH, Johnson R (1999) Caffeine overdose in a premature infant: clinical course and pharmacokinetics. Anaesth Intensive Care 27, 307-311

Aranda JV, Collinge JM, Zinman R, Watters G (1979) Maturation of caffeine elimination in infancy. Arch Dis Child 54, 946-949

Arnaud MJ (2011) Pharmacokinetics and metabolism of natural methylxanthines in animal and man. Handb Exp Pharmacol, 33-91

Ballanyi K (2004) Neuromodulation of the perinatal respiratory network. Curr Neuropharmacol 2, 221–243

Ballanyi K, Ruangkittisakul A (2009) Structure-function analysis of rhythmogenic inspiratory pre-Botzinger complex networks in "calibrated" newborn rat brainstem slices. Resp Physiol Neurobiol 168, 158-178

Ballanyi K, Lalley PM, Hoch B, Richter DW (1997) cAMP-dependent reversal of opioid- and prostaglandin-mediated depression of the isolated respiratory network in newborn rats. J Physiol 504, 127-134

Ballanyi K, Onimaru H, Homma I (1999). Respiratory network function in the isolated brainstem-spinal cord of newborn rats. Prog Neurobiol 59, 583-634

Ballanyi K, Panaitescu B, Ruangkittisakul A (2010) Control of breathing by nerve glue. Sci Signal 3, pe41

Bancalari E (2006) Caffeine for apnea of prematurity. N Engl J Med 354, 2179-2181

Benowitz NL, Jacob P 3rd, Mayan H, Denaro C (1995) Sympathomimetic effects of paraxanthine and caffeine in humans. Clin Pharmacol Ther 58, 684-691

Berthou F, Guillois B, Riche C, Dreano Y, Jacqz-Aigrain E, Beaune PH (1992) Interspecies variations in caffeine metabolism related to cytochrome P4501A enzymes. Xenobiotica 22, 671-680

Bianchi AL, Denavit-Saubié M, Champagnat J (1995) Central control of breathing in mammals: neuronal circuitry, membrane properties, and neurotransmitters. Physiol Rev 75, 1-45

Bory C, Baltassat P, Porthault M, Bethenod M, Frederich A, Aranda JV (1979) Metabolism of theophylline to caffeine in premature newborn infants. J Pediatr 94, 988-993

Bouvier J, Thoby-Brisson M, Renier N, Dubreuil V, Ericson J, Champagnat J, Pierani A, Chédotal A, Fortin G (2010) Hindbrain interneurons and axon guidance signaling critical for breathing. Nat Neurosci 13, 1066-1074

Brockhaus J, Ballanyi K (1998) Synaptic inhibition in the isolated respiratory network of neonatal rats. Eur J Neurosci 10, 3823-3839

Brockhaus J, Ballanyi K (2000) Anticonvulsant A_1 receptor-mediated adenosine action on neuronal networks in the brainstem-spinal cord of newborn rats. Neuroscience 96, 359-371

Brown EM, MacLeod RJ (2001) Extracellular calcium sensing and extracellular calcium signaling. Physiol Rev 81, 239-297

Capogna M (1998) Presynaptic facilitation of synaptic transmission in the hippocampus. Pharmacol Ther 77, 203-223

Charles BG, Townsend SR, Steer PA, Flenady VJ, Gray PH, Shearman A (2008) Caffeine citrate treatment for extremely premature infants with apnea: population pharmacokinetics, absolute bioavailability, and implications for therapeutic drug monitoring. Ther Drug Monit 30, 709-716

Conde SV, Obeso A, Vicario I, Rigual R, Rocher A, Gonzalez C (2006) Caffeine inhibition of rat carotid body chemoreceptors is mediated by A2A and A2B adenosine receptors. J Neurochem 98, 616-628

Dahan A, Aarts L, Smith TW (2010) Incidence, Reversal, and Prevention of Opioid-induced Respiratory Depression. Anesthesiology, 112, 226-238

Daly JW (2000) Alkylxanthines as research tools. J Auton Nerv Syst 81, 44-52

Daly JW (2007) Caffeine analogs: biomedical impact. Cell Mol Life Sci 64, 2153-2169

Del Negro CA, Morgado-Valle C, Hayes JA, Mackay DD, Pace RW, Crowder EA, Feldman JL (2005) Sodium and calcium current-mediated pacemaker neurons and respiratory rhythm generation. J Neurosci 25, 446-453

Del Negro CA, Hayes JA, Pace RW, Brush BR, Teruyama R, Feldman JL (2010) Synaptically activated burst-generating conductances may underlie a group-pacemaker mechanism for respiratory rhythm generation in mammals. Prog Brain Res 187, 111-136

Duan L, Yang J, Slaughter MM (2009) Caffeine inhibition of ionotropic glycine receptors. J Physiol 587, 4063-4075

Dzhala V, Desfreres L, Melyan Z, Ben-Ari Y, Khazipov R (1999) Epileptogenic action of caffeine during anoxia in the neonatal rat hippocampus. Ann Neurol 46, 95-102

Feldman JL, Del Negro CA (2006) Looking for inspiration: new perspectives on respiratory rhythm. Nature Rev Neurosci 7, 232-242

Ferré S, Guix T, Sallés J, Badia A, Parra P, Jané F, Herrera-Marschitz M, Ungerstedt U, Casas M (1990) Paraxanthine displaces the binding of [3H]SCH 23390 from rat striatal membranes. Eur J Pharmacol 179, 295-299

Fredholm BB, Battig K, Holmen J, Nehlig A, Zvartau EE (1999) Actions of caffeine in the brain with special reference to factors that contribute to its widespread use. Pharmacol Rev 51, 83–133

Gargaglioni LH, Hartzler LK, Putnam RW (2010) The locus coeruleus and central chemosensitivity. Respir Physiol Neurobiol 173, 264-273

Gray PA, Rekling JC, Bocchiaro CM, Feldman JL (1999) Modulation of respiratory frequency by peptidergic input to rhythmogenic neurons in the preBotzinger complex. Science 286, 1566-1568

Gray PA, Hayes JA, Ling GY, Llona I, Tupal S, Picardo MC, Ross SE, Hirata T, Corbin JG, Eugenín J, Del Negro CA (2010) Developmental origin of preBötzinger complex respiratory neurons. J Neurosci 30, 14883-14895

Guerreiro S, Toulorge D, Hirsch E, Marien M, Sokoloff P, Michel PP (2008) Paraxanthine, the primary metabolite of caffeine, provides protection against dopaminergic cell death via stimulation of ryanodine receptor channels. Mol Pharmacol 74, 980-989

Harinath S, Sikdar SK (2005) Inhibition of human TREK-1 channels by caffeine and theophylline. Epilepsy Res 64, 127-135

Hawke TJ, Allen DG, Lindinger MI (2000) Paraxanthine, a caffeine metabolite, dose dependently increases [Ca(2+)](i) in skeletal muscle. J Appl Physiol 89, 2312-2317

Hilaire G, Viemari JC, Coulon P, Simonneau M, Bevengut M (2004) Modulation of the respiratory rhythm generator by the pontine noradrenergic A5 and A6 groups in rodents. Respir Physiol Neurobiol 143, 187-197

Hille B (2001) Ion channels of excitable membranes. Sunderland, MA: Sinauer Associates

Howell LL (1993) Comparative effects of caffeine and selective phosphodiesterase inhibitors on respiration and behavior in rhesus monkeys. J Pharmacol Exp Ther 266, 894-903

Howell LL, Coffin VL, Spealman RD (1997) Behavioral and physiological effects of xanthines in nonhuman primates. Psychopharmacology (Berl) 129, 1-14

Jefferys JG (1995) Nonsynaptic modulation of neuronal activity in the brain: electric currents and extracellular ions. Physiol Rev 75, 689-723

Johansson B, Georgiev V, Kuosmanen T, Fredholm BB (1996) Long-term treatment with some methylxanthines decreases the susceptibility to bicuculline- and pentylenetetrazol-induced seizures in mice. Relationship to c-fos expression and receptor binding. Eur J Neurosci 8, 2447-2458

Kajana S, Goshgarian HG (2008) Administration of phosphodiesterase inhibitors and an adenosine A1 receptor antagonist induces phrenic nerve recovery in high cervical spinal cord injured rats. Exp Neurol 210, 671-680

Kantor C, Panaitescu B, Kuribayashi J, Ruangkittisakul A, Lee TF, Cheung PY, MacTavish D, Jhamandas J, Ballanyi K (2012) Electrophysiological imaging of early network oscillations in brain slices from newborn rats and piglets. In Isolated Central Nervous System Circuits (Ed K Ballanyi), Neuromethods Series Vol 73 (Ed W Walz). Springer Science+Business Media, LLC, New York, NY, 315-356

Kennedy JS, Leduc BW, Scavone JM, Harmatz JS, Shader RI, Greenblatt DJ (1987) Pharmacokinetics of intravenous caffeine: comparison of high-performance liquid chromatographic and gas chromatographic methods. J Chromatogr 422, 274-280

Kilb W, Sinning A, Luhmann HJ (2007) Model-specific effects of bumetanide on epileptiform activity in the in-vitro intact hippocampus of the newborn mouse. Neuropharmacology 53, 524-533

Konnerth A, Heinemann U, Yaari Y (1986) Nonsynaptic epileptogenesis in the mammalian hippocampus in vitro. I. Development of seizurelike activity in low extracellular calcium. J Neurophysiol 56, 409-423

Kubo Y, Miyashita T, Murata Y (1998) Structural basis for a Ca2+-sensing function of the metabotropic glutamate receptors. Science 279, 1722-1725

Kulik A, Haentzsch A, Lückermann M, Reichelt W, Ballanyi K (1999) Neuron-glia signaling via α_1 adrenoceptor-mediated Ca^{2+} release in Bergmann glia in situ. J Neurosci 19, 8401-8408

Kuwana S, Okada Y, Natsui T (1998) Effects of extracellular calcium and magnesium on central respiratory control in the brainstem-spinal cord of neonatal rat. Brain Res 786, 194-204

Law PY, Wong YH, Loh HH (2000) Molecular mechanisms and regulation of opioid receptor signaling. Annu Rev Pharmacol Toxicol 40, 389-430

Lee TC, Charles BG, Steer PA, Flenady VJ (1996) Saliva as a valid alternative to serum in monitoring intravenous caffeine treatment for apnea of prematurity. Ther Drug Monit 18, 288-293

Leon AE, Michienzi K, Ma CX, Hutchison AA (2007) Serum caffeine concentrations in preterm neonates. Am J Perinatol 24, 39-47

MacVicar BA, Crichton SA, Burnard DM, Tse FW (1987) Membrane conductance oscillations in astrocytes induced by phorbol ester. Nature 329, 242-243

Martin RJ, Abu-Shaweesh JM (2005) Control of breathing and neonatal apnea. Biol Neonate 87, 288-295

Mellen NM, Janczewski WA, Bocchiaro CM, Feldman JL (2003) Opioid-induced quantal slowing reveals dual networks for respiratory rhythm generation. Neuron 37, 821-826

Miller MJ, Martin RJ (1992) Apnea of prematurity. Clin Perinatol 19, 789-808

Mitchell ES, Slettenaar M, vd Meer N, Transler C, Jans L, Quadt F, Berry M (2011) Differential contributions of theobromine and caffeine on mood, psychomotor performance and blood pressure. Physiol Behav 104, 816-822

Montandon G, Qin W, Liu H, Ren J, Greer JJ, Horner RL (2011) PreBotzinger complex neurokinin-1 receptor-expressing neurons mediate opioid-induced respiratory depression. J Neurosci 31, 1292-1301

Moraidis I, Bingmann D (1994) Epileptogenic actions of xanthines in relation to their affinities for adenosine A1 receptors in CA3 neurons of hippocampal slices (guinea pig). Brain Res 640, 140-145

Nichols CG, Lopatin AN (1997) Inward rectifier potassium channels. Annu Rev Physiol 59, 171-191

Okada Y, Sasaki T, Oku Y, Takahashi N, Seki M, Ujita S, Tanaka KF, Matsuki N, Ikegaya Y (2012) Preinspiratory calcium rise in putative pre-Bötzinger complex astrocytes. J Physiol (Epub ahead of print)

Onimaru H, Homma I (2003) A novel functional neuron group for respiratory rhythm generation in the ventral medulla. J Neurosci 23, 1478-1486

Onimaru H, Arata A, Homma I (1990) Inhibitory synaptic inputs to the respiratory rhythm generator in the medulla isolated from newborn rats. Pflugers Arch 417, 425-432

Onimaru H, Homma I, Iwatsuki K (1992) Excitation of inspiratory neurons by preinspiratory neurons in rat medulla in vitro. Brain Res Bull 29, 879-882

Onimaru H, Ballanyi K, Homma I (2003) Contribution of Ca2+-dependent conductances to membrane potential fluctuations of medullary respiratory neurons of newborn rats in vitro. J Physiol 1, 727-741

Oyamada Y, Ballantyne D, Muckenhoff K, Scheid P (1998) Respiration-modulated membrane potential and chemosensitivity of locus coeruleus neurones in the in vitro brainstem-spinal cord of the neonatal rat. J Physiol 513, 381-398

Pace RW, Mackay DD, Feldman JL, Del Negro CA (2007) Role of persistent sodium current in mouse preBötzinger Complex neurons and respiratory rhythm generation. J Physiol 580, 485-496

Pesce AJ, Rashkin M, Kotagal U (1998) Standards of laboratory practice: theophylline and caffeine monitoring. National Academy of Clinical Biochemistry. Clin Chem 44, 1124-1128

Pagliardini S, Adachi T, Ren J, Funk GD, Greer JJ (2005) Fluorescent tagging of rhythmically active respiratory neurons within the pre-Bötzinger complex of rat medullary slice preparations. J Neurosci 25, 2591-2596

Ptak K, Yamanishi T, Aungst J, Milescu LS, Zhang R, Richerson GB, Smith JC (2009) Raphé neurons stimulate respiratory circuit activity by multiple mechanisms via endogenously released serotonin and substance P. J Neurosci 29, 3720-3737

Rekling JC, Champagnat J, Denavit-Saubi M (1996a) Electroresponsive properties and membrane potential trajectories of three types of inspiratory neurons in the newborn mouse brain stem in vitro. J Neurophysiol 75, 795-810

Rekling JC, Champagnat J, Denavit-Saubié M (1996b) Thyrotropin-releasing hormone (TRH) depolarizes a subset of inspiratory neurons in the newborn mouse brain stem in vitro. J Neurophysiol 75, 811-819

Richter DW, Spyer KM (2001) Studying rhythmogenesis of breathing: comparison of in vivo and in vitro models. Trends Neurosci 24, 464-472

Richter DW, Ballanyi K, Schwarzacher S (1992) Mechanisms of respiratory rhythm generation. Curr Opin Neurobiol 2, 788-793

Richter DW, Lalley PM, Pierrefiche O, Haji A, Bischoff AM, Wilken B, Hanefeld F (1997) Intracellular signal pathways controlling respiratory neurons. Respir Physiol Neurobiol 110, 113-123

Ruangkittisakul A, Ballanyi K (2006) Reversal by phosphodiesterase-4 blockers of in vitro apnea in the isolated brainstem-spinal cord preparation from newborn rats. Neurosci Lett 401, 194-198

Ruangkittisakul A, Ballanyi K (2010) Methylxanthine reversal of opioid-evoked inspiratory depression via phosphodiesterase-4 blockade. Respir Physiol Neurobiol 172, 94-105

Ruangkittisakul A, Schwarzacher SW, Ma Y, Poon B, Secchia L, Funk GD, Ballanyi K (2006) High sensitivity to neuromodulator-activated signalling pathways at physiological [K^+] of confocally-imaged respiratory centre neurons in online-calibrated newborn rat brainstem slices. J Neurosci 26, 11870-11880

Ruangkittisakul A, Secchia L, Bornes TD, Palathinkal DM, Ballanyi K (2007) Dependence on extracellular Ca^{2+}/K^+ antagonism of inspiratory centre rhythms in slices and en bloc preparations of newborn rat brainstem. J Physiol 584, 489-508

Ruangkittisakul A, Schwarzacher SW, Secchia L, Ma Y, Bobocea N, Poon BY, Funk GD, Ballanyi K (2008) Generation of eupnea and sighs by a spatiochemically organized inspiratory network. J Neurosci 28, 2447-2458

Ruangkittisakul A, Panaitescu B, Kuribayashi J, Ballanyi K (2010) Caffeine reversal of opioid-evoked and endogenous inspiratory depression in perinatal rat en bloc medullas and slices. Adv Exp Med Biol 669, 123-127

Ruangkittisakul A, Panaitescu B, Ballanyi K (2011) K(+) and Ca²(+) dependence of inspiratory-related rhythm in novel "calibrated" mouse brainstem slices. Respir Physiol Neurobiol 175, 37-48.

Ruangkittisakul A, Secchia-Ballanyi L, Panaitescu B, Bobocea N, Kuribayashi J, Iizuka M, Kantor C, Ballanyi K (2012) Anatomically ‘calibrated‘ isolated respiratory networks from newborn rodents. In Isolated Central Nervous System Circuits (Ed K Ballanyi), Neuromethods Series Vol 73 (Ed W Walz). Springer Science+Business Media, LLC, New York, NY, 61-124

Schnell C, Fresemann J, Hülsmann S (2010) Determinants of functional coupling between astrocytes and respiratory neurons in the pre-Bötzinger complex. PLoS One 6, e26309

Shi D, Padgett WL, Daly JW (2003) Caffeine analogs: effects on ryanodine-sensitive calcium-release channels and GABAA receptors. Cell Mol Neurobiol 23, 331-347

Smith JC, Ellenberger HH, Ballanyi K, Richter DW, Feldman JL (1991) Pre-Bötzinger complex: a brainstem region that may generate respiratory rhythm in mammals. Science 254, 726-729

Somani SM, Khanna NN, Bada HS (1980) Caffeine and theophylline: serum/CSF correlation in premature infants. J Pediatr 96, 1091-1093

Somjen GG (2002) Ion regulation in the brain: implications for pathophysiology. Neuroscientist 8, 254-267

Ståhle L, Segersvärd S, Ungerstedt U (1991) Drug distribution studies with microdialysis. II. Caffeine and theophylline in blood, brain and other tissues in rats. Life Sci 49, 1843-1852

Turmen T, Louridas TA, Aranda JV (1979) Relationship of plasma and CSF concentrations of caffeine in neonates with apnea. J Pediatr 95, 644-646

Ukena D, Schudt C, Sybrecht GW (1993) Adenosine receptor-blocking xanthines as inhibitors of phosphodiesterase isozymes. Biochem Pharmacol 45, 847-851

Uneyama H, Harata N, Akaike N (1993) Caffeine and related compounds block inhibitory amino acid-gated Cl- currents in freshly dissociated rat hippocampal neurones. Br J Pharmacol 109, 459-465

Zhao J, Gonzalez F, Mu D (2011) Apnea of prematurity: from cause to treatment. Eur J Pediatr 170, 1097-1105

Zhao MG, Hülsmann S, Winter SM, Dutschmann M, Richter DW (2006) Calcium-regulated potassium currents secure respiratory rhythm generation after loss of glycinergic inhibition. Eur J Neurosci 24, 145-154

Zucker RS (2005) Minis: whence and wherefore? Neuron 45, 482-484